Dottorato di Ricerca in Ingegneria Civile
Graduate School in Civil Engineering
Sede: Facoltà di Ingegneria - Università di Pavia - via Ferrata 1 – 27100 Pavia – Italy

Dottorato di Ricerca in Ingegneria Civile XI Ciclo

Performance-based Design by Structural Control for Suspension Bridges

Ph.D. Thesis
Fabio Giuliano

Supervisor:
  Prof. Franco Bontempi

Examiner:
  Prof. Lucia Faravelli

Febbraio 2007

III

Dottorato di Ricerca in Ingegneria Civile

Settore:	Ingegneria
Sede Amministrativa non consortile:	Università degli Studi di PAVIA
Durata del dottorato in anni:	3
Numero studenti:	3 ogni anno
Periodo formativo estero in mesi:	come previsto dal regolamento del Dottorato di Ricerca
Numero minimo di corsi:	6

Recapiti

Dipartimento di Meccanica Strutturale
via Ferrata 1 - 27100 Pavia - Italy
Tel. 0382 / 505450   Fax 0382 / 528422

Dipartimento di Ingegneria Idraulica e Ambientale
via Ferrata 1 - 27100 Pavia - Italy
Tel. 0382 / 505300   Fax 0382 / 505589

Coordinatore

CASCIATI Fabio - Professore Ordinario di Scienza delle Costruzioni (H07A)

Dipartimento di Meccanica Strutturale
via Ferrata 1 - 27100 Pavia – Italy   Tel. 0382 / 505458   Fax 0382 / 528422
e-mail: fabio@dipmec.unipv.it

Collegio dei Docenti

CAUVIN Aldo	-	Professore Ordinario di Teoria e Progetto delle Costruzioni in Calcestruzzo Armato e Precompresso (H07B)
CIAPONI Carlo	-	Professore Associato di Idraulica (H01A)
FARAVELLI Lucia	-	Professore Ordinario di Sicurezza e Affidabilità delle Costruzioni (H07A)
FUGAZZA Mario	-	Professore Associato di Sistemazione dei Bacini Idrografici (H01B)
GOBETTI Armando	-	Professore Associato di Dinamica delle Strutture (H07A)
MACCHI Giorgio	-	Professore Ordinario di Tecnica delle Costruzioni (H07B)
MOISELLO Ugo	-	Professore Ordinario di Idrologia (H01B)
PAPIRI Sergio	-	Professore Associato di Infrastrutture Idrauliche (H01B)
SALA Roberto	-	Professore Associato di Macchine (H04C)

Organizzazione del corso

Il dottorato di ricerca in *Ingegneria Civile* presso la Facoltà di Ingegneria dell'Università degli Studi di Pavia è stato istituito nell'anno accademico 1994/95 (X ciclo).

Il corso consente al dottorando di scegliere tra due curricula: idraulico o strutturale. Egli svolge la propria attività di ricerca rispettivamente presso il Dipartimento di Ingegneria Idraulica e Ambientale o quello di Meccanica Strutturale.

Durante i primi due anni sono previsti almeno sei corsi, seguiti da rispettivi esami, che il dottorando è tenuto a sostenere. Il Collegio dei Docenti, composto da professori dei due Dipartimenti, organizza i corsi con lo scopo di fornire allo studente di dottorato opportunità di approfondimento su alcune delle discipline di base per entrambe le componenti, idraulica e strutturale. Corsi e seminari vengono tenuti da docenti di Università nazionali ed estere.

Il Collegio dei Docenti, cui spetta la pianificazione della didattica, si è orientato ad attivare ad anni alterni corsi sui seguenti temi:

− Meccanica dei solidi e dei fluidi
− Metodi numerici per la meccanica dei solidi e dei fluidi
− Rischio strutturale e ambientale
− Metodi sperimentali per la meccanica dei solidi e dei fluidi
− Intelligenza artificiale

più corsi specifici di indirizzo.

Al termine dei corsi del primo anno il Collegio dei Docenti assegna al dottorando un tema di ricerca da sviluppare sotto forma di tesina entro la fine del secondo anno; il tema, non necessariamente legato all'argomento della tesi finale, è di norma coerente con il curriculum, scelto dal dottorando (idraulico o strutturale).

All'inizio del secondo anno il dottorando discute con il Coordinatore l'argomento della tesi di dottorato, la cui assegnazione definitiva viene deliberata dal Collegio dei Docenti.

Alla fine di ogni anno i dottorandi devono presentare una relazione particolareggiata (scritta e orale) sull'attività svolta. Sulla base di tale relazione il Collegio dei Docenti, "previa valutazione della assiduità e dell'operosità dimostrata dall'iscritto", ne propone al Rettore l'esclusione dal corso o il passaggio all'anno successivo.

Il dottorando può svolgere attività di ricerca sia di tipo teorico che sperimentale, grazie ai laboratori di cui entrambi i Dipartimenti dispongono, nonché al Laboratorio Numerico di Ingegneria delle Infrastrutture.

Il "Laboratorio didattico sperimentale" del Dipartimento di Meccanica Strutturale dispone di:

1. una tavola vibrante che consente di effettuare prove dinamiche su prototipi strutturali;
2. opportuni sensori e un sistema di acquisizione dati per la misura della risposta strutturale;
3. strumentazione per la progettazione di sistemi di controllo attivo e loro verifica sperimentale;
4. strumentazione per la caratterizzazione dei materiali, attraverso prove statiche e dinamiche.

Il laboratorio del Dipartimento di Ingegneria Idraulica e Ambientale dispone di:

1. un circuito in pressione che consente di effettuare simulazioni di moto vario;
2. un tunnel idrodinamico per lo studio di problemi di cavitazione;
3. canalette per lo studio delle correnti a pelo libero.

A partire dall'anno accademico 1997/98 al dottorando viene data la possibilità di frequentare la "Scuola Avanzata di Formazione Integrata" dell'Istituto Universitario Studi Superiori, che si articola in tre anni e la cui finalità è quella di integrare le attività post-laurea di tipo specialistico con studi a carattere interdisciplinare adatti ad assicurare un più ampio bagaglio culturale.

Elenco delle tesi

Marco Battaini (X Ciclo)   "Sistemi strutturali controllati: progettazione e affidabilità"

Claudia Mariani (X Ciclo)   "Problemi di ottimizzazione per strutture bidimensionali anisotrope"

Antonella Negri (X Ciclo)   "Stima delle perdite idrologiche nei bacini di drenaggio urbani"

Aurora Angela Pisano (XI Ciclo) "Structural System Identification: Advanced Approaches and Applications"

Carla Saltalippi (XI Ciclo)   "Preannuncio delle piene in tempo reale nei corsi d'acqua naturali"

Eugenio Barbieri (XI Ciclo) "Termofluid dynamics and topology optimisation of an active thermal insulation structure"

Massimiliano Barbolini (XII Ciclo) "Dense snow avalanche avalanches: computational models, hazard mapping and related uncertainties"

Paolo Espa (XII Ciclo)   "Moti atmosferici generati da forze di galleggiamento: simulazioni numeriche e studio su modello fisico"

Lorenza Petrini (XII Ciclo)   "Shape Memory Alloys: Modelling the Martensitic Phase Behaviour for Structural Engineering Exploitation"

Stefano Podestà (XIII Ciclo) "Risposta sismica di antichi edifici religiosi in muratura: sviluppo di nuovi modelli per l'analisi di vulnerabilità"

Daniele Sturla (XIII Ciclo)   "Simulazioni lagrangiane di flussi rapidamente variati nell'approssimazione di acque poco profonde"

Francesco Marazzi (XV Ciclo) "Semi-active control of civil structures: implementation aspects"

Roberto Nascimbene (XV Ciclo) "Sail Modelling for Maximal Speed Optimum Design"

Massimo Giudici (XVI Ciclo) "Progettazione in regime non lineare di strutture in CAP a cavi aderenti e non aderenti"

Matteo Mutti (XVI Ciclo) "Stability analysis of stratified three-phase flows in pipes"

Gabriella Petaccia (XVI Ciclo) "Propagazione di onde a fronte ripido per rottura di sbarramenti in alvei naturali"

Sara Casciati (XVII Ciclo) "Damage Detection and Localization in the Space of the Observed Variables"

Tiziana D'Amico (XVI Ciclo) "Ricerca e Sviluppo di Metodologie Diagnostiche per il Recupero di Edifici monumentali: Prove Vibro-acustiche sul Tufo"

Marco Domaneschi (XVIII Ciclo) "Structural Control of Cable-stayed and Suspended Bridges"

Olga Janet Barco (XVII Ciclo) "Modeling the quantity and quality of storm water runoff using SWMM"

Joanna Boguniewicz (XVIII Ciclo) "Integration of monitoring and modelling in the surface water state evaluation process of a sub-Alpine lake watershed"

Laura Bornatici (XVIII Ciclo) "L'impiego degli algoritmi generici per la risoluzione dei problemi di progetto di reti di distribuzione idrica"

Maria Cristina Collivignarelli (XVIII Ciclo) "Trattamento di rifiuti liquidi mediante processi biologici aerobici termofili e mesofili e processi avanzati di ossidazione chimica in diversa sequenza"

Botond Ráduly (XVIII Ciclo) "Artificial neural network applications in urban water quality modeling"

Carla Antoci (XVIII Ciclo) "Simulazione numerica dell'interazione fluido-struttura con la tecnica SPH"

Federica Cappabianca (XVIII Ciclo) "La valutazione del rischio valanghivo attraverso la modellazione dinamica"

Arianna Callegari (XVIII Ciclo) "Applicazione di tecnologie di monitoraggio on-line per la gestione dei processi di trattamento reflui"

Acknowledgments

Index

Chapter 5
Structural Control of the Pylon of a Suspension Bridge 185

INTRODUCTION

The final target of the present thesis is the investigation of the capabilities of passive control strategies for the reduction of the wind response of the pylons of long span suspension bridges. This aim is inserted and interacts into the more general framework of the Performance-based Design, a modern approach for design suitable to innovative structures.

The primary motivation of the work is related to the design of the challenging long span suspension bridge in the Strait of Messina, Italy, described in the Appendix B of the thesis. The aim was the investigation of the effectiveness of passive strategies like the provision of Tuned Mass Dampers in the pylons as already done in flexible and low damped structures. At this regard the application of these technologies against wind loading has been experienced mainly for skyscrapers, but for the mitigation of the wind response of the pylons of long span bridges this solution has been experienced only for the Akashi Kaikyo Bridge, Japan, and only few works have been produced, with no adequate description of the critical aspects of the design.

The specific problem in object must be considered in a more general context, presented in Chapter 1, where the innovative nature of the structure, for which there is no experience concerning several features, suggests the adoption of the

modern Performance-based Approach for the design. The complexity of the problem, related to the mechanical nonlinearities, the interaction mechanisms and the uncertainties can be faced through a Systemic Approach adapted from the System Engineering: the structural system, the design environment, the contingency scenarios and the complex of performance are identified, decomposed and hierarchically organized. For the evaluation of the performance capabilities each subsystem needs to be modelled in an adequate scale of description through a multilevel modelling (*layering*), practiced through a Guyan substructuring technique inside the finite element method, while the response under uncertain loading and boundaries are investigated through the techniques of the *experimental design* to provide reliable for technical judgement, the design refinement and final choice. The coupling of Performance and Systemic Approach provide the reasons, the targets and the means to the suppliers which must find technical solution to satisfy the Users' needs.

This general framework is the methodology guideline for the development of the thesis, in the applicative parts of Chapter 2 and 5.

Chapter 2 presents an exemplification of the Systemic-Performance Approach , used for the evaluation of the performance of the Messina Strait Bridge: the structural and performance decomposition, the multilevel modelling for specific performance, and the experimental method for the exploration of the response. Some critical aspects of modelling and results of the investigations on the serviceability performance of the bridge conducted during the first year of the Ph. D. course are also presented.

Once introduced and exemplified the philosophy and the methodology of the Performance-Systemic Approach, before coming back to the design of the control system of the pylon, an overview on the nature and description of the wind loading, on the aeroelastic effects and on the modelling of the soil-foundation boundaries involving the pylons of suspension bridge is briefly presented in Chapter 3.

The state of art of the design of bridges considers the tools of Structural Control technically enough mature to be applied for specific problems, distinguishing active, semi-active and passive strategies, but sometimes not enough reliable or economically convenient. In the specific case of suspension bridges, active/hybrid strategies have been used for the erection stages, while passive control has been more deeply adopted to correct the structural response under accidental events or transient phases such as the constructive stages. The

attention in Chapter 4 is focused the Tuned Mass Dampers, on their main properties, on their optimization criteria for the design and on the role of Structural Control for the design of suspension bridges, with specific attention to the pylons.

Chapter 5 is the final applicative part of the thesis, where the methodology presented in Chapter 1 and 2 (decomposition, substructuring and experimental approach), the loadings and modelling aspects of Chapter 3, the capabilities of Tuned Mass Dampers and the role of Structural Control presented in Chapter 4 are conveyed to put in evidence significant design aspects that are specific for the pylons.
Many researches and applications have been already developed concerning the wind design of long span bridge pylons during the erection stages, showing the effectiveness of active or hybrid control strategies. Yet the targets of the design and the specific performance are usually not explicitly documented neither expressed in terms of increase of structural robustness and reliability.
Concerning the service life, it has to be noted that the structural problem changes radically in respect the erection stages when the pylon has a cantilever-type configuration: the boundaries impose a different static and scheme, different dynamic properties, different sensitivity to uncertainties and loading vulnerability. For this stages, less critical than the free-standing configurations, there is no adequate documentation in literature about the advantages of structural control in the mitigation of the response, because the problem becomes relevant just for very high slenderness ratios, while for shorter structures the *strengthening* strategies have been always preferred. It is not casual that the Akashi Kaikyo Bridge, the longest suspension bridge of the world, is the only applying Tuned Mass Dampers to guarantee structural safety in the world. For this bridge the design of the control system has been successfully implemented using the well-established criteria of design for single-degree-of-freedom systems subjected to harmonic loads (approximating the vortex loading), but with no satisfactory focus on the performance under gust loading (also for the truss configuration of the towers) and on the mechanisms which affect the *Dependability* of the control system.

In the perspective of the Performance-based Design, criteria of *Dependability* are proposed in Chapter 5 to provide a guideline for the design of the control system from the erection to the service life: *Efficiency*, *Robustness* and *Redundancy*, with different hierarchical order along the constructive process, and strictly dependent on the natural environment (i.e. soil interaction effects).

Starting from the available data and design, the system is analyzed in its constructive stages, with particular attention towards the free-standing configuration (before the main cable assemblage) and in the service configuration. The passage from the free to the service configuration represents a critical *snap-through*, where the dynamic properties and the structural problem perform a sudden change and the targets and the technologies of the structural control need to be adapted.

Simple modelling of the system, with few degrees of freedom, suitable for analytical treatment and well acknowledged in literature by the fifties, is not adequate, because of the high impact of the uncertain boundaries and of geometry on the dynamic characterization of the system.

Consequently a substructured finite element modelling, representing explicitly the soil and its layered stratification, the geometry of the foundations, the boundaries on the top of the pylon through the saddle elements is necessary to obtain a likely characterization of the system and a reliable response. The numerical investigations are at first focused on the gust response of the uncontrolled structural configuration, through analyses in the time domain, in order to check the structural safety in respect the design loads. Analyses in the frequency domain (in the hypothesis of stationary loadings and linear response) have been also performed in order to assess the qualitative soil impact along the constructive process and to identify the need of performance of the control system from the erection to the service life.

After the identification of the properties of the system, the design of a passive control system, using Tuned Mass Dampers is approached, starting from the minimum damping to be provide against the vortex induced lock-in phenomena, and further to give adequate reduction of the gust response, and consequently of the secondary moments, of the corresponding induced distortions (evaluable through the Erection Factors Reduction Procedure (*ERF*)) and of possible fatigue effects. It is worthnoting that the need or the convenience of the control provisions is strictly related to the preliminary design and the locked data, and to the margin of benefit allowed for the control strategies as explicitly declared in the Design Specifications. In other words, the decision on the installation of the control system rely on the role of Structural Control assumed in the Design Specification, as receipted from the experience and the external state of art.

The evolution of the demand of efficiency, robustness and redundancy of the control system is identified along the constructive process, while the design parameter optimization is conducted through the presented *experimental*

approach, leading to optimal configuration, from single-efficient TMD to multiple configuration (MTMD), increasing the system robustness in the expected scenarios.

The analyses, with a brief extension also to the seismic performance (which require different optimal design parameters than wind loading), put in evidence a dichotomic relationship between the targets of efficiency and robustness, the prevalence of the efficiency demand in the *free-standing* configurations and the increase of the robustness demand in the service one, for which multiple-TMD configurations, with spreading of devices frequencies, are recommended.

The final solution, synthesis of the whole design process, can be identified – before an inescapable *real-time* tuning and correction - through an optimization reliability-based method, conceived to identify the optimal control configuration minimizing the probability failure (violation of a performance hyper-surface) and keep the passive nature of the provisions. It allows also to quantify the capabilities of *monitoring*, *identification* and *model updating* during the erection in increasing the reachable efficiency, in front of adequate reduction of the robustness demand. This approach can be conducted through Monte Carlo simulations considering the soil and other mechanical and loading uncertainties, and keeps in this sense the experimental nature of the methodology adopted in the pre-design stages, and is realized as a support to the decision process about the technical and economical convenience of the installation in respect of the traditional *strenghtening* strategies.

5
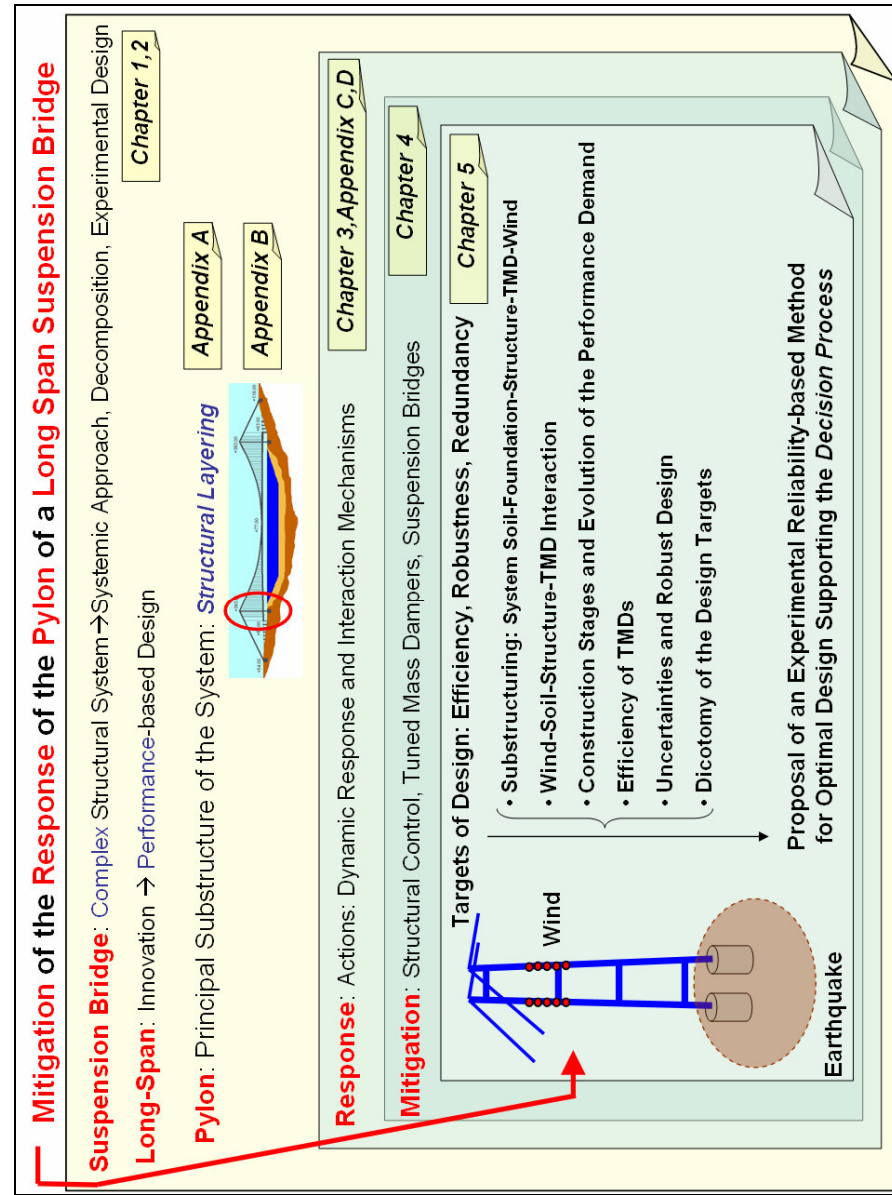
Chapter 1

THE PERFORMANCE-BASED DESIGN OF COMPLEX STRUCTURES

- The Performance-based Design Philosophy
- Statement of Users' Needs and Requirements
  - Performance Decomposition - Dependability
- Complex Systems – Systemic Approach for the Design
  - Structural Decomposition – Multilevel Layering
- Quantified Performance Criteria
- Experimental Methods for Evaluation
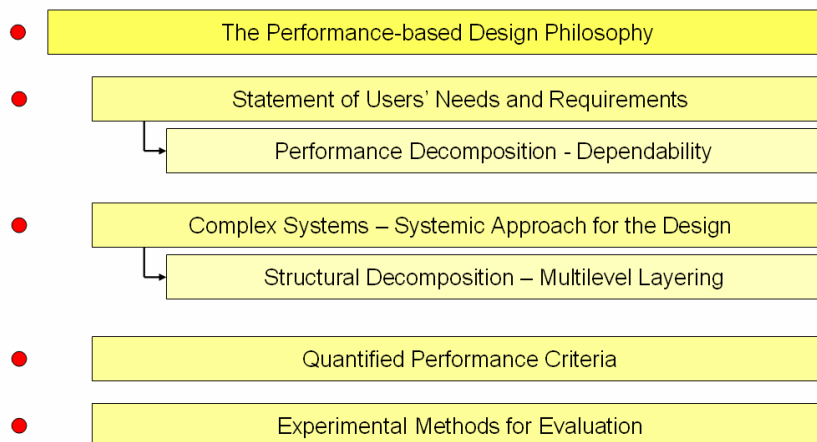
Abstract

This Chapter presents the framework of a *performance oriented approach* for the design of complex structural systems.

The modern concept of construction may enlarge the spectrum of the structural solutions, employing new materials and technologies. For such challenges the traditional design approaches appear inadequate, for the amount of prescriptions often not suitable for innovative works. Design approaches, oriented towards the performance instead of the prescriptions, have been already introduced as a more versatile mean to take advantage of the availability of new technologies and to support their development.

For complex structural system the design, and particularly the performance oriented one, require a *Systemic approach*, directly adapted from the System Engineering. The evaluation and the optimization of the performance capabilities is simplified through a Structural and Performance multilevel decomposition.

The complexity and the multitude of interrelated factors, each of them able to modify the structural performance, suggest the adoption of an experimental approach for the exploration of the response and the feedback-negotiation activity during the Specification draft.

1.1 Introduction

The activity of production of designs is one of the most important tasks of Engineers. It consists of the transformation of natural materials and of the natural environment in such a way to produce a service for the people.

It requires activities of research, comparison, validation, verification, choice, to make decision and find final solutions, even in presence of uncertain or fragmentary data, and limiting risks as much as possible.

These purposes are achieved through the use of numerical models able to simulate the physical phenomena.

The design research has the target of guaranteeing the users' requirements in safe manner. In this sense the structural design is a synthesis and the choice of the optimal solution to realize a certain structure.

In the last years a large amount of innovation has been recorded in Mechanical and Civil Engineering, in terms of numerical tools and technology availability, capable to introduce deep modernization in the design and construction practice. Unfortunately, Civil Engineering is traditionally reluctant to acquire such news, because of the relevance of tradition, culture, confidence on experience in the constructive practice. In addition, and to guarantee the Users' safety, the Building Codes have a strong prescriptive content, leaving very small freedom to the designers: in fact an excessive flexibility or release of the laws could have encouraged dangerous hazards in the constructive practice.

Furthermore some accidents occurred to innovative structures (i.e. the disaster of Tacoma Bridge), restricted the need of innovation when well-established solutions were available.

Nowadays the availability of new tools and technologies give new challenges to the designers, increasing performance and capabilities of structural typologies, and realizing also more slender, elegant and demanding solutions for structures. These challenges require that many prescriptions strictly related to ordinary problems and their traditional technologic solutions are outdated, and awakened public opinion and engineers to the need of renewal. In this sense the traditional

prescriptive approach for the design, especially for innovative and complex structural system, appears now to be inadequate and promotes the development and the adoption of performance oriented codes for the whole constructive process.

1.2 The Performance-based Design (PBD) Philosophy

A simple but effective definition of the Performance Approach is that of Gibson (1982), as the "*practice of thinking and working in terms of ends rather than means.* […] *It is concerned with what a building or a building product is required to do, and not with prescribing how it is to be constructed.* […] *A prescriptive approach describes means as opposite to ends, and is concerned with type and quality of materials, method of construction, workmanship, etc.*"

The content of the prescriptive approach is oriented to the description of how to reach the design targets how to build structures, which means may be employed: it is based on experience and the knowledge of what works well, and imposes specific prescriptions to prevent disasters.

For example, in the design of civil structures, a prescriptive approach makes sure to define all the loads applied and to verify that stresses and strains are within admissible levels; generally speaking, a prescriptive approach leads to an acceptable technical solution, being the margins of freedom quite limited, while a performance oriented approach states explicitly which are the performance requested, and eventually the levels to be guaranteed, giving more freedom to the designer, who can choose the optimum in a range of possible solutions.

As a consequence, the main advantages of a prescriptive approach are:

- the simplicity of the application for a designer;
- the easiness for any controller;
- the consolidation in the tradition and in the experience of specialists.

Yet it represents also an obstacle to innovation and to the design of structures of which there is no experience, and for which most of the prescriptions cannot be applied or even represent a non-sense. Furthermore, in a prescriptive context the proposal of alternative solutions creates procedural difficulties, for the need of

demonstrating that the alternative solution is able to get equal performance levels, using equivalence criteria between non-homogeneous solutions.

Another disadvantage of prescriptive codes concern the difficulty for the international trade of construction products: at this regard the *World Trade Organization (WTO)* stated in the clause 28 of the "*Agreement on Technical Barriers to Trade*" (WTO 1997), that "*wherever opportune, the Members shall specify technical regulations based on product requirements in terms of performance rather than design or descriptive characteristics*". So the subscribers of this Agreement committed themselves to use the performance language in trade.

Generally speaking, the Performance-based Design, represents a modern, continuously growing and versatile option to overcome these difficulties. In a project, it makes sure of fixing directly the performance guideline required and moves, in the space of the free variables, using extensively the capabilities of materials and the composition of the sub-structures maximizing the possible levels of efficiency, if the capabilities of materials and technologies are demonstrated to be adequate for the targets with satisfactory levels of performance (safety, functionality, etc.).

A Performance-based Approach to the design requires a clear description of the requested performance, not related to the final specific technical solution, while the levels of performance could be expressed also in reliability terms to keep into account possible uncertainties. Consequently in this process a new relevance is given to the *Clients/Users*, who pay for the work but must declare their needs, while the *Suppliers/Designers* have the task of offer a technical solution, including the estimated performance. The way of establishing, verifying and validating the performance is the open area of research.

The greater freedom for the designers, now free from many prescriptions, stimulates innovation but is paid in terms of need of a greater knowledge of the phenomena and, broadly speaking, implies an increase of responsibility.

In general, the final agreement between Designers and Users, established in the draft of the *Design Specification*, are a "mix" of prescriptive and performance

statements: more performance-oriented the statements are, and more freedom the designer will have to provide different alternative solutions (Figure 1.1).

A low-level specification has a high prescriptive content, and gives low margins of freedom; for high-level of performance specification the designers' freedom grows but it is more difficult to establish universal criteria of evaluations.
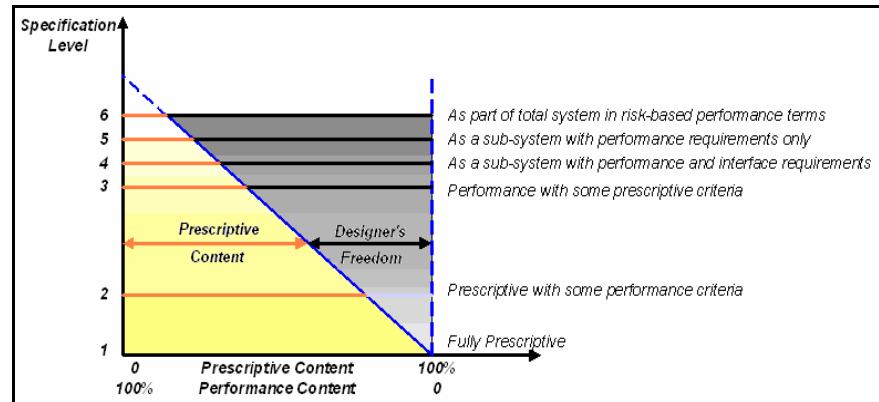
Figure 1.1. Prescriptive vs Performance Based Approach (Bontempi, 2003).

If a product is considered as a matrix of components - *Parts* - and *Attributes*, the main difference between the traditional prescriptive approach and the performance oriented one can be summarized as in Figure 1.2:

- following the prescriptive approach the components of the product are specified with an adequate level of description, leading to a product with certain attributes;
- following the performance approach only the requirements and the performance to be satisfied are fixed, and the absolute freedom to get them in different ways is left, with different combinations of constructive components (*Parts*). This focus on the performance to be guaranteed extend the fields of the constructive technologies and areas of research.
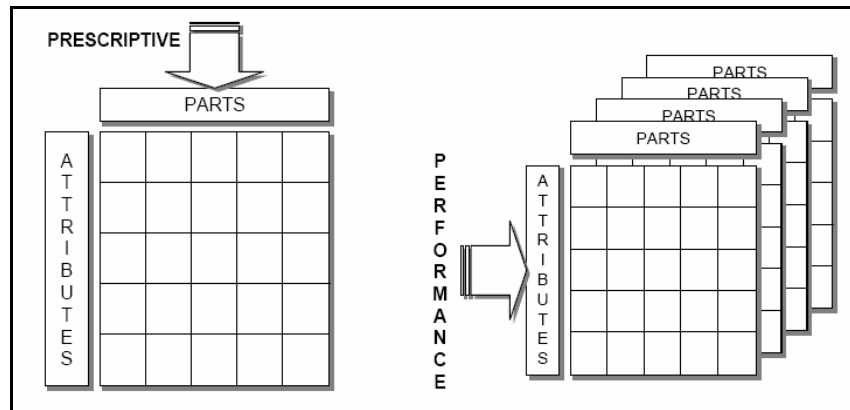
Figure 1.2. Prescriptive vs Performance approach: Attribute Specifications and Parts (Foliente, 2000).

The Performance Approach, as it applies to building, is not new; it can be traced back thousands of years. King Hammurabi of Babylon, who reigned from BC 1955 to 1913, is credited for the first recorded building regulation. The Article 229 of the Hammurabi Code states: "*The builder has built a house for a man and his work is not strong and if the house he has built falls in and kills a householder, that builder shall be slain*". King Hammurabi provided a performance statement, addressing structural safety entirely in terms of user requirements, did not state how to construct the building, and did not refer to building structure or building materials.

The modern development of Performance-based and objective-based codes starts in the seventies with the "Nordic Model" (NKB 1978): this model contains one of the key characteristics of the Performance approach, the dialog and the negotiation between the WHY + WHAT and the HOW, shown in the summary diagram of Figure 1.3.

The goals and the user needs (WHY) are expressed by explicit functional statements and performance requirements (WHAT), and transformed in acceptable solutions (HOW) by the suppliers, who must demonstrate their technical validity.

13
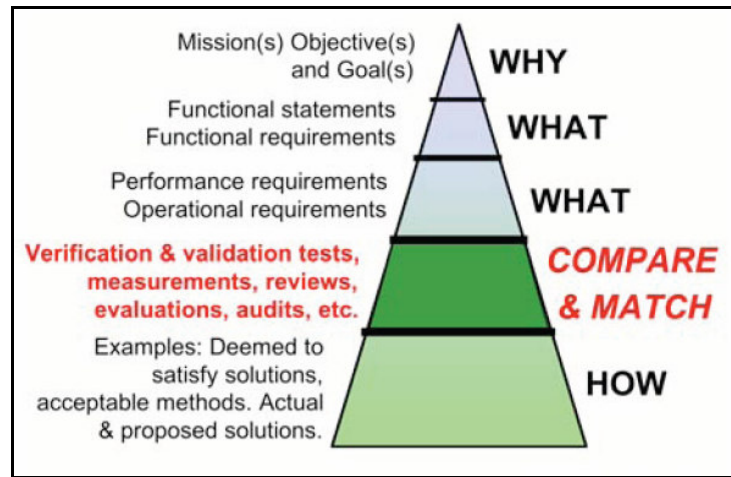
Figure 1.3. The Nordic Model Approach for Design (Szigeti & Davis, 2005).

This new relationship between Client and Supplier, requires (Figure 1.4):
- the use of two languages, one proper of the demander and one proper of the provider. The dialog is possible through a systematic decomposition of the object performed by the supplier, and the creation of a set of explicit and coherent performance requirements by the users;
- the need of validating and verifying the satisfaction of the Users' requests and the target performance, and of comparing alternative solutions: it happens through measures, computation, tests and a feedback interrelationship in the spirit of negotiation and collegial choice.

1.3 Statement of Users' Needs and Requirements

In the Performance-based Design, the Users' need and the functional requirements must be explicitly declared at the project initiation and definition stages. The Clients must have the opportunity to measure and evaluate the satisfaction of these performance by the Suppliers' solutions through

established validation procedures which can be also included in the tender Specifications.
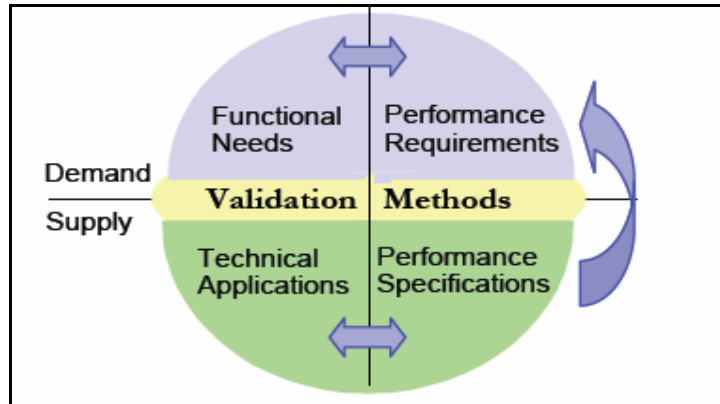
Figure 1.4. Translation and validation (PeBBu Final Report, 2005).

The targets and their hierarchy must be stated in a precise, unambiguous, measurable way, in form of attributes of the product, in order to define univocal criteria of choice for the alternative design solutions (Figure 1.5).
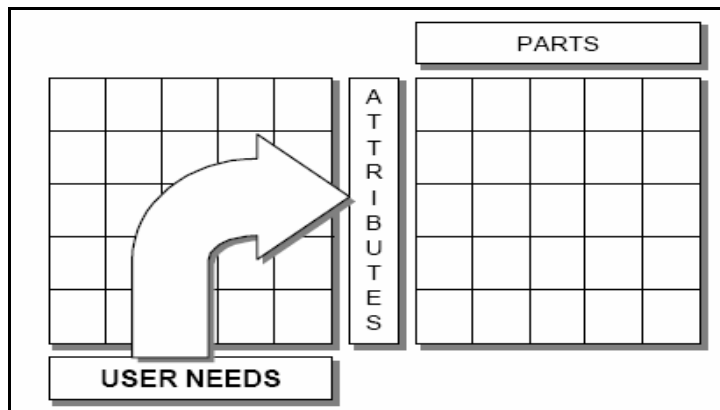
Figure 1.5. Performance-based Design: Users' request and Specifications (Foliente, 2000).

15

The quantification of the expected performance levels must consider possible incomplete knowledge and require also the application of probabilistic methods, concerning the possible environmental interactions, the material uncertainties, the human factors. For innovative design this phase results particularly critical: there is generally a lack of information, and the judgement of experts already involved in similar works is desirable or even necessary.

Furthermore the definition of the performance requirements is generally done in the early stages of the design, when there is a lack of quality information for the process control. In this stage there is a lot of flexibility for process control. As the design-build process progresses, this flexibility decreases while more and more refined information become available (Figure 1.6).
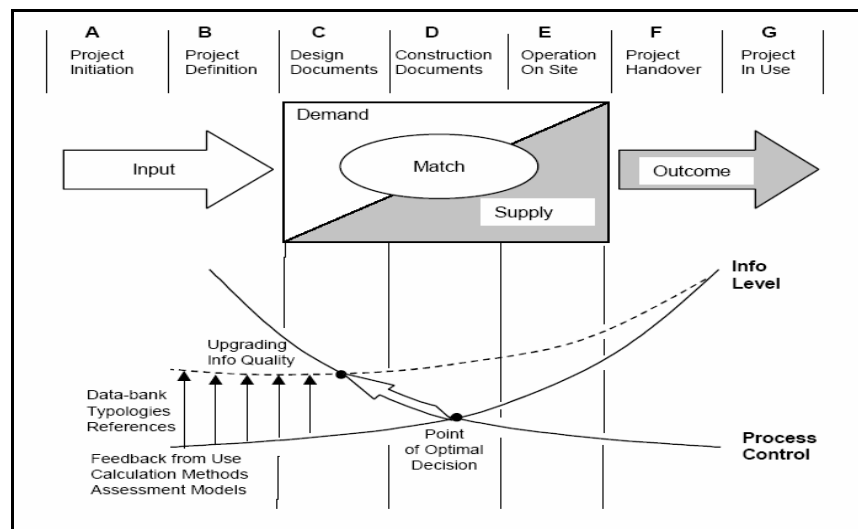
Figure 1.6. Application of the Performance Approach in the Design Process (Ang and Wyatt, 1998).

The collection and management of the information is an important tool to optimize the performance levels of the product: a possible strategy consists of

setting a database (*data-bank*) of information of similar products already realized and in service, of which also mathematical models are available.

Such aspects emphasise the role of monitoring and model updating in the design and in the constructive process: a dynamic project management during the construction allows an increase of the product performance, as it will be exemplified in Chapter 5.

1.3.1 Performance Decomposition and *Dependability*

The design and the construction of the object must be developed in such a way to get an optimum level of *Dependability*.

The term is used to describe the availability of performance and its influencing factors: reliability, performance, maintainability performance and maintenance support performance. Dependability is generally used for general descriptions in non-quantitative terms and it is a time-related aspect of quality.

It can be considered, as a whole, by the complex of performance (*Attributes*) and its influencing factors (*Threats*) (Figure 1.7).
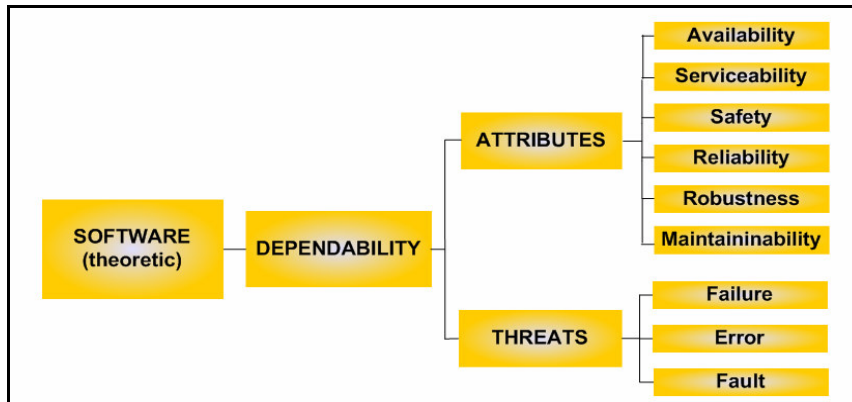
Figure 1.7. Scheme of Performance Decomposition of a Structural System (Bontempi, Gkoumas, Arangio, 2005).

The *Attributes* include the characteristics of the product as required by the Client. In particular the following performance (each corresponding to minimum levels expected, and with different hierarchic relevance in the decision process):

- *Availability*, which is the degree of effectiveness for the users;
- *Serviceability*, which is the degree of functionality performance of the system;
- *Safety*, which represent absence or tolerable levels of danger for humane life and environment;
- *Reliability*, which represents the ability of the system to perform Safety and Serviceability during time;
- *Robustness*, which is the capability of not being damaged by accidental loads, like fire, explosions, airplane impact or consequences of human error, to an extent disproportionate with the severity of the triggering event;
- *Maintainability*, which is the ease and the speed by which any activity related to the preservation and upgrade of the structure can be carried out on the system or its parts.

Each of the attribute defined for the product finds expression in a list of specific demands of expected performance.

The *Threats* for a system can be classified as:

- *Failure*, which is the system deviance from compliance with the system specifications for a specified period of time;
- *Errors*, which is an incorrect state of the system: it may be or may not be a possible cause of failure for the system;
- *Fault*, which is a defect and represents a potential cause of error, active or dormant: it can be due to natural causes (environment, materials, etc.) or to human-made causes (accidental or deliberated).

Concerning structures, the Attributes and the requirements are motivated by the following main aspects:

- the *Structural Serviceability*: Availability, Functionality, Comfort.
- the *Structural Safety*: Resistance, Stability, Rigidity, Ductility;
- the *Structural Robustness*;
- the *Durability*.

Structural Serviceability can be defined as the ability of the structure to satisfy the functional requests during the service life.

Structural Safety can be defined as the ability of the structure to guarantee the resistance requirements.

Structural Robustness can be defined as the ability of a structure to absorb proportional damage for exceptional and accidental cause (impact, fire, explosion).

Durability can be defined as the ability of the structure to keep correctly in the time the previously seen qualities, if an opportune maintenance plane is provided.

The confidence on the fulfilment of these requirements must be supported by analytical results, obtained by reliable numerical models representing the behaviour of the structure *as designed* with an adequate degree of accuracy.

The computed performance offered by the structure are compared within *Limit States* corresponding on:

- *Service Limit States (SLE)* for Serviceability;
- *Ultimate Limit States (SLU)* for Safety;
- *Structural Integrity Limit States (SLIS)* for Robustness.

Limit States correspond to conditions beyond which the defined tasks are not satisfied.

1.4 Complex Systems and Systemic Approach for

Design

Structures can be defined as unitary entities conceived as on organized and positioned constitutive elements in space in which the character of the whole depends on the interrelationship between the parts and dominates it. The traditional approaches of design, which evaluate the response from a set of input

data, is a trivial but effective approach in the case of simple structures, as experienced for many years.

Nowadays the need of more hazardous and challenging infrastructures make the simple structural conception inadequate to describe the nature of innovative structure.

In fact for complex structures, and more for complex structural systems, the traditional approaches for design, construction, maintenance are not adequate, and must be integrated by the tools of the System Engineering and of the Knowledge-Management Sciences.

The term "complex" introduces into the object of the present investigation the existence of a set of parts, strictly connected but intrinsically distinct, whose mutual relationship gives to the whole object a behaviour which is not referable to a simple and regular scheme. For example, a complex structural behaviour is that resulting from:

- mechanical uncertainties;
- mechanical nonlinearities;
- interaction mechanisms.

Moreover, the passage from a "structure" to a "system" implies the existence of a set of interrelated components which interact with one another in an organized fashion towards a common purpose (NASA SE Handbook, 1995).

For complex structural systems the Systemic approach, directly adapted from the System Engineering, is the most effective way to conduct the design and the related operative phases, keeping simultaneously into account the unitary nature of the whole and the multiple interrelationships between the parts, which allows an optimal implementation and integration of the components.

For the previous considerations, the design of complex structural systems the Performance-based Systemic Approach is the overall framework to organize efficiently and effectively all the aspects and details of the synthesis problem.

The Performance-oriented Approach to the design of a complex and innovative structural system requires an assessment of the performance capabilities, basic for its feasibility, its availability and its level of satisfaction of the Users' needs,

and so its technical and economic value. In this case, for the design of a complex structural system, the design difficulties are related to:

- the multitude, complexity, uncertainty and interrelation of the variables;
- systemic arrangement;
- the consequent difficult acquisition of the system performance and capabilities.

The systemic approach allows a methodological simplification of the problem. After the identification of the *design variables* (subdivided into locked data, free variables, environmental data and external inputs) and of the complexities that affect the problem (nonlinearities, interactions and uncertainties), the Performance-based Design, and the exploration of the capabilities of the system, can be conducted through a series of simplifications (*decompositions*) of the problem. In this way an organic description, modelling, and analysis reduces the performance problem in a sum of easier problems. Inside each decomposition, the simplification is formalized through a *hierarchical layering*, as a general tool for the representation of the structural *multilevel* complexity.

1.4.1 **Structural Decomposition and** *Multilevel Layering*

The identification of the Performance Functions can be complicate also for possible *size effects*: some global performance depend on micro-scale behaviour and vice-versa. At this regard large sized structures, with many components interrelated, can be decomposed and organized at different levels by components that can be generally named as *substructures*; they are subjected to actions at different levels (intensities) and they shall satisfy performance requirements both at the global and at the local scales.

The structural decomposition organizes all the components of the systems (*substructures*), with their logical relationship and hierarchical role in the system architecture.

This representation takes advantage of a distinction, inside the system, between two or more levels, from global (*Macro-level*) to local (*Micro-level*) one, logically separated for the modelling but physically and organically

interconnected, resulting any global response as the integration of all the local aspects (Table 1.1, Figure 1.8). It is to note that the structural decomposition includes also the complex of physical and technical equipment for *monitoring*, data transmission and elaboration from the design to the service life, interconnected with *software* tools for data-collecting, model updating and increasing the system knowledge in a recursive way.

Macro-level	**Principal, Secondary, Auxiliary Macro-systems**
Meso-level	**Structures and Substructures**
Micro-level	**Structural Elements**

Table 1.1. Decomposition of the structural system.
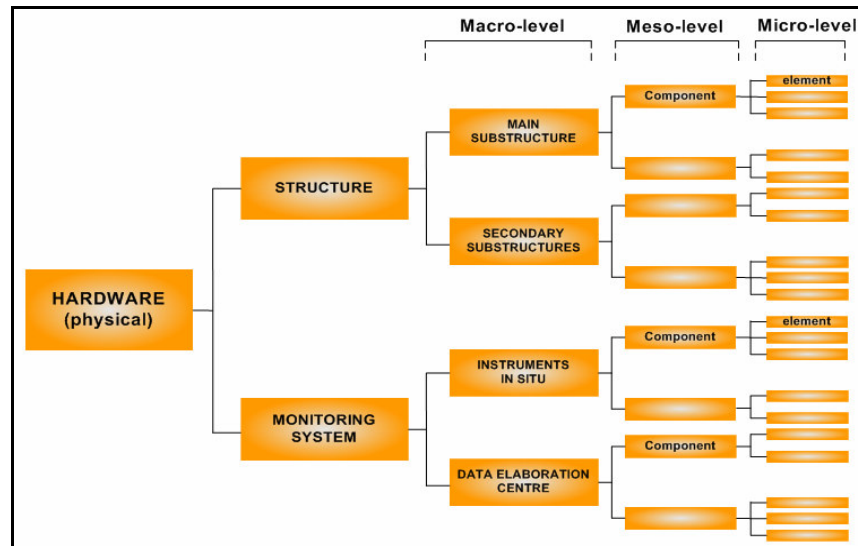
Figure 1.8. Scheme of the Performance decomposition of a structural system (Bontempi, Gkoumas, Arangio, 2005).

Each level of description corresponds to performance that must be evaluated by proper models. So, the *Macro-level* performance that depend only on all-

embracing factors, are evaluated by functions F_i (models) which depend only on wide-ranging variables: the global models cannot represent the local aspects but just the integral response of all the interconnected substructures.

On the contrary, the *Micro-level* performance that depend only on small level factors are evaluated by functions F_i (models) that depend only on minute variables: the local models represent what happens in a small portion of the system, that in general does not affect directly the global response.

Furthermore, it is possible that some *Macro-level* variables have a heavy impact on *Micro-level* performance: so the generic performance P_i is identified by a more complicated function F_i (i.e. model) that depends both on *Meso-level* and *Macro-level* variables: the "*interface*" models can represent at the same time the global response with focus on local and critical behaviours.

In conclusion, for each performance P_i a function or a mathematical model can be defined, keeping into account the relationship and the relevant factors, at different levels of description: this multilevel vision of the modelling is synthesized with the name of *layering*, as idealized in Figure 1.10.

These multilevel vision of the system architecture in the modelling stages, for the evaluation of performance and capabilities, can be practiced, in a finite element method for evaluation, through a Guyan-type substructure approach, as referred in Appendix A.

1.5 Quantified Performance Criteria and Design

The satisfaction of the user requirements, transferred to Attributes for the structure, must verified through performance criteria and analytical/numerical tools.

A *Performance Criterion* is an explicit statement of the features that a product must have to satisfy a certain performance (i.e. structural safety, fire resistance, thermal comfort, etc.).
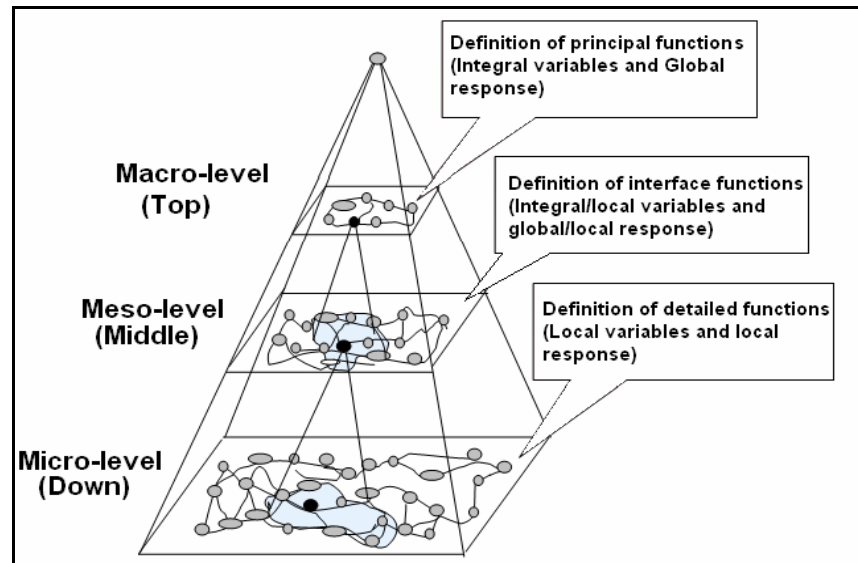
Figure 1.10. Recursive Modelling: hierarchical layering (Bontempi, 2003).

When the Performance Criterion is expressed in quantitative form, a mathematical relation is written, relating the Performance and all the parameters that play a significant role.

These statements can be deterministic (*Technology-Based Performance criteria*) or expressed in a probabilistic context (*Risk-Based Performance criteria*), and in general involve:

-   the mechanical behaviour: nonlinearities, uncertainties, size effects;
-   the expected performance: large amount and different scales of description;
-   the influent factors: environment, actions, interactions effects and linked uncertainties;
-   the external requirements and prescriptions: locked data;
-   the innovative nature of the design and the possible suspicions;
-   the arbitrary ranking of the performance.

The degree of the satisfaction of the performance requirements is quantified through Evaluation Methods, which state a set of equations as

$$\underline{P} = \underline{F}\left(\underline{x}_f, \overline{\underline{x}}_l, \underline{x}_r; \overline{\underline{E}}\right); \qquad P_i \geq \overline{P}_i \ \forall i$$

where

$\underline{P} = \left[P_1, P_2, \dots P_i, \dots P_n\right]^T$ is the vector of the performance established to be guaranteed;

$\underline{x}_f$ is the vector of the free variables of design;

$\overline{\underline{x}}_l$ is the vector of the locked variables of design (established);

$\underline{x}_r$ is the vector of the variables that vary within a defined interval: $x_{rj} \in \left[a_j, b_j\right]$;

$\overline{\underline{E}}$ represents the design environment;

$\overline{P}_i$ represents the minimum expected value for the i-th performance.

The vector of the Performance Functions $\underline{F} = \left[F_1, F_2, \dots F_i, \dots F_n\right]^T$ gathers accurately the functions that relate the performance of the system to the design variables.

Possible solutions of the problem (Suppliers' solutions) are all the combinations of the design variables satisfying the stated equations.

The aspect remarking the difference between the Performance-based Approach and the traditional prescriptive one is that if the problem has no solutions, some release can be made for some range of the variables or in the expected performance (*negotiation*) to gain a possible solution. This negotiation process is identified, ordered and clarified to all the Stakeholders. When more than one solution is possible, since each performance identifies different optimal combinations of the design variables, an arbitrary (in some sense) establishment of hierarchies of the performance induces the final choice. This is the deep essence of design: a decision process, essentially rationally based but intrinsically and inescapably subjective, sometimes addressed as heuristically based.

25

1.6 Experimental Evaluation Methods

Once decomposed the structural system the performance to be satisfied and their levels, it is necessary to discover their logical link, and to state acceptable methods of measuring or calculating them.

Coming back to the performance notation of Par.1.5, the identification of Evaluating Methods correspond to that of the Performance Functions F_i for the research of optimal combinations of the design variables.

Analytical treatments of the problem for complex structures are surely prohibitive while the exploration of the performance capability in the multidimensional space of the design variables (*Experimental Design*) is more accessible, especially when it is possible to know in advance which are the most significant ones, for each performance. In this approach, the performance functions F_i can be substituted by mathematical models (i.e. Finite Element Models) built *ad hoc.*, and the evaluations conducted through deterministic/probabilistic (Monte Carlo Simulations) analyses.

The exploration starts from the *sensitivity analysis* of the response around admitted combinations of the design variables: this step allows the identification of *stiff* (insensitive) and *soft* (sensitive) performance with respect to certain design variables. *Stiff* performance with respect to most of the design variables are robust and reliable but can be subjected to small improvements if no changes are made in the boundaries of the problem; on the contrary, *soft* performance can be improved by optimal design but can be affected by heavier uncertainties (Figure 1.11).

The framework of the experimental design for the evaluation of the sensitivity, the exploration of the performance and of their robustness is summarized in the scheme of Figure 1.12, where it is assumed that a certain performance P_i depends only on two design parameters x_1, x_2. Here one can consider in sequence:

a) the <u>sensitivity of the model</u>, with the classification of stiff and soft behavior as defined previously, represented by the gradients $\partial p / \partial x_i$;

b) the <u>parametric exploration of the response</u> where one considers, for example, more levels of the design parameter x_1, (i.e. which can be labeled as *low*, *normal* and *high*) and explores the performance if the other variable is fixed: $U\left(x_1, \bar{x}_2\right)$;

c) the <u>definition of a set of suitable levels</u> of the design variables to develop a combinatory exploration of the response;

d) the <u>reliability definition of the response</u>, based on a statistic treatment of the various experiments. At this regard an attractive tool is represented by the probabilistic-experimental methods such as the Monte Carlo simulations.

This framework represent the approach followed in the applicative part of Chapter 2 for the evaluation of the serviceability performance of the long span suspension bridge of Appendix B, and, more extensively, in Chapter 5, for the Performance-based design of a passive MTMD control system for the pylon of the same structural system.
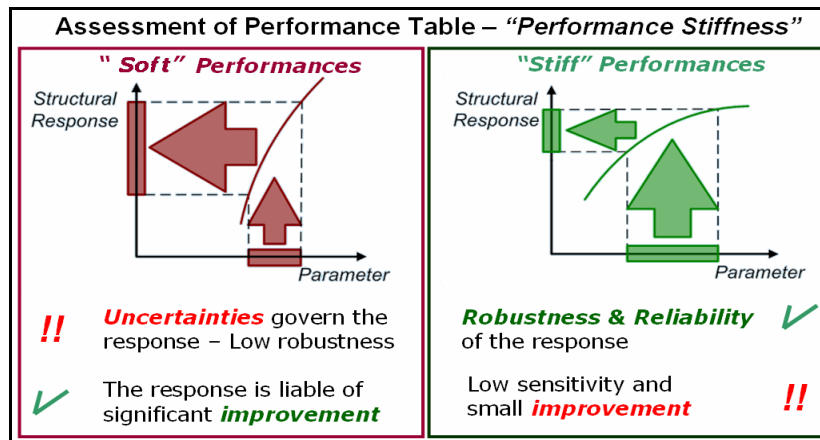
Figure 1.11. Robustness of performance and reliability of the response (Bontempi & Giuliano, 2005).
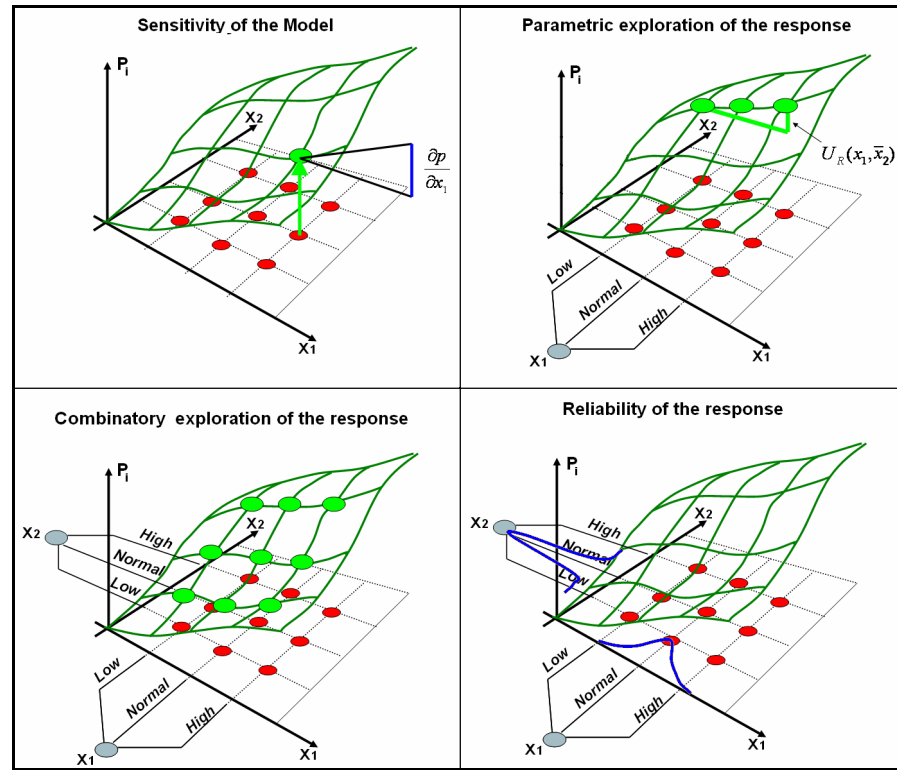
Figure 1.12. Experimental Design (Bontempi & Giuliano, 2005).

Chapter 2

P.B.D. AND LONG SPAN SUSPENSION BRIDGES

- Suspension Bridges: State of Art and Complexity
- The Performance-Systemic Approach for the Design of Suspension Bridges
  - Structural Decomposition – Multilevel Modelling
  - Performance Decomposition – Multilevel Specifications
  - Experimental Design: Exploration of the Serviceability Response
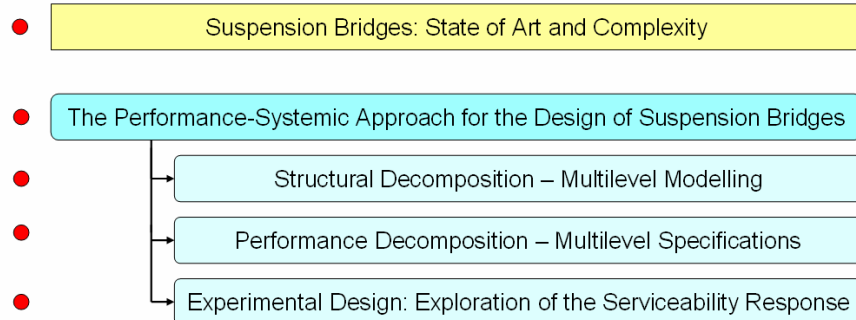
Abstract

In this Chapter the Systemic-Performance-based Approach outlined in Chapter 1 is transferred to the case of long span suspension bridges.

The innovative nature of long span suspension bridge suggests also a Performance oriented Approach for the Design: the structure is designed to guarantee minimum levels of the expected performance, but its Dependability features are adapted to the structural capabilities.

The mechanical complexity of the structure, inserted also in a complex environment, suggests the adoption of the Systemic Approach, which organizes the structural system and its performance in multi-level arrangements, according to the multi-scale impact of actions and response, and to the interrelationships between the different scales of description. It is realized through the multi-level modelling (*layering*) of the substructures, while the satisfaction of the requested performance is verified through finite element models and experimental analyses, simulating likely load scenarios and critical scenarios of contingency.

3.1 Suspension Bridges: State of Art and Complexity

Cable-supported bridges are a structural typology conceived to overcome large span. The first cable-supported bridges were built around the mid of the XIX century in Great Britain and in the United States of America. Since that time a large amount of cable-supported bridges have been realized in all the world, with also a progressive increase of the maximum span length covered.

All the cable-supported bridges have a principal structural system divided into four main parts:

- the cable system;
- the pylons (or towers);
- the anchor blocks;
- the girder and the supported deck.

These bridges are also distinguished into two main families according to the configuration of the cable system:

- the *suspension bridges*, whose cable system is composed by a couple of parabolic main cables and a system of hangers connecting the main cables and the stiffening girder;
- the *cable-stayed bridges*, which have straight cables connecting girders and pylons, with harp/fan configuration.

Between these two families combined solutions are feasible, while different configurations and typologies are also possible for pylons, girder, suspension system, giving different features in terms of geometry, covered spans, traffic functionality, deck composition and also aerodynamic/aeroelastic properties.

For high spans, it is well-known that the suspension typology is the most efficient: actually the current maximum span covered is that of the Akashi Kaikyo Bridge, a 1990 m long suspension bridge, completed in Japan in 1998 to link the islands of Honshu and Shikoku (Figure 2.1).
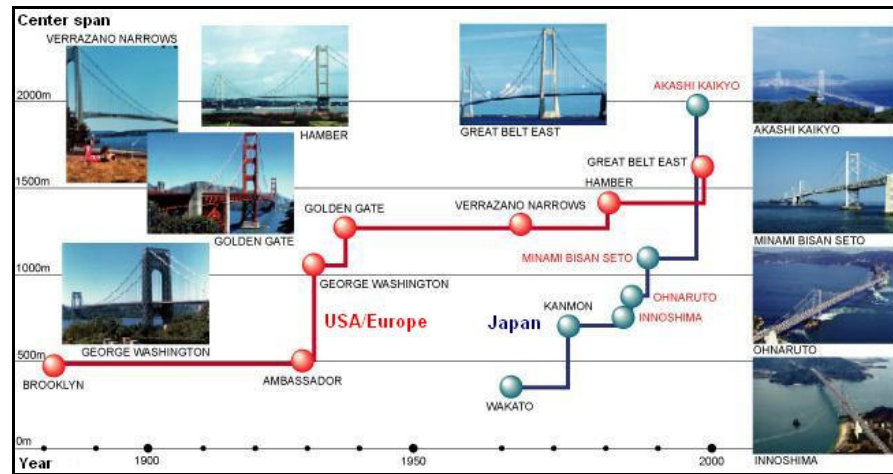
Figure 2.1. Evolution of suspension bridge span in USA/Europe and Japan (http://www.jb-honshi.co.jp/english/technologies/progress.html).

The design of this kind of structures, for the intrinsic structural conception and their insertion in a natural environment, requires that a large amount of complexities are simultaneously considered:

- *structural complexities*: mechanical arrangement and composition of substructures, nonlinearities for geometry (i.e. cable system) or for material (i.e. the mechanical devices, soil, etc.);
- *loading complexities*: from environment (wind, earthquake, temperature, chemical agents) or from the human use (i.e. traffic actions);
- *interaction mechanisms*, i.e. soil-structure interaction, wind-structure interaction (vortex-shedding, buffeting, galloping, flutter), traffic-structure interaction, interaction between deck, towers and suspension system, etc.;
- *performance complexities*: serviceability, safety, robustness, durability can be identified as the main performance to be guaranteed. The performance and the allowable levels are also time-varying, defining

32

different expected levels during the whole bridge life, from the erection to the service time.

All these complexities must be kept into account in the design stages and in the operative life, also by the mean of continuous or discrete monitoring activities, leading to a technically optimal and cost-effective decision process.

3.2 The Performance-Systemic Approach for the Design of Suspension Bridges

The Performance-Systemic Approach, the multilevel modeling and the experimental exploration of the structural capabilities can be the guidelines for the assessment of the structural performance, the optimization of the design of complex and innovative structures such as long span suspension bridges.

The performance approach for the structural design is based on the verification of the exact suitability of the structure with respect to fixed requisites connected to serviceability and safety (Figure 2.2).
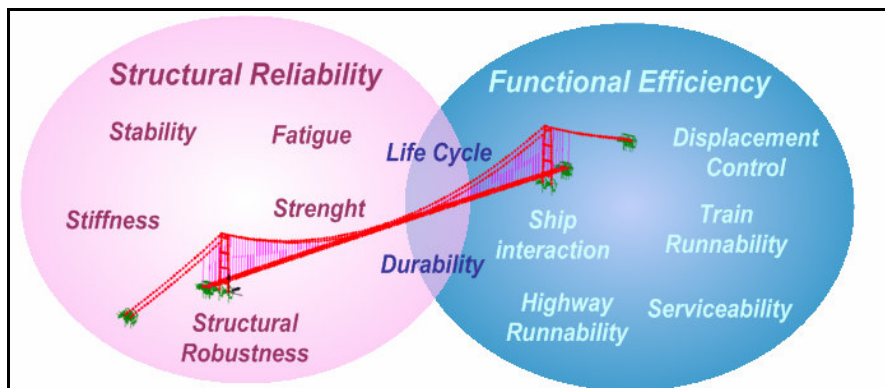
Figure 2.2. Expected performance of a suspension bridge (Bontempi & Silvestri, 2003).

The process starts from the knowledge of structural and geometric variables already stated, such as the geometry, the structural typology, the composition of deck and the users, the geographic coordinates of main points, the span length, the pylon height, etc., declared as not modifiable (*locked variables*).

The evolution of the Project and possible limitations imposed by the National Authorities can restrict the domain of the design variables, so that the Designers can progressively move with almost total freedom just in the space of the secondary design variables, while several restraints are imposed on the primary ones, and others are absolutely locked. The restrictions on some primary variables (as the height of the pylons) have an important impact on some kinematical performance, distinctively relevant for serviceability.

The assessment of the performance of the bridge consists of the identification of the sensitive variables for each of them, through mathematical models which keep into account all the structural criticities and complexities and give robust and reliable numerical results.

The solution of the Performance Problem needs the exploration of the mechanical properties of the bridge and the identification of hierarchies of dependence between actions and structural responses.

The Methodology to obtain such information can take advantage of:
- structural decomposition and multi-level modelling (*layering*);
- performance decomposition;
- experimental approach for the numerical exploration.

In the perspective of the *Performance Based Design*, possible unsatisfied performance standard produce a change in the design or reduce the expected serviceability (*availability*), while satisfied performance can allow further optimization and update the design under the suggestions of Experts and the experiences of other bridges. The structural properties of the bridge drive the levels of the actions (traffic loads, wind speed) beyond which the serviceability performance is not satisfied: in this sense, it is important to recognize that in a Performance-based Design of a long span bridge, the actions (i.e. traffic loads) are not a standard input for the analysis and the judgment, but a design variable,

calibrated on the properties of such a flexible superstructure, and on the unavoidable requirements of safety and serviceability of users. This criterion imposes that the bridge operability is judged in expected scenarios *(contingency scenarios)*, likely to happen during the service life.

2.2.1 Structural Decomposition of the Bridge and Multi-level Modelling

According to the Systemic Methodology outlined in the Chapter 1, the object of the study – a long span suspension bridge – is decomposed in all its physical parts (*substructures*).

The structural complexity, the multitude of the design variables, their interrelationship to form a multi-level well-organized system, with multilevel distribution of performance induce to decompose the bridge in *Macro/Meso/Micro-levels* of description, as described in Figure 2.3.

The decomposition is useful and necessary to identify, with regards to the failure eventualities, a structural hierarchy, with ordered sequences of elements, in accordance with their structural role and criticity in the global robustness of the bridge.

The structural elements can be also distinguished on the basis of their reparability and maintenance features. In this way, all of them can be classified as primary or secondary elements:

-   primary elements are considered critical and not repairable or repairable only with a long out of service for the bridge (foundations, anchorages, pylons, main cables, hangers system (globally), transverse girders);
-   secondary elements are those repairable, subjected to ordinary maintenance program without or with very short out of service for the bridge (single hangers, girders, expansion joints, devices, secondary and auxiliary systems).

An opportune evaluation of the loss of safety and serviceability after a failure of each element is necessary to classify it and to determine the robustness of the global performance.
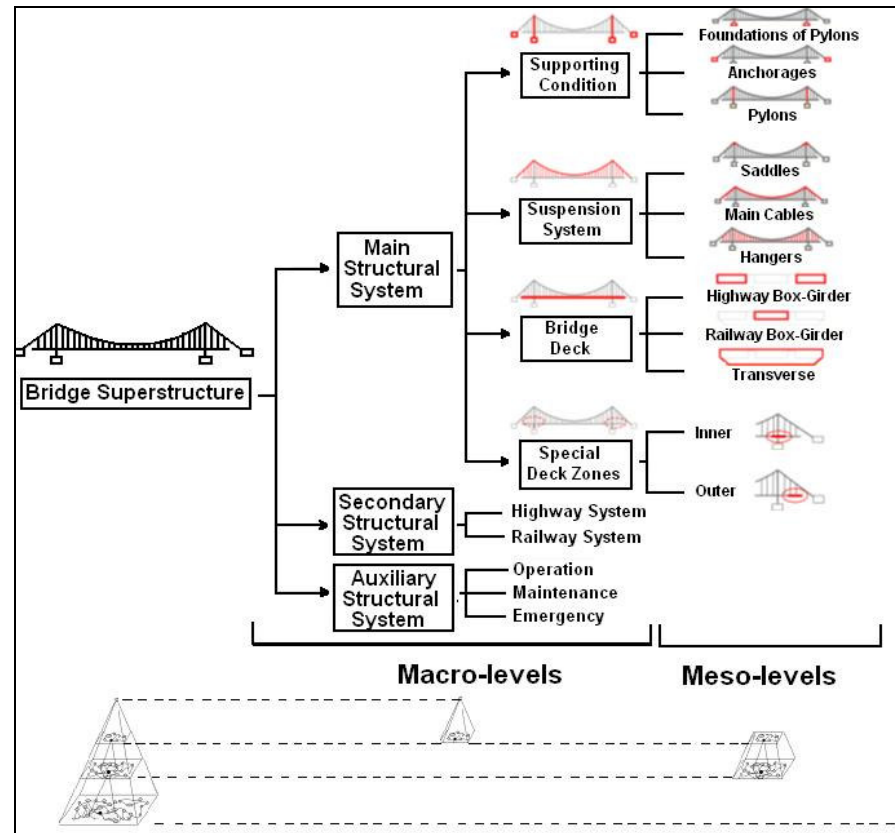
Figure 2.3. Structural Decomposition of the bridge (Bontempi & Giuliano, 2005).

The multilevel organization of the structure, has a dual correspondence in the multilevel organization of the performance: *Macro-level* (global) actions can have impact on *Micro-level* performance, while *Micro-level* details (i.e. control devices, aerodynamic flaps, etc.) can change the global response.

This hierarchic organization of the structural system creates an exchange of information and mechanical relationship from a scale of description to another, and determine the need of a multi-level (layered) mathematical modelling.

In general *global models* are used to describe the relationship between global response and global variables (actions or design parameters): the description of the structure in the *Macro-level* scale gives response in terms of macroscopic effects using a reasonable but limited number of elements, where each one represents a synthesis of all its component substructures. This is an usual strategy in structural analysis: for instance, the beam element used to represent a girder is the synthesis of the behaviour of a more complicated steel structure inside.

Moving towards *Micro-level* size (*Top-Down Path*), it is possible to use more refined finite element typology and models to assess the performance of a smaller scale of description but strictly dependent on the global response of the structure. The performance computed using global descriptions in general must be considered an approximation of those obtained by refined models (local models), which have a larger amount of degrees of freedom.

With reference to Figure 2.4, the layout of this multilevel vision is formalized for a suspension bridge as follows:

- the first level of the layering (*Top*) catches the global performance using three-dimensional frame models;
- the second level of the layering (*Middle*) catches the *Meso-level* performance by refined interface models realized through the *sub-structuring* technique: two- and three-dimensional elements are combined with the frame types. The *interface regions* between solid/shell elements introduce diffusive regions with complex stress and strain response, in general with a smaller degree of reliability but which extinguishes with the distance;
- the third level of the layering (*Down*) pertains to the investigation on detail effects such as stress peaks, relevant also for fatigue effects, the crack propagation along the engraving. It requires accurate modelling of geometry, material properties and loads for the incremental stress,

37

counting method (i.e. rainflow method) and damage laws (i.e. SN curves).
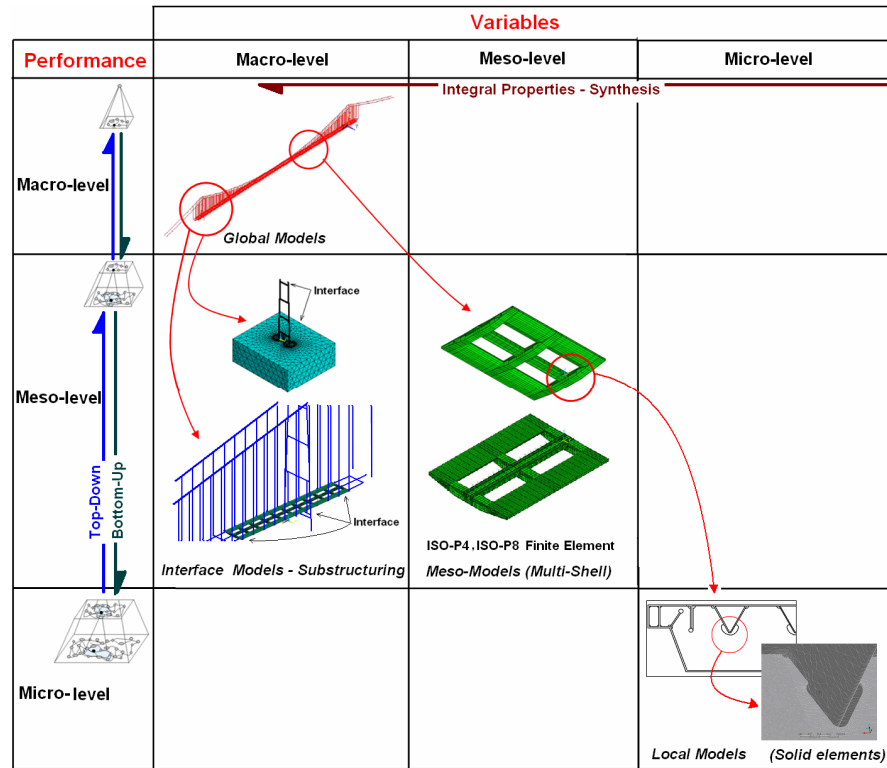
Figure 2.4. Multilevel modelling for the bridge performance assessment (Bontempi & Giuliano, 2005).

The global *3D* frame models are used for analyses of safety and serviceability for traffic and environmental load scenarios at *Macro-level* size: stresses on the main structures (cables, hangers system, and pylons) and the global deformations induced.

The mathematical formulation must admit large displacements but allows small strains for the structure; the analyses can be conducted in the static and dynamic field, in the domain of time, or of the frequency when nonlinear effects are negligible. For preliminary evaluations, simple P-Δ analyses can also be accepted.

The global models are not adequate to evaluate all the performance: specific quantities require substructured numerical models realized *ad hoc*. Among them, the peaks of the horizontal curvatures of the deck under the pylon under transversal wind load, that are a 2nd order derived quantity from the computed displacements:

$$\chi(x) = \frac{1}{r(x)} = \frac{u_x''(x_0)}{\left\{1 + [u_x'(x_0)]^2\right\}^{\frac{3}{2}}}$$

These curvatures can be locally critical for the railway serviceability, because of their congruence with the curvature of the tracks, (Figure 2.5).

They are a Meso-level (local) quantity but related to the Macro-level response; so numerical models that catch the global response and let the evaluation of local aspects in their proper scale are necessary and the only frame models are not adequate for this target. In fact the curvatures are computed from the nodal displacements through a finite difference scheme, where the step Δx must be enough small, and requires a fine mesh of the structure.

In conclusion it is necessary to realize models sensitive to global effects and capable to provide local information: the sub-structured *interface-models*, coupling frame and shell elements are adequate for this purpose (Figure 2.6).

Concerning the kinematical behaviour, the congruence of the deformed configurations of the frame and the sub-structured models validates the local quantities computed, in terms of stresses and strains. Figure 2.7 shows, for example, the comparison of the diagram of the horizontal curvatures for a transversal wind scenario, in the static field, for the global (frame) model and for the substructured one, computed with the same step $\Delta x = 30m$.

39
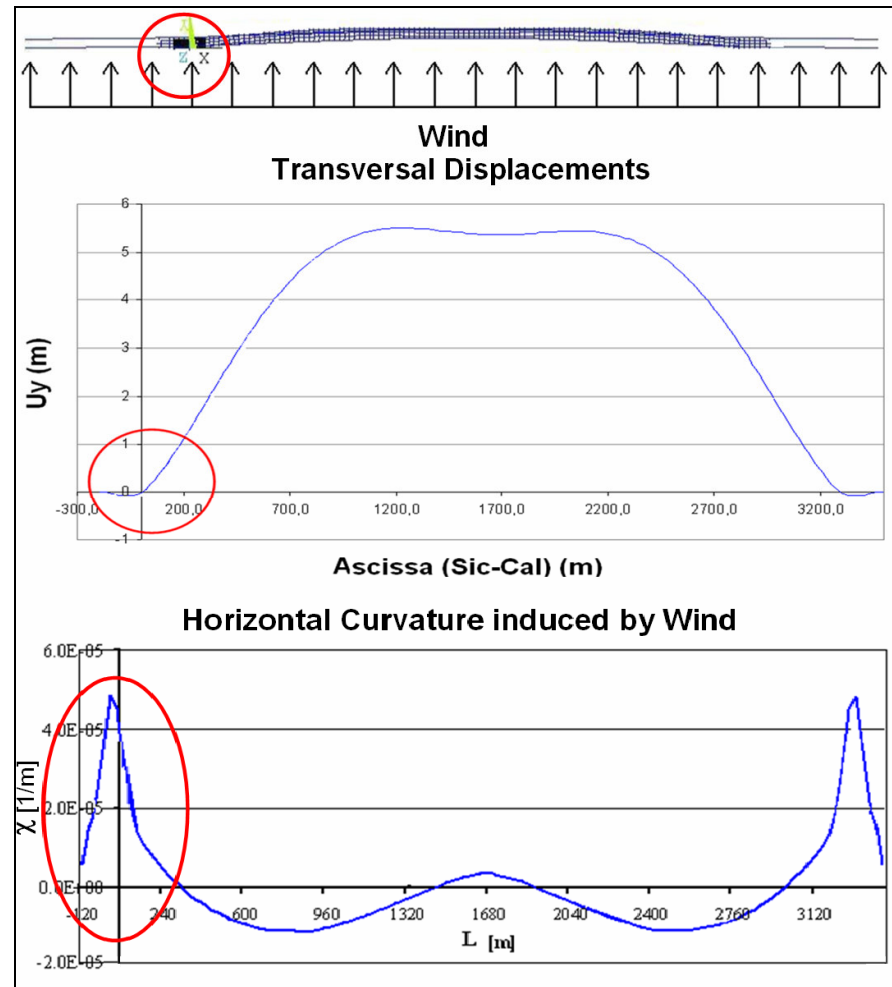
Figure 2.5. Deformed configuration under transversal wind and horizontal curvature of the deck (global models). (Bontempi & Giuliano, 2004).
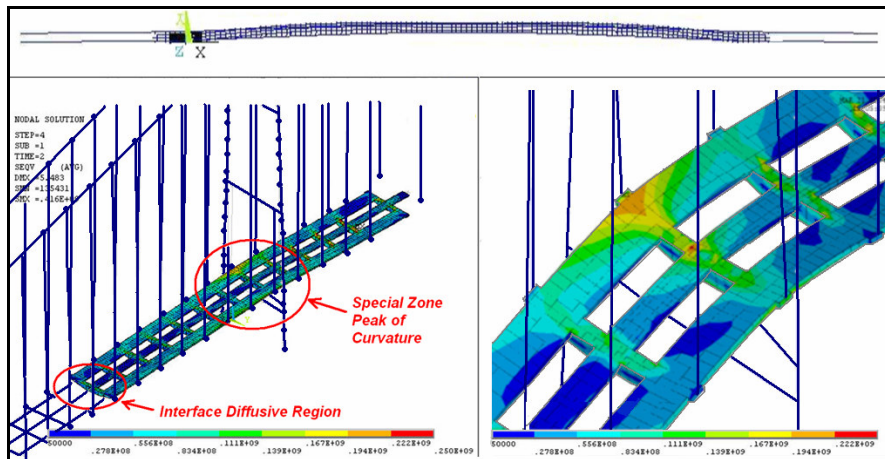
Figure 2.6. Deformed configuration under wind load and stress response of *sub-structured* model (Giuliano, Gkoumas, Petrini, 2005).
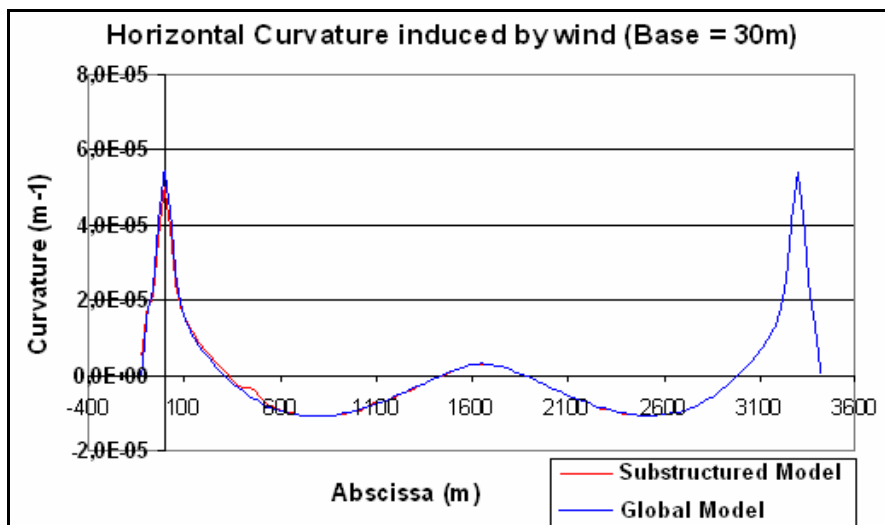
Figure 2.7. Validation of the multilevel modelling: horizontal curvature under transversal wind (Bontempi & Giuliano, 2004).

41

The refinement introduced by the sub-structured model, with its finer mesh, allows the computation of local curvatures in their proper micro-scale, increasing the reliability of the judgment of railway serviceability. Figure 2.8 and 2.9 show the different refinement of punctual information such as the deck transversal displacements and curvatures provided by models with different scale of description (step of computation of curvatures $\Delta x = 30m;\ \Delta x = 2.6m$).

The diagram of the horizontal curvature computed in the micro-scale emphasize the shear deformation of the deck system composed by girders and transverses, congruent with that of the tracks and constituting a base for the evaluation of safety and comfort for the *Users*. Starting from the trajectory imposed by the deformed tracks, coupled with the deck motion computed in the time-domain, train run simulations taking into account the mechanical properties of the subsystem (car body masses, damping and stiffness of suspensions and expected ranges for different train typologies), can assess, for different wind scenarios, the train speeds compatible with the established performance levels.
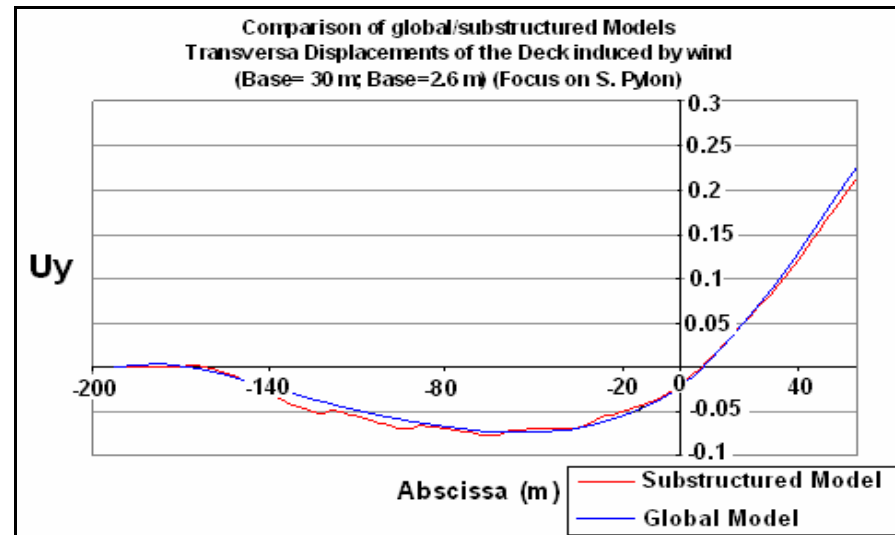
Figure 2.8. Discretization and refinement of the displacements: Global/Substructured model. (Bontempi & Giuliano, 2004).

42
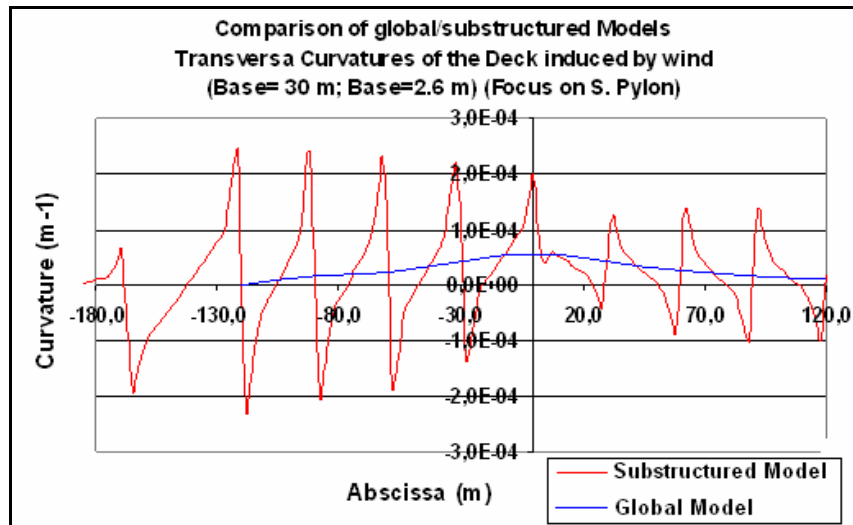
Figure 2.9. Discretization and refinement of the transv. curvatures computed with different bases: Global/Substructured Models.(Bontempi, Giuliano, 2005).

2.2.2 Performance Decomposition and Multilevel Specifications

Concerning the Attributes of Dependability, the main characters which must be contained and specified in detail in the documents (*Design Specifications*) containing the expected performance of a suspension bridge are respectively:

- the Robustness features;
- the Safety features;
- the Serviceability features.

Table 2.I and Figure 2.10 report possible general schemes of the expected performance for the case-study suspension bridge presented in Appendix B.

From a general point of view, for load scenarios with small period of return, serviceability performance, related to the structural deformability, govern the design (*SLS* Limit States); for more severe intensities of the loads, related to higher periods of return, loss of serviceability is gradually admitted and

structural safety, related to strength, governs the design. For rare environmental actions, the structural problem is governed by robustness criteria while absence of serviceability is admitted (*SLIS* Limit States).

Level	Check	Return Period	Safety Performance	Serviceability Performance
1	SLS1	50 years	No Damage Elastic behavior	Complete Serviceability (CF)
	SLS2	200 years		Only Railway Serviceability (FF)
2	SLU	2000 years	• Integrity of the main structural system • Repairable damage only to secondary components	Temporary Out of Service (AF)
3	SLIS	10000 years	Surviving of the main structural system	Out of service (AF)

Table 2.I. Performance decomposition of the bridge.
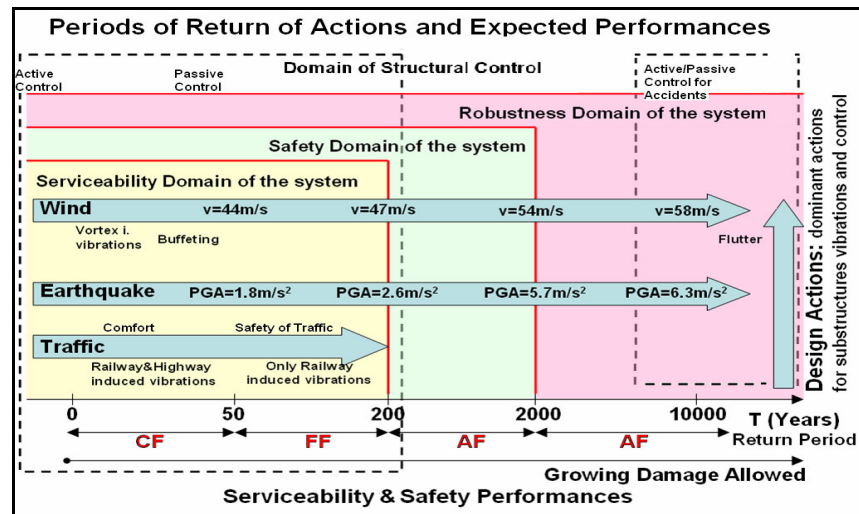
Figure 2.10. Expected domain of performance and control and return periods of actions (Giuliano, 2005).

44

Concerning safety, different levels of damage are defined: each structural element, with its role in the structural decomposition, can be subjected to levels of damage according to their role in the bridge hierarchy, and is consequently designed. The damage scales established for elements go from absolute absence of damage (elastic behaviour, Level 1) to increasing damage levels, with fatigue damage, plastic strain and even collapse (local and limited to secondary elements for the most severe load scenarios, Level 2 and 3).

In the same way, related to serviceability features, more than one level can be fixed, in order to relate full serviceability, reduction (limitations to some vehicular typologies) or absolute no serviceability to periods of return and load scenarios.

The scheme of Figure 2.10 represents also the possible role of structural control for the mitigation of the structural response of the bridge: it can support the serviceability capabilities, while it is considered not reliable to rely on it for the achievement of safety requirements; furthermore, it can support the robustness of the bridge as a redundant resort against extreme accidents.

In the specific case of serviceability performance of a long span suspension bridge, different groups of requirements are identified; their allowable levels are generally established on the basis of other bridge experiences or according to experts' suggestions. Other specific performance levels are obtained by adapting serviceability criteria used for ordinary bridges to a superstructure that experiences significant movements under traffic and environmental loads, with possible dynamic and interaction effects.

The innovative nature of the work and the stochastic nature of many design factors get the confidence on some performance smaller than that of others. So the uncertainties of the response and of the performance should be limited as much as possible from the design to the construction through continuous monitoring activities. Any error and fault should be small enough to be controlled or corrected in real-time, through small rearrangements in the local configurations or by control techniques.

In respect of the safety requirements, the improvement of the serviceability kinematical and dynamic performance is generally a more difficult problem, because most of them depend on global properties which are locked data for the design (i.e. the span, the height of the pylons, the deck composition, the environment), and have generally a *stiff* nature. On the contrary, the nonlinear nature and the intrinsic flexibility of the structure, give high attitude to deformations and vibrations which cannot be improved significantly, and get the serviceability requests more critical, also for the economic value of the work which is related to the *availability*.

The expected levels of serviceability, expressed in general terms in Table 2.I are further decomposed and classified and established according to:

- the requiring users category;
- the Performance criterion (with the allowable values);
- the scale of description (suitable models) for the evaluation.

The evaluation of the achievable performance represents the basis of the decision process because defines its Dependability.

In this context the Performance approach allows a negotiation between client (and users) and suppliers (designers): whenever the bridge cannot guarantee certain serviceability performance, a real-time management unit decides on the operability, adapting its availability to the environmental context.

For example, since it has been demonstrated that the vertical deflection of the bridge exceeds the established limit during the contemporary transit of two heavy trains, such transit will not be allowed when the navigation channel must be clear for the need of the maritime traffic; similarly the availability of the bridge to certain vehicular typologies may be forbidden when the wind speed exceed established levels.

The evaluation of the capabilities of the bridge, requires that the structure is analyzed in likely but severe scenarios: an experimental approach appears to suitable to satisfy this purpose.

Users	Performance (Limit values established)	Structure-Environment System Level	Performance Level	Scale of Description (Suitable Models)
Maritime traffic	Clearance of the established navig. channel	Macro-Level	Macro-Level	*Global Models*
Railway serviceability	Railway longitudinal slope	Macro-Level	Macro-Level	*Global Models*
Railway and Roadway traffic safety	Transversal slope of deck and road	Macro-Level	Macro-Level	*Global Models*
Railway traffic safety	Rate of change of cant of the tracks	Meso-level	Micro-level	*Interface Models*
Railway and Roadway traffic safety and serviceability	Joint displacements	Macro-Level	Macro-Level	*Interface Models*
	Vertical acceleration of the deck	Macro-Level	Micro-level	*Global & Interface Models*
Railway traffic safety and serviceability	Non-compensated acceleration	Meso-Level	Micro-level	*Meso-level Models (Multi-scale)*
	Roll speed	Meso-Level	Micro-level	
	Recoil	Meso-Level	Micro-level	
	Derailment	Meso-Level	Micro-level	
	Overturning	Meso-Level	Micro-level	
Comfort Performance	Comfort Indexes	Meso-Level	Micro-level	

Table 2.II. Performance for Serviceability and Safety of the traffic and suitable models (Giuliano).

2.2.3 Experimental Design: Exploration of the Serviceability Response

Some of the serviceability performance of Table 2.II, and specifically the mean longitudinal/transversal slope of the bridge, are global quantities which depend on the effects of global actions. For their evaluation the 3D frame global models are suitable. Furthermore, even if the actions on the bridges are intrinsically dynamic, some performance can be evaluated with reliable accuracy also through analyses in the static field because of the structural mass and the low dynamic impact of the actions.

In the perspective of delimiting the structural capabilities and of updating the Messina Strait Bridge project, whose structure is better described in Appendix B, *experimental-type* numerical investigations have been conducted coherently with the general framework presented in the previous Paragraphs.

The serviceability performance here presented are:

- *the conventional longitudinal mean slope of the deck*: it is defined as the mean slope of the deck, computed with different length bases, between the head and the end of the trains crossing the bridge. This performance is a specific request of one of the *Clients* of the Project, the National Railway Authority (RFI), because of its particular relevance on the railway *runnability*, and on the demand of power when trains restart their run after a stop on the bridge in the worst possible location;
- *the maximum transversal slope of the deck*: it is related to the torsional stiffness of the bridge. This performance represents a need of two *Clients*: the National Railway Authority (RFI) and the Roadway one (ANAS), which specified two different allowable levels of the maximum longitudinal development of the bridge with transversal slope close to critical values for the safety of railway and roadway traffic, and the maximum development with transversal slope (inclusive of that for water efflux) smaller than critical values for the safety related to the aquaplaning phenomena;

- *the maximum vertical acceleration of the deck*, significant for the availability features of the bridge and for the traffic management;
- *the peaks of horizontal curvature under the pylon*, is significant for the railway *runnability*.

For each performance allowable levels are established as compatible with Complete Functionality (*CF*) (Table 2.III).

Performance	Expected Levels (CF)
Longitudinal mean slope (%)	1.80 % (one train running) 2.00% (two trains running)
Transversal slope (%)	7%
Deck acceleration (m/s^2) (dynamic analyses)	0.70 m/s^2
Peak of horizontal curvature (1/m)	

Table 2.III.   Expected levels of the performance related to Complete Functionality.

Each performance is more sensitive to some actions type than others: the most impacting actions must be identified and their intensity must be chosen in a selected likely range. At this regard, Table 2.IV reports, for each performance of Table 2.III, the actions expected having the highest impact and used for the investigations. Table 2.V and Figure 2.11 represent the intensities of the loads, with likely values for the service life, to explore and delimit the serviceability capabilities of the bridge.

The environmental/traffic loads are organized in geometric schemes, composing critical but likely *load scenarios* for each performance (Figure 2.12).

The combination of loads and scenarios allows the identification of the dependence of Performance on actions and structural arrangements.

Performance	Expected Levels (CF)
Longitudinal mean slope (%)	Intensity of Railway Loads
	Intensity of Roadway Loads
Transversal slope (%)	Intensity of Railway Loads
	Intensity of Roadway Loads
Peak of horizontal curvature (1/m)	Wind speed
	Gap of the transversal control devices
Deck acceleration (m/s^2) (dynamic analyses)	Wind speed
	Train speed
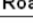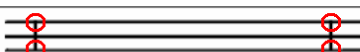
Table 2.IV. Serviceability performance and high impacting loadings.
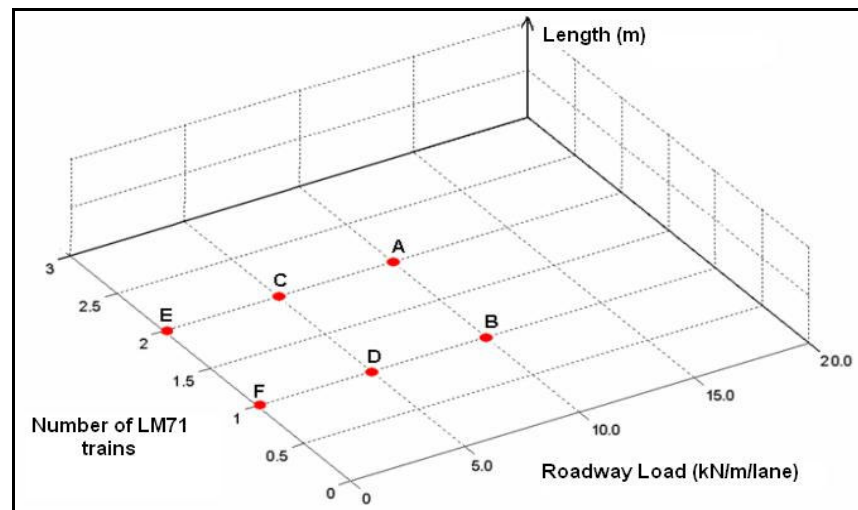
Figure 2.11. Exploration of the serviceability of the bridge: Longitudinal/Transversal slopes – Levels of Traffic actions (Giuliano).

50

Loading	Intensity	
Railway Loads: Number of LM71 trains (Eurocode2)	Low	0
	Medium	1
	High	2
Train speed (constant) (km/h)	Low	0.0
	Medium	40.0
	High	80.0
Intensity of Roadway Loads (KN/m/lane)	Low	0
	Medium	5.0
	High	10.0
Wind mean speed (m/s)	Low	0.0
	Medium	21.0
	High	42.0
Configuration	Intensity	
Free gap of the transversal control devices (cm)	Low	0
	Medium	30
	High	50

Table 2.V. Discrete levels of design loads for the exploration of the response.

Figure 2.12. Serviceability performance and geometric schemes of the Loads (Giuliano).

Figures 2.13, 2.14, 2.15, 2.17 separately contain the experimental histograms that approximate the idealized analytical functions F_i, relating the performance and couples of design variables considered sensitive.

Figure 2.13 represents the mean longitudinal slope under one/two trains, computed using its severe scenario: the requested level associated to the expected traffic scenarios is largely satisfied, while from the gradients of the bars, it appears clear the higher dependence of the slope on the railway loads, because heavier than the roadway ones.

On the contrary Figure 2.14 shows that the rotation of the deck is governed by the roadway traffic, even if significantly lighter than the railway loads. It defines the tolerance of the bridge towards traffic queues.

Figure 2.15 shows the deck acceleration vs wind speed and train speed: it is obtained by dynamic analyses in the time-domain (turbulent wind+crossing train), and shows that for the case-study bridge wind has the most pronounced dynamic impact on the availability and comfort features of the bridge.

Figure 2.17 shows also the impact of the free gap of the transversal devices installed under the pylon (Figure 2.16) on the curvature of the deck in case of

transversal wind, measured by static analyses. It can be tuned to obtain acceptable curvatures paid by greater transversal displacements of the deck.
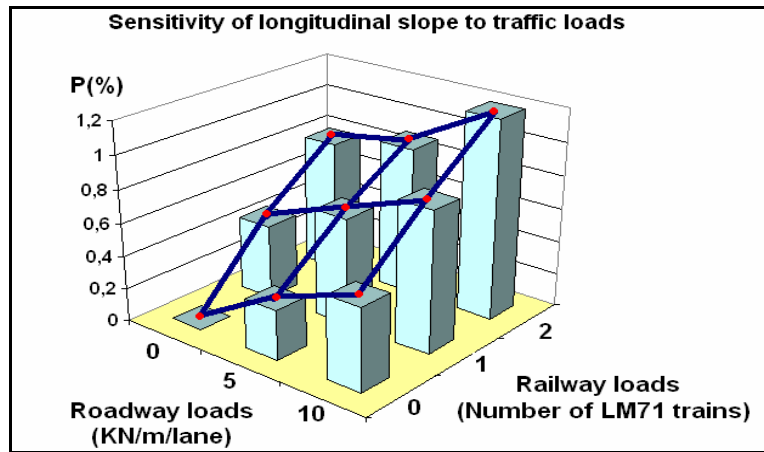
Figure 2.13. Experimental design: Sensitivity of conventional mean longitudinal slope to traffic loads (Giuliano).
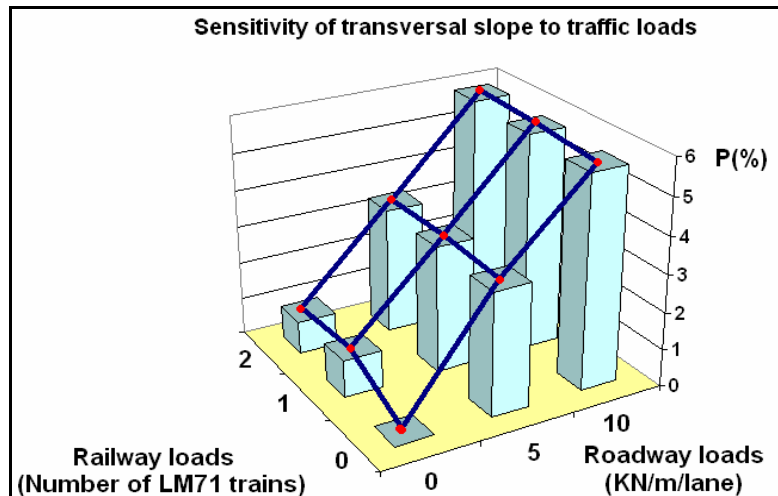
Figure 2.14. Experimental design: Sensitivity of maximum transversal slope to traffic loads (Giuliano).

53
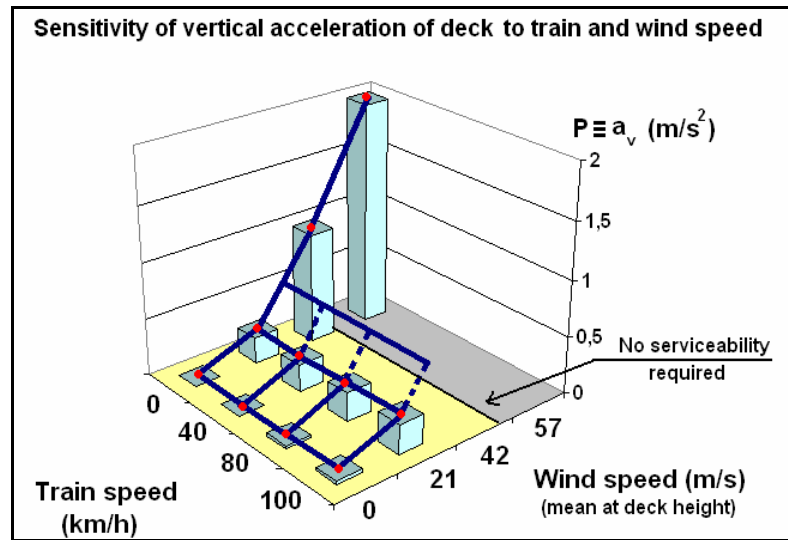
Figure 2.15. Experimental design: Sensitivity of vertical acceleration of the deck to train and turbulent wind speeds (Giuliano).
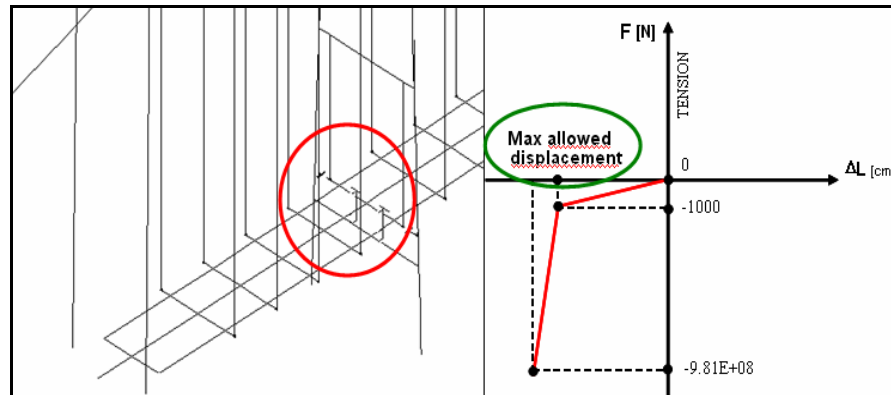
Figure 2.16. Passive Control device configuration under the pylon to limit transversal/longitudinal displacements and constitutive law.
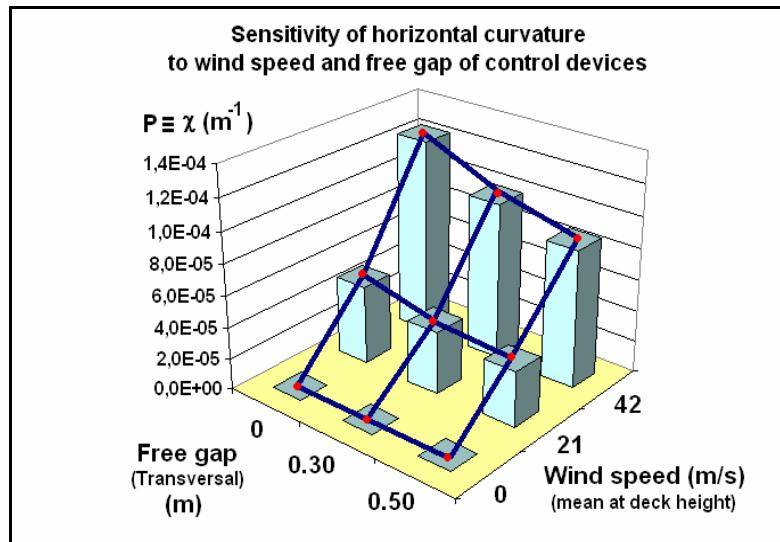
Figure 2.17. Experimental design: combination of variables and serviceability performance (Giuliano).

Summarizing, an experimental approach allow to identify a hierarchy of relevance of actions (and structural solutions) towards each performance.

It is qualitatively represented through chromatic matrices such as that of Figure 2.18, and allow to identify the relationship between performance and actions (sometimes negotiable if related to the use), and similarly between the performance and the technical solutions provided.

The degree of sensitivity of each performance to changes on actions, and the degree of uncertainty of each action, induce to identify also a scale of robustness for the performance, identifiable, for example, by the variance of the numerical response: robust (stiff) performance have small variance because insensitive to change in the actions, while performance with high variance (soft) are those on which to be less confident (Figure 2.19).

55

For example, it appears clear that the railway loads have high impact on the vertical sag, on the longitudinal slope of the deck, on the vertical curvature. The knowledge of the load characteristics, robust in the scale of a long span bridge, and with a low dynamic impact, allows to be confident on the computed levels of the sensitive performance. On the contrary, the performance whose levels are sensitively affected by loading uncertainties and by interaction effects, whose effects can be amplified in the macro-scale of the bridge, are those on which the supplier is less confident, and for which experiments and full-scale tests are required.

In any case the effectiveness of the whole process is realized if the amount of the uncertainties will not affect, during the construction or in the service life of the bridge, the minimum levels of the expected performance, leaving to Structural Control just the opportunity – not decisive – to improve the response.

Hierarchy of Actions for Messina Strait Bridge and Calibration

Serviceability Performances	Anthropic and Environmental Actions				
	Railway	Roadway	Wind	Earthquake	Temperature
Vertical sag	!!				!!
Longitudinal Displ.	!!			!!	!!
Longitudinal Slope	!!				
Transversal Slope		!!	!!		
Horizontal Curvature			!!		
Vertical Curvature	!!				
Deck Accelerations			!!		

Figure 2.18. Hierarchy of Actions and degree of dependence of Serviceability Performance (Giuliano).

Figure 2.19. Uncertainties of Actions and Reliability of Serviceability Performance (Giuliano).

57

Chapter 3

INTERACTION MECHANISMS

- ● Environmental Actions: Wind Gust Loading
  - → Wind Velocity Representation for Complex Structures
  - → Spectral Description of Turbulence

- ● Wind-Structure Interaction (WSI)
  - → Vortex Shedding and Lock-in
  - → Buffeting

- ● Soil-Structure Interaction (SSI)
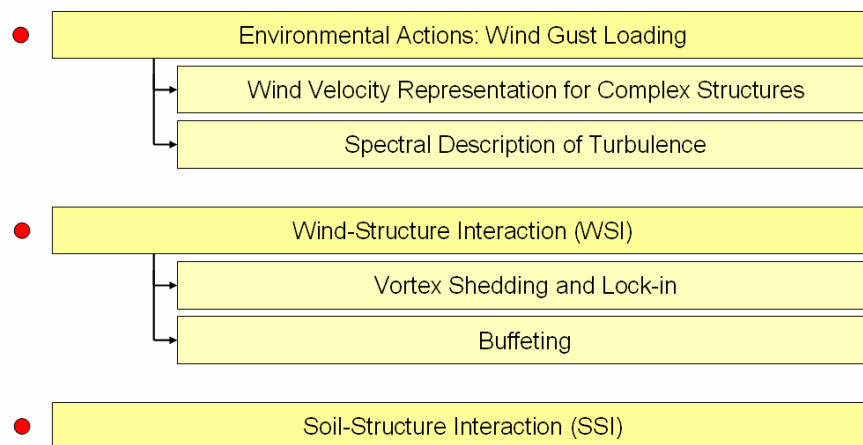
Abstract

This Chapter describes some aspects of the possible interaction mechanisms between the environmental actions and the structures, and some analytical and numerical models developed to investigate the structural response. The natural and anthropic actions, and the interaction effects have an intrinsic dynamic nature, and in many cases the dynamic impact is so high that the static analyses are inadequate for design purposes.

Among them, the Chapter contains the hypotheses and the procedures adopted for the modelling phases of the application presented in Chapter 5.

The attention is focused in particular on three aspects:

-   the turbulent wind loading and its numerical representation;
-   the wind-structure mechanisms of interaction: the aerodynamic attitude to vortex-shedding, the vortex-induced vibration and the *lock-in* synchronization, buffeting;
-   the soil-structure interaction (SSI): types of interaction, rheologic models, modelling aspects and solution methods.

3.1   Introduction

The previous Chapter focused on the experimental approach used for the case-study bridge described in Appendix B to give technical judgement about some serviceability performance, valuable through static nonlinear analyses of selected load scenarios, because of the well-known low dynamic impact of the actions on the monitored performance.

Yet the complex of actions on a structure such as a long span bridge are more complex and some performance cannot be evaluated in the static field. In fact in general they have a dynamic and intrinsically stochastic nature, while the interaction effects can change significantly the structural response and must be kept into account in order to obtain reliable response results.

The *Design Environment* can be defined as the complex of external actions which interact with the structure, stress it, change its properties and its operative regime. In a broad sense, this complex of actions concerns both the use of the structure by the users and its insertion in the natural environment.
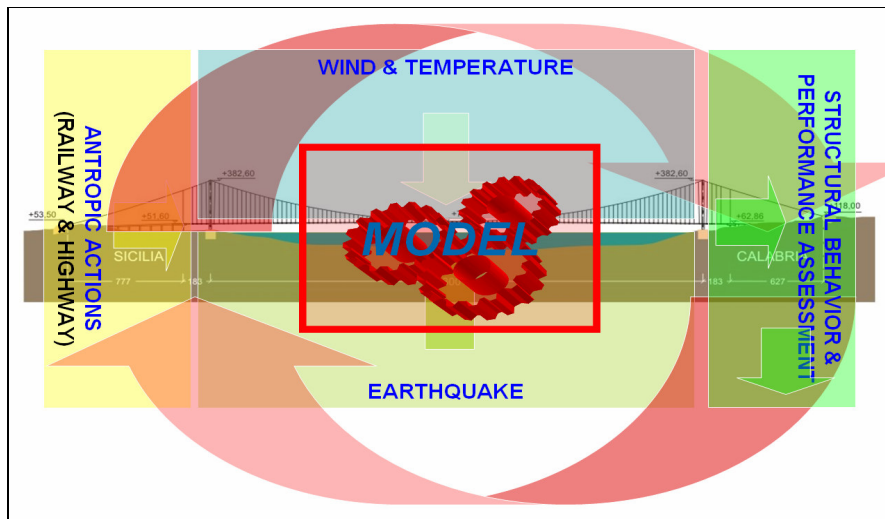
Figure   3.1. The Design Environment of a suspension bridge and the role of modelling in the assessment of the performance. (Bontempi, 2005).

61

The former can have various formats, from the vertical loads for buildings, traffic/pedestrian actions for bridges, operative loadings for machines; the latter comprise, for civil structures, the seismic action, the wind loadings, the thermo-hygrometric loadings, chemical agents. Their description is generally more complex for their spatial and time distribution, and for the difficulty of represent them in a reliability and statistical context in the design and analysis stages.

Furthermore the effect of environmental action on structures is not a simple cause-effect process, but has a *feedback* nature: the actions change the structural response and its attitude, and such changes change the actions themselves, and so on. Such feedback relationship is common in several natural phenomena and gets their simulation more complicate. In many case the complexity becomes so high that any numerical modelling is a rough approximation of the actual response, and the experimentation becomes decisive in the evaluation of the response.

In the case of civil structures, especially the complex and large-sized ones, the laboratory tests are useful tools but cannot be the only mean: the out-of-scale effects can decrease the accuracy and the reliability of the model results.

In most cases it can be asserted that the final prototype of the structure can be only the structure itself.

In the following paragraphs some interaction mechanisms between wind loading and structures and between soil and structures are presented, with focus on numerical representation and modelling strategies, some of which are those adopted in the applicative parts of the present thesis, in Chapter 5.

3.2 Environmental Actions: Wind Gust Loading

Wind speeds vary randomly with time for the turbulent nature of the wind flow. The fluctuant nature of the wind speed gives a fluctuant nature to the loads on the structures, with possible dynamic and resonant effects that must be evaluated; furthermore the aerodynamic response of bodies is related to the turbulent content of the air flow.

The real wind is turbulent, because the passage over irregularities of the ground surface disturb the stable stratification of the flow, or for lapse of temperature rate than the adiabatic value, or for thermal instabilities (convective gusts).

The standard description of the wind loading consists of the superposition of a logarithmic profile of the mean speed with height and a statistical description of turbulence. The turbulence is described, through semi-empirical relations, primarily on a ground roughness parameter, chosen in accordance with the smoothness of the reference site.

The characteristics of wind loading distinguishing it from earthquake are:
- the duration;
- a mean load value, with no reversal of deformations;
- the random nature in the time and in the space over the structure;
- the effects on the structures are significant in a large range of frequency.

The dynamic response of structures to gust loads, depending on the structural inertia, can be evaluated by spectral approach in the frequency domain, where a description of the energetic content of wind loading (*power spectrum*) in the frequencies is available. The Fourier integral approach, in the frequency domain, allows also the assessment of a special correlation of quasi-static pressures, which is dominated by the action of frequency components in general smaller than any resonant frequency of the structure, and for which the inertial effects are negligible.

In a severe temperate-climate windstorm, the mean wind speed and the statistical description can be approximately considered stationary for a sufficient duration so that sometimes the analyses in the frequency domain using power spectra can be attractive, especially when the nonlinear effects, in terms of inelastic or geometric deformation are small. When the nonlinearities become relevant in the structural problem, the time-domain approach is recommended.

3.2.1 Wind Velocity Representation in Complex Structures

As previously said, wind velocity is usually represented as a sum of a mean value $\overline{U}(\underline{x})$, in general function of the position $\underline{x}$ and a stationary zero-mean fluctuation $\underline{u}(\underline{x},t)$ function of position and time:

$$\underline{U}(\underline{x},t) = \overline{\underline{U}}(\underline{x}) + \underline{u}(\underline{x},t)$$

The projections of $\overline{U}(\underline{x})$ and $\underline{u}(\underline{x},t)$ along the axes of a reference system identified by the unit-vectors $\underline{e}_1$, $\underline{e}_2$, $\underline{e}_3$, where $\underline{e}_3$ vertical directed.

If one assumes a discrete spatial domain composed by N nodes (Figure 3.1), representing the point of the structural model where the aerodynamic forces will be applied, N vectors $\underline{x}^{(k)}$ $(k = 1,...,N)$ of coordinates are determined.

The wind field is then represented in these points, resulting in N vectors $\overline{\underline{U}}^{(k)} = \overline{\underline{U}}(\underline{x}^{(k)})$ $(k = 1,...,N)$ for the mean velocity vectors and N vectors $\underline{u}^{(k)}(t) = \underline{u}(\underline{x}^{(k)},t)$ $(k = 1,...,N)$ for the turbulence vectors.

For each node local reference systems can be defined, with unit-vectors $\underline{f}_1^{(k)}$, $\underline{f}_2^{(k)}$, $\underline{f}_3^{(k)}$, $(k = 1,...,N)$, so that $\underline{f}_3^{(k)}$ is parallel to $\underline{e}_3$ and $\underline{f}_1^{(k)}$ with the direction of the horizontal projection of the mean velocity $\overline{U}^{(k)}$:

$$\underline{f}_1^{(k)} = \frac{\overline{U}^{(k)} - U_3^{(k)}\underline{e}_3}{\sqrt{\left\|\overline{U}^{(k)}\right\|^2 - U_3^{(k)2}}}, \quad \underline{f}_2^{(k)} = \underline{e}_3 \times \underline{f}_1^{(k)}, \quad \underline{f}_1^{(k)} = \underline{e}_3$$
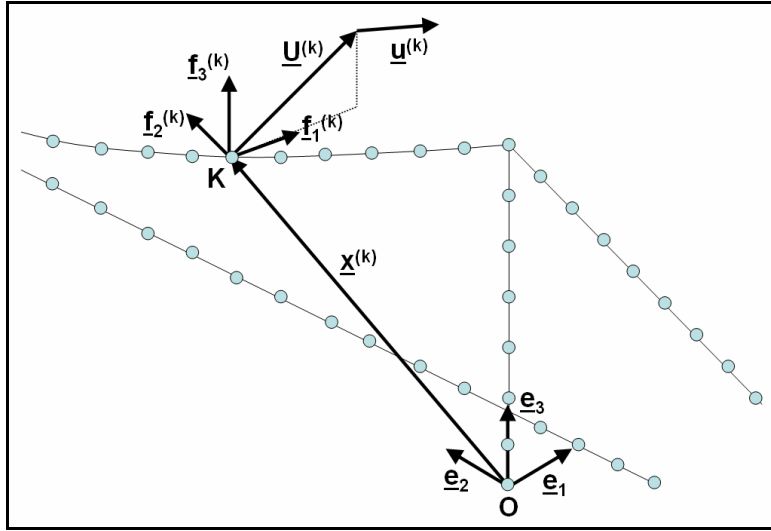
Figure 3.1. Global and local systems, mean and turbulent velocity vectors (Solari, 2005).

The projections of the turbulence vectors along the unit-vectors $\underline{f}_1^{(k)}$, $\underline{f}_2^{(k)}$, $\underline{f}_3^{(k)}$ represent the longitudinal $v_1^{(k)}$, lateral $v_2^{(k)}$ and vertical $v_3^{(k)}$ components of turbulence in the generic k-th node.

Modelling of mean wind velocity

For regions with flat terrain and uniform roughness, the mean wind velocity varies with the elevation z according to the Ekman spiral profile, that depends on the intensity of velocity, the roughness of the terrain, the geographic latitude and the thermal stratification of the atmosphere. Near the ground surface, in the inner boundary layer, the mean wind velocity has constant direction and has logarithmic profile for neutral stratification condition:

$$\overline{\underline{U}}(\underline{x}) = 2.5u_* \ln\left(\frac{x_3}{z_0}\right)\underline{w}$$

where u_*: shear velocity; z_0: roughness length;

65

$\underline{w}$: unit-vector which has the direction of the wind on the ground.

Other models or procedures from wind tunnel experiments have been proposed for non-homogeneous terrain roughness or regions with topographic irregularities.

Modelling of wind turbulence

As previously introduced, the atmospheric turbulence $\underline{u}$ can modelled as a stationary Gaussian zero-mean random process.

In general the turbulent components are assumed small in comparison of the mean terms, stationary and with zero mean value.

The spectrum defines the strength of an infinite number of infinitesimally spaced sinusoid components sustained so that the steady state response is attained for each component. The randomness of the process is related to the complex beat phenomena between the components; the magnitudes are expressed in mean-square terms: the spectrum describes the distribution of the variance of the process on a frequency abscissa: the ordinate are square values of the process per unity of frequency.

In wind engineering the basic spectrum used is in the single-sided form with frequency n, $S(n)$: its numerical values are 4π times the values for the double-sided circular frequency form $S(\omega)$.

Furthermore, the spectra in wind engineering are usually represented in normalized non-dimensional format of $nS(n)/\sigma^2$ plotted on a logarithmic scale abscissa n.

The complete characterization of the process is obtained by the cross-power spectral density function $S_{u_i u_j}(\underline{x}_1, \underline{x}_2, n)$ of any pair of turbulent components u_i, u_j, $i, j = 1,2,3$ in the points $P_1(\underline{x}_1)$, $P_2(\underline{x}_2)$, where n is the frequency.

The characterization of the process requires the modelling of the turbulence in the sense that the auto-spectrum and the coherence of the components of turbulence were introduced; the two-points coherence of any component of

turbulence must be such that it decreases if the distance of the points and the frequency increase: generally the dependence has exponential law.

The power spectral density matrix of the turbulent term $\underline{u}$ for the N-node structure has the following general expression:

$$[S_{\underline{uu}}(n)] = diag([R^{(1)}] \ \ldots \ [R^{(N)}]) * \begin{bmatrix} [S_{\underline{v}^{(1)}\underline{v}^{(1)}}(n)] & \ldots & \ldots & [S_{\underline{v}^{(1)}\underline{v}^{(N)}}(n)] \\ \ldots & \ldots & & \ldots \\ \ldots & \ldots & & \ldots \\ \ldots & & \ldots & \ldots \\ [S_{\underline{v}^{(N)}\underline{v}^{(1)}}(n)] & \ldots & \ldots & \ldots & \ldots & [S_{\underline{v}^{(N)}\underline{v}^{(N)}}(n)] \end{bmatrix} * diag([R^{(1)}] \ \ldots \ [R^{(N)}])^T$$

where $\left[S_{\underline{v}^{(h)}\underline{v}^{(k)}}(n)\right]$: matrices 3x3 containing the cross-power spectral density functions of the three turbulence components in the nodes h and k ;

$[R^{(k)}]$ $(k = 1,...,N)$: rotation matrices whose components are defined as

$$R_{ij}^{(k)} = \underline{e}_i \cdot \underline{f}_j^{(k)} \ \ , \ i, j = 1,2,3 \ ; \ k = 1,...,N$$

If the turbulent components are defined in the global reference system $\left(\underline{f}_j^{(k)} = \underline{e}_j\right)$, the matrices $[R^{(k)}]$ become identity matrices.

The cross-power spectral density function can be expressed in terms of auto-spectra and coherence functions:

$$S_{v_i v_j}\left(\underline{x}^{(1)}, \underline{x}^{(2)}; n\right) = \sqrt{S_{v_i v_i}(\underline{x}_1; n) S_{v_j v_j}(\underline{x}_2; n)} Coh_{v_i v_j}\left(\underline{x}^{(1)}, \underline{x}^{(2)}; n\right)$$

$$i, j = 1,2,3$$

where

$Coh_{v_i v_j}\left(\underline{x}^{(1)}, \underline{x}^{(2)}; n\right)$: coherence of turbulence components $v_i\left(\underline{x}^{(1)}, t\right)$ and $v_j\left(\underline{x}^{(2)}, t\right)$;

$S_{v_i v_i}(\underline{x}; n)$: auto-spectrum of the component $v_i(\underline{x}, t)$.

The area of the spectral plot is the variance of the turbulent component process $v_i(\underline{x}, t)$:

$$\sigma_{v_j}^2 (\underline{x}) = \int_0^\infty S_{v_j v_j} (\underline{x}; n) dn \quad i = 1,2,3$$

Cross-Spectra of velocity fluctuations

The cross-spectrum of two continuous records represents their degree of correlation.

If longitudinal turbulence is considered, it is defined as

$$S_{u^{(1)}u^{(2)}}^{cr}(r,n) = S_{u^{(1)}u^{(2)}}^{C}(r,n) + i S_{u^{(1)}u^{(2)}}^{Q}(r,n)$$

where $S_{u^{(1)}u^{(2)}}^{C}(r,n)$ and $S_{u^{(1)}u^{(2)}}^{Q}(r,n)$ are the co-spectrum and the quadrature spectrum of the random process u measured in the points P_1, P_2 whose reciprocal distance is r.

The coherence function is

$$C(r,n) = [Coh(r,n)]^2 = c_{u_1 u_2}^2 (r,n) + q_{u_1 u_2}^2 (r,n)$$

where

$$c_{u_1 u_2}^2 (r,n) = \frac{\left[S_{u^{(1)}u^{(2)}}^{C}(r,n)\right]^2}{S_{u^{(1)}u^{(1)}}\left(x_3^{(1)},n\right)S_{u^{(1)}u^{(1)}}\left(x_3^{(2)},n\right)} ; q_{u_1 u_2}^2 (r,n) = \frac{\left[S_{u^{(1)}u^{(2)}}^{Q}(r,n)\right]^2}{S_{u^{(1)}u^{(1)}}\left(x_3^{(1)},n\right)S_{u^{(1)}u^{(1)}}\left(x_3^{(2)},n\right)} ;$$

$S_{u^{(1)}u^{(1)}}\left(x_3^{(1)},n\right)$, $S_{u^{(1)}u^{(1)}}\left(x_3^{(2)},n\right)$: spectra of the longitudinal velocity fluctuations at points P_1, P_2.

The two-point coherence of any turbulence component decreases increasing the separation distance and frequency. Such dependency is traditionally modelled through simple exponential laws.

Davenport (1968) proposed the following expression for the square root of the coherence function:

$$Coh(r,n) = \exp\left(- \hat{f}\right)$$

where

$$\hat{f} = \frac{n\left[C_{1z}^2 \left(x_3^{(1)} - x_3^{(2)}\right)^2 + C_{1y}^2 \left(x_2^{(1)} - x_2^{(1)}\right)^2\right]^{1/2}}{U(10)} \quad \text{or}$$

$$\hat{f} = \frac{n\left[C_z^2\left(x_3^{(1)} - x_3^{(2)}\right)^2 + C_y^2\left(x_2^{(1)} - x_2^{(2)}\right)^2\right]^{1/2}}{\frac{1}{2}\left[U\left(x_3^{(1)}\right) + U\left(x_2^{(1)}\right)\right]}$$

The *exponential decay coefficients C* must be determined experimentally.
In homogeneous turbulence the quadrature spectrum vanishes; furthermore in
the atmosphere the ratio of quadrature spectrum to co-spectrum is small, so that
the coherence function can be approximated to the reduced co-spectrum $c_{u_1 u_2}$.

A common expression used is

$$S_{v_i v_j}\left(\underline{x}^{(1)}, \underline{x}^{(2)}; n\right) = \sqrt{S_{v_i v_i}\left(\underline{x}_1; n\right) S_{v_j v_j}\left(\underline{x}_2; n\right)} Coh_{v_i v_j}\left(\underline{x}^{(1)}, \underline{x}^{(2)}; n\right),$$

where $\hat{f}$ is determined assuming $C_z = 10$, $C_y = 16$.

The exponential decay coefficients are larger for rough surfaces, but depend
also on height and on wind speed. The uncertainties on cross-spectra and their
decay coefficients, are related to those of the integral scales of turbulence. Other
models propose a relation between longitudinal coherence, turbulence intensity
distance and integral scale $L_u^x(z)$.

The exponential coherence function for longitudinal, vertical and lateral
turbulence for a N-node structure can be generalized by the following
expression:

$$Coh_{v_j^{(h)} v_j^{(k)}}\left(\underline{x}^{(h)}, \underline{x}^{(k)}, n\right) = \exp\left[-\frac{n\left\|\left(\left[C_j^{(h)}\right] + \left[C_j^{(h)}\right]\right)\left(\underline{x}^{(h)} - \underline{x}^{(k)}\right)\right\|}{\left\|\underline{U}^{(h)}\right\| + \left\|\underline{U}^{(k)}\right\|}\right],$$

$$\left(j = 1,2,3 \quad h, k = 1, ..., N\right)$$

where $\left[C_j^{(h)}\right] = \sum_{s=1}^{3} C_{js} \underline{f}_s^{(k)} \otimes \underline{f}_s^{(k)}$, $\quad \left(j = 1,2,3; k = 1, ..., N\right)$ (second-order

tensor);

C_{js}: exponential decay coefficient to the turbulent component v_j versus a separation distance in longitudinal direction $(s = 1)$, lateral $(s = 2)$, vertical $(s = 3)$.

Generally it is assumed that the lateral turbulence component v_2 is uncorrelated with respect to the longitudinal and vertical components v_1 and v_3, while it is known that v_1 and v_3 have negative single-point coherence.

3.2.2 Spectral Description of Turbulence

The properties of the turbulent content can be summarized by the atmospheric turbulence quantities:

-   the turbulence intensity;
-   the integral scales of turbulence;
-   the spectra of turbulent fluctuations of velocity.

Turbulence intensity

The longitudinal turbulence intensity is defined as

$$I(z) = \frac{\sqrt{\overline{u(z)^2}}}{U(z)}$$

where $U(z)$: average value of velocity at elevation z;

$u(z)$: fluctuation, parallel to $U(z)$; $\sqrt{\overline{u(z)^2}}$ = rms value of the fluctuation.

The lateral and vertical turbulence intensity can be defined in similar way.

Integral scales of turbulence

The fluctuation of the wind speed can be considered the result of the superposition of eddies transported by the flow, each causing periodic fluctuation with circular frequency $\omega = 2\pi f$, while the wave length $\lambda = U/f$ is a measure of their size.

The integral scales are measures of the average size of the turbulent eddies of the flow; nine scales can be defined corresponding to the dimensions of the

70

eddies associated with the components of the longitudinal, vertical, transversal fluctuations.

Consequently, for instance, L_u^x, L_u^y, L_u^z are measures of the eddy associated with the longitudinal fluctuation u of the mean speed (x =direction of the mean speed U and of fluctuation u).

In particular L_u^x is defined as $L_u^x = \dfrac{1}{\overline{u}^2} \displaystyle\int_0^\infty R_{u_1 u_2}(x)dx$

where $R_{u_1 u_2}(x)$: cross-covariance function of the longitudinal component $u_1 = u(x_1, y_1, z_1, t)$ and $u_2 = u(x_1 + x, y_1, z_1, t)$.

By definition, integral scales are small if the cross-covariance decay rapidly with distance: velocity fluctuations of points enough far each other in respect of the integral scales are uncorrelated. When the integral scales are small compared with the size of a structure, the effect of the longitudinal wind fluctuation on the overall wind loading is small; when the integral scales grow, the effect of eddies on the structural response becomes relevant.

If we assume that the flow disturbance travels with $U(z)$, the fluctuation is such that

$$u(x_1, \tau + t) = u(x_1 - Ut, \tau), \text{ and } L_u^x = \frac{U}{\overline{u}^2} \int_0^\infty R_u(\tau)d\tau$$

where $R_u(\tau)$ is the auto-covariance function of the fluctuation $u(x_1, t)$.

In general the scales of turbulence depend on the length of the record, on the stationary nature of the signal and vary with height of elevation and terrain roughness.

Spectra of longitudinal velocity fluctuations

The fluctuation of wind velocity can be considered as the result of a superposition of eddies, at different frequencies n, and the total kinetic energy of the turbulent motion can be regarded as the sum of the eddies of the flow.

The function $E(n)$ represent the dependence of the energy contribution on frequency, the energy spectrum of the turbulent motion.

71

It is possible to show, starting from the equations of the motion of the turbulent flow, that the inertial terms of the equations are associated with transfer of energy from larger eddies to smaller ones, while the viscous terms, related to energy dissipation, are effected mostly by the smallest eddies where the shear and viscous stress and deformation are large.

For small viscous effects the decay time is long, and the energy of these eddies can be considered steady if we have perfect balance of the energy transferred by the large eddies with that dissipated by viscous effects: the small motion of the eddies is due to the rate of energy transfer ε (dissipation) and by viscosity. In these conditions (Kolmogorov's first hypothesis) the small eddy motion is related only to internal mechanisms and does not depend on boundary, so that perfect local isotropy is reasonable.

A further hypothesis regards the concentration of dissipation in the smallest eddies (Kolmogorov's second hypothesis): at the lower end of the higher frequency range to which the Kolmogorov's first hypothesis applies, the influence of the viscosity on the eddy motion is small, and depends only on the rate of energy transfer (*inertial sub-range*).

Inertial sub-range - Assuming the wave number $K = \dfrac{2\pi n}{U} = \dfrac{2\pi}{\lambda}$ (λ: wave length), in the inertial sub-range a dimension relation between $E(K)$ and ε for high values of K can be stated:

$$E(K) = a_1 \varepsilon^{2/3} K^{-5/3}$$

For longitudinal velocity fluctuation the spectrum $S(K) = a\varepsilon^{2/3} K^{-5/3}$, $a \cong 0.5$.

Inertial (high frequency) sub-range - The balance energy production and dissipation in horizontally homogenous neutrally stratified flow can be written as

$$\varepsilon = \frac{\tau_0}{\rho} \frac{dU(z)}{dz}$$

where

ρ : density of air; $U(z) = \dfrac{1}{k} u_* \ln \dfrac{z}{z_0}$; $u_* = \left(\dfrac{\tau_0}{\rho} \right)^{\frac{1}{2}}$:shear velocity of the flow.

It follows

$$\varepsilon = \frac{u_*^3}{kz}$$

Substituting and assuming $K = \dfrac{2\pi n}{U(z)}$, we obtain the reduced spectrum of the longitudinal velocity fluctuations, function of the height:

$$\frac{nS(z,n)}{u_*^2} = 0.26 f^{-2/3}$$

where $f = \dfrac{nz}{U(z)}$: Monin similarity coordinate.

The expression above of the spectrum can be considered representative for many cases in the high-frequency range, and conservative for $f > 0.2$.

Spectra in the lower-frequency range – The lower frequency range is defined between $n = 0$ and the lower end of the inertial sub-range. In this range similarities cannot be defined and no universal relation are valid. However, some statement can be done:

A. $S(n = 0) = S(0) = \dfrac{4\overline{u^2} L_u^x}{U}$;

B. $\dfrac{dS}{dn}\bigg|_{n=0} = 0$;

C. $S(n)$ is monotonically decreasing;

D. $S(n)$ is continuous at the lower end of the inertial subrange.

The length of the record used to evaluate U , $\overline{u^2}$, L_u^x must be representative of the storms expected in the region of the construction in the associated period of return and conventionally is of one hour (spectral gap).

In literature a relation between the frequency n_{peak} at which the curve $nS(n)$ has a maximum and L_u^x has been stated as

$$L_u^x = \frac{1}{2\pi}\frac{U}{n_{peak}}$$

Yet the evaluation of the integral scale from measurements of U and n_{peak} can fail for the uncertain shape of the spectrum in the range of n between 0 and n_{peak}, that affects the estimation of L_u^x.

The spectral distribution in the lower-frequency range in general does not affect the building response, but for tall and slender structures the natural frequencies can be close to those of the lower-frequency range, and affect the response significantly.

Spectra of literature

In literature many expression of spectra have been proposed on the basis of measurements and used for design. Some are reported in Table 3.I, containing comments.

Spectra of Vertical and Lateral Velocity Fluctuations

Concerning the spectrum of vertical fluctuations up to 50 m the following formula has been proposed:

$$\frac{nS_w(z,n)}{u_*^2} = \frac{3.36f}{1+10f^{5/3}}$$

The cross-spectrum of vertical fluctuations at points P_1, P_2 of elevation z may be expressed as

$$S_{w_1 w_2}(\Delta y, n) = S_w(z,n)e^{-\frac{8n\Delta y}{U(z)}}$$

where Δy is the horizontal distance between the two points.

For the lateral velocity fluctuation a proposed spectrum is

$$\frac{nS_v(n)}{u_*^2} = \frac{15f}{(1+9.5f)^{5/3}}$$

74

In the case of flat and homogeneous terrain, Solari and Piccardo have developed a model applicable within the inner boundary layer and in neutral regime. The auto-spectrum of the three components of turbulence is given in the form

$$S_{v_j v_j}(\underline{x};n) = \frac{\sigma_{v_j}^2(\underline{x})\lambda_j \dfrac{L_{v_j}(\underline{x})}{\|U(\underline{x})\|}}{\left(1+1.5\lambda_j n \dfrac{L_{v_j}(\underline{x})}{\|U(\underline{x})\|}\right)^{\frac{5}{3}}} \qquad j=1,2,3$$

where $\lambda_1 = 6.868$, $\lambda_1 = 9.434$, $\lambda_1 = 6.103$;

L_{v_j} : integral scale of the gust component $v_j(\underline{x},t)$.

3.3   Wind-Structure Interaction (WSI)

3.3.1 Aerodynamics and Aeroelasticity

For civil engineering the application of aerodynamics and aeroelastics deals with the evaluation of the forces and the interaction effects between structure and flows, i.e. wind, at relatively low speed and incompressible, affected by local conditions such as topography and turbulence of the boundary layer of the atmosphere.

Aerodynamics

The aerodynamic behaviour of bluff bodies like most of the civil structures are investigated by the synergy of experiments, analytical models and the modern tools of computational fluid dynamics (CFD) and of computational wind engineering (CWE): for complex structures the use of only one of these tool at the moment is not able to give absolutely reliable basis for the design.

In Table 3.II are summarized some definitions and hypotheses generally used for the air flows.

Author	Spectrum	Comments
T. Von Karman (1948)	$$\frac{nS(n)}{u_*^2} = \frac{4\beta \frac{nL_u^x}{U}}{\left[1 + 70.8\left(\frac{nL_u^x}{U}\right)^2\right]^{5.6}}$$	Non consistent with $\frac{nS(z,n)}{u_*^2} = 0.26 f^{-2/3}$ of the inertial sub-range, because at high frequency the spectrum is not affected by the large scale features of turbulence that determine L_u^x. Feasible for structures with high inertial response to low-frequency loads (structures with high periods of vibration).
R.I. Harris (1968)	$$\frac{nS(n)}{u_*^2} = 4.0 \frac{x}{\left(2 + x^2\right)^{5/6}}$$ $$\left(x = \frac{1800n}{U(10)}\right)$$	The spectrum proposed does not depend on height. $\left(L_u^x \neq 0\right)$
J.C.Kaimal (1972)	$$\frac{nS(z,n)}{u_*^2} = \frac{200 f}{\left(1 + 50 f\right)^{5/3}}$$ $$\left(f = \frac{nz}{U(z)}\right)$$	It implies $\overline{u^2} = 6u_*^2$. Good approximation of the inertial sub-range. Requirements A,B not satisfied; feasible for structure with fundamental frequencies in the inertial sub-range (high frequencies).

Table 3.I. Longitudinal turbulence spectra of literature for design.

Fluid nature			
Real fluids		$[\sigma] = -p[I] + [\tau]$	Isotropic and deviatoric components of stress
	Newtonian	$\tau_{ij} = \lambda\,div\underline{v}\,\delta_{ij} + \mu\left(\dfrac{\partial v_i}{\partial x_j} + \dfrac{\partial v_j}{\partial x_i}\right)$	
Inviscid fluids		$[\sigma] = -p[I]$	

Table 3.II. Fluid classification and definitions.

The governing equation of the fluid dynamics are summarized in Table 3.III: for incompressible flows the only equations closing the system are the equation of continuity and the equations of momentum, because we have only four independent state variables and no state equation is required.

The fluids like air have mass and viscosity, that appear and have role in the equations of the motion; at normal atmospheric pressure the viscosity is small but have an important role because it governs the formation of the boundary layers, in which the air speed vary from zero (no slip, at the surface) to the full value, creating a typical profile.

The prevalence of inertial or viscous terms in the motion allows simplification in the mathematical problem and changes also the nature of the flow; this dicotomic relation between viscosity and inertia can be represented by the nondimensional Reynolds number:

$$Re = \frac{\rho U B}{\mu} = \frac{U B}{\nu}$$

that represents the ratio between the inertial and viscous forces in the flow.
(U =mean speed of the flow; ρ =fluid density; μ =fluid viscosity; ν =kinematic viscosity of air; B =characteristic length for the flow).

For flows of practical interest the range for Reynolds numbers is about $0\text{-}10^9$.

Principle	Equation	General form	Particular forms
Mass conserv.	Equation of continuity	$\dfrac{\partial \rho}{\partial t} + div(\rho\underline{v}) = 0$	Incompressible fluid $\rho = const \rightarrow div\underline{v} = 0$ Irrotational flow (inviscid) $\underline{v} = \underline{gradU} \rightarrow \nabla^2 U = 0$ + Bernoulli's theorem $\dfrac{1}{2}\rho U^2 + p = const$
Conserv. of momentum	Equations of Navier-Stokes	$\rho\dfrac{d\underline{v}}{dt} =$ $= -\underline{\nabla}p + \underline{\nabla}\cdot[\tau] + \rho\underline{f}$	Incompressible and Newtonian fluid $\rho\dfrac{d\underline{v}}{dt} = -\underline{\nabla}p + \mu\nabla^2\underline{v} + \rho\underline{f}$ Incompressible Inviscid fluids (Euler's equation) $\rho\dfrac{d\underline{v}}{dt} = -\underline{\nabla}p + \rho\underline{f}$

Table 3.III. General Equations of fluid dynamics

Let's consider a circular cylinder subjected to laminar flow (Figure 3.2): for a specific range of Reynolds number alternating vortices are shed from the cylinder and move off downstream at a lower speed than that of the fluid.

At low Reynolds numbers the flow remains attached to the body and overpasses it undisturbed; at $Re \cong 20$ the flow separates and creates two big vortices that remain attached to the body; at $Re \cong 30 - 5000$ the vortices are broken and a continuous vortex shedding, cyclically alternating is generated; for higher values, $Re \geq 5000$, the inertia force predominate and a turbulent wake is formed behind the body.

The boundary-layer separation occurs when the fluid particles in the boundary layer are sufficiently decelerated by inertial forces that the flow near the surface becomes reversed, for adverse pressure gradients in the flow.
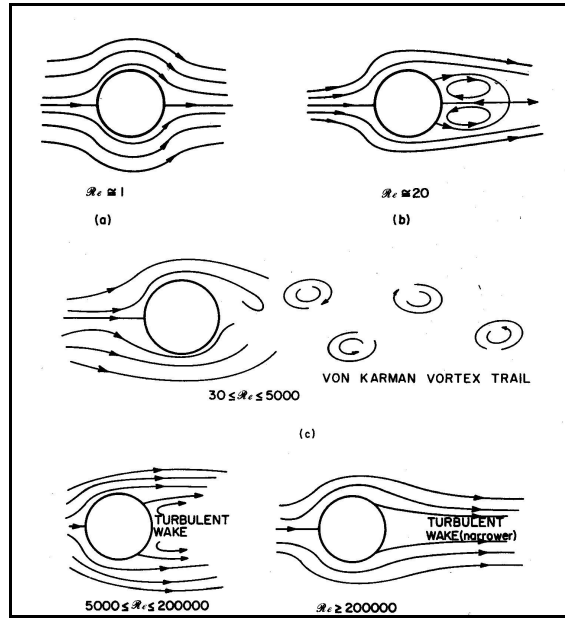
Figure 3.2. Flow past a circular cylinder (Simiu & Scanlan, 1996).

Analogous phenomenon is observed for a sharp-edged plate, where the corners are prone to create such pressure gradients adverse to the flow speed. In Figure 3.3 is represented the nature of the flow from small values of Reynolds number, when viscous effects dominate, to higher values when the inertial effects do.

If $Re \geq 1000$, the inertia force predominate and a turbulent wake is formed behind the plate, with a small shear layer of vortices separating the smooth and the turbulent flow.

Other bluff bodies like triangles, prisms, rectangles give rise to analogous vortex-shedding phenomena.

The regularity of the vortex wake was investigated by Strouhal, who discovered that the frequency of shedding N_s is related to the mean speed of the uniform flow U by the following relation:

79

$$S = \frac{N_s B}{U} \, ,$$

where the Strouhal number S depends on the shape of the cross section invested by the flow and B is a characteristic dimension of the body.

$Re \cong 0.3$ $Re \cong 10$

$Re \cong 250$ $Re \geq 1000$
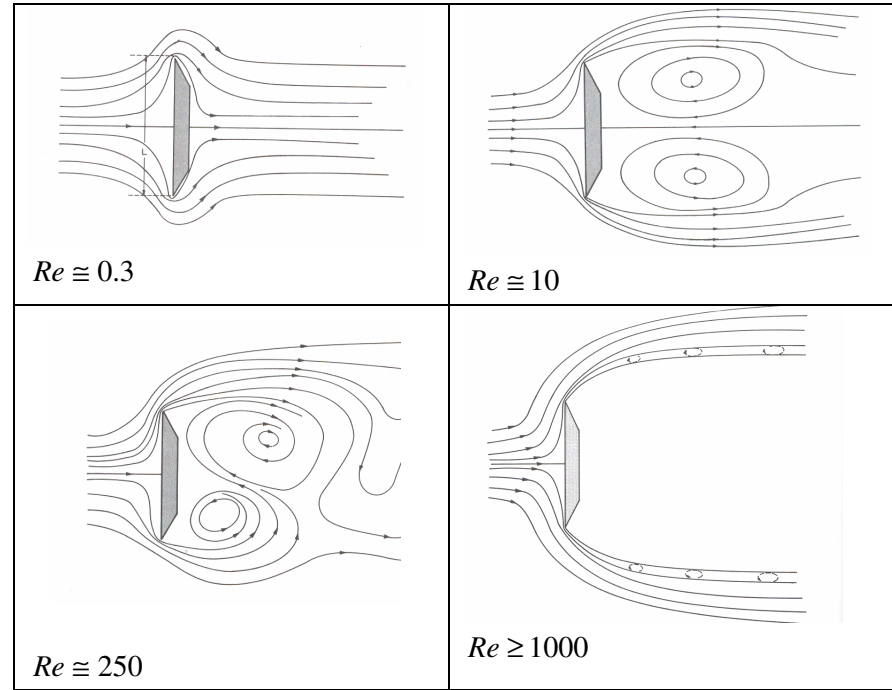
Figure 3.3. Flow past a sharp edged plate (Simiu & Scanlan, 1996).

In the range of speed of vortex-shedding, the degree of dependence of S on Re is small.

For any bluff body, the shedding is not a purely sinusoidal phenomenon, because a range of more component frequencies than the spectral peak govern it. Considering just the spectral peak, an approximation of the across-flow force per unit length at the peak Strouhal frequency is given by the expression

80

$$F_L = \frac{1}{2} \rho U^2 B \overline{C}_L \sin \omega t,$$

where $\omega = 2\pi N_s$ and $\overline{C}_L$ is a mean coefficient that depends on the section shape (in fact the coefficient is not constant but varies with time and with angle of attack).

The integration of the pressure over the surface of the body gives a net force and moment (*aerodynamic forces*): the component of the force in the along-flow and across-flow directions are the *drag force* F_D and the *lift force* F_L (as forces for unit of length). Such forces are affected by the shape of the body and the Reynolds number.

The pressures measured at a structural surface or the aerodynamic forces can be referred to the mean dynamic pressure $1/2\,\rho U^2$ (see Bernoulli's theorem), and corresponding aerodynamic coefficients can be defined (Table 3.IV).

Aerodynamic coefficients	
Pressure Coefficient (p-p$_0$=difference between local and far upstream pressure p$_0$)	$C_p = \dfrac{p - p_0}{1/2\,\rho U^2}$
Lift Coefficient	$C_L = \dfrac{F_L}{1/2\,\rho U^2 B}$
Drag Coefficient	$C_D = \dfrac{F_D}{1/2\,\rho U^2 B}$
Moment Coefficient	$C_M = \dfrac{M}{1/2\,\rho U^2 B^2}$

Table 3.IV. Aerodynamic coefficients.

The relationship between Reynolds number and drag coefficient is shown in the diagram of Figure 3.4 for circular cylinders: there is a region of sharp drop between $2\times10^5 < \mathrm{Re} < 5\times10^5$, called *critical region*, with transition from laminar to

81

turbulent flow in the boundary layer on the surface of the cylinder. The turbulent mixing in the boundary layer lets transport fluid with higher momentum towards the surface of the cylinder; separation occurs much farther back and the wake narrows, producing a value of the mean drag coefficient lower than in the subcritical region. For higher Reynolds number, in the supercritical and transcritical regions, the coefficients increases but remains lower than the subcritical values and less sensitive to Reynolds number.

Sharp-cornered and short sections have, on the contrary, drag practically unchanging with Reynolds number; the early separation of the flow and the shortness of the afterbody precludes the possibility of reattachment. In general the sections with well defined points of detachment of the flow are Reynolds number insensitive (and the aerodynamic coefficients can be assembled in tables of constants), while the sections with extended regions of possible detachment have drag coefficient Reynolds number dependent.
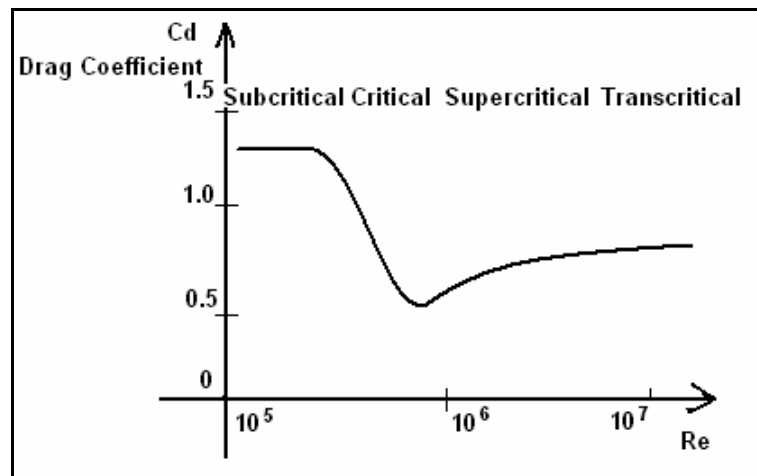
Figure 3.4. Evolution of drag coefficient with Reynolds Number for a circular cylinder.

As concerns the turbulence influence, it has been demonstrated that the drag coefficients are generally lightly modified on respect the values obtained by smooth flow; this justify the use of smooth flows to assess the aerodynamic features in the wind tunnel tests.

Possible influence of turbulence occurs:

- when the ratio between the sides of the body does not allow flow reattachment: high turbulence gives higher drag and smaller separation layers;
- when the ratio between the sides of the body can allow flow reattachment: if the turbulence is enough high to provide reattachment, it gives lower drag and larger separation layers than if the turbulence is low and does not allow reattachment.

The characteristics of the flow in terms of aerodynamic forces, that vary with time, can be summarized by time-histories and spectral densities, with peaks corresponding to the frequency of vortex shedding (governed by Strouhal number), and others related to the fact that the fluctuation of the forces are not purely sinusoidal but have several contents in frequency.

Aeroelasticity

The time-dependent nature of aerodynamic forces on a body is high if the flow is turbulent and more if the body has oscillations, with possible mutual influence between flow and body motion. *Aeroelasticity* is the science that investigates the interaction between the aeroelastic forces and the structural motion.

The aerodynamic instability is a phenomenon inside the flow, producing divergent wake or trail of vortices; the aeroelastic instability is related to the divergent oscillatory movement of the body, for the negative damping of the system fluid-structure and the inability to dissipate the energy introduced into the system.

Yet some aerodynamic phenomenon of instability such as vortex shedding, can generate oscillation on the invested body, with aeroelastic effects of coupling

that change the aerodynamic forces as consequence of the motion (self-excited forces).

In what follows the vortex shedding and lock-in phenomenon, and the buffeting effects are presented, significant for the application of Chapter 5.

3.3.2 Vortex Shedding and *Lock-in*

As presented in the previous Paragraph, under certain conditions bluff bodies shed alternating vortices with frequency N_s related to the mean speed of the uniform flow by the Strouhal number.

The time-histories of the forces induced on the body (integral of the pressure on the surface) depend in a complex way on the geometry, but the frequency N_s of the shedding is equal to that of the principal harmonic of the transversal force induced on the body, while that of the force in the flow direction is equal to $2N_s$.

The amplitudes, the direction or even the frequencies of forces can be affected by local or global structural movements, making aeroelastic effects.

The structures subjected to vortex shedding are excited periodically at a frequency related to the Strouhal number; when this frequency is close to the across-wind natural frequency of the structure, it starts to interact strongly with the flow: the structure is excited with alternate resonant forces, the frequency of vortex shedding and the natural frequency of the structure become syncronous and the natural frequency of the structure controls the vortex shedding even in a larger range of wind speeds, in which the vortex shedding occurs at the same frequency of the structure even if the nominal Strouhal frequency is different of some percent. This phenomenon is known as *lock-in* (*synchronization*).

In the diagram of Figure 3.5 is represented the evolution of vortex-shedding frequency with wind velocity over an elastic structure: in the *lock-in* region the vortex-shedding frequency is constant and is not a linear function of the wind velocity as the Strouhal relation would.
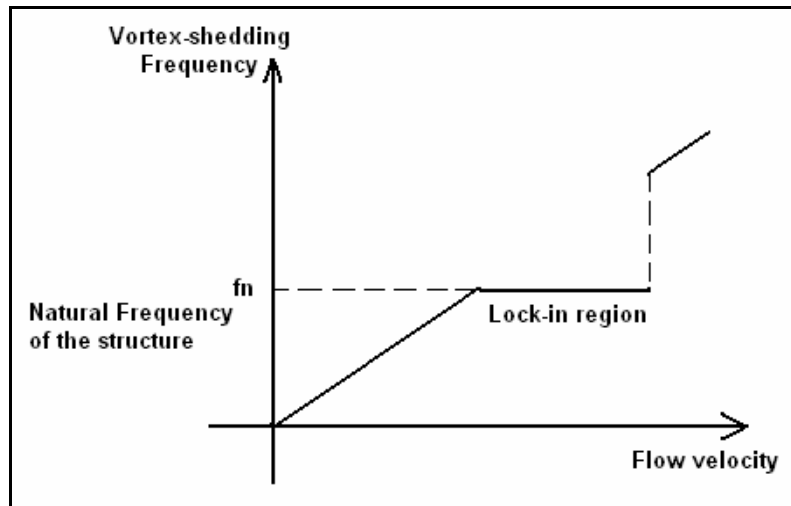
Figure 3.5. Vortex-shedding frequency and wind speed for elastic structures (Simiu & Scanlan, 1996).

So before *lock-in* the structural oscillations have a density spectrum of displacements with a peak on the structural natural frequency f_n and a smaller peak on the Strouhal frequency N_s, and the shedding frequency is $f_s < N_s$; the same happens for high speed, after *lock-in*, but $f_s > N_s$; at *lock-in* the frequencies coincide $f_s = N_s$ and the amplitude of the vibrations experiences the maximum value.

Two are the typical aspect of the vortex shedding:

-   the wake of the bluff body, composed of a street of alternately shed vortices, has the characters of a separate oscillator, coupled with the structure;
-   the self-excited vortex induced oscillations do not diverge but remain in a cycle of relatively modest level (self-limitation).

No completely satisfactory analytical models have been developed; actually the response of structures is evaluated by a synergy of results of wind tunnel tests, analytical, CFD and Finite Elements models, 2D and 3D.

85

Numerical models

At the moment neither numerical or physical modelling provide the solution of the problem, and so the prediction of the full-scale response must rely on semi-empirical models supported by full-scale experiments.

Vickery developed mathematical models for the prediction of lateral response of tall structures such as chimneys to vortex-shedding (Table 3.V). The developed forces are decomposed into two parts:

- a vortex associated narrow-band force, whose complete spectrum has an energy content also at low frequency associated to large scale turbulence, that has only a small contribution at lock-in, when the resonant effects are predominant;
- a motion dependent force (aeroelastic), expressed in terms of aerodynamic nonlinear damping.

The aerodynamic parameters of the model need an experimental full-scale procedure of identification.

The model assumes linear superimposition of the modal responses:

$$y(z,t) = \sum_i \alpha_i(t)\phi_i(z),$$

where α_i = i-th modal coefficient; $\phi_i(z)$=i-th modal shape.

Even if the model refers to towers, simple for section and structural geometry, the nature of the solution (rms of amplitude) is also for more complex systems described in the form

$$\frac{\sigma_a}{d} = \frac{C}{\left[K_S - K_{ao}\left(1 - \left(\frac{\sigma_y}{\lambda d}\right)^2\right)\right]^{1/2}},$$

where

$$K_s = \frac{m\zeta_s}{\rho d^2} = \text{Scruton number}; \quad \zeta_s = \text{structural damping};$$

$$C = \phi\left(\frac{h}{d}, m, C_L, l, B, St\right).$$

86

Vickery's model (1983, 1990)	
Vortex-shedding force: Narrow-band random force $w(z,t)$ **with normal distribution**	
Spectrum of $w(z,t)$:	$$\frac{f S_w(f)}{\sigma_w^{\,2}} = \frac{1}{B\sqrt{\pi}} \exp\left[-\left(\frac{(1-f/f_s)}{B}\right)^2\right];$$ (f_s =Shedding frequency; B =bandwidth)
Variance of $w(z,t)$: (for $f = f_s$)	$$\sigma_w^2 = \tilde{C}_L \left(\frac{1}{2}\rho U^2\right)^2 d^2$$ ($\tilde{C}_L$ =rms lift coefficient; ρ =air density; U =wind speed; d =diameter)
Co-spectrum	$$Co(w, z_1, z_2) = \sqrt{S_w(z_1, f) * S_w(z_2, f)} * R(z_1, z_2)$$ $$R(z_1, z_2) = \cos\left(\frac{2r}{3l}\right)\exp\left[-\left(\frac{r}{3l}\right)^2\right]; \; r = \frac{2|z_1 - z_2|}{[d(z_1) + d(z_2)]};$$ l =correlation lenght in diameters $(\cong 1)$.
Aeroelastic force: nonlinear aerodynamic damping force $w_d(z,t)$	
Aeroelastic Force at a section z:	$$w_d(z,t) = 4\pi\rho d^2 f_1 K_{ao}\left(1-\left(\frac{\sigma_y}{\lambda d}\right)^2\right)\dot{y} = 2m\omega_1\zeta_a \dot{y};$$ (f_1: fundamental frequency; σ_y: rms displacement y; λd: limiting rms of the aeroelastic response in diameters; m :mass per unit length; ω_1: fundamental circular frequency; ζ_a: aerodynamic damping) $$K_{ao} = \phi\left(\frac{\overline{U}}{f_1 d}, I_u, \mathrm{Re}\right); I_u$$: intensity of longitudinal turbulence.

Table 3.V. Vickery's model for vortex response of towers.

87

The solution is such that three different regions can be identified (Figure 3.6):

1) a *lock-in* region with small value of m or ζ_s ($K_S/K_{ao} \ll 1$, low Scruton number), in which the response is independent on C and on the vortex forces, it is governed by the nonlinear damping: and has a quasi-sinusoidal history, with rms

$$\frac{\sigma_a}{d} = \alpha\left[1 - \frac{K_S}{K_{ao}}\right]^{\frac{1}{2}}$$

2) a small-amplitude region, ($K_S/K_{ao} \gg 1$, higher Scruton number), in which the response has a random nature with linear positive damping , with rms

$$\frac{\sigma_a}{d} = \frac{C}{[K_S - K_{ao}]^{\frac{1}{2}}}$$

3) a transition region ($K_S/K_{ao} \cong 1$).
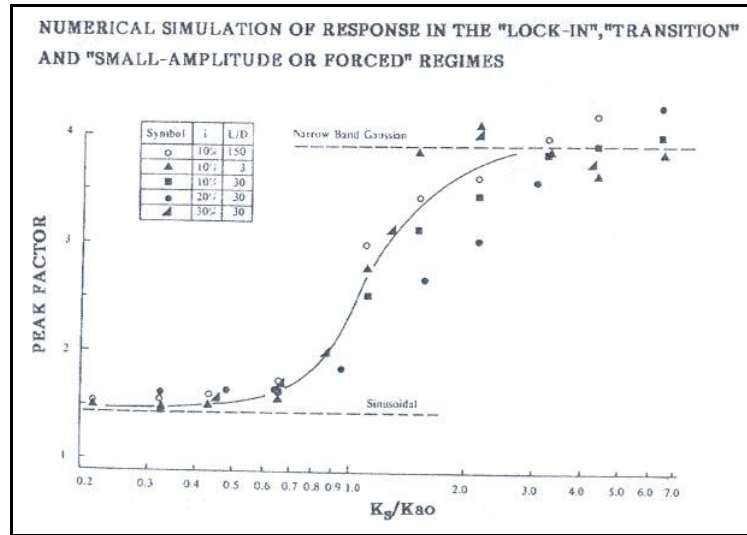
Figure 3.6. Vortex response: Lock-in and small amplitude region (Simiu & Scanlan, 1996).

It follows that the lock-in phenomenon is governed by the Scruton number, representing the damping and the ability of the structure to dissipate energy. At low Scruton number the structure cannot dissipate energy and amplifies the vibrations (*lock-in* regime). The suppression of such vibrations requires the provision of a positive damping, by structural rearrangement or the use of mechanical devices, in order to exit from the critical region.

3.3.3 Buffeting with Aeroelastic Effects

Buffeting is the unsteady loading of a structure due to the fluctuating velocity of the oncoming flow.

Several researches have been made to solve the problem of the buffeting of structures subjected to atmospheric turbulence over different typologies of homogeneous terrain, and analytical models have been developed in order to obtain the buffeting response of structures with or without aeroelastic interaction with the wind forces.

Structures like towers and deck of suspension bridges are subjected to buffeting and may exhibit aeroelastic effects.

When a linelike structure, with spanwise coordinate x is buffeted by atmospheric turbulence and the oscillations of the structure related to the first modes are small, the aerodynamic behaviour of the structure is linear: the aerodynamic forces consist of a superposition of *self-excited* forces (flutter-type) and buffeting forces induced by turbulence.

a. *Self-excited forces*: for a body oscillating with circular frequency ω in the torsional and flexural modes, the *self-excited* lift L_h and moment M_α can be expressed as follows:

$$L_h(K) = \frac{1}{2}\rho U^2 B\left[KH_1^*(K)\frac{\dot{h}}{U} + KH_2^*(K)\frac{B\dot{\alpha}}{U} + K^2 H_3^*(K)\alpha + K^2 H_4^*(K)\frac{h}{B}\right]$$

$$M_\alpha(K) = \frac{1}{2}\rho U^2 B^2\left[KA_1^*(K)\frac{\dot{h}}{U} + KA_2^*(K)\frac{B\dot{\alpha}}{U} + K^2 A_3^*(K)\alpha + K^2 A_4^*(K)\frac{h}{B}\right]$$

where $K = \dfrac{B\omega}{U}$ (reduced frequency); B: characteristic dimension;

and H_i^*, A_i^* are nondimensional functions of K (Scanlan's flutter derivatives).

Since the random buffeting load action on a structure can be considered as the superposition of harmonic loads, in the linear hypotheses the vibrations of a structure can be seen as the superposition of harmonic responses induced by them, with each oscillation inducing an elementary self-excited load expressed by the previous equations.

b. *Buffeting forces*: for turbulence intensities typical of winds in the atmospheric boundary layer, and for turbulence components with frequency of interest, it is possible to assume that the squares and products of the velocity fluctuations are negligible with respect to the square of mean velocity U and that the aerodynamic coefficients C_D, C_L, C_M are independent of frequency.

So the expression of buffeting forces of the quasi-steady theory are acceptable and the drag, lift, moment loads can be expressed as follows (small oscillations):

$$D(t) = \frac{1}{2}\rho B C_D(\alpha_0)\frac{A}{B}\left[U + u(x,t)\right]^2 \cong \frac{1}{2}\rho U^2 B C_D(\alpha_0)\frac{A}{B}\left[1 + 2\frac{u(x,t)}{U}\right]$$

$$L(t) = -\frac{1}{2}\rho B C_L(\alpha_0)\frac{A}{B}\left[U + u(x,t)\right]^2 + \left[\left.\frac{dC_L}{d\alpha}\right|_{\alpha=\alpha 0} + \frac{A}{B}C_D(\alpha_0)\right]\frac{w(x,t)}{U} \cong$$

$$\cong -\frac{1}{2}\rho U^2 B C_L(\alpha_0)\frac{A}{B}\left[1 + 2\frac{u(x,t)}{U}\right] + \left[\left.\frac{dC_L}{d\alpha}\right|_{\alpha=\alpha 0} + \frac{A}{B}C_D(\alpha_0)\right]\frac{w(x,t)}{U}$$

$$M(t) = \frac{1}{2}\rho B^2\left[C_M(\alpha_0) + C_D(\alpha_0)\frac{Ar}{B^2}\right]\left[U + u(x,t)\right]^2 + \left.\frac{dC_M}{d\alpha}\right|_{\alpha=\alpha 0}\frac{w(x,t)}{U} \cong$$

$$\cong \frac{1}{2}\rho U^2 B^2\left[C_M(\alpha_0) + C_D(\alpha_0)\frac{Ar}{B^2}\right]\left[1 + 2\frac{u(x,t)}{U}\right] + \left.\frac{dC_M}{d\alpha}\right|_{\alpha=\alpha 0}\frac{w(x,t)}{U}$$

where

A : across-wind area per unit length projected on the plane normal to the mean wind speed U ;

r : distance between the body and the effective rotation axis;

$U + u(t)$: wind speed component in the along-wind direction;

$w(t)$: wind speed component in the transversal direction;

α_0 : mean angle of attack under wind action (reference of small oscillation).

3.4   Soil-Structure Interaction (SSI)

3.4.1 Types of SSI Effects

The dynamic interaction between soil and structure consists of the exchange of mutual forces between them when dynamic loads excite the system, like earthquake and wind. When such effects are relevant, the structural response must be evaluated including the soil in the mathematical model, because such forces change the motion of soil and structure in respect of the free models.

The interaction between soil and structure can be put in evidence in different ways:

- the soil instability (i.e. soil motion, liquefaction, etc.) leading to instability of the structures;
- the soil deformability, transmitting displacement to foundations and structures;
- the accelerations transmitted by the seismic motion, and the consequent increase of pressure on the foundations;
- the structural motion and the consequent stresses and displacement with possible rupture of the soil.

Concerning the effects of soil deformability, in general the soil motion produces motion of the foundations and of the main structure, changing the reactions and the mutual forces between soil, foundations and structures.

The global response depends on the stiffness, damping, mass of the whole system soil+foundations+structure: the contact pressures between structure and

91

soil are determined by imposing the equations of equilibrium and congruence to the systems structure and foundations (Figure 3.7).
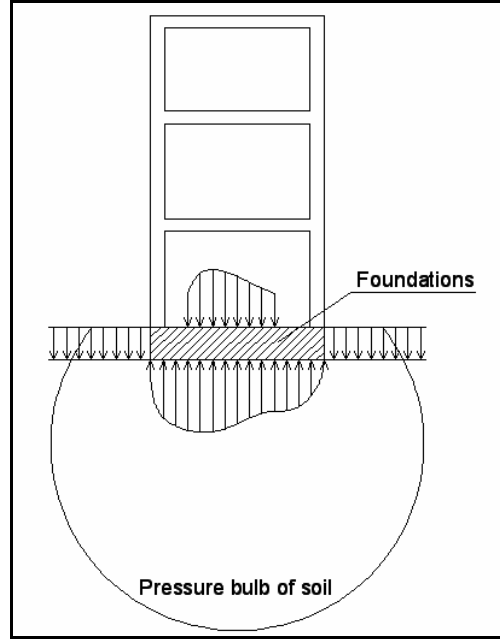
Figure 3.7. System structure+foundations+soil, distribution of actions and contact pressures.

The propagation of the of waves (i.e. seismic) in the soil creates solicitations to the structure that depend on topography, geology, contact between soil and foundation.

In general, for seismic excitation or wind forces, the equations of the motion are

$$\begin{bmatrix} M_{ss} & M_{sf} \\ M_{fs} & M_{ff} \end{bmatrix} \begin{Bmatrix} \ddot{u}_s \\ \ddot{u}_f \end{Bmatrix} + \begin{bmatrix} C_{ss} & C_{sf} \\ C_{fs} & C_{ff} \end{bmatrix} \begin{Bmatrix} \dot{u}_s \\ \dot{u}_f \end{Bmatrix} + \begin{bmatrix} K_{ss} & K_{sf} \\ K_{fs} & K_{ff} \end{bmatrix} \begin{Bmatrix} u_s \\ u_f \end{Bmatrix} = \begin{Bmatrix} W \\ E \end{Bmatrix}$$

where W is the wind load on the structure, E is the seismic load on the foundation, while s, f, sf represent the structure/foundation/coupled terms.

This schematization neglects the effects of the structure motion on the soil motion and the force E itself.

A primary role in the interaction problem is that of the relative stiffness between the system structure+foundations and the soil. The relative stiffness between structure and foundations governs the distribution of the forces between them and varies during the constructive stages.

If the foundations are stiff the actions transmitted to the soil can be computed by using fixed boundaries, assuming that the structure does not influence the interaction between foundations and soil, while the model used for the soil behaviour does not affect the description of the actions transmitted to the structure by the soil itself.

For flexible foundations the actions transmitted depend on the soil-structure interaction, on the soil model assumed, on the loads and their geometric distribution (Figure 3.8).

When the soil under the structure is stiff, the interaction effects are low or even negligible. Consequently, the seismic loads can be applied directly on the bottom of the structure, hypothesized having a fixed base. The stiffness of the soil, in fact, make the foundation deformations be negligible. In this case the structural response is not dependent on the soil properties, and its modelling can be unnecessary.
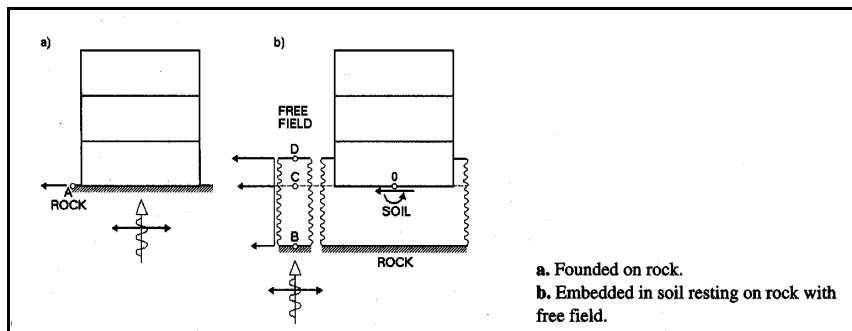
Figure 3.8. a) Foundation on rock b) Foundation on a soil layer on a rock basement.

When the soil under the structure is flexible, the structural response, and the *free field* seismic motion can be modified.

In general the introduction of soil in the mechanical model reduces the fundamental frequency in respect of that obtained by *fixed-base* models.

The soil can change the dynamic response of the structure through three mechanisms of interaction:

- *free field motion*;
- *cinematic interaction*;
- *inertial interaction*.

Free field motion

The free field motion consists of the modification of the surface motion of the soil (for seismic excitation, typically) due to a flexible soil layer. This effects is generally related to the local seismic effects, whose analysis is useful to determine design spectra, dynamic stress and strain, evaluation of liquefaction risk, etc.

A complete local seismic analysis should reproduce the mechanism of rupture in the formations on the rock basement and determine how the motion in surface is transformed in consequence of the mechanical properties of the deeper layers. This evaluation is generally very complex and empirical methods and seismic risk analyses are more common. So the seismic response problem concerns the evaluation of the response of the soil to the basement rock motion.

Kinematical interaction

The shape, the mass and the stiffness of the foundations in general change the motion of the surrounding soil, induced by any dynamic excitation, with alteration of the motion of the structure.

The cinematic interaction consists of the limitation of one or more components of the motion of the free surface due to the foundation stiffness, as represented in Figure 3.9.

In Figure 3.9(a) the flexural stiffness of a plate contrasts the vertical displacements of the free surface; in Figure 3.9.(b) the stiffness of the foundation block contrasts the horizontal displacements, while the axial

stiffness of a plate contrasts the incoherent motion of the free surface Figure 3.9(c).
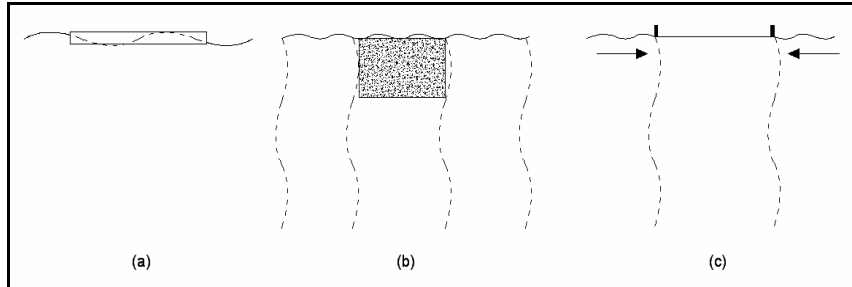
Figure 3.9. Kinematical interaction.

The cinematic interaction can change the modes of a structure.

If we consider a fixed foundation (Figure 3.10) subjected to S waves propagating in vertical direction and having wave length comparable with the foundation height, an inversion of the moment is possible, generating an oscillatory motion in addition to the translation, also if the soil motion is of pure translation. For different frequencies the wave length can be small and no rotations are allowed. The propagation of waves in the horizontal direction can also induce torsion vibration to the foundation.
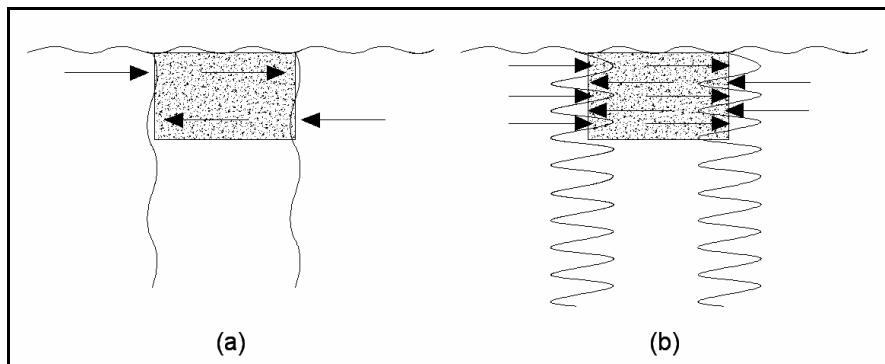
Figure 3.10. Foundation and compatible motion.

95

The relevance of the cinematic interaction is greater when the stiffness of the foundation is very different than the soil, and when the dimensions of the foundations grows. The differences in respect the free field motion can be noticeable.

Inertial interaction

When the structure has great mass, the soil motion induces on it high inertial force, with change also in the relative motion between foundation and soil.

The main effect is the increase of the natural period of the structure, and a decrease of the shear on the base of the structure induced by seismic loads.

The complex of cinematic and inertial interaction describes completely the soil structure interaction.

The most important effects of the SSI can be represented using a single-degree-of-freedom system mounted on a stiff foundation, with no mass and on an elastic soil, as represented in Figure 3.11(a).

The structure has mass m, stiffness k and a damping coefficient c.

If the supporting soil is stiff, the natural frequency of the system is

$$\omega_o = \sqrt{\frac{k}{m}}$$

and the hysteretic damping ratio is $\xi = \dfrac{c\omega_o}{2k}$.

If the supporting soil is soft, the foundations can translate and rotate. The characteristics of the soft structure-soft foundation can be represented by spring and damper elements (Figure 3.11(b)). The foundation dampers represent both the material damping for the inelastic properties of the soil and the radiation damping related to the soil deformation and energy propagation. The damping of the material increases with the level of deformation of the soil, while the geometric radiation damping does not depend on the strain amount. It is often dominant in respect the material damping.

The flexibility of the foundations can make the total displacement of the structure and its foundations be different; it produces a reduction of the natural frequency of the structure in respect of the fixed base assumption, increasing also the effective damping ratio of the structure itself.
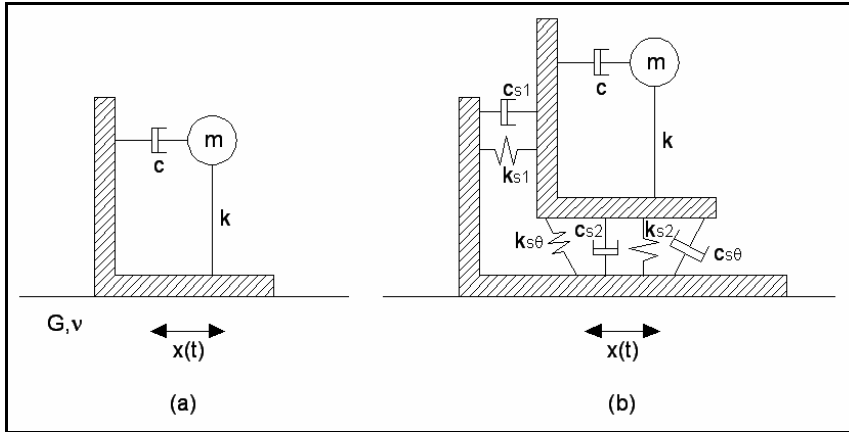
Figure 3.11. Inertial interaction.

The study of the soil-structure interaction is generally conducted assuming for the soil a linear visco-elastic behaviour, where the mechanical properties are modelled by spring and dampers in the *impedance method*.

The *impedance* is a complex variable, where the real part represents the stiffness and the imaginary part represents the geometric damping. If a punctual harmonic load is supposed acting on the surface of a semi-space, the soil motion is harmonic too, with amplitude decreasing with the distance. The impedance is the ratio between force and motion at the point of application of the load. It depends on the frequency of the load, and it is in general unknown for each design situation. The evaluation of the stiffness is conducted iteratively, by the use of impedance tables in the domain of the frequencies and the study of the harmonic motion of soils; specialist software are available also for stratified layers.

The damping is computed mode by mode to account the dependence on the frequency, and proper corrections are done to account also the material damping and also reductions to consider the stratification instead of the theoretical radiation in a semi-infinite homogeneous elastic domain.

97

There are also formulations that allow the representation of the soil by distribution of masses, springs and dampers that let avoid the impedance evaluation and the dependence on frequency.

3.4.2 Constitutive Law and Dissipative Effects for Soils

A relevant aspect in the interaction is the dissipation of energy inserted in the system (by seismic loads or by the structural vibrations induced by wind): the dissipation depends on hysteresys of the material, especially for high levels of stress and strains, and the radial propagation (radiation) of waves in the semi-space. In fact in a linear homogeneous and elastic mean the waves run with constant amplitude, but in the real soil they decrease the amplitude during the propagation. Some of the propagating energy is converted in heat, and such conversion is paid in decrease of the wave amplitude.

The viscous nature of the materials of the structure and soil is to be taken into account in the interaction problems: the solution becomes time-dependent, with re-distribution of stresses and pressure, and also variation in the stiffness of the soil for primary consolidation effects.

The viscosity of materials changes also the stress on structures (increasing) and soil (decreasing), and so also the relative stiffness ratio.

When the knowledge of soil properties is not complete, simplifications on the hypotheses are accepted: homogeneous, isotropic and elastic behaviour can be suitable for certain problems, but unfeasible for research on soil-structure interaction.

Furthermore the modelling of possible anisotropies and non-homogeneities of soil are difficult to be modelled and probabilistic methods can be more feasible.

The modelling of the soil properties, by spring+dampers or by finite elements, require that the parameters (i.e.< Young modulus, Poisson ratio, damping, density) are determined. Experimental tests use cyclic loads or propagation of waves to asses the dynamic behaviour of soils.

In general the shear modulus G decreases with the distortion γ, while the damping increases.

The most common models representing the response are the nonlinear elastic (i.e. response of rocks, at amplitude of deformation of $10^{-7} - 10^{-5}$ and frequency of some thousand of Hertz), the linear visco-elastic and the elasto-plastic.

Visco-elastic models

For moderate levels of strain, the behaviour of soils can be represented by equivalent linear visco-elastic models. This kind of model account the damping during the propagation of the waves and the energetic dissipation inside the soil, which is not a real linear phenomenon but it can be sufficient to describe the global damping for a range of frequencies and for a given amplitude.

Experimental procedures have been established to characterize the parameters of the model.

The use of linear visco-elastic models let establish relations between attenuation of waves and frequency. In Figure 3.12 it is represented the attenuation as function of the frequency for different models.

The expressions of the attenuation as function of frequency are reported in Table 3.VI and Figure 3.12, where E:Young modulus; ω:circular frequency; η: coefficient of viscosity.

Rheologic models	Attenuation Q^{-1}
Maxwell	$\dfrac{E}{\omega\eta}$
Kelvin-Voigt	$\dfrac{\omega\eta}{E}$
Zener	$\dfrac{\omega\eta E}{E_V(E+E_V)+\omega^2\eta^2}$
Maxwell generalized	$\dfrac{E(\eta_1+\eta_2)}{\eta_1^2}\dfrac{1}{\omega}+\dfrac{\eta_2}{E}\omega$

Table 3.VI. Rheologic models and attenuations.

99
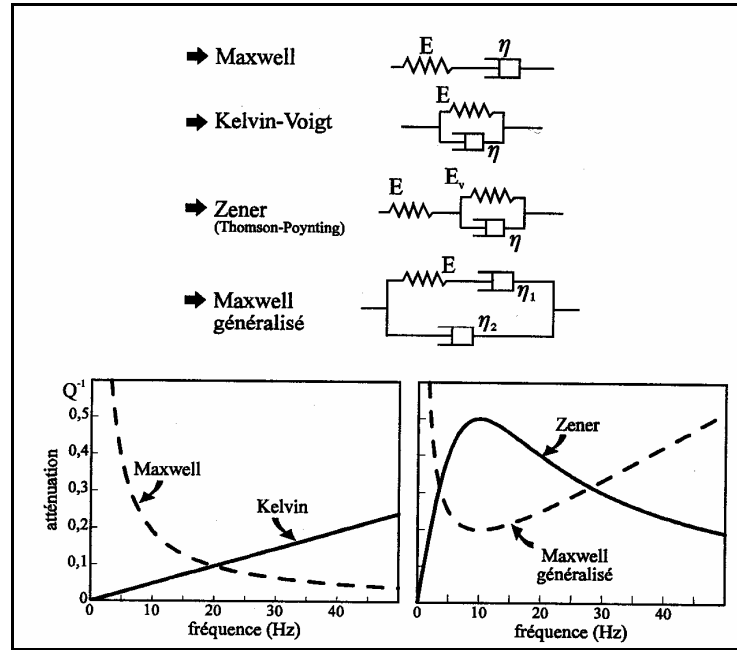
Figure 3.12. Rheologic models and attenuation curves (Mestat & Prat, 1999).

The models of Maxwell and Maxwell generalized have infinite attenuation at frequency zero (no instantaneous elastic response). The models of Zener and Maxwell generalized have maximum/minimum attenuation in a well-defined frequency bandwidth.

The expression of the attenuation for the Maxwell generalized is for low damping $(\xi \leq 20\%)$ appreciatively the same of the Rayleigh damping.

$$\text{If } [C] = a[K] + b[M] \Rightarrow Q^{-1} \approx 2\xi = a\omega + \frac{b}{\omega}.$$

Elasto-plastic models

The cyclic dynamic behaviour of the soil depends on the amplitude of the solicitation, the velocity of loads, the load time-history, the degree of saturation, etc.

Several models have been proposed, keeping into account such dependences.

A hyperbolic hysteretic cyclic model is that of Hardin & Drnevich, represented in Figure 3.13.
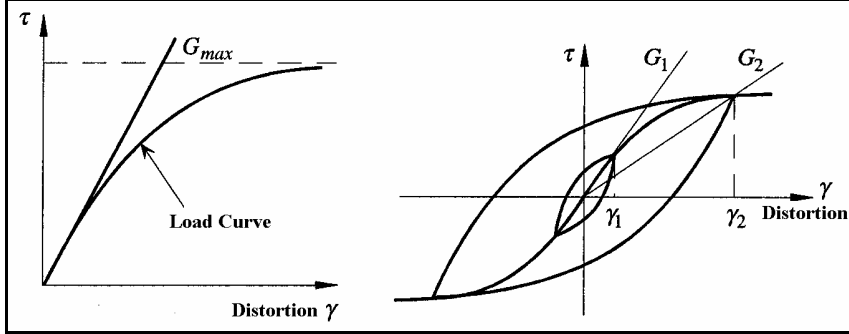
Figure 3.13. Hysteretic model.

For a single load cycle the soil response can be represented by two parameters: the shear modulus G and the damping ratio D (Figure 3.14).

These parameters vary with the shear strain γ impressed to the element; three range of behaviour can be identified: small/medium/large strain (Figure 3.15).

Starting from the model of Hardin & Drnevich, Heitz proposed a numerical method for the propagation of the waves in the soil. The expression of the relationship between the shear stress τ and the distortion γ is

$$\tau = G(\gamma)\gamma + \eta(\gamma)\dot{\gamma}$$

Assuming a nonlinear visco-elastic behaviour close to the hysteretic model, the G modulus and the viscosity η are expressed as function of distance x and frequency f:

$$G(x,f) = G_0[\delta(f) - \Phi(x,f)]$$

$$\eta(x,f) = \frac{2G_0}{\omega}[\beta_0\delta(f) - (\beta_m - \beta_0)\Phi(x,f)]$$

101
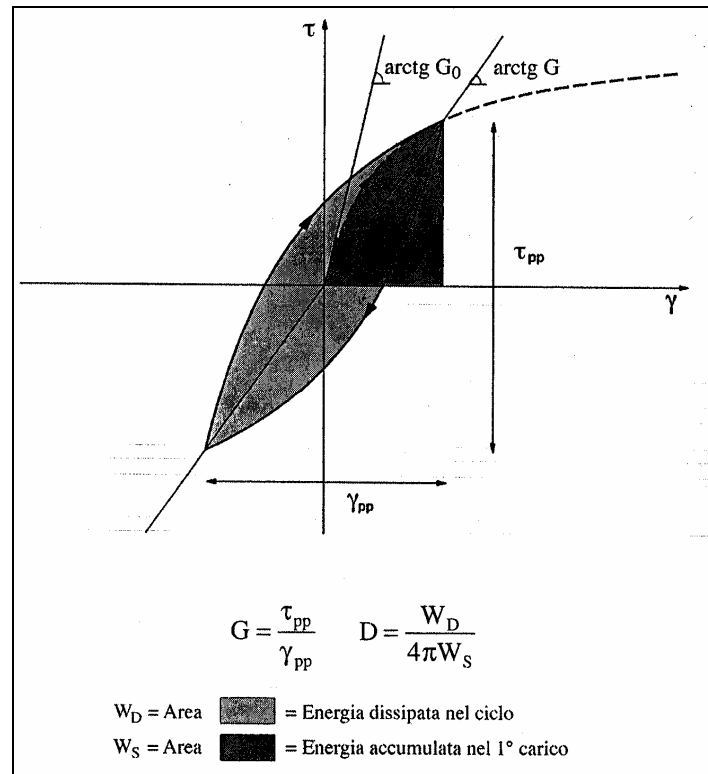
Figure 3.14. Definition of the shear stiffness (G) and damping ratio (D) in a shear load cycle (Caputo, 1995).
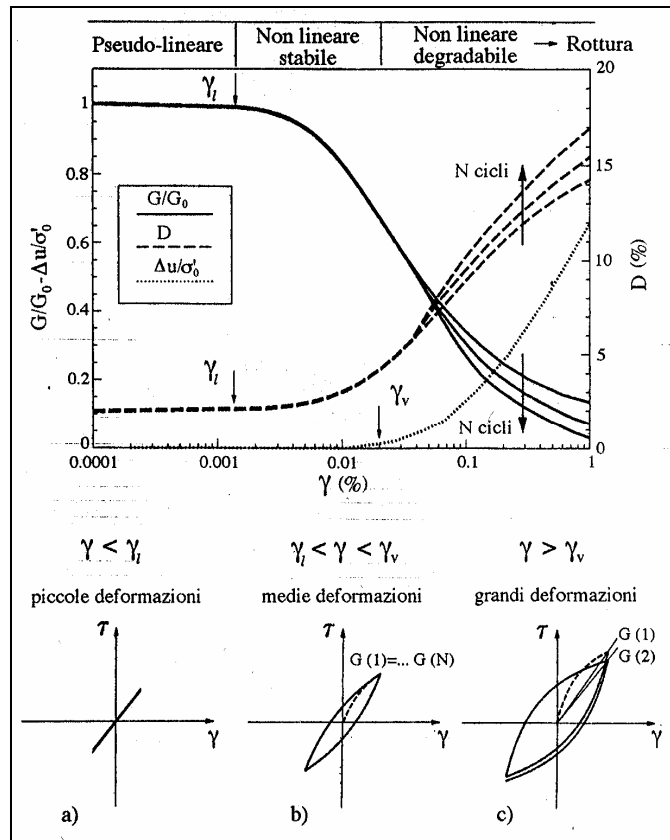
Figure 3.15. Levels of strain and mechanical behaviour of soil in case of cyclic shear load (Caputo, 1995).

3.4.3 SSI Modelling and Methods of Solution

The most attractive approach to study the soil-structure interaction is the finite element method. It requires a suitable modelling of the soil involved by the structure.

The interaction phenomena between soil and structure in general involve both the seismic and the wind response.

Two groups of procedures for the analysis of the interaction are available:

103

- the direct method;
- the substructure method.

The analyses can be conducted in the time or in the frequency domain.

In the frequency domain the excitation and the response are decomposed in series of Fourier and the response is determined for each frequency.

The main disadvantage of the frequency domain analyses is that they are linear and nonlinear properties of structure and soil behaviour are neglected.

In the domain of frequency it is possible to use the complex modulus to simulate the hysteretic damping, for linear elastic means, for which the superposition of effects must be applied.

Possible nonlinearities can also be kept into account by equivalent linear analyses, approximating the nonlinear response.

In the time domain the nonlinearities can be better accounted, also because only in this domain the semi-infinite soil models can be represented.

The most attractive approach to analyze the SSI consists of the modelling of the system soil-foundations-structure by a finite element discretization.

This approach has some difficulties, related to the indefinite dimension of the soil, and the simulations should account it.

Under static loads it is sufficient to model a small portion of the soil involved; for dynamic loads the boundaries of the model reflect the waves and do not allow the radiation and the dissipation of the energy (Figure 3.16).

This circumstance requires that the modelling reproduce the non-finite domain of interaction, and the radiation of the waves through the mean. If it is not accounted, an overestimation of the structural response is produced.

A possible solution is the realizing of large size meshes, paid with higher computational costs. The use of high order finite elements let reduce the number of elements and increase their size, but the high-frequency components can be suppressed if too large elements are employed.

The common methods for the study of the SSI effects are distinguished in (Figure 3.17):

- *substructure methods*.
- *direct methods*.

Both the methods use a regular and an irregular zone, separated by a layer on which the seismic excitation is applied.
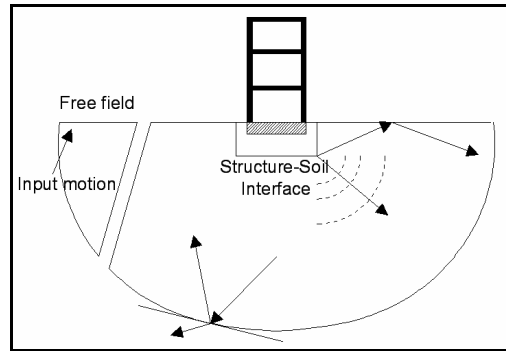
Figure 3.16. Wave radiation and artificial boundary.
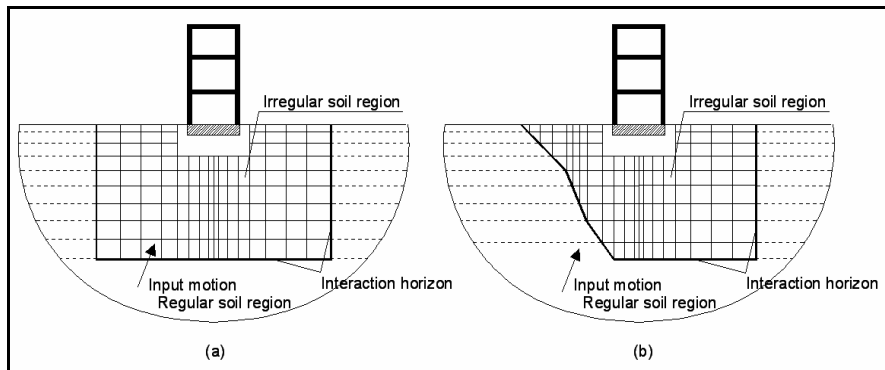
Figure 3.17. Model for the *direct method* (a) and model for the *substructure method* (b).

Substructure Method

The substructure method consists of the decoupling of the problem into two sub-problem: soil and structure are separated. For each substructure the dynamic equilibrium equations are written; the global equilibrium and the congruence on the common nodes to the two systems are imposed.

105

The analysis is divided into three steps (Figure 3.18):
1. the input motion to the foundations is considered, and the cinematic interaction effects;
2. the impedance function is determined; it describes the stiffness and the damping effects of the SSI, in terms of ratio between the amplitude of harmonic force with frequency ω and that of the foundation displacement;
3. the response of the structure with a dynamic impedance matrix as boundary and subjected to the forces corresponding to the accelerations of the cinematic interaction.

Direct method

In the direct approach an opportune portion of soil under the structure is modelled, i.e. by finite elements, on a contour with proper boundaries to simulate the soil neglected. (Figure 3.18). This approach is suitable for large structures and soil extensions involved.

The size of the soil mesh is related to the load and the structural size.
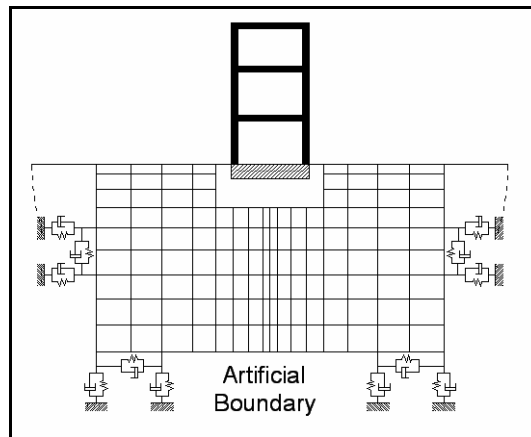
Figure 3.18. Finite element mesh and artificial boundary for the *direct method*.

The main problem is the reproduction of the dissipation of the energy in the three directions. It follows that an accurate modelling of the boundaries must be

done. The modelling of infinite soil is a problem to be fronted for any numerical method used for the solution. The methods of the integral equations let the modelling of the infinite mean, while the finite element methods require that the reflection phenomena are reduced. In fact even if one enlarges the model size, he cannot be sure about the reflection of the waves by the boundaries. This problem is fronted by two main techniques (Figure 3.19):

-   the use of *adsorbing elements*, connected to the border of the mesh: they adsorb an amount of incident energy and reduce the amplitude of the reflected wave. The technique of the adsorbing elements allow the adsorption of the energy in the border of the mesh. The characteristics (stiffness, damping) of the element must be calibrated according to the soil and excitation properties.
-   the use of *infinite elements*, that use functions of decrease of the amplitude in the element formulation.
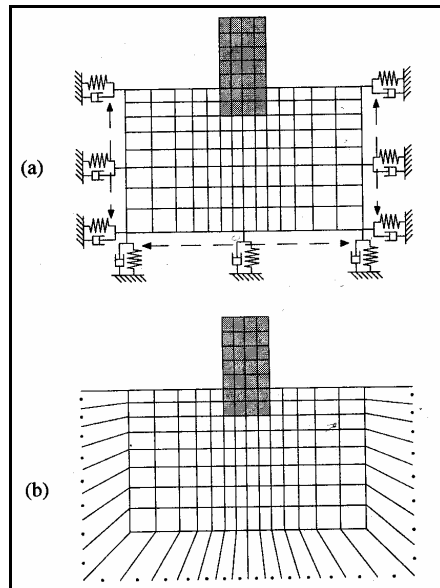
Figure 3.19. Elimination of reflection: (a) adsorbent elements; (b): infinite elements (Mestat & Prat, 1999).

107

In the finite element approach, more than one constraint can be used for the borders (Figure 3.20):

- Simple constraints;
- Adsorbing boundary elements; Infinite elements;
- Rheologic models (i.e. *viscous boundaries*, proposed at first by Lysmer and Kuhlemeyer (1969);
- Boundary elements, introduced by Lysmer and Waas (1972).
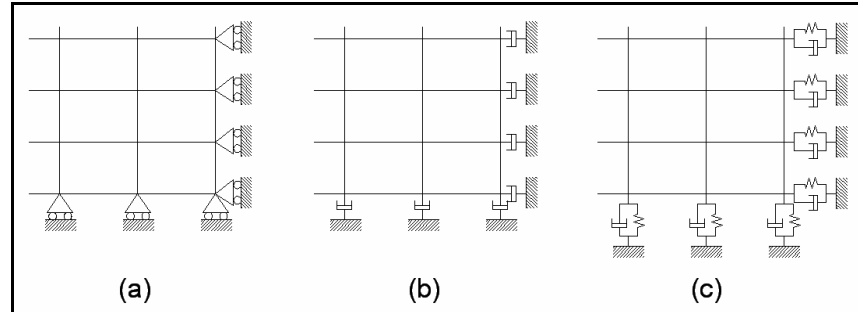
Figure 3.20. Types of boundaries.(a): simple constraints; (b): viscous constraints; (c): congruent constraints.

For *simple constraints* forces or displacements are imposed. They are used to fix some degrees of freedom of the mesh. This kind of boundary does not adsorb energy, that is kept inside the model. Yet it is possible that the waves are reflected in the adjacencies of the boundaries and surface waves are determined, moving in the contour surfaces, without coming back to the structure. In this case the foundation is not by the loss of radiation of the model. This phenomenon can be useful but requires that the boundaries are not close to the SSI zone.

If the frequency of excitation are lower than the natural frequency of the layer the radiation problem is not relevant (i.e. wave motion and off-shore structures). For the seismic case the frequency bandwidth is larger ($\left(\approx 0.3 - 0.15 Hz \right)$ and the benefit of the phenomenon concerns a portion of the band.

The use of simple boundaries is helpful when the internal damping of the soil is high; in this case the energy content of the reflected waves to the SSI zone are negligible (i.e. soil with high deformation such as in case of intense seismic excitation)

Adsorbing boundary elements:

In general the enlarging of the mesh and the use of element such as the adsorbent elements or the infinite elements allow the reduction of the reflection on the border of the mesh and the disturb of the exact solution.

Let consider a of 1D finite element model, with horizontal displacement imposed at the extreme border of the mesh (Figure 3.21), and a parallel spring+damper at the end.
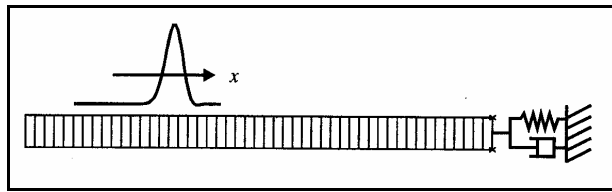
Figure 3.21. Adsorbent element (1D) (Mestat & Prat, 1999).

The mechanical properties of the boundary elements are calibrated according to the soil and the solicitation characteristics, in such a way to compensate the impedance effects in the border and to adsorb the energy of deformation due to the solicitation.

If a positive unit displacement incident wave is imposed, different response in terms of reflected wave is expected for different damping. For low damping the reflected wave is still positive (undisturbed in case of free border), while for strong damping it is negative (approximating -1 for infinitely rigid border) (Figure 3.22).
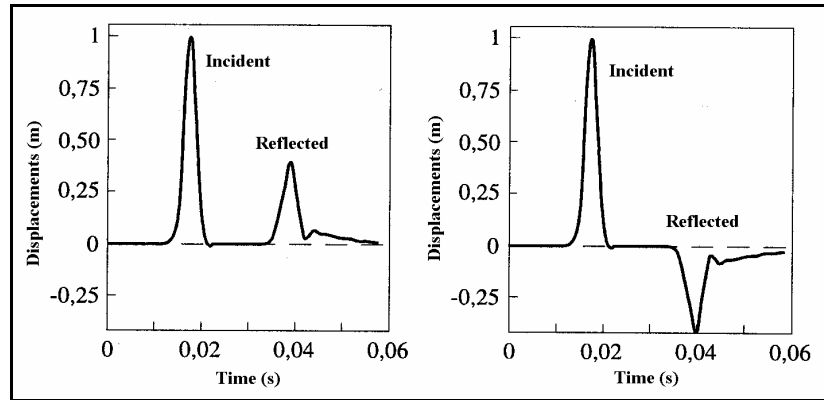
Figure 3.22. Reflection of waves in FEM and boundary element damping. (a): Low damping; (b): High damping (Mestat & Prat, 1999).

The optimal value is that neutralizing the incident wave (Figure 3.23).
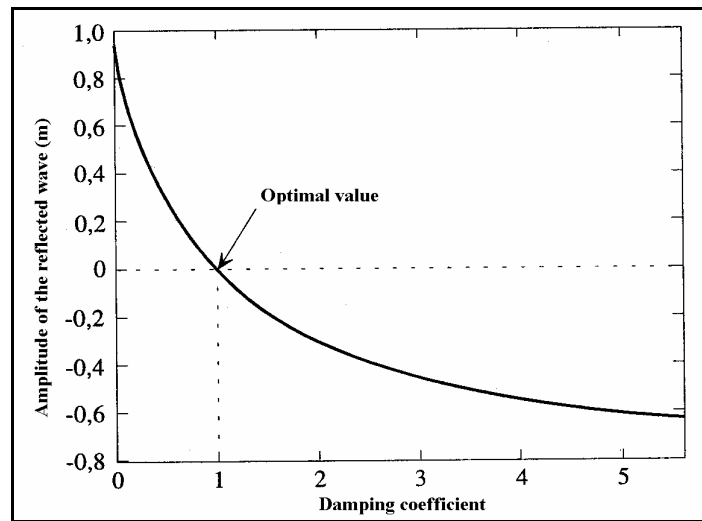
Figure 3.23. Reflection of waves in FEM: Optimal damping of boundary element (Mestat & Prat, 1999).

Chapter 4

STRUCTURAL CONTROL, TUNED MASS DAMPERS AND SUSPENSION BRIDGES

- Classification of Structural Control: Passive/Active/Hybrid/Semiactive Control

- Tuned Mass Dampers (TMD)
  - Physical Properties and Response – Harmonic Excitation
  - Transfer Functions
  - Types of Excitation and Response: Criteria of Optimal Design
  - Equivalence SDOF-MDOF
  - Multi-TMD Systems (MTMD)

- Structural Control and Suspension Bridges
  - The Experience of the Akashi-Kaikyo Bridge: Control of the Pylon

Abstract

This Chapter outlines the main strategies actually available for the Structural Control, paying particular attention to passive systems such as Tuned Mass Dampers (TMD).

The physical properties of TMDs, their response to harmonic and white noise excitation and criteria for optimal design are resumed, with also an introduction to the transfer function characterization of the multi-device configuration adopted in the application of Chapter 5.

In the third part of the Chapter the role of structural Control in the design of cable-supported bridge is reported, with also a reference to the mitigation of the pylon response of the Akashi Kaikyo Bridge in Japan.

4.1 Introduction

As previously mentioned, the design of civil structures is conducted in order to achieve specified performance or goals in terms of safety, serviceability and robustness against all the likely load scenarios (*scenarios of contingency*) that could affect the structure.

The actions such as earthquake, wind, traffic in general have dynamic and stochastic nature, that must be taken into account leaving the traditional approach of design in the static field.

Furthermore in the last years the diffusion of slender structures like tall buildings and long span bridges, with small damping capabilities and high deformability, enlarged the dominion of motion-oriented structural problems, where motion and vibrations, proper of serviceability checks, become a more severe requirement than the structural strength, related to Ultimate State Limits.

Slender structures are generally prone to vibrations under wind actions, particularly for vortex-shedding and buffeting phenomena, affecting serviceability, comfort and capable of fatigue damage.

Researches conducted by various academics and industries in the last two decades indicate that the adoption of active, semi-active, passive and hybrid control schemes, using smart materials and devices, offer promising future for the subject matter.

The structural control is a new area of research and development, a meeting point between structural dynamics and control theory, with the challenging ambition of building innovative, flexible and reliable structure.

The traditional design of structure exposed to dynamic loading relies on strengthening strategies, acting on structural mass and stiffness, or on damping strategies, which dissipates energy to survive under severe loads.

Structural control interacts with the dynamical loads transferred to the structure, reducing the amount of forces transferred (base isolation systems), controlling the motion through inertial forces (Tuned Mass Dampers), or increasing the internal dissipation.

In the civil engineering passive control strategies have been successfully employed in the mitigation of seismic hazards, and for the reduction of the wind response.

At the moment alternative strategies have not found the same diffusion, because of the higher costs of use and maintenance and of the lower reliability. In most cases the active strategies are allowed if they assure a redundant resource, and guarantee the same performance of passive strategies in case of out-of-service.

4.2   Classification and Basic Principles of Structural Control

In the following Paragraphs a classification of the possible strategies used to control the structural response is presented.

The feedback design objectives for structural systems can be stated in terms of keeping the response (stresses, strains, displacements and accelerations - *outputs* yi, i= 1,2,3...) at a specified set of locations within the structure below specified bounds in the presence of any disturbances (winds, earthquakes etc.) less than a certain size.

The structural control strategies are distinguished into four main families.

The basic principles of the control schemes above can be expressed using as sample a SDOF system, with mass m, stiffness k and damping c subjected to an earthquake load with ground acceleration $\ddot{x}_g(t)$. If $x(t)$ is the degree of freedom of the system, the equation of the motion is (Figure 4.1(a))

$$m\ddot{x} + c\dot{x} + kx = -m\ddot{x}_g$$

Passive Control strategies

If we add a passive energy dissipation device to the SDOF model, the equation of the motion becomes (Figure 4.1(b))

$$m\ddot{x} + c\dot{x} + kx + \Gamma x = -\left(m + \overline{m}\right)\ddot{x}_g$$

where $\overline{m}$ is the mass of the device and the force transmitted by the device is

Γx, and Γ is a generic integro-differential operator that depends on the device type. The addition of the Γx term modify the structural properties, so that it can be adjust in order to enhance the structural response under dynamic loads.

Passive control systems do not require any external power sources, but impart forces that are developed in response to the natural motion of the structure.

These systems are characterized by their capability to enhance energy dissipation in the structural systems in which they are installed. They encompass materials and device for enhancing damping, stiffness and strength, and are used for seismic hazard mitigation and for structural rehabilitation.

Passive strategies include also base isolation.

Active Control strategies

Active systems has a configuration as in Figure 4.1(c), consisting of sensors, measuring external excitations and/or structural response, controllers, processing the information and computing the control forces according to a given algorithm, actuators, producing the forces for the structure.

If $u(t)$ is the applied control force, the equation of motion of the SDOF system becomes

$$m\ddot{x} + c\dot{x} + kx = -mu(t) - m\ddot{x}_g$$

If we use a feedback configuration in which the control force is designed to be $u(t) = \Gamma x/m$, the equation becomes

$$m\ddot{x} + c\dot{x} + kx + \Gamma x = -m\ddot{x}_g$$

The effect of the control is again a change on the structural properties, but here the term Γx is not fix but is governed by the chosen control law, which can change according to the excitation.

Active systems act simultaneously with the hazardous excitation to enhance the structural behaviour, using control system with one or more external source powers control actuators that apply forces to the structure according to a prescribed algorithm. The signals sent to the actuators are functions of the external loads (forward control), or of the response of the system (feedback control) or of both (feedback-forward control), measured with physical sensors and processed by evaluators/controllers.

115
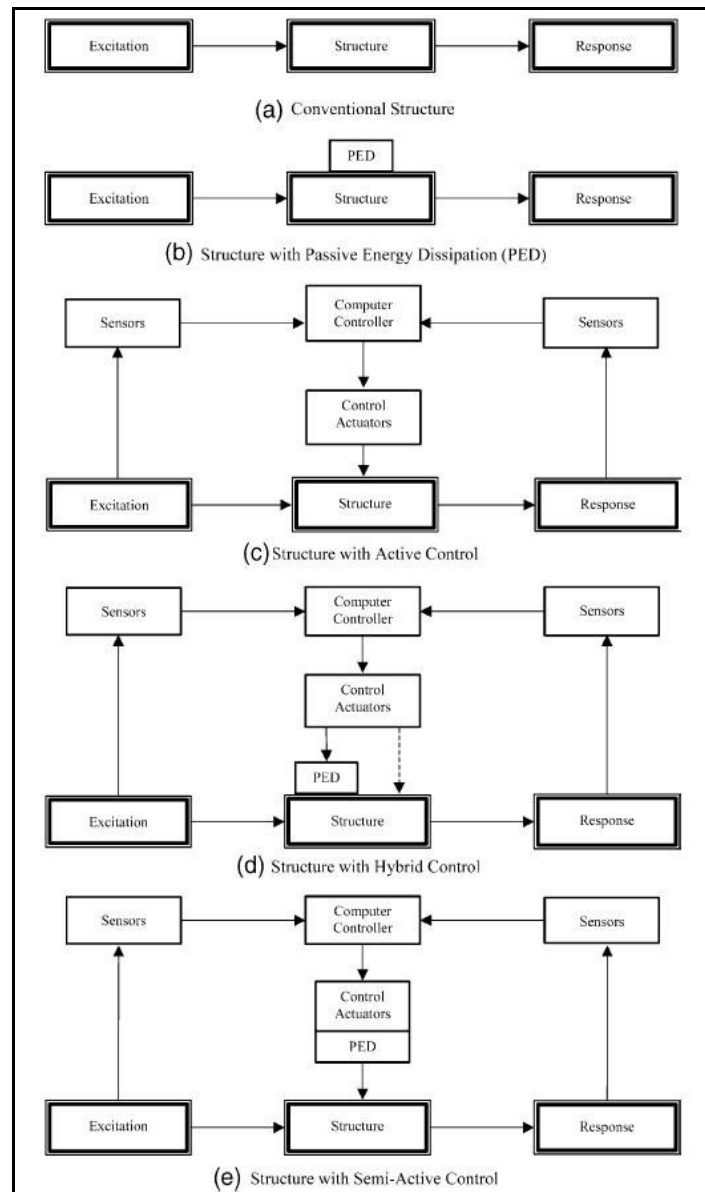
Figure 4.1. Classification of control strategies (Spencer & Soong, 1999).

Hybrid Control strategies

Hybrid control systems combine active and passive control: a portion of the control targets are pursued by the passive system, so that less power resource is involved by active control system (Figure 4.1(d)).

Semi-active Control strategies

Semi-active control has also both the characteristics of active and passive, but the actuators do not insert *directly* energy into the structure, and so work as time-varying dampers: bounded-input/bounded-output guarantee system stability (Figure 4.1e).

These strategies use passive systems that are in the mean time controllable by active control systems, and with smaller external energy requirements.

A benefit of hybrid and semi-active control systems is that in the case of power failure, the passive components of the control continue to offer some degree of protection, unlike the fully active control systems.

Most of the application in civil structures are passive, for the lower costs of installation and maintenance and for their high reliability; yet it has been demonstrated that the smart strategies, with active, semi-active and hybrid control schemes, where feedback control is implemented, can improve significantly the structural response under dynamic loading.

The Design Specification of challenging structure such as skyscrapers or long-span bridges, may allow and encourage the adoption of active control systems if reliable: in general they must guarantee minimum performance levels also in case of energy fault or out-of-service: in this sense *semi-active* strategies seem to be the most attractive.

4.2.1 Passive Control Systems

When a structure is subjected to dynamic loads and vibrate, it dissipates energy for internal stressing, rubbing, cracking, plastic deformations.

All passive control devices for the reduction of the response increase the energy dissipation by augmenting the damping, or acting on the stiffness or on the strength of the system.

With the advent of new technology and developments in materials science,

117

passive control is likely to become an indispensable tool for protecting structures and facilitating the comfort and safety of human occupants.

Dissipative mechanisms

In what follows, a classification of the main passive mechanisms of energy dissipation and the corresponding devices is presented.

1. ***Inelastic deformation of metals - Metallic Yield Dampers***: they dissipate energy through the development of plastic strains.
    They are used as torsional or flexural beams, U-strip energy dissipators, realized by different materials, from lead to shape-memory alloys. They are long-term reliable, with a stable hysteretic behaviour, and not very sensitive to temperature effects.

2. ***Frictional Dampers***: they use sliding interfaces to dampen the motion of the structure they are embodied in, providing energy dissipation. (i.e. X-braced friction dampers). These devices provide good performance and their behaviour is not significantly affected by loading amplitude, frequency, or even the number of loading cycles. Generally friction devices have rectangular hystereticloops similar to the characteristics of the Coulomb friction.

Both frictional and metallic yield dampers have good energy dissipations characteristics which can be understood from the experimental force-displacement response (hysteretic loop). The area enclosed within the loop is a measure of the amount of dissipated energy. For an effective design employing these devices, the modelling and the characterization of the hysteretic behaviour of these materials under arbitrary cyclic loadings, as in an earthquake, must be done. The non-linear nature of the device requires non-linear structural analyses for the response, regardless of the linearity of the system they are integrated in.

3. ***Viscoelasticity – Visco-elastic and Viscous Fluid Dampers***: they use viscoelastic materials such as copolymers and glassy substances, that dissipate energy through shear deformation and have been found to be effective against seismic and non-seismic vibrations. This, along with the linear behaviour of these materials over a wide range of strain, has made viscoelastic dampers a useful tool for structural engineering.

4. ***Viscoelasticity – Viscous Fluid Dampers***: these compact devices primarily consist of a cylindrical piston immersed in a visco-elastic fluid, containing a number of small orifices through wich the fluid may pass from one side of the piston to the other. The devices (considering stroke and output force) provide a linear viscous response over a broad frequency range and are insensitive to temperature changes. As the piston moves in the fluid, the forces generated by the viscous fluid oppose the motion and are out of phase with displacement.

5. ***Inertial Forces - TMD and TLCD***: they use the motion of secondary masses to dissipate energy. The concept of Tuned Mass Damper was proposed in 1940's by Den Hartog: it consists of a secondary mass with properly tuned spring and damping elements, used to reduce vibrations at the tuned frequency. These systems have a clear efficiency in reducing wind-induced structural vibrations, but their efficiency on reducing the earthquake response is more questionable. In fact they are efficient in reducing the response for resonant ground motions for which they are properly tuned, but the efficiency decreases as the frequency of the ground motion gets away from the structure's natural frequency. Furthermore TMD can only be tuned to a single structural frequency, so that just the first mode of a MDOF system can be reduced, but the higher modes can be relevant too (i.e. if the number of stores of a building increases). At this regard several researchers have proposed the use of multiple tuned mass dampers (MTMD's) tuned to different dominant frequencies. In designing these systems, the engineer is limited also by practical considerations such as the amount of additional mass to provide (in general placed on the top of buildings) and the allowable TMD travel distance. For obtaining an optimal configuration, the designer must select the type of TMD (e.g. spring-mass type, pendulum type, etc.) and pay attention to the friction characteristics of the sliding surface, which determine the minimum level of excitation that the system can respond to.

Similar in concept to TMD's, tuned liquid damper systems (TLD) dissipate energy using a secondary mass in the form of a body of liquid introduced into the structural system and tuned in such a way to act as a dynamic vibration adsorber. They do not require a threshold level of excitation to be activated. The relation between the frequency of vibration and the response is related to the side lengths of the tank. For example, a rectangular tank may be used to dampen a structure with two different fundamental frequencies in two directions. One major difficulty in the design of these systems is the nonlinear for the nature of the liquid sloshing motion, and for the orifices. Installations of these systems in structures, have shown that they are effective in reducing wind-induced vibrations in tall structures.

4.2.2 Active Control Systems

In the last years a growing interest around active/hybrid/semi-active control has been developed, for the coordinated research efforts mainly in Japan and USA, for the promising capabilities of these strategies in enhancing the structural response in respect of those of the traditional strategies.

The development of active control in civil engineering grows thanks to the synergic integration of diverse disciplines, some of which are not within the domain of traditional civil engineering: computer science, data processing, control theory, material science, sensing technology, as well as stochastic processes, structural dynamics, wind and earthquake engineering.

As alluded to earlier, the development of active, hybrid, and semi-active control systems has reached the stage of full-scale applications to actual structures, like in building structures and towers, and also for the erection of bridge towers active systems have been employed.

The observed performance of these full-scale systems subjected to actual wind forces and ground motions and provided information in terms of:

1. validating analytical and simulation procedures used to predict the system performance;
2. verifying complex electronic-digital-servo hydraulic systems under

actual loading conditions;

3. verifying capability of these systems to operate or shutdown under prescribed conditions.

Active systems in general have a configuration as schematized in Figure 4.2, consisting of:

- sensors distributed along the structure to measure external excitations and/or structural response variables, for feedback/forward/feedback-forward control: the information is used to live update the control forces;
- controllers, that process the information and compute the control forces according to a given algorithm (Figure 4.3);
- actuators, powered by external sources and producing the required forces.
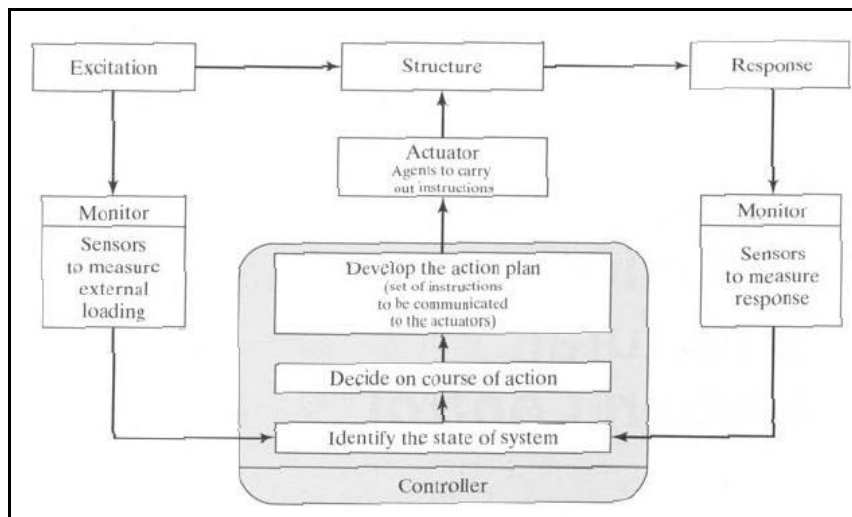
Figure 4.2. Components of an active control system (Avrenli, Gencturk, Keten, Lus, 2004).

The main advantages of active systems in respect of the passive ones consists of

121

1. the possible change of the structural properties according to the excitation;
2. the enhanced effectiveness in the response control;
3. the applicability to multi-hazard mitigation situations (wind, earthquake, impacts…)
4. the possible selectivity of control targets: during non critical times serviceability and comfort algorithms can be used, while during more severe loading algorithms for increased structural safety can be considered.
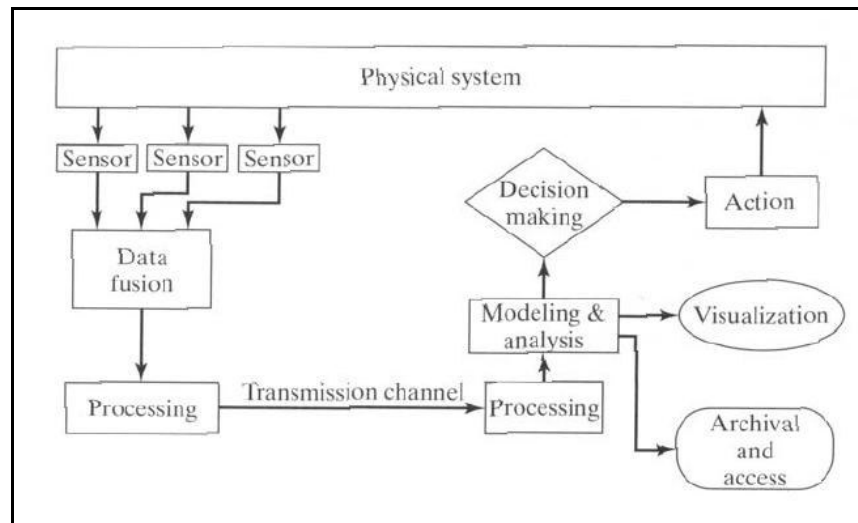
Figure 4.3. Information processing (Avrenli, Gencturk, Keten, Lus, 2004).

Active control can improve the dynamic response of structures, but since there is an input of energy into the system, there is the risk of destabilizing the structure. This occurs when there are considerable modelling errors and the control energy is amply large.

Four are the main types of modelling errors, namely parameter errors, errors in model order, neglected disturbances, neglected non-linearities, associated with

physical properties and disturbances such as earthquake and wind, limited number of sensors and actuators, complexity on actuators behaviours.

No control algorithm can simultaneously deal with all of these error types: *Adaptive Control*, for instance, can treat parameter errors, while a well chosen model reduction approach can get around the model order errors.

Several control schemes have been implemented within the branch of active control, and each has its own advantages and disadvantages:

- <u>Optimal Control</u> involves minimizing or maximizing a specified performance measure, so as to get the "best" design by some criterion; this scheme can be used to find the optimal mix of passive and active control in order to minimize the active control energy and to optimize both the structure and control parameters of interest;

- <u>Stochastic Control</u>, is also frequently employed by civil engineers for the importance of uncertainties on modelling and of reliability methods of design utilized in many engineering fields, from hydraulics to structural dynamics.

  Stochastic control encompasses a number of functions, such as:

  • Determination of a control policy for a dynamic system subject to random disturbances, with possible noisy measurement outputs, in order to attain some objective;

  • Estimation of the states of a dynamic system from incomplete and noisy output measurements;

  • Synthesis of a controller matching some prescribed second-order statistics;

  • Assessment of the robustness of a dynamic system to uncertainty in its parameters and inputs;

  • System and parameter identification.

  The stochastic models are especially useful in modelling the uncertainties inherent in the structure and the exogenous forces that it is subjected to, as well as that uncertainty brought about by the sensors used for measurement in active control systems.

- Adaptive Control, utilizes controllers with adjustable parameters, incorporating a mechanism for the fine-tuning of these parameters. This scheme is generally used to control plants whose parameters are unknown or uncertain.

  1.   Direct and indirect control are utilized in adaptive control: the former adjusts the parameters so as to minimize the error between the measured and desired outputs, while the other utilizes online estimations for the modification.

  2.   Intelligent control, proposed by Fu in 1971 for the enhancement of automatic control systems, encompasses artificial neural networks or fuzzy logic to deal with uncertain, qualitative and incomplete information. Neural networks are common in modelling and control of dynamic systems: they learn by experience and utilize neurocontrollers to change the system response. Fuzzy logic uses imprecise data and "soft" computing techniques to reason and derive control actions.

  3.   Sliding mode control, is another method considered in the context of adaptive control: a hypersurface, called the sliding surface, is defined in the state space and the error between the measured and desired response is zero when the state falls on the sliding surface. Different control laws dominate different regions of the state space, so this method is also considered a variable structural control scheme.

- Robust control, focuses on the issues of performance and stability in the presence of uncertainty in system parameters and exogenous inputs.

All of these control schemes discussed under the name of active structural control have their strengths and weaknesses based on the area of application and system characteristics that can't be solely governed by the control parameters, such as hysterisis and nonlinearity.

4.2.3 Hybrid Control Systems

A hybrid control system employs passive and active devices combined, using the advantages of both systems and compensating for the limitations that exist with each system acting alone. Due to this increase in reliability, most of the

structures that have been built with a feedback control system have hybrid configurations.

Until now, research in this area has primarily involved hybrid mass damper systems and active base isolation systems.

Hybrid Mass Dampers (HMD) are the most common control devices employed in full-scale civil engineering applications: they combine a Tuned Mass Damper (TMD) and an active control actuator: while the TMD's natural motion significantly helps with the dynamics of the system, the forces from the active element boost the efficiency of the system and makes it more adept in reacting robustly to changes in the dynamic characteristics of the structure. In addition to this, the forces and energy requirements are significantly reduced compared to an AMD (Active Mass Damper) system acting alone to put out a comparable performance. The use of passive Tuned Liquid Dampers working in conjunction with an active actuator is another possible option.

In case of severe constraints such as space limitations, the use of HMD can be precluded: in these cases the recourse to fully active systems such as Active Mass Dampers (AMD) can be the most convenient or feasible choice.

Hybrid base isolation consists of a passive base-isolation system combined with a supplementary control actuator to manage a higher level of performance in terms of inter-story drift and maximum base displacement, without a major increase in the cost.

4.2.4 Semi-active Control Systems

Extensive studies have indicated that appropriately implemented semi-active systems perform significantly better than passive devices and have the potential to achieve the majority of the performance of fully active systems, thus allowing for the possibility of effective response reduction during a wide array of dynamic loading conditions.

The inability of active systems to operate in cases of power failure has been a major source of criticism for the implementation of these systems alone in structures. Even with the use of hybrid schemes, the full capacity of the system cannot be available during power failure, which makes these systems inefficient

in cases of major earthquakes. Yet as stated before, passive systems do not require external energy, but they are not as effective in reducing responses as active systems. Appropriately designed semi-active systems have shown great promise in serving that purpose and have the capability of operating on battery power, which makes them the favoured control technology for the near-term implementations.

Providing the adaptability of active and hybrid control systems with much lower energy requirements is not the only benefit of semi-active control devices: in fact these devices do not bring in any mechanical energy into the system, hence wouldn't by themselves cause any destabilization. Such systems are in general compact, reliable and economic.

Various semi-active devices have been developed:
- controllable friction devices, that utilize forces generated by surface friction to dissipate vibratory energy in a structural system; the force at the interface can be changed by adjusting the controllable slippage amount;
- variable-stiffness devices;
- controllable impact dampers;
- controllable tuned liquid dampers;
- variable orifice fluid dampers, that have controllable valves that can be used to alter the resistance to flow of a conventional hydraulic fluid damper;
- controllable fluid dampers, that have a similar working principle of the variable orifice dampers, but differ in the control methodology used: they do not contain any valves or moving parts other than the piston, and rather than changing the flow conditions of the fluid through valves or orifices, these devices operate through the utilization of fluids that can have adaptable flow characteristics. Two classes of fluids, called *electro-rheological (ER)* or *magnetorheological (MR) fluids*, have the ability to transform from a free-flowing, linear viscous fluid to a semisolid with a controllable yield strength when exposed to either a

magnetic (MR fluids) or an electric (ER fluids) field. In absence of any fields, these fluids flow freely and behave as Newtonian, while when the field is applied, a common model used to describe their behaviour is the Bingham plastic model.

In this model the plastic viscosity is defined as the slope of the measured shear stress versus shear strain rate data. The total yield stress is given by

$$\tau = \tau_{y(field)}\,\mathrm{sgn}(\dot{\gamma}) + \eta_p \cdot \dot{\gamma}$$

where

$\tau_{y(field)}$: yield stress caused by the applied field; $\dot{\gamma}$: shear strain rate;

η_p : plastic viscosity, defined as the slope of measured stress versus shear strain rate data.

The transition can happen amazingly fast, in a few milliseconds, which enables construction of devices with high bandwidth. Their ease of implementation, insensitivity to impurities and low voltage requirements make these devices highly practical.

4.3   Tuned Mass Dampers

A tuned mass damper (TMD) is a device consisting of a mass, a spring and a damper attached to a structure and tuned to a particular structural frequency in order to reduce the structural response under dynamic excitation: when that frequency is excited, the damper resonate out of phase with the structural motion, and dissipates energy through the inertia forces exerted on the structure. The concept of TMD was first applied by Frahm in 1909 to reduce the rolling motion of ships and ship hull vibrations.

The theory of TMD was presented later by Ormondroyd and Den Hartog (1928), and the discussion of optimal tuning and damping parameters was developed by Den Hartog in "Mechanical Vibrations" in 1940, with regard to single-degree-of-freedom systems (SDOF) subjected to harmonic force excitation. Warburton and Ayorinde (1980) have derived the optimum damper

parameters using Den Hartog's procedure for base-acceleration for all the input frequencies, and for other kinds of harmonic excitation.

Den Hartog's solution has been extended by Wiesner for single degree of freedom systems subjected to white noise wind excitation, and by Wirsching et al., Kaynia et al. for similar systems subjected to white noise ground excitation.

Extensions of the theory of TMDs has been investigated also by Randall et al. (1981), Warburton (1981,1982), Tsai and Lin (1993), in order to determine explicit formulae for the optimum parameters and different types of excitation. Fujino and Abe (1993) derived optimal TMD parameters under various types of loading using a perturbation technique.
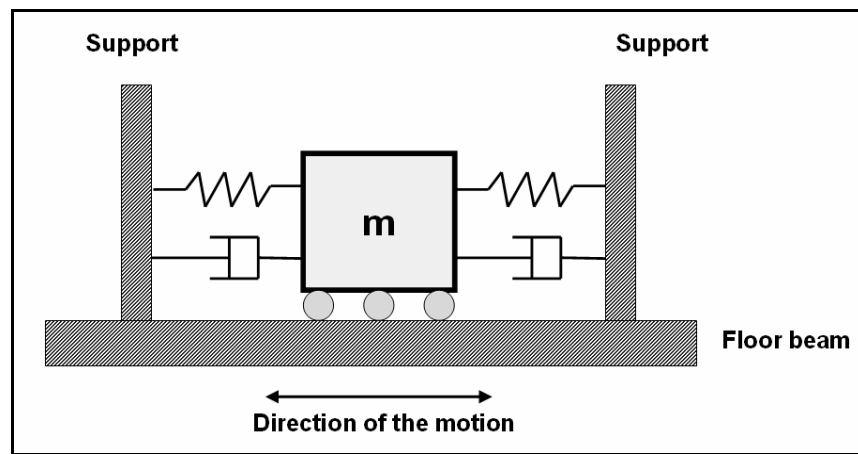
Figure 4.4. Example of translational TMD.

4.3.1 Physical Properties: Response and Efficiency under Harmonic Excitation

Undamped systems – harmonic force exciting

The behaviour of an undamped single-degree-of-freedom system (SDOF), with mass M and stiffness K, depends on its dynamic properties: if it is subjected

to sinusoidal force with circular frequency ω very close or even coincident with the structural frequency $\Omega = \sqrt{K/M}$, resonance phenomenon occurs. This growing and undesirable motion can be prevented by changing the stiffness of the spring (or the mass) or the exciting frequency in order to avoid their coincidence.

An alternative method to prevent resonance or excessive vibrations consists of the introduction of vibration absorber: it consists of a vibratory system k, m attached to the main mass M: the system has a degree-of-freedom and a resonant frequency more.
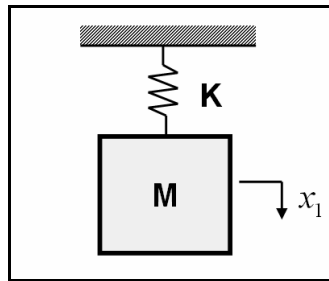
Figure 4.5. Undamped mass.
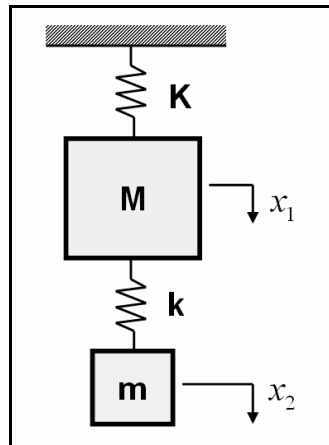
Figure 4.6. Two d.o.f. system.

129

Let's consider a so composed two-degrees-of-freedom-system whose main mass M is subjected to a sinusoidal force $P = P_o \sin \omega t$.

The equations of the motion of the system are

$$\begin{bmatrix} M & 0 \\ 0 & m \end{bmatrix} \begin{Bmatrix} \ddot{x}_1 \\ \ddot{x}_2 \end{Bmatrix} + \begin{bmatrix} K+k & -k \\ -k & k \end{bmatrix} \begin{Bmatrix} x_1 \\ x_2 \end{Bmatrix} = \begin{Bmatrix} P_0 \sin \omega t \\ 0 \end{Bmatrix}$$

Since in the equations do not contain the first derivatives $\dot{x}$, the forced vibration can be expressed by pure sinusoidal functions:

$$\begin{cases} x_1 = \hat{x}_1 \sin \omega t \\ x_2 = \hat{x}_2 \sin \omega t \end{cases}$$

By substituting in the previous equations and dividing by $\sin \omega t$ we obtain algebraic equations:

$$\begin{cases} \hat{x}_1 \left(-M\omega^2 + K + k \right) - k\hat{x}_2 = P_o \\ -k\hat{x}_1 + \hat{x}_2 \left(-m\omega^2 + k \right) = 0 \end{cases}$$

The previous equations lead to the following dimensionless relations (amplification factors):

$$\begin{cases} \dfrac{\hat{x}_1}{x_{st}} = \dfrac{1 - \omega^2 / \omega_a^2}{\left(1 - \dfrac{\omega^2}{\omega_a^2} \right)\left(1 + \dfrac{k}{K} - \dfrac{\omega^2}{\Omega^2} \right) - \dfrac{k}{K}} = \dfrac{1 - \omega^2 / \omega_a^2}{\left(1 - \dfrac{\omega^2}{\omega_a^2} \right)\left(1 + \dfrac{k}{K} - \lambda^2 \right) - \dfrac{k}{K}} \\[4ex] \dfrac{\hat{x}_2}{x_{st}} = \dfrac{1}{\left(1 - \dfrac{\omega^2}{\omega_a^2} \right)\left(1 + \dfrac{k}{K} - \dfrac{\omega^2}{\Omega^2} \right) - \dfrac{k}{K}} = \dfrac{1}{\left(1 - \dfrac{\omega^2}{\omega_a^2} \right)\left(1 + \dfrac{k}{K} - \lambda^2 \right) - \dfrac{k}{K}} \end{cases}$$

where

$x_{st} = \dfrac{P_o}{K}$: static deflection of the main system;

$\omega_a = \sqrt{\dfrac{k}{m}}$: natural frequency of the absorber;

$\Omega = \sqrt{\dfrac{K}{M}}$: natural frequency of the main system; $f = \omega_a \big/ \Omega$: frequency ratio;

$\lambda = \omega \big/ \Omega$: forced frequency ratio; $\mu = m \big/ M$: mass ratio.

If the natural frequency of the absorber ω_a is chosen equal to the frequency of the disturbing force ω, the main mass M does not vibrate at all, while the secondary mass m vibrates in such a way that its spring force is at all instants equal and opposite to the external force; there is no net force acting on the main mass and it cannot move. The critical scenario is the resonant condition, $\omega = \Omega$, but as previously declared, if the exciting frequency is equal to the absorber one $\omega = \omega_a$, the main mass does not move $\hat{x}_1 = 0$, while the secondary mass is subjected to a sinusoidal motion with static amplitude

$$\hat{x}_2 = -\frac{K}{k} x_{st} = -\frac{P_o}{k} :$$

$$x_2 = -\frac{P_o}{k} \sin \omega t$$

while the elastic force is $- P_o \sin \omega t$.

Such relations are valid for any ratio ω / Ω; yet they assume particular relevance in proximity of resonance.

If the frequency of the absorber coincides with the main frequency $\omega_a = \Omega$, ($k \big/ m = K \big/ M$), the expressions of the dynamic factors of the system become

$$\begin{cases} \hat{x}_1 = x_{st} \cdot \dfrac{1 - \lambda^2}{\left(1 - \lambda^2\right)\left(1 + \mu - \lambda^2\right) - \mu} \\[4mm] \hat{x}_2 = x_{st} \cdot \dfrac{1}{\left(1 - \lambda^2\right)\left(1 + \mu - \lambda^2\right) - \mu} \end{cases}$$

Obviously the denominators of such expressions are equal: when the main motion x_1 diverges, also the secondary motion x_2 does, for the infinite intensity of the elastic force transmitted by the connecting spring.

The resonant natural frequencies of the system can be obtained by imposing the previous denominators equal to zero, solving a quadratic equation:

$$\lambda^4 - \lambda^2(2+\mu) + 1 = 0$$

whose solutions are $\lambda^2 = (1+0.5\mu) \pm \sqrt{\mu + 0.25\mu^2}$.

This result is represented in the following diagram, showing the resonant frequencies of systems with $\omega_a = \Omega_n$, for different values of μ .
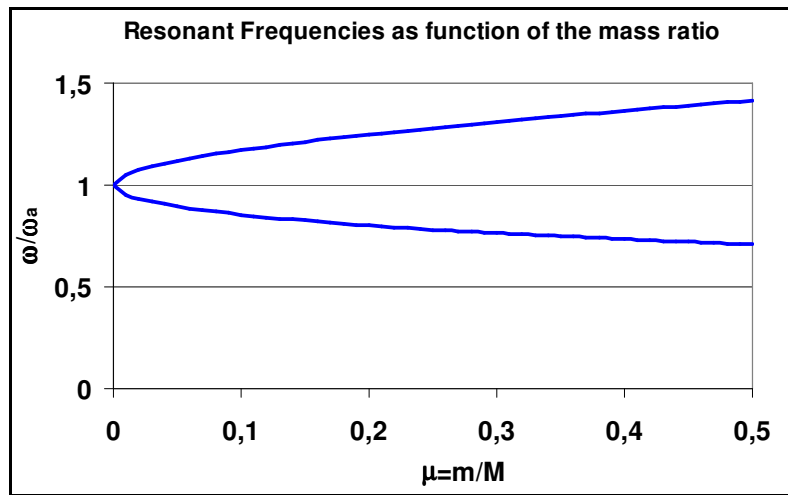
Figure 4.7. Resonant frequencies vs mass ratio.

It possible to observe that for $\mu = 0$ (SDOF) there is only one resonant frequency, and the introduction of the secondary mass (and the related degree-of-freedom) adds a resonant frequency and shifts the resonant excitation frequencies. The insertion of a TMD shifts the resonant frequency and prevent

resonant oscillation if the exciting frequency is the same as that of the main system, as often occurs for industrial machines.

Keeping the hypothesis $\omega_a = \Omega$, and fixing an arbitrary value for the mass ratio μ, it is possible to study the amplitudes of the motions $\hat{x}_1/x_{st}$, $\hat{x}_2/x_{st}$ for growing values of the ratio ω/Ω.

In the following diagram are represented, for $\mu = 0.1$, the motion amplitude of the primary and of the secondary mass, the resonant frequencies (0.85 and 1.17 times the original frequency) and the relative motion dimensionless amplitude.

If $\omega = \omega_a = \Omega$ the main system does not move.
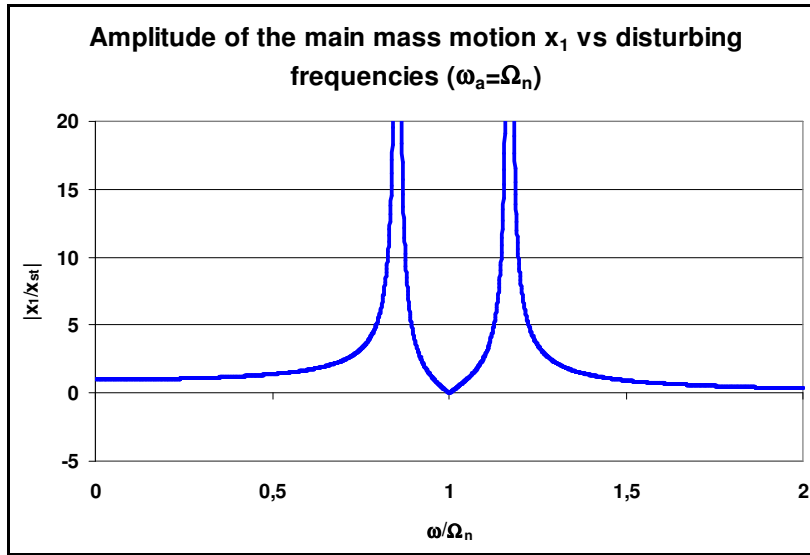
Figure 4.8. Amplitude of the main mass motion vs exciting frequencies.
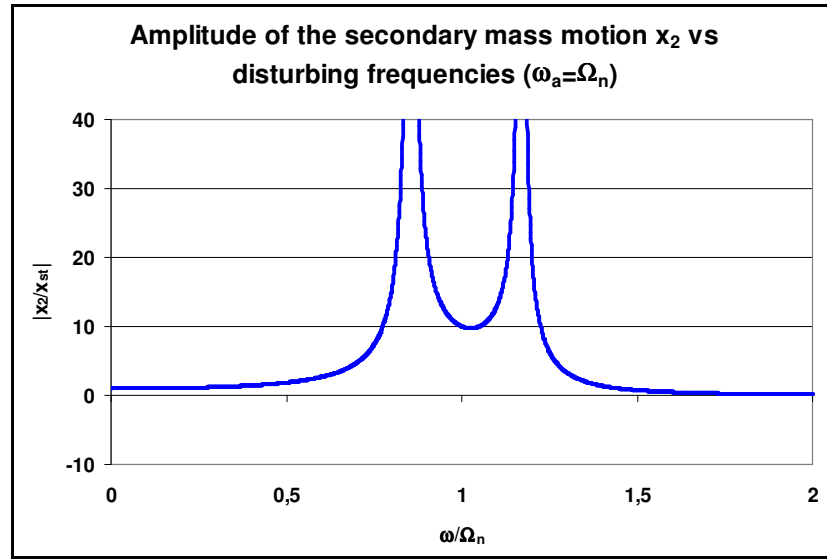
Figure 4.9. Amplitude of the secondary mass motion vs exciting frequencies.

Remarks: Main effects of the introduction of the adsorber on undamped SDOF system subjected to harmonic force.

1. The system has **two DOF and two resonant frequencies** instead of one.

2. The resonant frequencies of excitation is shifted in accordance with the mechanical parameters of the system.

3. If $\omega = \omega_a$: the main mass M **does not move** for any ratio ω/Ω .

4. If $\omega_a = \Omega$:

> 4a. **Arbitrary shift of the resonant frequencies** is possible if adequate value to the mass ratio μ is assigned;

> 4b. The amplitudes $\hat{x}_1/x_{st}$, $\hat{x}_2/x_{st}$ depend only on the ω and μ .

Undamped system and damped absorber – harmonic force exciting

Let's consider the two-degrees-of-freedom system introduced and add a dashpot arranged parallel to the damper spring between M and m .

The design consists of the attribution of values to the secondary mass m, stiffness k and damping coefficient c, in order to obtain specific requested reduction of the response.
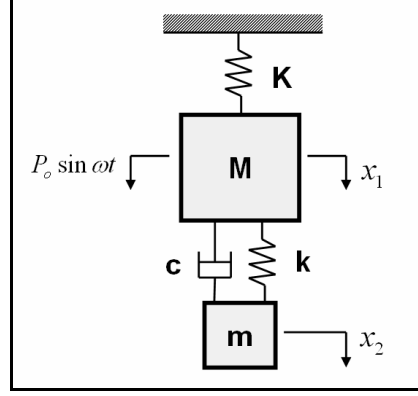
Figure 4.10. Damped adsorber and Main structure: two d.o.f. configuration.

If the main mass is still subjected to harmonic load, the equations of the motion become

$$\begin{bmatrix} M & 0 \\ 0 & m \end{bmatrix} \begin{Bmatrix} \ddot{x}_1 \\ \ddot{x}_2 \end{Bmatrix} + \begin{bmatrix} c & -c \\ -c & c \end{bmatrix} \begin{Bmatrix} \dot{x}_1 \\ \dot{x}_2 \end{Bmatrix} + \begin{bmatrix} K+k & -k \\ -k & k \end{bmatrix} \begin{Bmatrix} x_1 \\ x_2 \end{Bmatrix} = \begin{Bmatrix} P_0 \sin \omega t \\ 0 \end{Bmatrix}$$

The solution in the polar form has amplitudes

$$\begin{cases} \hat{x}_1 = \dfrac{P_o}{K} H_1 \\[2mm] \hat{x}_{rel} = \dfrac{P_o}{K} H_3 \end{cases}$$

where $x_{rel} = x_1 - x_2$

$$H_1 = \frac{\sqrt{\left[f^2 - \lambda^2\right]^2 + \left[2\xi_a \lambda f\right]^2}}{\left|\left(1 - \lambda^2\right)\left(f^2 - \lambda^2\right) - \mu\lambda^2 f^2 + 2j\xi_a \lambda f\left[1 - \lambda^2(1 + \mu)\right]\right|}$$

$$H_3 = \frac{g^2}{\left|\left(1 - \lambda^2\right)\left(f^2 - \lambda^2\right) - \mu\lambda^2 f^2 + 2j\xi_a \lambda f\left[1 - \lambda^2(1 + \mu)\right]\right|}$$

where $\xi_a = \dfrac{c}{c_c} = \dfrac{c}{2\sqrt{k \cdot m}}$: damping in respect of the critical.

The previous relations show that x_1 is function of seven variables: P_o, ω, c, K, k, M, m. Yet four are effectively independent:

The governing amplitude ratio is:

$$\frac{\hat{x}_1}{x_{st}} = \sqrt{\frac{(2\xi_a \lambda f)^2 + (\lambda^2 - f^2)^2}{(2\xi_a \lambda f)^2(\lambda^2 - 1 + \mu\lambda^2)^2 + \left[\mu f^2 \lambda^2 - (\lambda^2 - 1)(\lambda^2 - f^2)\right]^2}}$$

If the frequency of the damper is that of the main system $\omega_a = \Omega$ $(f = 1)$, and fixing the mass ratio μ, the amplitude of the motion of the main mass depends on the frequency of excitation ω and on the damping of the system ξ_a. So the curves for x_1 and x_2 can be plotted for different values of the damping.

If $c = 0$ no work is done and resonance has infinite peak at two resonant frequencies. If $c/c_c > 1$ or even $c/c_c = \inf$ the absorber is practically clamped with the main mass, no relative motion occurs and damping does not make any work, so that there is only one resonant frequency as the SDOF system. For intermediate values of the damping, with two or one resonant responses, two resonant peaks are observed, with finite values for the amplitude, according with the properties of damped systems that are able to dissipate energy doing work in the relative displacement of the masses.

Consequently between $c = 0$ and $c = \inf$ there is an optimal value of the damping for which the work of the damping force is maximum and the peak

(amplitude of the motion of M) gets a minimum: a general objective is to bring the resonant peak as much as possible so that smaller amplification over a wide frequency bandwidth with g close to unity.
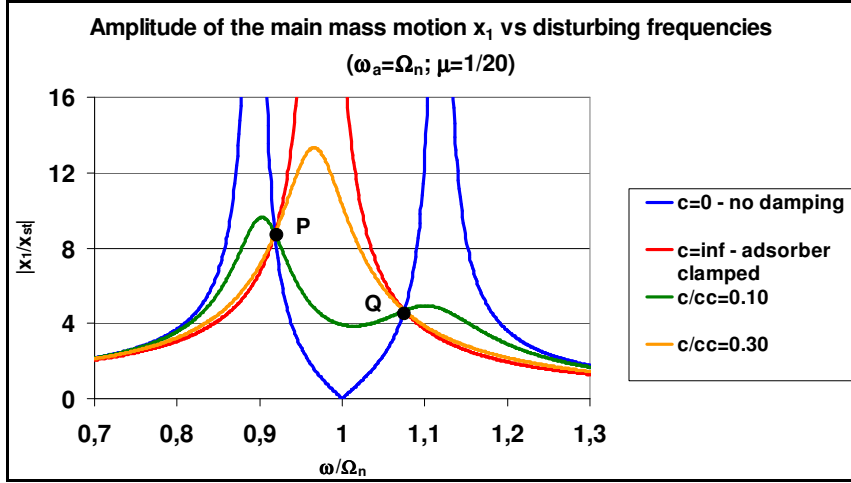
Figure 4.11. Effect of damper damping on the main mass motion (f=1).

It is possible to observe also that all the curves pass through two points, named P and Q, whose location and the corresponding amplification do not depend on the damping: the optimum damping is that for which at the highest of the two points the tangent of the response curve is horizontal, so that the maximum amplitude for the main mass corresponds to the ordinate of that point.

Obviously the location of P and Q depends on the frequency ratio $f = \omega_a / \Omega_n$, so that by tuning f one point goes up and the other down; the optimum choice of f is that giving the same ordinate to the two points.

The points P and Q can be determined by imposing that $\hat{x}_1 / x_{st}$ does not depend on the damping; from the expression of $\hat{x}_1 / x_{st}$ such condition is verified when

$$\left(\frac{1}{\lambda^2 - 1 + \mu\lambda^2}\right)^2 = \left(\frac{\lambda^2 - f^2}{\mu f^2 \lambda^2 - \left(\lambda^2 - 1\right)\left(\lambda^2 - f^2\right)}\right)^2$$

The locations of P and Q depend on f and μ.

Solving the equation the trivial solutions $\lambda^2 = 0$ corresponding to non-harmonic loads and static deflections are obtained; furthermore the two values λ_1^2 and λ_2^2 giving the fixed points are determined.

If the frequency ratio f is not free, the optimization is conducted looking for the value of the damping c for which at the highest of the fixed points the tangent of the curve is horizontal.

If the frequency ratio f is free, the optimum tuning must fix the points P and Q at the same ordinate: such request is satisfied if $f = 1/(1+\mu)$, as the following diagram shows. If the frequency of the damper is tuned in accordance with $f = 1/(1+\mu)$, the dimensionless amplitude on fixed point, indipendent of damping, is

$$\hat{x}_1 / x_{st} = \sqrt{1 + \left(2/\mu\right)}$$
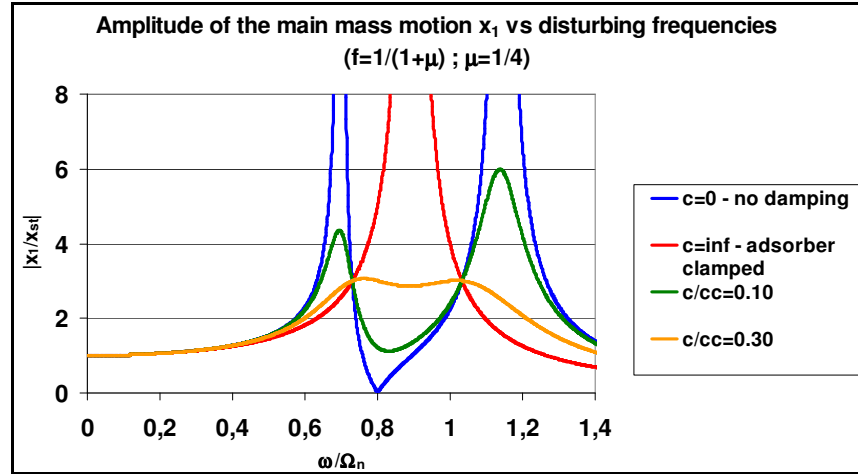
Figure 4.12. Effect of damper damping on the main mass motion (f=f$_{opt}$).

This relation shows that an increase in damper mass, at optimum tuning for the TMD, reduces the maximum amplification factor.

If the frequency ratio $f = 1$, the ordinates of the peaks are different and the solution of the quadratic equation is $\lambda^2 = 1 \pm \sqrt{\mu/(2+\mu)}$.

Considering the left peak (minus sign in the solution roots) the dimensionless amplitude on fixed point is

$$\frac{\hat{x}_1}{x_{st}} = \left(-\mu + (1+\mu)\sqrt{\frac{\mu}{2+\mu}}\right)^{-1}$$

The objective of the design is to find the optimal damping, for which the curve is horizontal in the highest fix point. By differentiating the general expression of $\hat{x}_1/x_{st}$ with respect to λ, thus finding the slope, and equate that slope to zero for the fixed point, and extracting the damping, we obtain:

- for optimal tuning $f = 1/(1+\mu)$, the optimal damping is

$$(\xi_a)_{opt} = \left(\frac{c}{c_c}\right)_{opt} = \sqrt{\frac{\mu}{8(1+\mu)^3}\left(3 - \sqrt{\mu/(\mu+2)}\right)} \quad \text{(fixed point is P);}$$

$$(\xi_a)_{opt} = \left(\frac{c}{c_c}\right)_{opt} = \sqrt{\frac{\mu}{8(1+\mu)^3}\left(3 + \sqrt{\mu/(\mu+2)}\right)} \quad \text{(fixed point is Q).}$$

An approximation often used is the average of the two values

$$\left(\frac{c}{c_c}\right)_{opt} = \sqrt{\frac{3\mu}{8(1+\mu)}}$$

- if $f = 1$, $\left(\frac{c}{c_c}\right)_{opt}^2 = \frac{\mu(\mu+3)}{8(1+\mu)}\left(1 + \sqrt{\mu/(\mu+2)}\right)$
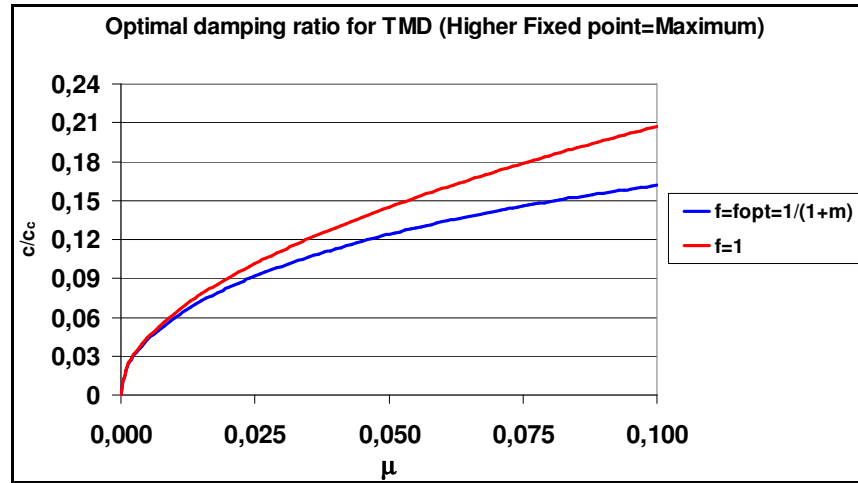
Figure 4.13. Optimal damping vs mass ratio for different tuning ratio.

In the following diagrams the resonance curves of undamped, infinite damping and optimized damping absorber are represented for $f = 1$ and for optimal tuning $f = 1/(1 + \mu)$ $(\mu = 0.05)$.
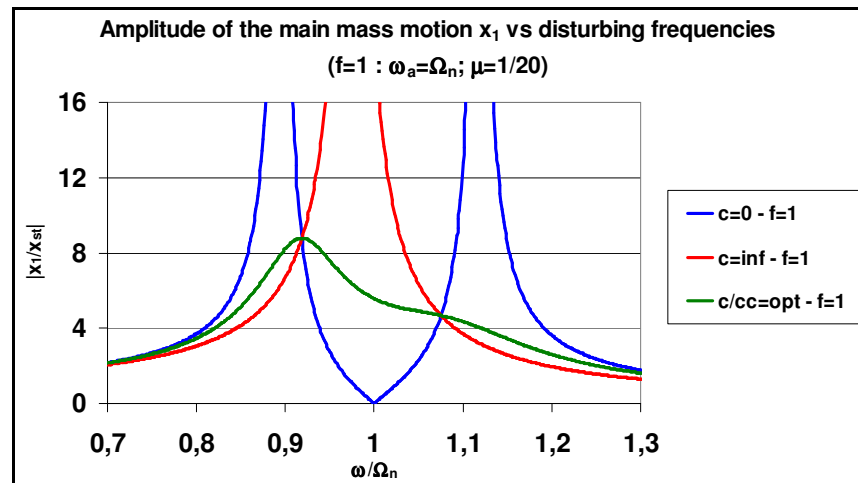
Figure 4.14. Optimization of damping ratio (f=1).
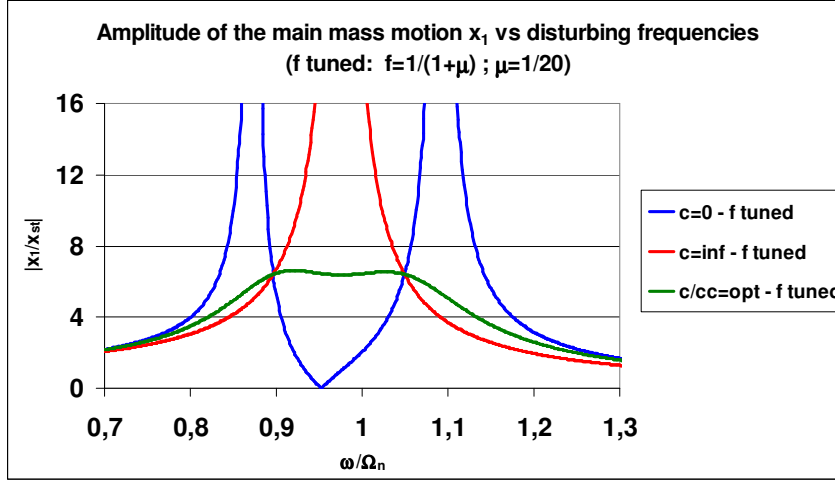
Figure 4.15. Optimization of damping ratio ($f=f_{opt}$).

In both cases it is possible to observe that at optimal damping the maximum (slope equal to zero) is at one of the fixed points; for optimal tuning the fixed points have the same (smaller) ordinate. For values of the damper damping higher than the optimal, the peaks merge and the amplitude increase beyond the optimal value.

The response diagrams show that the effect of the damper is to limit the motion in a frequency range centred on the natural frequency of the primary mass and extending about $0.2\Omega_n$, while outside this range the motion is not significantly influenced by the damper. Consequently the performance of the damper are very sensitive to the tuning: possible mistuning can reduce the performance of the damper or even increase the structural response. In this sense the Tuned Mass Dampers are intrinsically non robust.

If the damping is optimized, the ordinate of the highest fixed point represents the amplitude of the motion of the main mass, with the expression of $\hat{x}_1/x_{st}$ already written for $f=1$ and for optimal tuning $f=1/(1+\mu)$ and represented in Figure 4.16.

141
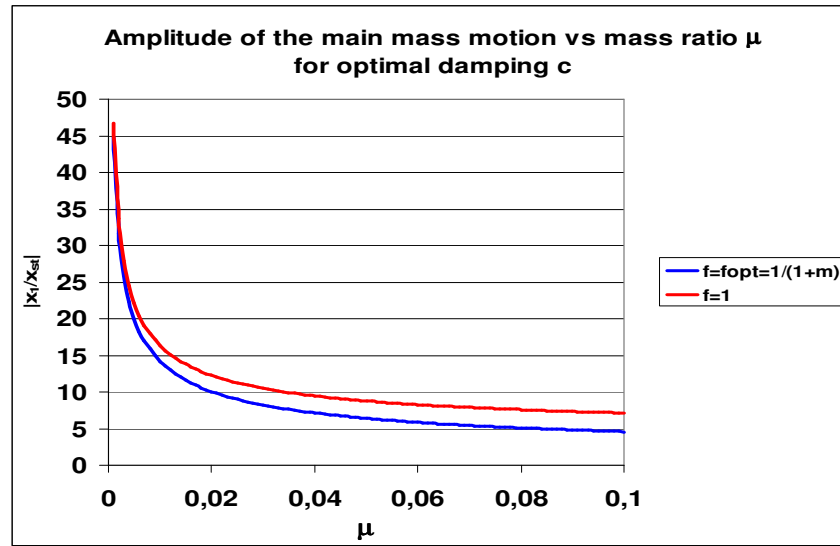
Figure 4.16. Effects of mass ratio for optimal damping ratios on the main mass motion.

It is to observe that the efficiency of the insertion of a TMD increases with the mass ratio, but with decreasing marginal benefit.

The dimensionless amplitude of the relative motion of masses is

$$\left(\frac{\hat{x}_{rel}}{x_{st}}\right)^2 = \frac{\hat{x}_1}{x_{st}}\frac{1}{2\mu\lambda\xi_a}$$

it is represented for $f = 1$ and for optimal tuning $f = 1/(1+\mu)$ in the Figure 4.17.

It is possible to observe that the relative motion, or spring extensions is large in comparison with the main motion: the design of the damper spring must keep into account possible fatigue effects and the available space for the motion.
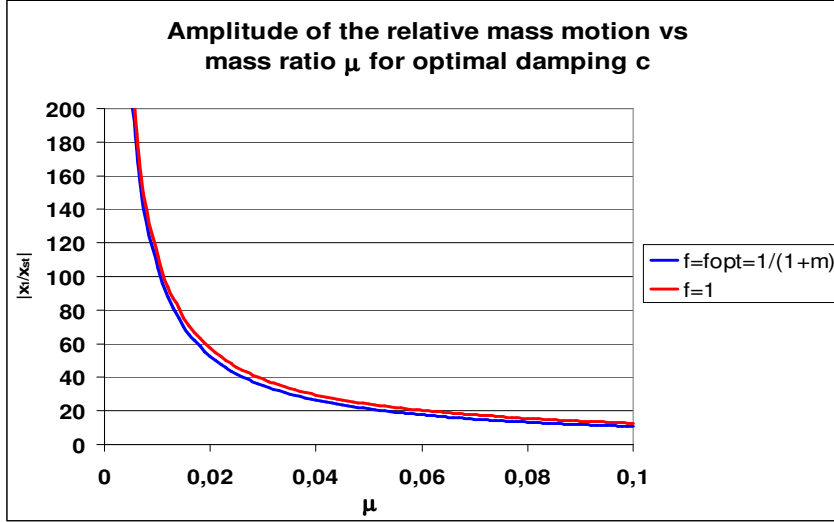
Figure 4.17. Effects of mass ratio for optimal damping ratios on the relative motion.

Remarks: Effects of the introduction of a damped adsorber on SDOF subjected to harmonic loads

1. The amplitude ratio $\hat{x}_1/x_{st}$ depends on **four dimensionless parameters**: μ, f, λ, ξ_a.

2. If $\omega_a = \Omega$, ($f = 1$) and the mass ratio μ is fixed, the **damping** of the absorber governs the response in terms of resonant frequency and amplitude of the motion.

For any value of f the **optimum damping** is the one that gives minimum amplitude to the motion of the main mass: it can be checked imposing that the response curve has horizontal tangent at the highest of the two fix points.

3. If the frequency ratio f is free, the **optimum tuning** $f = 1/(1+\mu)$ fixes the points P and Q at the same minimum ordinate; the **optimum damping** is still

143

that provides horizontal tangent on the fix points (absolute maximum of the curve).

4. The response diagrams show that the effect of the damper is to limit the motion in a frequency range centred on the natural frequency of the primary mass and extending about 0.2Ω. Outside this range the motion is not significantly influenced by the damper. Any cause of mistuning can reduce the damper efficiency or even increase the response: the TMDs are intrinsically non robust.

Undamped system and damped absorber – harmonic ground acceleration

If the same system SDOF+TMD of case 2a is subjected to ground acceleration $\ddot{x}_g$, the governing equations of the motion become

$$\begin{bmatrix} M & 0 \\ 0 & m \end{bmatrix}\begin{Bmatrix} \ddot{x}_1 \\ \ddot{x}_2 \end{Bmatrix} + \begin{bmatrix} c & -c \\ -c & c \end{bmatrix}\begin{Bmatrix} \dot{x}_1 \\ \dot{x}_2 \end{Bmatrix} + \begin{bmatrix} K+k & -k \\ -k & k \end{bmatrix}\begin{Bmatrix} x_1 \\ x_2 \end{Bmatrix} = \begin{Bmatrix} -M \\ -m \end{Bmatrix}\ddot{x}_g$$

If the ground acceleration is harmonic $\ddot{x}_g = \hat{\ddot{x}}_g \sin \omega t$, the solution in polar form can be written as

$$\begin{cases} \hat{x}_1 = -\dfrac{\hat{\ddot{x}}_g M}{K} H_2 e^{i\delta_2} \\[4mm] \hat{x}_{rel} = -\dfrac{\hat{\ddot{x}}_g M}{K} H_4 e^{i\delta_4} \end{cases}$$

where

$$H_2 = \frac{\sqrt{\left[(1+\mu)f^2 - \lambda^2\right]^2 + \left[2\xi_a\lambda f(1+\mu)\right]^2}}{\left|(1-\lambda^2)(f^2-\lambda^2) - \mu\lambda^2 f^2 + 2j\xi_a\lambda f\left[1-\lambda^2(1+\mu)\right]\right|}$$

$$H_4 = \frac{1}{\left|(1-\lambda^2)(f^2-\lambda^2) - \mu\lambda^2 f^2 + 2j\xi_a\lambda f\left[1-\lambda^2(1+\mu)\right]\right|}$$

Since the mass ratio μ is usually small, by comparing the expressions of the main motion amplitude factors of H_2 (case 2b) and H_1 (case 2a), it is possible

144

to observe that they are essentially equal. Similar conclusions may be done for phases, here omitted. So the results expressed previously for harmonic force excitation are extendible to harmonic ground motion case.

Damped system with damped absorber – harmonic force exciting

All real systems contain some damping; so even if TMD usually are introduced into lightly damped structures, assessing the effect of damping of the main structure on the optimal tuning is an important point of the design process.

Also for this case analytical expressions of the amplification factors are possible; the main difference with the previous case consists of the absence of the invariant points P, Q.

For damped structure with damped absorber and subjected to external force $F(t)$, the equation of the motion is

$$\begin{bmatrix} M & 0 \\ 0 & m \end{bmatrix} \begin{Bmatrix} \ddot{x}_1 \\ \ddot{x}_2 \end{Bmatrix} + \begin{bmatrix} C+c & -c \\ -c & c \end{bmatrix} \begin{Bmatrix} \dot{x}_1 \\ \dot{x}_2 \end{Bmatrix} + \begin{bmatrix} K+k & -k \\ -k & k \end{bmatrix} \begin{Bmatrix} x_1 \\ x_2 \end{Bmatrix} = \begin{Bmatrix} F \\ 0 \end{Bmatrix}$$

where C: structural damping coefficient.
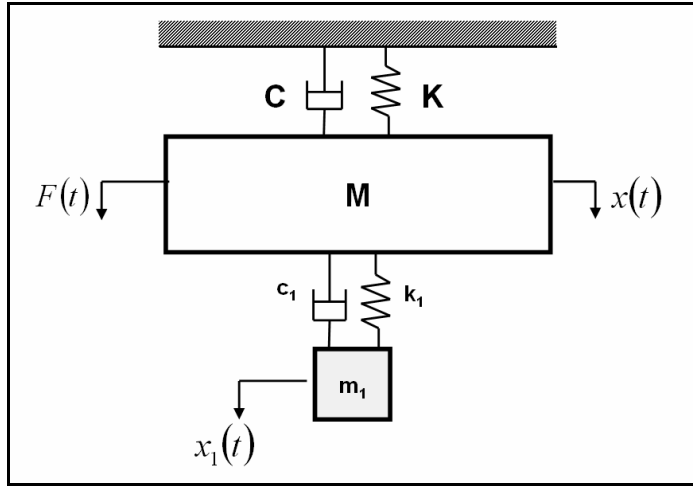
Figure 4.18. Damped structure and absorber.

145

For harmonic excitation ($F = P_0 \sin \omega t$), the general solution of the motion for harmonic excitation is

$$\hat{x}_1 = \frac{P_0}{K} A_1 e^{i\delta_1}; \quad \hat{x}_{rel} = \frac{P_0}{K} A_2 e^{-i\delta_2}$$

where the dimensionless amplitudes of the displacement response are

$$A_1 = \frac{\hat{x}_1}{x_{st}} = \frac{\sqrt{\left[f^2 - \lambda^2\right]^2 + \left[2\xi_a\lambda f\right]^2}}{\left[-f^2\lambda^2\mu + \left(1-\lambda^2\right)\left(f^2-\lambda^2\right) - 4\xi\xi_a f\lambda^2\right]^2 + 4\left[\xi\lambda\left(f^2-\lambda^2\right) + \xi_a f\lambda\left(1-\lambda^2\left(1+\mu\right)\right)^2\right]}$$

$$A_2 = \frac{\hat{x}_{rel}}{x_{st}} = \frac{g^2}{\left[-f^2\lambda^2\mu + \left(1-\lambda^2\right)\left(f^2-\lambda^2\right) - 4\xi\xi_a f\lambda^2\right]^2 + 4\left[\xi\lambda\left(f^2-\lambda^2\right) + \xi_a f\lambda\left(1-\lambda^2\left(1+\mu\right)\right)^2\right]}$$

$$\xi = \frac{C}{2\sqrt{K \cdot M}} : \text{damping ratio in respect the critical of the main structure;}$$

$$\xi_a = \frac{c}{2\sqrt{km}} : \text{damping ratio in respect the critical of the device.}$$

The relations above involve ξ; so it is not possible to establish analytical expressions of the optimal tuning frequency and optimal damping ratio in terms of the only mass ratio, because these parameters depend also on ξ, nor to fill a table like the previous for the undamped structure subjected to harmonic/random force/base acceleration. Numerical simulations can be done to evaluate the motion amplitudes for a range of λ (excitation frequency), given the values for μ, ξ, f, ξ_a. If we start with a specific combination of values of μ, ξ, it is possible to evaluate $\hat{x}_1/x_{st}$ versus λ for different values (range) of f, ξ_a. Each $\hat{x}_1/x_{st}$ - λ plot has a peak value of $\hat{x}_1/x_{st}$; the optimum combination of f, ξ_a is that corresponding to the lowest peak for $\hat{x}_1/x_{st}$. The process can be repeated for different values of μ and ξ, and the parameter governing the behaviour and necessary for the design of the damper system are obtained.

At resonance $\omega = \Omega_n$ the solution of the motion in terms of amplitude is

146

$$\hat{x}_1 = x_{st}\frac{1}{\mu}\sqrt{\frac{1}{1+\left(\dfrac{2\xi}{\mu}+\dfrac{1}{2\xi_a}\right)^2}}\;;\hat{x}_2 = \left(1+\frac{1}{2\xi_a}\right)\hat{x}_1$$

Consequently the relative motion amplitude is $\hat{x}_r = \dfrac{1}{2\xi_a}x_1$

and the response is

$$\begin{cases} x_1 = \hat{x}_1\sin(\omega t + \alpha) \\ x_2 = \hat{x}_2\sin(\omega t + \alpha + \beta) \end{cases},$$

where $\tan\alpha = -\left[\dfrac{2\xi}{\mu}+\dfrac{1}{2\xi_a}\right];\;\; \tan\beta = -\dfrac{\pi}{2}.$

The response of the tuned mass is 90° out of phase with the response of the main mass; this difference produces the energy dissipation contributed by the inertia force.

If no damper is provided the amplitude of the motion of the primary mass is

$$\frac{\hat{x}_1}{x_{st}} = \frac{1}{2\xi}$$

The introduction of the damper can be considered as the introduction of an equivalent damping ξ_{eq}, so that $\dfrac{\hat{x}_1}{x_{st}} = \dfrac{1}{2\xi_{eq}}$,

where $\xi_{eq} = \dfrac{\mu}{2}\sqrt{1+\left(\dfrac{2\xi}{\mu}+\dfrac{1}{2\xi_a}\right)^2}$.

The previous expression shows the contribution of the damper parameters to the total damping: increasing the mass ratio increases the damping, and decreasing the damping of the absorber increases the total damping but also the relative motion x_r that can be a restrictive requirement in the design stage; so in the design a reasonable compromise between total damping and limited secondary motion is adopted.

Remarks: Effects of damped adsorber on a damped SDOF system at resonance

1. The effect of the introduction of a damper adsorber on a damped SDOF system is equivalent to giving an equivalent damping to the system:

$$\xi_{eq} = \frac{\mu}{2}\sqrt{1 + \left(\frac{2\xi}{\mu} + \frac{1}{2\xi_a}\right)^2} \ .$$

1a. Increasing the mass ratio μ increases the damping;

1b. Decreasing the damping of the absorber ξ_a increases the total damping

but also the relative motion between the connected masses $x_r = \dfrac{1}{2\xi_a} x_1$.

Damped system with damped absorber – harmonic ground acceleration

In the case of ground acceleration at the bounds of the system the equations of the motion are

$$\begin{bmatrix} M & 0 \\ 0 & m \end{bmatrix}\begin{Bmatrix} \ddot{x}_1 \\ \ddot{x}_2 \end{Bmatrix} + \begin{bmatrix} C+c & -c \\ -c & c \end{bmatrix}\begin{Bmatrix} \dot{x}_1 \\ \dot{x}_2 \end{Bmatrix} + \begin{bmatrix} K+k & -k \\ -k & k \end{bmatrix}\begin{Bmatrix} x_1 \\ x_2 \end{Bmatrix} = \begin{Bmatrix} -M \\ -m \end{Bmatrix}\ddot{x}_g$$

If the acceleration has a harmonic content ($\ddot{x}_g = \hat{\ddot{x}}_g \sin \omega t$), the generalized solution in polar form is

$$\hat{x}_1 = -\frac{\hat{\ddot{x}}_g M}{K} A_3 e^{i\delta_3}; \ \hat{x}_{rel} = -\frac{\hat{\ddot{x}}_g M}{K} A_4 e^{-i\delta_4}$$

where the dimensionless amplitude of the motion are

$$A_3 = \frac{\sqrt{\left[(1+\mu)f^2 - \lambda^2\right]^2 + \left[2\xi_a \lambda f(1+\mu)\right]^2}}{\left[-f^2\lambda^2\mu + (1-\lambda^2)(f^2-\lambda^2) - 4\xi\xi_a f\lambda^2\right]^2 + 4\left[\xi\lambda(f^2-\lambda^2) + \xi_a f\lambda(1-\lambda^2(1+\mu))^2\right]}$$

$$A_4 = \frac{\sqrt{1+[2\xi\lambda]^2}}{\left[-f^2\lambda^2\mu + (1-\lambda^2)(f^2-\lambda^2) - 4\xi\xi_a f\lambda^2\right]^2 + 4\left[\xi\lambda(f^2-\lambda^2) + \xi_a f\lambda(1-\lambda^2(1+\mu))^2\right]}$$

148

4.3.2 Transfer Functions

For each problem the response at excitation frequency can be written in non-dimensional form as $H(\omega)e^{i\omega t}$, where $H(\omega)$ is the complex transfer function

$$H(\omega) = \frac{A + iB}{C + iD}$$

where A, B, C, D are functions of:

the type of excitation and the response parameter;

$\lambda = \omega/\Omega$: excitation frequency ratio $\left(\Omega^2 = K/M\right)$;

$f = \omega_a/\Omega$: tuning ratio $\left(\omega_a^2 = k/m\right)$;

$\mu = m/M$: mass ratio;

$\xi_a = c/\left(2\sqrt{km}\right)$: absorber damping ratio.

$\xi = C/\left(2\sqrt{KM}\right)$: main structure damping ratio.

The non-dimensional amplitude of the response R can be expressed as

$$R = |H(\omega)| = \sqrt{\frac{A^2 + B^2}{C^2 + D^2}}$$

In Table 4.I are represented the transfer functions determined for different types of excitation and response parameters.

In particular one can observe that the optimal tuning ratio to reduce the displacements induced by base acceleration is quite lower than for the other cases. Such circumstance and precisely, the distinction of optimal values for type of excitation (force/base-acceleration) produce a significant discrepancy for the design of Tuned Mass Dampers against wind/earthquake scenarios.

149

Case	Excitation	Response	R	A	B
1	Force on the main mass $Pe^{i\omega t}$	x : Main displ.	$\dfrac{Kx}{P}$	$f^2 - \lambda^2$	$2\xi_a \lambda f$
2		$\dot{x}$: Main velocity	$\dfrac{K\dot{x}}{P\Omega}$	$-2\xi_a \lambda^2 f$	$\lambda\left(f^2 - \lambda^2\right)$
3		$\ddot{x}$: Main acceleration	$\dfrac{M\ddot{x}}{P}$	$-\lambda^2\left(f^2 - \lambda^2\right)$	$-2\xi_a \lambda^3 f$
4		F : Frame reaction	$\dfrac{F}{P}$	$f^2 - \lambda^2 - 4\xi_a \xi f \lambda^2$	$2\xi_a \lambda f + {}+2\xi\lambda\left(f^2 - \lambda^2\right)$
5	Base-accel. $\ddot{X}_0 e^{i\omega t}$	$Y = x - x_1$: Relative motion	$\dfrac{\Omega^2 Y}{\ddot{X}_0}$	$f^2(1+\mu) - \lambda^2$	$2\xi_a \lambda f(1+\mu)$
6		$\ddot{x}$: Main acceleration	$\dfrac{\ddot{x}}{\ddot{X}_0}$	$f^2 - \lambda^2 - 4\xi_a \xi f \lambda^2$	$2\xi_a \lambda f + {}+2\xi\lambda\left(f^2 - \lambda^2\right)$
7		x : Main displacement	$\dfrac{\Omega^2 x}{\ddot{X}_0}$	$-\dfrac{f^2}{\lambda^2} + 1 + 4\xi_a \xi f$	$-\dfrac{2\xi_a f}{\lambda} - {}-\dfrac{2\xi}{\lambda}\left(f^2 - \lambda^2\right)$
$C = \left(f^2 - \lambda^2\right)\left(1 - \lambda^2\right) - \mu f^2 \lambda^2 - 4\xi_a \xi f \lambda^2$					
$D = 2\xi_a \lambda f\left(1 - \lambda^2 - \mu\lambda^2\right) + 2\xi\lambda\left(f^2 - \lambda^2\right)$					

Table 4.I. Complex transfer function of damped structure+TMD.

4.3.3 Criteria of Optimal Design: Types of Excitation and Response Parameters

In the past years the optimization of the response of structures subjected to dynamic loads have been extensively investigated, and many criteria have been analyzed in order to   increase safety and integrity of the structure (displacements criteria), or to improve serviceability, fatigue, and comfort features (accelerations criteria), under different excitation types.

The optimum parameters for absorbers minimizing the vibration response of a complex systems have been evaluated by treating the structure as a single degree-of-freedom system. This is correct if the natural frequencies are well separated. Simple expressions of optimal parameters have been derived for undamped SDOF systems subjected to harmonic and white noise excitation, in terms of force or base-acceleration applied, and various response parameters.

Optimization under harmonic loads

For harmonic excitation various optimization criteria of minimizing the response amplitude can be written, depending on the type of excitation (force/base-acceleration) and on the response parameters to be limited.

For example, concerning the minimization of displacements, the optimization is stated as

$$
\begin{cases}
\dfrac{\partial\left(\dfrac{\hat{x}_1}{x_{st}}\right)}{\partial f} = \dfrac{\partial R}{\partial f} = 0 \\[4ex]
\dfrac{\partial\left(\dfrac{\hat{x}_1}{x_{st}}\right)}{\partial \xi_a} = \dfrac{\partial R}{\partial \xi_a} = 0
\end{cases}
$$

This particular optimization gives the values of f_{opt}, $\xi_{a,opt}$, for which the response at the fix points (frequency at which the response does not depend on the damping ratio) is equal. The response at the fix point is maximum and is assumed as optimized maximum response.

In Table 4.II the optimal values of tuning and damping ratio are reported with reference to harmonic excitations on undamped structures $(\xi = 0)$, obtained by Den Hartog (1956), Neubert (1964), Warburton (1982).

In general the reduction of the response increases with the mass ratio, while the optimal tuning ratio f_{opt} decreases while μ increases.

151

Excitation	Response	R	R_{opt}	f_{opt}	$(\xi_a)_{opt}$
Force on the main mass $Pe^{i\omega t}$	x Main displ.	$\dfrac{Kx}{P}$	$\sqrt{1+\dfrac{2}{\mu}}$	$\dfrac{1}{1+\mu}$	$\sqrt{\dfrac{3\mu}{8(1+\mu)}}$
	$\dot{x}$ Main vel.	$\dfrac{K\dot{x}}{P\Omega}$	$\sqrt{\dfrac{2(1+\mu/2)}{\mu(1+\mu)}}$	$\dfrac{\sqrt{1+\mu/2}}{1+\mu}$	$\sqrt{\dfrac{3\mu(1+\mu+5\mu^2/24)}{8(1+\mu)(1+\mu/2)^2}}$
	$\ddot{x}$ Main accel.	$\dfrac{M\ddot{x}}{P}$	$\sqrt{\dfrac{2}{\mu(1+\mu)}}$	$\sqrt{\dfrac{1}{1+\mu}}$	$\sqrt{\dfrac{3\mu}{8\left(1+\mu/2\right)}}$
	F Frame react.	$\dfrac{F}{P}$	$\sqrt{1+\dfrac{2}{\mu}}$	$\dfrac{1}{1+\mu}$	$\sqrt{\dfrac{3\mu}{8(1+\mu)}}$
Base-accel. $\ddot{X}_0 e^{i\omega t}$	$Y = x - x_1$ Rel. displ.	$\dfrac{\Omega^2 Y}{\ddot{X}_0}$	$\sqrt{\dfrac{2}{\mu}(1+\mu)}$	$\dfrac{\sqrt{1-\mu/2}}{1+\mu}$	$\sqrt{\dfrac{3\mu}{8(1+\mu)\left(1-\mu/2\right)}}$
	$\ddot{x}$ Main accel.	$\dfrac{\ddot{x}}{\ddot{X}_0}$	$\sqrt{1+\dfrac{2}{\mu}}$	$\dfrac{1}{1+\mu}$	$\sqrt{\dfrac{3\mu}{8(1+\mu)}}$
	x Main displ.	$\dfrac{\Omega^2 x}{\ddot{X}_0}$	$\sqrt{\dfrac{2}{\mu}\left(1+2\mu+2.125\mu^2+...\right)}$ (series)	$\dfrac{\sqrt{1-\mu/2+\sqrt{1-3\mu-...}}}{2(1+\mu)^2}$ (series)	$\sqrt{\dfrac{3\mu(1-3\mu+1.5\mu^2-...)}{8(1-3.5\mu-...)}}$ (series)

Table 4.II. Harmonic excitation and optimal parameters (undamped structures).

The Figures 4.19, 4.20, 4.21 show that:

    a. the non-dimensional response decrease as the mass ratio increase (Figure 4.19); the largest optimized response (R_{opt}) is for case 7, followed by 5,1,2,3.

    b. the optimal values for the tuning ratio f_{opt} decrease as the mass ratio increases (Figure 4.20); the largest value is for case 3, followed by 2,1,5,7.

  c. the optimal values for the damping ratio $\left(\xi_a\right)_{opt}$ increases as the mass ratio increases (Figure 4.21); the smallest value is for case 2, followed by 1,3,5,7.

The same optimization can be conducted for damped structure: the resulting equations are solved by numerical methods to obtain f_{opt} and $\left(\xi_a\right)_{opt}$.

Harmonic excitation
Response (R) vs mass ratio
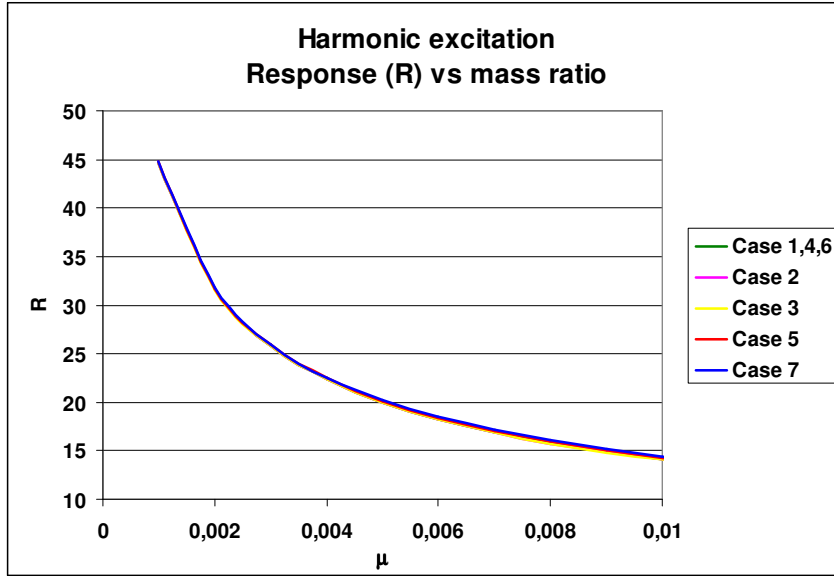
Figure 4.19. Response parameters vs mass ratio for various types of harmonic excitation.
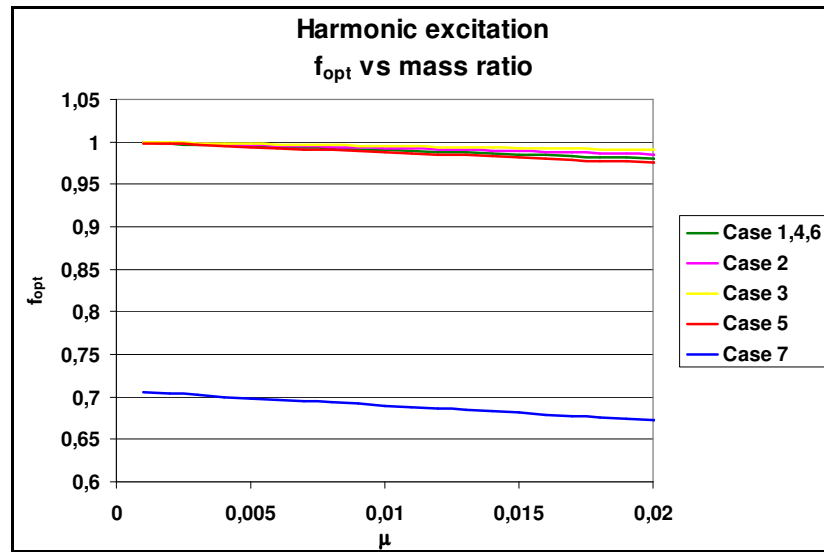
Figure 4.20. Optimal tuning ratios vs mass ratio for various types of excitation.
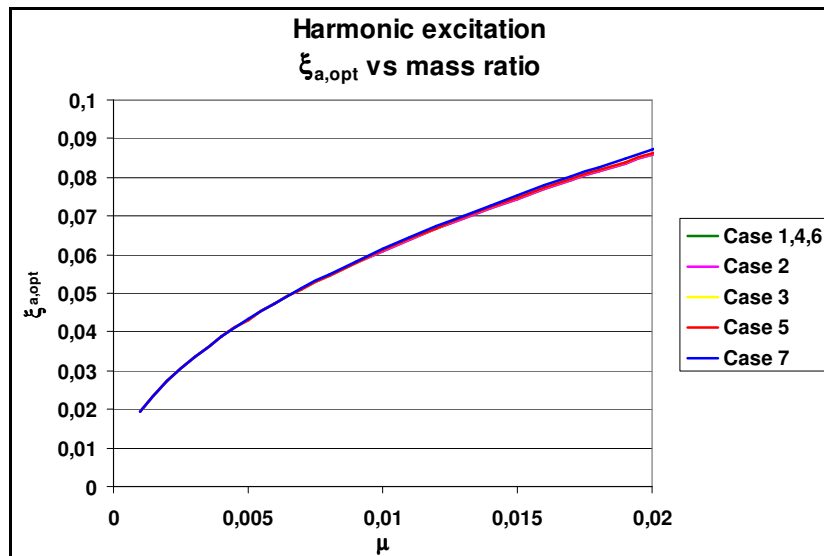
Figure 4.21. Optimal damping vs mass ratio for various types of excitation.

Optimization under random loads

Wind and earthquake are intrinsically stochastic and non stationary, but sometimes they are approximated by stationary white-noise processes, whit constant spectral density. For such spectral distribution the expressions of the optimal values of the TMD parameters for undamped structures are particularly easy.

If the excitation is a stationary random process, of spectral density $S_0(\omega)$, the variance of a response quantity x, σ_x^2, is given by

$$\sigma_x^2 = \int_{-\infty}^{+\infty} S_0(\omega) \cdot |H(\omega)|^2 \, d\omega$$

(mean square value of a random quantity with zero-mean).

Closed form expressions for σ_x^2 have been obtained by Crandall&Mark (1963).

The optimization conditions can be written as follows

$$\begin{cases} \dfrac{\partial \sigma_{x_1}^2}{\partial f} = 0 \\[3mm] \dfrac{\partial \sigma_{x_1}^2}{\partial \xi_a} = 0 \end{cases}$$

and lead to optimal values of the tuning and the damping ratios.

In Table 4.III are reported the excitation types, the definition of optimized response parameters (non-dimensional variance), their optimal value and the optimal values of the absorber parameters reported in literature (Warburton, 1982) for undamped structures.

The relationship between the optimal response, tuning ratio and damping ratio versus mass ratio for undamped structures excited as in Table III are represented in Figures 4.22,23,24.

155

Excitation	Resp.	R (non dim.)	R_{opt}	f_{opt}	$\left(\xi_a\right)_{opt}$
Force on the main mass	x Main displ.	$R \equiv \dfrac{\sigma_x^2 K^2}{2\pi S_0 \Omega}$	$\sqrt{\dfrac{1+0.75\mu}{\mu(1+\mu)}}$	$\dfrac{\sqrt{1+0.5\mu}}{1+\mu}$	$\sqrt{\dfrac{\mu(1+0.75\mu)}{4(1+\mu)(1+0.5\mu)}}$
	$\dot{x}$ Main vel.	$R \equiv \dfrac{\sigma_{\dot{x}}^2 K^2}{2\pi S_0 \Omega^3}$	$\sqrt{\dfrac{1}{\mu(1+\mu)}}$	$\dfrac{1}{\sqrt{1+\mu}}$	$\dfrac{\sqrt{\mu}}{2}$
Base-accel.	$Y = x - x_1$ Rel. displ.	$R \equiv \dfrac{\sigma_y^2 \Omega^3}{2\pi S_0}$	$\sqrt{\dfrac{1}{\mu}\left(1-\dfrac{\mu}{4}\right)(1+\mu)}$	$\dfrac{\sqrt{1-\mu/2}}{1+\mu}$	$\sqrt{\dfrac{\mu(1-0.25\mu)}{4(1+\mu)(1-0.5\mu)}}$

Table 4.III. White noise excitation and optimal parameters (undamped structures).
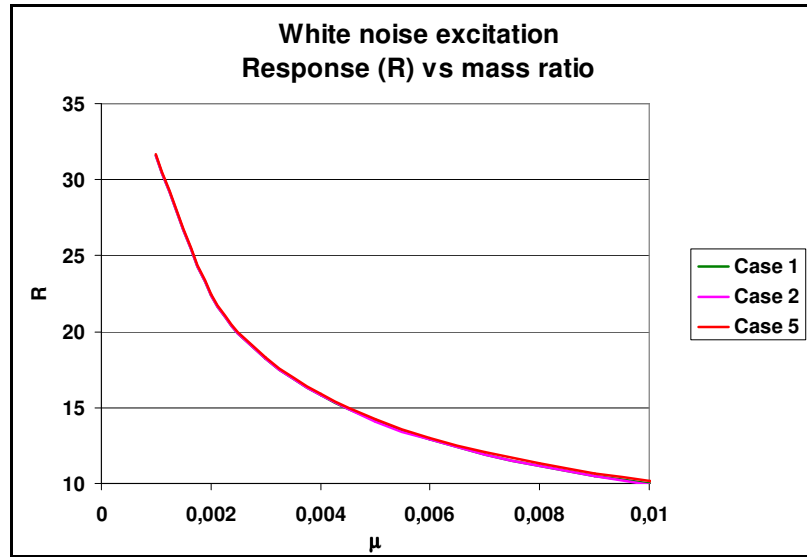
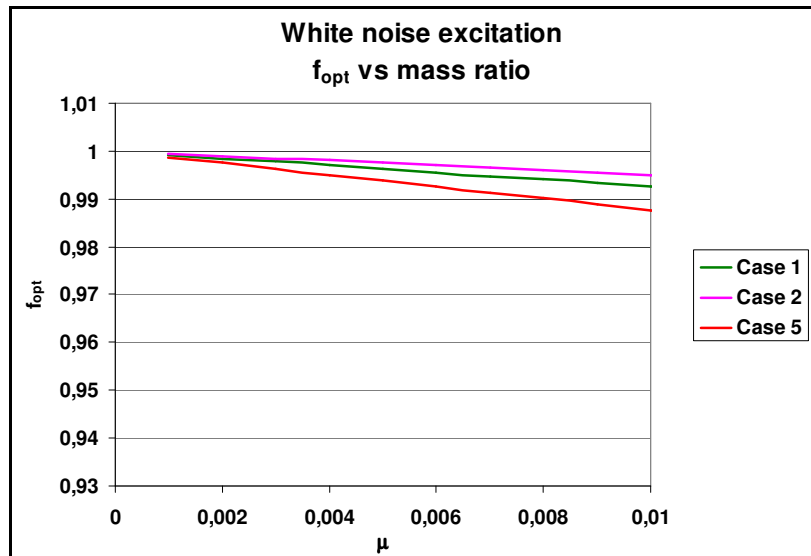**Figure 4.22.** Response vs mass ratio for various types of harmonic excitation.

156

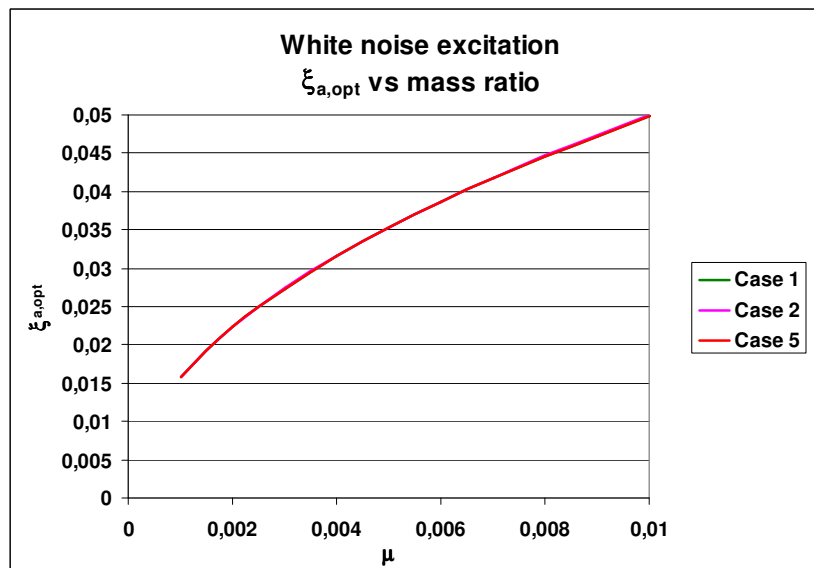**Figure 4.23.** Optimal tuning vs mass ratio for harmonic excitation.

Figure 4.24. Optimal damping ratio vs mass ratio for harmonic excitation.

157

For a given type of excitation and mass ratio μ there is a slight increase on the values of f_{opt} and a reduction of the optimal damping ratio $(\xi_a)_{opt}$ in respect the harmonic excitation.

Different type of excitations and response parameters produce different optimal values for the tuning and the damping ratios, while minimum response reduction (performance) is strictly related to the mass amount installed, for each response type considered.

The use of incorrect design criteria (for type of excitation or for kind of response optimization) produce greater structural response than the optimum. Such difference increases quickly if the mass ratio increases.

If a multiple combination of performance must be satisfied, a combination of design parameters (μ, f, ξ_a) must be identified in order to obtain the minimum levels of performance admitted. A possible approach consists of the identification of a main performance for which the tuning ratio and the absorber damping will be optimized, and secondary performance whose satisfaction require opportune mass ratio corresponding to non optimal tuning and damping. In this sense the role of the mass ratio, increasing the structural performance as it increases, produce a collection of possible solution for the design. In general the final choice will be that assuring the expected performance using the minimum mass amount possible.

For damped structures the evaluation of the non dimensional response (related to the variance in Table 4.III for the various cases of excitation) is conducted using the integrals of Crandall & Mark:

$$R = \frac{1}{2\pi} \int_{-\infty}^{+\infty} |H(\lambda)|^2 \, d\lambda = \frac{I(\mu, f, \xi_a, \xi)}{L(\mu, f, \xi_a, \xi)}$$

where

$$L(\mu, f, \xi_a, \xi) = 4\left\{ \mu f \xi_a^2 + \xi_a \xi \left[1 - 2f^2 + f^4(1+\mu)^2 + 4f^2 \xi_a^2(1+\mu) + \right.\right.$$
$$\left.\left. + 4f \xi_a \xi (1 + f^2(1+\mu)) + 4f^2 \xi^2 \right] + \mu f^3 \xi^2 \right\}$$

158

and $I(\mu, f, \xi_a, \xi)$ has different expression for different excitations:

Case	$I(\mu, f, \xi_a, \xi)$
1	$\xi_a\left[1 - f^2(2+\mu) + f^4(1+\mu)^2\right] + \mu f^3 \xi + 4 f^2 \xi_a^3 (1+\mu) +$ $+ 4 f \xi_a^2 \xi\left[1 + f^2(1+\mu)\right] + 4 f^2 \xi^2 \xi_a$
2	$\xi_a\left[1 - 2f^2 + f^4(1+\mu)\right] + \mu f^3 \xi + 4 f^2 \xi_a^3 + 4 f^2 \xi_a^3 \xi +$ $+ 4 f^2 \xi^2 \xi_a$
5	$\xi_a\left[1 - f^2(2-\mu)(1+\mu)^2 + f^4(1+\mu)^4\right] + \xi\left[f\mu^2 + \mu f^3(1+\mu)^2\right] +$ $+ 4 f^2 \xi_a^3 (1+\mu)^3 + 4 f (1+\mu)^2 \xi_a^2 \xi\left[1 + f^2(1+\mu)\right] + 4 f^2 \xi^2 \xi_a (1+\mu)^2$

The conditions of optimization

$$\frac{\partial R}{\partial f} = 0, \quad \frac{\partial R}{\partial \xi_a} = 0$$

lead to two nonlinear equations in f, ξ_a, whose solution is determined numerically.

For lightly damped SDOF structures with TMD and subjected to random white noise acceleration with spectral density S_o applied to the base, the optimum absorber parameters have been evaluated by Warburton (1982) using the optimization criterion on the non dimensional displacement variance $R = \sigma_{x_1}^2 \Omega_n^3 / 2\pi S_o$ are represented in the following diagrams.

The diagrams show that for each value of μ the optimized response decreases if the structural damping ξ increases, especially for lower mass ratios: this confirms that the insertion of a TMD is equivalent to an increase of the structural damping.

The optimal tuning f_{opt} and damping $(\xi_a)_{opt}$ are less sensitive to structural damping ξ in the common ranges and for reasonable mass ratios.

Such results can be extended to other types of excitations.
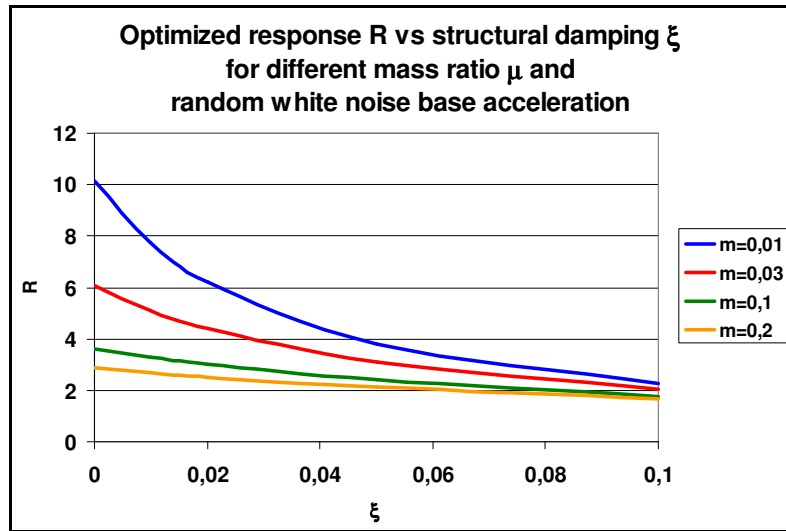
Figure 4.25. Structural damping and mass ratio effects on the response for white noise base acceleration.
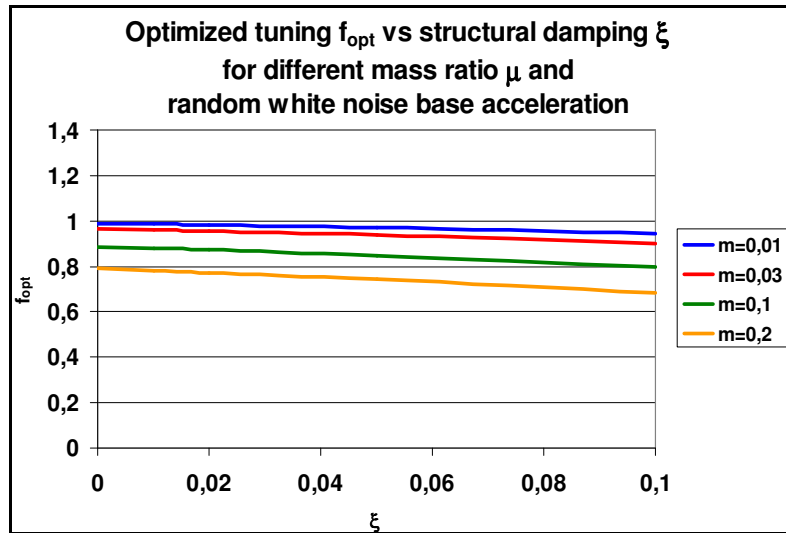
Figure 4.26. Structural damping and mass ratio effects on optimal tuning for white noise base acceleration.

160
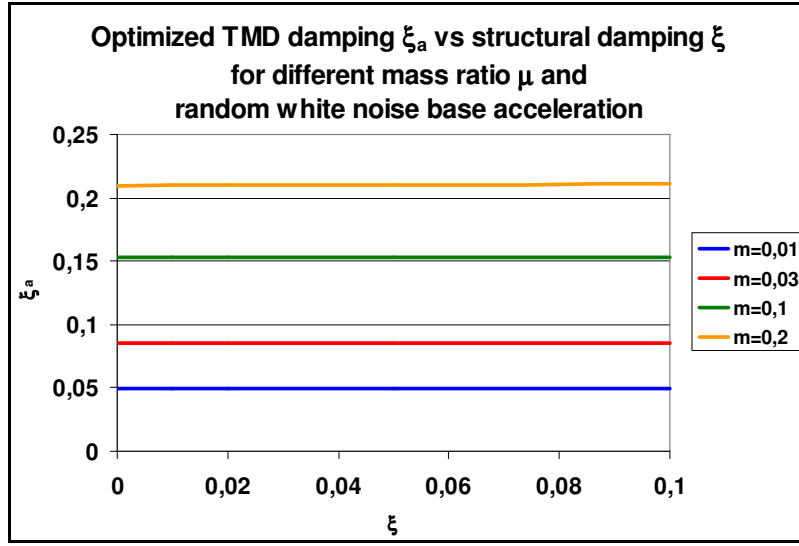
Figure 4.27. Structural damping and mass ratio effects on optimal damper damping for white noise base acceleration.

Criteria of literature
In Table 4.IV are reported some criteria proposed by researchers in the past, and used in particular to tune optimal TMD frequencies for undamped structures.

Maximum effective damping criterion
A particular optimization criterion is that introduced by Luft: it consists of the maximization of the effective damping of the combined structure+TMD system. The expression of the effective damping for an undamped structure is

$$\xi_e = \frac{\xi_a \mu f}{1 + \left[4\xi_a^2(1+\mu) - (\mu+2)\right] f^2 + (1+\mu)^2 f^4}.$$

Maximizing ξ_e in respect of f and ξ_a one gets the optimum values in terms of μ:

161

$$f_{opt} = \sqrt{\frac{1}{1+1.5\mu}}$$

$$\xi_{opt} = \sqrt{\frac{\mu}{4}\left(1-0.75\mu\right)}$$

Criterion – Response parameter	Author
Minimum Displacement of the main structure	Den Hartog (1956) Thompson (1981) Jacquot and Hoppe (1981) Fujino and Abe (1993)
Maximum dynamic stiffness of the main structure	Falcon et al. (1987)
Maximum effective damping of combined structure/TMD system	Luft (1979)
Minimum travel of the secondary mass relative to the main structure	Luft (1979)
Mixed criterion: Frequency tuning with displacement criterion and TMD damping by maximum effective damping criterion	Luft (1979)
Minimum velocity of main structure	Warburton (1982)
Minimum acceleration of main structure	Ioi and Ikeda (1978) Warburton (1982)
Minimum force in the main structure	Warburton (1982)

Table 4.IV. Optimization criteria of literature.

4.3.4 Equivalence MDOF-SDOF

Real systems have an infinite number of degrees of freedom and are usually modelled by multi-degree-of-freedom systems (MDOF), i.e. by the finite elements method.

The expressions of the non-dimensional response and of the optimal values for the absorber parameters are useful for complex systems only if the replacing real systems by equivalent SDOF system is reasonable.

In order to study the effect of natural frequency distribution, Warburton (1981) determined the optimal values for two-degree-of-freedom system, minimizing the response for a harmonic excitation including the two resonant conditions for the system. It has been demonstrated that as ω_2/ω_1 increases, the optimum parameters are asymptotic to Den Hartog's values.

If a real system is represented by an equivalent SDOF system, contributions to response by higher modes are neglected, but the numerical effect of such approximation must be investigated for different excitation types.

Two separate problems should be considered: the predict response and the optimal parameters for the absorber.

If the dynamic transfer function of the MDOF system is approximately that of the SDOF system, the analogy can be used to determine the response.

Analogy SDOF-MDOF in case of base-motion

Let's consider an undamped MDOF system: the equations of the free vibrations are

$$[M]\ddot{\underline{x}} + [K]\underline{x} = \underline{0}$$

The analogy with SDOF system in case of base-motion excitation (imposed displacement) is considered.

If the MDOF system has S masses $M_1, M_2...M_S$, with displacements $x_1, x_2...x_S$, connected to the base by springs of stiffness $k_1, k_2...k_S$ parallel to the displacement axes, the equations of the motion for forced vibration are

$$[M]\ddot{\underline{x}} + [K]\underline{x} = \underline{p}X_0 e^{i\omega t}$$

where $p_i = k_i \quad i \le S$, $p_i = 0 \quad i > S$.

The i-th modal mass, m_i is

$$\underline{\Phi}_i^T [M]\underline{\Phi}_i = m_i$$

163

If ω_i is the natural frequency of the i-th mode, one obtains

$$\underline{\Phi}_i^T [K] \underline{\Phi}_i = m_i \omega_i^2$$

If the response is represented by the i-th modal contribution

$$\underline{x} = \underline{\Phi}_i q_i$$

By substitution and pre-multiplying by $\underline{\Phi}_i^T$ and using the previous equations, one obtains

$$m_i \ddot{q}_i + m_i \omega_i^2 q_i = \underline{\Phi}_i^T \underline{p} X_0 e^{i\omega t} = \sum_{n=1}^{S} \Phi_{in} k_n X_0 e^{i\omega t}$$

If the absorber is attached to the mass M_a with the absorber displacement x_A in the same direction as x_a, the equation of the motion of the absorber is

$$M_A \ddot{x}_A + c_A \dot{x}_A + k_A x_A - c_A \dot{x}_a - k_A x_a = 0$$

The insertion of the absorber adds an additional term on the left side of the a-th equation of the system:

$$- c_A \dot{x}_A - k_A x_A + c_A \dot{x}_a + k_A x_a$$

Assuming $\dot{x}_a = i\omega x_a$, $\ddot{x}_a = -\omega^2 x_a$ and using the absorber equation to eliminate x_A from the additional term, the modal equation of the motion becomes

$$\left[m_i \left(\omega_i^2 - \omega^2\right) + \Phi_{ia}^2 \left(k_A + i\omega c_A\right) - \frac{\Phi_{ia}^2 \left(k_A + i\omega c_A\right)^2}{k_A - M_A \omega^2 + i\omega c_A} \right] q_i = \sum_{n=1}^{S} \left(\Phi_{in} k_n\right) X_0 e^{i\omega t}$$

If one wants to minimize the displacement response of M_n, x_n, and the input is the base acceleration $\ddot{X}_0 e^{i\omega t}$, from the previous equation one obtains

$$F(\omega) x_n = -\sum_{l=1}^{S} \frac{\Phi_{il} \ddot{X}_0}{\omega^2} e^{i\omega t} \left(k_A - M_A \omega^2 + i\omega c_A\right)$$

where

$$F(\omega) = \left[m_i \left(\omega_i^2 - \omega^2\right) + \Phi_{ia}^2 \left(k_A + i\omega c_A\right) \right] \left(k_A - M_A \omega^2 + i\omega c_A\right) - \Phi_{ia}^2 \left(k_A + i\omega c_A\right)^2$$

The effective mass of the main system M_{eff} is defined as that giving the same kinetic energy, if placed at the same coordinate of the absorber, as that of the main system, when both vibrates in the i-th mode:

$$\frac{1}{2}M_{eff}\dot{x}_a^2 = \frac{1}{2}\underline{\dot{x}}^T[M]\underline{\dot{x}}$$

Using the modal representation and the modal mass one obtains

$$M_{eff}\Phi_{ia}^2 = m_i$$

The effective stiffness k_{eff} is defined as that giving the strain energy in the i-th mode: $\frac{1}{2}k_{eff}q_i^2$.

Assuming $\quad k_{eff} = m_i\omega_i^2, \quad \mu_{eff} = \dfrac{M_A}{M_{eff}}, \quad \lambda = \dfrac{\omega}{\omega_i}, \quad f = \dfrac{\omega_A}{\omega_i}, \quad \omega_A = \sqrt{\dfrac{k_A}{M_A}},$

$\xi_A = \dfrac{c_A}{2\sqrt{k_A M_A}}$, the previous equation can be written in terms of non-dimensional displacement quantity:

$$\frac{\omega_i^2 x_n}{\ddot{X}_0} = \frac{\Phi_{in}\sum_{n=1}^{S}(\Phi_{in}k_n)}{k_{eff}}\left(\frac{A+iB}{C+iD}\right)e^{i\omega t}$$

where $\quad A = -\dfrac{1}{r^2}(f^2 - \lambda^2); \quad B = -2\xi_A\dfrac{f}{\lambda}; \quad C = (f^2 - \lambda^2)(1-\lambda^2) - \mu_{eff}f^2\lambda^2;$

$D = 2\xi_A\lambda f(1 - \lambda^2 - \mu_{eff}\lambda^2)$.

The latter expression agree with the homologous values of Table 4.I - Case7, where μ is replaced by μ_{eff}. This circumstances establish the analogy between SDOF and the controlled mode. Optimum absorber parameters can be used, while the equivalence factor $\sum_{l=1}^{S}\dfrac{(\Phi_{il}k_s)\Phi_{in}}{k_{eff}}$ can be used to determine the optimized response of the MDOF system.

Similar analogy can be stated for exciting forces, with the same conclusions.

Yet the analogy SDOF-MDOF is not always possible. If an absolute quantity is the response parameter (i.e. a main displacement) the analogy exists; on the contrary when the response parameter is a relative quantity (i.e. relative displacement $(Y = x - x_1)$) there is no analogy.

In fact M_{eff} is defined in terms of absolute velocity and not relative. If one neglects it and assumes the same definition of M_{eff}, the non-dimensional equivalent of $F(\omega)$ is $C + iD$; for the analogy it is necessary that the square bracket in equation should be proportional to $(A + iB)$ of Case 5 of Table 4.I. It occurs if

$$\Phi_{na} M_{eff} = \sum_{l=1}^{n} \Phi_{nl} M_l$$

while the definition of M_{eff} can be written as

$$\Phi_{na}^2 M_{eff} = \sum_{l=1}^{n} \Phi_{nl}^2 M_l$$

This equations are not compatible in general. So for Case 5 it is not possible to establish an analogy.

In fact the concept of effective mass of the MDOF system is essential in the derivation of the analogy; its definition depends on the equivalence of kinetic energy, defined in terms of absolute velocities. This produce the breakdown of the analogy if the relative displacement is the response parameter.

The analogy SDOF-MDOF system breaks down also if the damping of the main system is included.

For harmonic excitation the absorber reduces the response minimizes the resonant response in proximity of ω_i, and the associated mode $\underline{\Phi}_i$; for white noise excitation the relations of the response and of optimal values are in terms of the fundamental frequency and mode ω_1, $\underline{\Phi}_1$. The effectiveness of the relations depends on the transfer function, that should be reduced in proximity

166

of ω_1 by the insertion of the TMD and be relatively small in proximity of the higher frequencies.

Equivalent SDOF system can be established for almost all the excitation type and response, and the expressions for the optimal parameters of TMD can be used, if the frequency separation is sufficient to justify the one-mode approximation.

The hypothesis of the analogy that allow the treatment of a single mode as a SDOF system to obtain the optimized structural response (and the related optimal values of the parameters), is that the response is represented by the fundamental mode. This is true if the frequencies are not close, and the ratio ω_2/ω_1 is high.

For harmonic excitation the equivalent SDOF+TMD system must give acceptable values for the two maxima of the complex transfer function $H(\omega)$ for the real system+TMD. In narrowband optimization the contribution of the other maxima are neglected.

For white noise excitation all the maxima of $H(\omega)$ give a contribution to the mean square response: the adoption of SDOF system is correct if the contribution of the higher maxima to the response is negligible.

Furthermore, in the real structures the structural damping reduce the high mode response.

Numerical investigations showed (Warburton 1981,1982) that for harmonic excitation and small values of the mass ratio μ_{eff} the response is well predicted by SDOF system if the ratio of the first two frequencies is such that $\omega_2/\omega_1 > 2$, while for random white noise excitation the criterion is more stringent. If the frequencies become closer, the optimal values diverge from Den Hartog's and Warburton's values, and this effect is more pronounced for high mass ratio μ.

If such conditions are not satisfied (i.e. closeness of frequencies or/and high mass ratio) the optimized values of SDOF can be just a first approximation and starting point for an iterative procedure to find the optimal design values.

167

4.3.5 Theory for MTMD Systems

The performance of TMDs are very sensitive to fluctuations of frequency and damping: in this sense they are intrinsically non robust. Possible change of the environment in respect of that modelled, related to variations on the load scenarios, or to boundary conditions, or possible discrepancies with values hypothesised, can modify the natural frequencies of the structure and reduce the efficiency of the installed devices.

The use of more than one TMD with different dynamic characteristics has been proposed and investigated in order to improve robustness to uncertainties in the primary or in the secondary system.

At this regard Xu & Igusa, Yamaguchi & Harnpornchai, Abe & Fujino, Kareem & Kline, et al. have proposed the adoption of multi-TMD systems (MTMD): the main structure is connected to a battery of TMDs, generally having different mechanical characteristics.

The system structure+MTMD can be schematized as in the Figure 4.28: the structure is idealized by a single oscillator with natural frequency equal to that of the mode to be controlled, neglecting the contribution of the other modes.
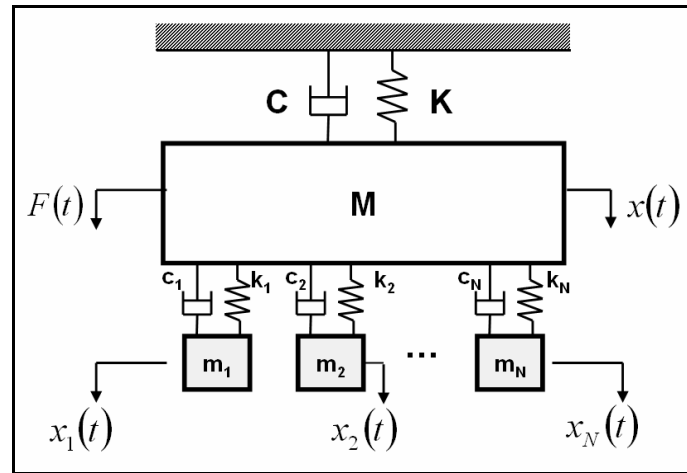
Figure 4.28. Structure+MTMD system.

The equations of the motion of the system has the following form

$$[M]\underline{\ddot{x}} + [C]\underline{\dot{x}} + [K]\underline{x} = \underline{F}(t),$$

where $[M] = \begin{bmatrix} M & 0 & 0 & ... & 0 \\ 0 & m_1 & 0 & ... & 0 \\ 0 & 0 & ... & 0 & ... \\ ... & ... & 0 & m_{N-1} & 0 \\ 0 & 0 & ... & 0 & m_N \end{bmatrix};$

M : mass of the primary structure (or generalized mass of the controlled mode); m_i : mass of the generic i-th installed device;

N : number of TMDdevices;

$$[K] = \begin{bmatrix} k' & \underline{k}_D^T \\ \underline{k}_D & [k] \end{bmatrix}; \qquad k' = K + \sum_{i=1}^{N} k_i \; ; \qquad \underline{k}_D = \begin{bmatrix} -k_1 \\ -k_2 \\ ... \\ -k_N \end{bmatrix};$$

$$[k] = \begin{bmatrix} k_1 & 0 & 0 & ... & 0 \\ 0 & k_2 & 0 & ... & 0 \\ 0 & 0 & ... & 0 & ... \\ ... & ... & 0 & k_{N-1} & 0 \\ 0 & 0 & ... & 0 & k_N \end{bmatrix};$$

K : stiffness of the primary structure;

k_i : stiffness of the generic i-th installed device;

analogous expressions are stated for the damping matrix $[C]$ and its elements.

The expression of the transfer function of the main system subjected to forces is

$$H_x(\omega) = \frac{1}{A + iB},$$

169

where $\quad A = 1 - \lambda^2 - \lambda^2 \sum_{i=1}^{N} \mu_i f_i^2 \left(\dfrac{f_i^2 - \lambda^2 + 4\xi_i^2 \lambda^2}{\left(f_i^2 - \lambda^2\right)^2 + 4\xi_i^2 \lambda^2 f_i^2} \right),$

$$B = 2\xi\lambda + \sum_{i=1}^{N} \mu_i \left(\dfrac{2\xi_i \lambda^5 f_i}{\left(f_i^2 - \lambda^2\right)^2 + 4\xi_i^2 \lambda^2 f_i^2} \right),$$

$\mu_i = \dfrac{m_i}{M}$: mass ratio of the generic i-th installed device;

$\lambda = \dfrac{\omega}{\Omega}$: ratio of exciting frequency to structural frequency;

$\omega_i = \sqrt{\dfrac{k_i}{m_i}}$: frequency of the generic i-th installed device;

$\xi_i = \dfrac{c_i}{2\sqrt{k_i m_i}}$: damping ratio in respect the critical of the generic i-th

device;

$f_i = \dfrac{\omega_i}{\Omega}$: *tuning* of the generic i-th installed device.

The MTMD in a parallel configuration modifies the transfer function of the system in respect of the single-TMD configuration, by flattening the typical peaks of the single-TMD response.

The expression of the transfer function emphasises that:

1. the contribution of each device to the response is independent on that of the others, and no mutual interaction occurs;
2. if the frequencies of the devices are equal, the MTMD system is equivalent to a single TMD connected to the main structure.

If the mechanical properties of the structure are known, it is possible to quantify the effectiveness of the devices by evaluating, for different exciting frequencies and of the design parameters, the Dynamic Amplification Factor, defined as

$$D = \sqrt{\dfrac{1}{A^2 + B^2}}$$

The adoption of a MTMD system introduces, in respect of the single TMD case, a multitude of supplementary parameters, that must be selected in such a way to increase robustness of the performance and keeping satisfactory levels.
The design of the device system consist of the determination of the following design parameters, as represented in the Figure 4.29:

- number of devices: N;
- geometric localization of the devices: $h_1, h_2 ... h_N$;
- total amount of installed mass: μ_{tot};
- criterion of distribution of masses: $\mu_1, \mu_2 ... \mu_N$;
- frequency range of devices: $\Delta\omega$;
- frequency spacing or frequency of each device: $\omega_1, \omega_2 ... \omega_N$;
- damping of the devices in respect of the critical: $\xi_1, \xi_2 ... \xi_N$.
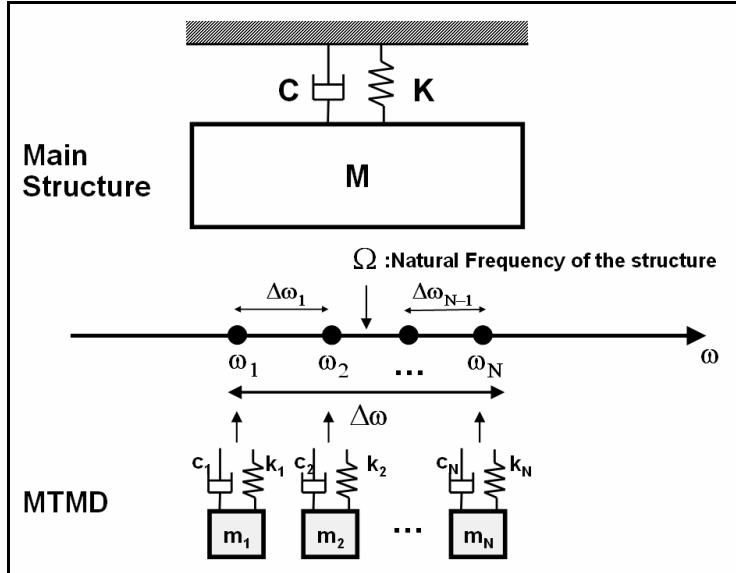
Figure 4.29. Structure+MTMD system and design variables.

Previous researches have showed that the MTMD system, with proper distribution of the frequencies of the devices, can increase, in respect the single-TMD configuration, the effectiveness and robustness performance, for their larger versatility in front of non-harmonic excitation and of possible *mistuning* scenarios.

Depending on the frequency range, the frequency response vary from a single-peaked function to a flattened curve, similar to that corresponding to an increase in damping for a single TMD.

The frequency range of MTMD is the most influencing parameter for effectiveness and robustness, while the damping ratio and the total number of devices play a secondary role, if the total mass ratio (and the achievable performance) is given.

Furthermore, the MTMD systems have the great advantage of redundancy, since can guarantee minimal levels of performance also in case of out-of-service of one or several devices.

Concerning practical aspects, the smaller size provide greater constructive, transport, installation and maintenance features.

All these attractive properties of MTMD will be emphasised in the Chapter 5 with reference to the case study presented.

4.3.6 Applicative Aspects

The effectiveness of TMD in suppressing the wind response have been well recognized and investigated in wind tunnel tests, full-scale tests, numerical investigations by many researchers. Such passive devices show to be less effective in case of seismic excitation, intrinsically non stationary, for two main reasons.

First, the earthquake excitation has a wider frequency bandwidth and the energy content at high frequency is higher, so that the higher modes are more involved with the response and the simplification of the structural behaviour with a SDOF system representing the first mode can be not adequate. Conventional TMD tuned to the fundamental frequency of the structure can suppress little or

even amplify the dynamic response of higher modes and so may fail in the reduction of the response.

Second, the first peak in the response time-history cannot easily reduced because TMD respond passively to the excitation induced by the structural movement and the mitigation happens through vibrations out-of-phase with the structural movement. They are not able to suppress in a short time the relative motion of the main system.

Concerning the first problem, a possible solution is the use of nonlinear TMD: for instance the spring with linear plus cubic behaviour provides a wider band of frequencies of vibration suppression. Another strategy to get wider suppression band consists of the combination of hardening absorber and softening structural spring.

Impact vibration absorber are effective at almost all excitation frequencies, while a significant increase of the suppression band is obtained by connecting the secondary mass to the main structure by viscoelastic materials like multiple rubber bearing.

The limits of passive devices have oriented the researchers towards active and hybrid mass dampers. Innovative approaches consist of the development of semi-active (SA) strategies, or hybrid mass damper or TMD with active capabilities (AMD) to mitigate the vibrations induced by wind and earthquake mainly used in tall building and towers; for these strategies the costs and the reliability must be kept into proper account.

4.4   Structural Control and Suspension Bridges

The design of challenge structures like suspension bridges, safety requirements are generally satisfied by the intrinsic structural properties, through an efficient structural organization, the use of dimensioning criterions adequate in respect of the expected loads, and on robust dependence hierarchies.

The attitude of long-span bridges to vibrate under dynamic loading depends mainly on their flexibility and low damping. The main actions developing structural vibrations are aerodynamic forces induced by wind, seismic loading and traffic loading.

The dynamic loading induced by wind is the most critical for long-span bridges because the vibrations induced by motion-dependent forces like wind aerodynamic forces are affect the performances of the bridge in terms of safety, serviceability, comfort. The motion of the bridges under wind loading makes an interaction effect between structure and flow that can emphasize the structural response: self excited forces can arise and increase the structural vibrations so much that even collapses have been experienced in the past (Tacoma Narrow Bridge, 1940).

The first type of wind-induced vibrations is due to vortex-shedding: at lock-in a resonant but self-limited amplification of the vibrations occurs.

Buffeting vibrations are due to the fluctuation of wind forces related to atmospheric turbulence; the gust response is a random process that increase with wind velocity.

For very high wind speed divergent oscillations may occur, depending on motion-dependent aerodynamic forces, in particular aerodynamic damping capable to get the system unconservative for negative damping and so unable to dissipate the energy introduced by the wind.

Concerning the wind-induced vibrations, their amplitude is related to wind mean speed as summarized in the following Figure.
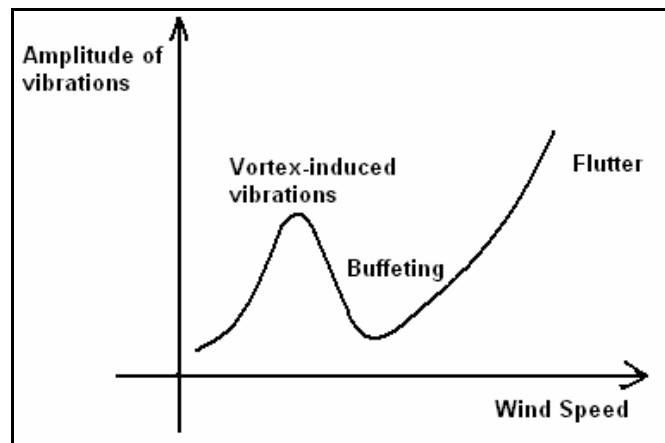
Figure 4.30. Wind-induced vibrations (Scanlan).

174

In the last decade it has been accepted that active control can be a viable technology for enhancing functionality and safety against natural hazards. Yet for long-span bridges many difficulties related to complex modelling, control design and implementation must be solved. Furthermore, active control for bridges has not been investigated as extensively as buildings.

Active control against flutter has been extensively studied using both mechanical and aerodynamic measures; while active seismic control of cable-supported bridges the first studies had been focused on exploring active cable tendon control and decentralized techniques by referring to simple structural models. Only in the last ten years the ASCE Task Committee on Structural Control Benchmarks has considered investigations of active/semiactive seismic response control in terms of detailed bridge models and allow for different control devices, giving a strong impulse to research.

In Table… is reported the state of art of the control strategies to suppress the wind-induced vibrations of different sub-structures of long-span bridges.

Girders

The most intuitive mean to front the problem of wind vibrations of girders is the shape or structural typology of the deck: at the moment two different trends distinguish the Japanese approach from the European one.

In Japan truss girders are deeply used in suspension bridges, for the high torsional stiffness and the smaller aerodynamic problems in respect of box girders: so the Akashi Kaikyo bridge, the longest ever built, has truss girders. The main targets of the wind-design of truss girders is related to the need of obtain high flutter wind speed, aerodynamic stability.

On the contrary box girders with high depth are subjected to galloping and vortex-induced vibrations, while flat box girders have classical (torsional) flutter and vortex induced vibrations: for these girders passive aerodynamic control is effective for the high sensitivity of aerodynamic forces to the geometry and to small changes on the sectional configuration by additional flaps (aerodynamic control).

Substructures	Vibrations	Structural and Passive control	Active Control
Pylons	Vortex induced vibrations	Corner-cut of section geometry	
	• During the erection	Mechanical control (TMD,TLD,Dampers) (Akashi)	AMD (Figure4.31)
	• During the operation life		
Cables	Vortex induced vibrations	Added masses	Semiactive devices
	Wake flutter		
Hangers	Vortex induced vibrations	Added masses	Semiactive devices (i.e. Ou&Li; Spencer; Ko&Ni)
	Interaction tower-hangers		
	Interaction with deck for relative motion	Passive dampers	
Deck	Vortex induced vibrations	• Section geometry (Diana) • Additional flaps	
	Buffeting	• Section geometry • Mechanical control (TMD,TLD, Dampers) (i.e. C.C. Chang et al.)	
	Flutter	• Section geometry • Additional flaps	Active flaps (Fujino)

Table 4.V. Control systems for the mitigation of the wind-induced vibrations of long-span bridges sub-structures.

The limit of aerodynamic control consists of the low versatility of the devices in respect of the aeroelastic phenomena that may occur, so that it is not simle to find aerodynamic devices effective for vortex-induced vibrations and for flutter/galloping.

Consequently the solution more commonly adopted consists of mechanical control devices such as Tuned Mass Dampers (TMD).

The effectiveness of such devices can be evaluated in wind-tunnel test; yet significant uncertainties can affect the prediction of the response: first the real structural damping that can be known only after the construction; second effective intensity of turbulence at the site. Such circumstances induce to install and calibrate the devices during the construction, with the support of monitoring data, and even during the service life.

Furthermore lower damping and turbulence can lead to underestimate the vortex-induced vibrations.

At the moment no control strategies have been used to control divergent vibrations, such as flutter or galloping, related to structural safety of the structure because of the long-term reliability and maintenance of the device.

Cables and Hangers

The vibration of cables is an important aspect affecting the serviceability and the fatigue of secondary elements of cable-stayed bridge: in general stays have low damping (about 0.1% critical damping ratio), resulting so the most vibrating structural members of this bridge typology. Furthermore the stays are subjected to wind and rain induced vibrations.

Such vibrations occur when particular conditions are verified, in terms of limited range of wind speed and velocity, moderate rainfall and smooth approaching of the wind. The vibrations have amplitude of the order of the cable diameters but involves more than the first modes. Inclined cables can experience also other types of self-excited vibrations.

In the case of twin parallel cables with a distance between 3 and 5 diametrs, a possible violent phenomenon is the wake galloping.

177

Also for parallel cables or hangers at reciprocal distance of the order of 10 diameters, violent vibrations due to wake-flutter may occur, as experienced in the suspender cables covered with PE in the Akashi Kaikyo bridge.

Vortex-induced vibrations are the most common for these members, but the amplitude is quite small and the provision of small damping can suppress them.

Another aspect pertaining the vibrations of the cables consists of the linear and nonlinear interactions with girders and pylons, the latter related to geometrical nonlinear effects due to the flexibility in respect of that of pylons and deck. The linear internal resonance occurs if the natural frequency ratio of the local cable to the girder/pylon global mode frequency is 1:1. The nonlinear interaction (autoparametric) is significant for ratios 1:2 and when cables have very low damping. These phenomena, proper of cable-stayed bridges, are not of great interest for gust response for the positive aerodynamic damping of the cables.

Cable and hangers are also subjected to fluctuating forces due to vortex shedding of the pylons under wind parallel in the longitudinal direction of the bridge. The wind tunnel test evidenced the possibility of high vibrations for this effect, especially for large pylons.

Possible system to control cable (stay,hangers) vibrations is connecting them by wires; such remedy increases stiffness but does not change the aerodynamic loading, so that damage n PE connections has been observed; so the most common control remedy is the installation of passive dampers near the anchorages, where the damping force is generated by the relative motion between cables and girders, but the damping that can be provided is low and its application is limited to short elements.

Pylons

Pylons are a principal sub-structure in the hierarchy of the components of a suspension bridge; though its vibrations are not more critical than the ones of the deck, their height and slenderness make them subjected to forced vibration for wind actions, for vortex shedding phenomena or for buffeting.

Such oscillations are critical during the constructive stages, when it is important the verticality of the structure, and it is more flexible, but must be limited also

178

during the service life, to reduce stresses, eccentricity and moments on the basement, and relate fatigue effects.

Vortex-shedding depends deeply on the sectional shape and geometrical optimization is generally conducted to reduce the phenomenon (*corner-cut* of rectangular sections).

At certain wind speed the vortex shedding is syncronized with the natural frequencies of the structure and generates aerodynamic alternate resonant forces (*lock-in*). For such excitation the only mechanism able to damp the vibrations is the structural damping; so the response of flexible steel structures with low damping can be affected from oscillations not allowable for the correct erection of the structure.

Furthermore the natural frequencies of the pylons decrease during the construction, and the structure becomes more sensitive at low wind speed: so tall steel pylons require temporal control for wind-induced vibrations. The construction of the pylon can require the provision of temporary stays to increase the stiffness, and passive/semi-active/active devices increasing the structural damping with time-depending performances. Aerodynamic control may be not suitable because it is needed for a short period, while mechanical control is more suitable because it can be removed when not necessary.

The design of the devices is conducted in order to reduce the oscillations of vibrations; this purpose is pursued after the evaluation of the energy content that the vortex shedding introduces into the structure. This specific quantity is currently determined by wind-tunnel tests.

Passive devices used are mainly Tuned Mass Damper, whose properties and capabilities have been described. Since each damper is tuned to a proper frequency and is ineffective for other frequency contents, each can control only one mode, at the closest frequency that can be excited by the wind.

Active control strategies, realized by masses and hydraulic actuators interacting by circuits and signals, have been an innovative opportunity experienced especially in Japan for the erection stages, with the use of actuators that move masses and produce damping forces according to different possible algorithms (Feedback Control, DVFB, H_∞ Control, Fuzzy Control, etc), in order to

mitigate the wind-induced and seismic effects (Figure 4.31). The versatility of this strategies, adaptive and controllable by proper algorithms, in front of time-varying structural and aerodynamic properties, and the possibility of controlling also the superior modes makes them particularly attractive, while the passive systems can operate just in limited frequency ranges.

Reasons of reliability suggest the use of active control for improvement of the response as an additional measure, able to guarantee minimum levels of protection also in case of out-of-service, by passive systems, and so as a redundant resort. In this sense hybrid strategies could be considered convenient for the erection and the service stages.

4.4.1 The Experience of the Akashi-Kaikyo Bridge

Honshu-Shikoku Bridge Authority conducted several investigations, analyses and wind-tunnel tests to improve the dynamic response of the pylons of Akashi Kaikyo Bridge under the action of wind.

These structure, 300m high, are flexible and prone to vibratory motion induced by the wind, especially in the erection stages, while during the service life the axial forces acting in the legs get this problem less relevant for the structural integrity.

The first measure to contrast wind induced vibration has been the *cut-off* of the section: the wind tunnel tests showed that a cruciform shape is able to reduce the amplitude of out-of-plane vibrations and to suppress the divergent torsional response at high wind velocities.

Yet during the design stages it has been observed that the amplitude of the vortex induced vibrations, occurring at wind speed lower than the design speed, were not compatible with the allowable stresses in the legs and in the structural joints. Consequently to satisfy safety requirements the control of the wind induced vibrations also the installation of damping devices was necessary.

It is important to underline that the control provision here is a safety measure in the project, and that it assume a decisive role together with the structural properties of the substructures to satisfy the Design Specifications.

Summary of bridge tower employing active control device during erection

Name of bridge	Years employed	Height, weight	Frequency range (Hz)	Moving mass, mass ratio (%[a])	Control algorithm	No. of controlled modes
Rainbow Bridge Pylon 1	1991–1992	119m 4800 tonf	0.26–0.95	6 ton×2 0.6	Feedback control	3
Pylon 2	1991–1992	117m 4800 tonf	0.26–0.55	2 ton 0.14	DVFB[b]	1
Tsurumi-Tsubasa Bridge[c]	1992–1993	183m 3560 tonf	0.27–0.99	10 ton×2 0.16	Optimal regulator DVFB	1
Hakucho Bridge Pylon 1	1992–1994	127.9m 2400 tonf	0.13–0.68	9 tonf 0.4	Sub-optimal feedback control	1
Pylon 2	1992–1994	131m 2500 tonf	0.13–0.68	4 ton×2 0.36	DVFB	1
Akashi Kaikyo Bridge Pylons 1 & 2	1993–1995	293m 24,650 tonf	–0.127–	28 ton×2 0.8	Optimal regulator DVFB	1
Meiko-Central Bridge[c] Pylon 1	1994–1995	190m 6200 tonf	0.18–0.42	8 ton×2 0.98–1.15	H_∞ Feedback control	1
Pylon 2	1994–1995	190 6200 tonf	0.16–0.25	0.17–0.38		
1st Kurushima Bridge Pylon 1	1995–1997	112m 1600 tonf	0.23–1.67	6 ton×2 0.15–2.05	Sub-optimal regulator control	3
Pylon 2	1995–1997	145m 2400 tonf	0.17–1.70	10 ton×2 0.3–2.6	H_∞ Feedback control	3
2nd Kurushima Bridge Pylon 1	1994–1997	166m 4407 tonf	0.17–1.06	10 ton×2 0.41	DVFB/H_∞	2
Pylon 2	1995–1997	143m 4000 tonf	0.20–1.45	10 ton×2 0.54–1.01	Fuzzy control	more than 3
3rd Kurushima Bridge Pylon 1	1995–1996	179m 4500 tonf	0.13–0.76	11 ton×2 0.3–2.4	Variable gain DVFB	1
Pylon 2	1994–1996	179m 4600 tonf	0.13–0.76	11 ton×2 0.3–2.4	H_∞ output feedback control	1
Nakajima Bridge[c]	1995–1996	71m 580 tonf	0.21–1.87	3.5 ton×2 1.0–10.6	Fuzzy control	3

[a] Percent of first modal mass.
[b] Direct velocity feedback.
[c] Cable-stayed bridge. Others are suspension bridges.

Figure 4.31. Examples of bridge tower employing active control during erection (Fujino, 2002).

Concerning the choice of the damping devices, Tuned Mass Dampers (TMD) and Hybrid Mass Dampers (HMD) (a combination of passive and semi-active type) were preferred to Tuned Liquid Damper (TLD), Friction Damper, etc. because their high reliability and low cost.

The design of the devices has been conducted for two different structural configurations:
-    the constructive stages;
-    the service life.

Each of them is associated to established levels for allowable stress in the steel plates, and correspond to amplitude values of the structural oscillations.

The attention of the designer has been paid on two families of vibrations, corresponding to two natural modes to be controlled:
-    the *out-of-plane* vibrations;
-    the *torsional* vibrations.

For each kind of vibrations different load scenarios have been assumed in the tunnel tests, with different levels of Permanent Loads, Live Loads, Thermal Loads, and Wind Loading. In particular the wind loading and its frequency content is chosen according to the frequency of the mode to be controlled: lower speed for the first out-of-plane mode, and a higher level for the torsional one.

In order to keep the vibratory amplitudes (and the stresses) until the established limits, for each mode of vibration target values for the damping were identified.

Through a numerical-experimental iterative procedure on two-degree-of-freedom system, starting from hypothesised values of the device mass, frequency and damping, and in the hypothesis of harmonic loading (because of the vortex shedding nature of the excitation) the equivalent damping is evaluated. The procedure took into account of tuning and damping uncertainties (in the range of $\pm5\%,\pm10\%$ respectively). The iteration stopped when the minimum mass value is obtained, giving the target equivalent damping.

Table 4.VI and Figure 4.32 show the control configuration provided during the erection and after the completion of the bridge.
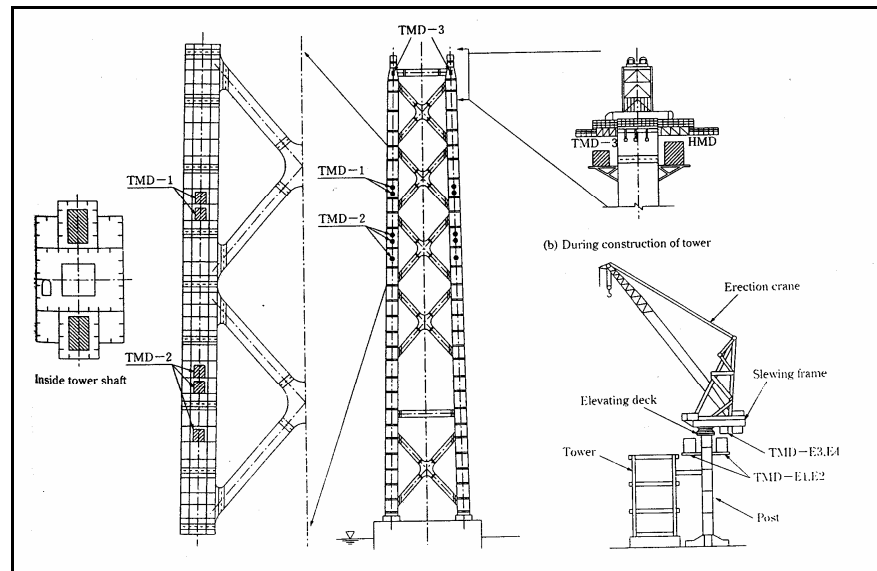
During the construction of the tower three kinds of provisions have been adopted:

- passive TMDs (TMD-E1, TMD-E2) and (TMD-E3, TMD-E4) on the top of the erection crane, with different tuning for different frequency content of wind loading;
- passive TMD (TMD-1, TMD-2) inside the towers to control out-of-plane and torsional vibrations, kept also in the service life;
- passive TMD (TMD-3) on the top of the tower;
- semi-active dampers (HMD) at the top of the tower for the early construction of the main cables.

For the service configuration only the passive devices TMD-1 and TMD-2 for the out-of-plane and torsional vibrations are kept, tuned at their proper frequency for the definitive structural configuration.

During the construction of the tower		
Frequency (Hz)	**Damping devices**	**Weight of TMDs**
0.6 – 1.3 (Torsional)	TMD-2 (inside tower)	114 ton
0.3 – 0.6 (Out-of-plane)	TMD-1 (inside tower)	84 ton
	TMD-3 (top of the tower)	21 ton
≈ 0.3	Semi-active damper (top of the tower)	
After completion of the bridge		
0.74 (Torsional)	TMD-2 (inside the tower)	114 ton
0.44 (Out-of-plane)	TMD-1 (inside the tower)	84 ton

Table 4.VI. Frequencies and TMDs used for the towers of the Akashi Kaikyo Bridge (Koshimura, Tatsumi, Hata, 1994).

Figure 4.32. Location of vibration control devices and crane (Koshimura, Tatsumi, Hata, 1994).

It is worthnoting to mention that during the construction a continuous monitoring of the tower behaviour has been conducted in order to:
-   identify the dynamic properties of the tower and of the devices, arranging a *mode- updating*;
-   evaluate the change on the response due to the installation, and the provided damping measured;
-   re-calibrate the properties of the devices with the collected data;
-   compare the experimental results with those of the tunnel tests, and evaluate the actual resonant wind speed (according with the Strouhal number), also for different wind orientations;
-   evaluate the safety of the structure in respect of the Design Specifications.

Chapter 5

CONTROL OF THE PYLON OF A SUSPENSION BRIDGE

- Decomposition, Substructuring, Characterization of the Soil-Foundation-Pylon System
- Targets of Design (System Dependability): Efficiency, Robustness, Redundancy
- Buffeting Response of the Pylon
- Structural Control from the Erection to the Service Life
- Experimental Approach for the Mitigation of the Wind Response by TMDs
  - Base of Design: Suppression of Lock-in Vibrations
  - Mitigation of Buffeting Response: Efficiency and Optimization of TMDs
  - Demand of Robustness and Robust Design: Performance of Multi-TMD
- Performance of TMDs under Seismic Loading
- Proposal of an Experimental Reliability-based Method (Monte Carlo Simulations) to support the final Decision Process

185

Abstract

In this Chapter the Systemic-Performance-based appraoach is applied for the design of a TMD passive control system of the pylon of a long span suspension bridge.

The attention is focused on:

- the characterization of the substructure inserted in:
    a)   the global structural system, through substructure analysis for *layering*;
    b)   a design environment, through a numerical (supported by experimental available data) investigation on the wind-structure-soil interaction effects from the erection to the service life in the uncontrolled configuration;
- the performance and the targets of the design of the control system;
- the evolution of the design targets during the construction phases;
- the experimental optimization of the control system and some dicotomic relationships between the established targets;
- the efficiency of the control system under seismic loading.

Finally a proposal of reliability-based method for the optimization of the design and supporting the decision process on the installation convenience is reported.

5.1 Introduction

The design of a TMD passive control system for the pylon of a suspension bridge a Systemic-Performance-based approach appears suitable because of the structural complexity of the whole structural system, of the loading actions, the possible scenarios of contingency from the erection to the service life, and the interaction mechanisms that can be baited.

The pylon, which is a principal substructure in the structural system, is considered inserted into a *Meso-Level* sub-system, the soil-pylon-suspension system. It is connected to the external substructures (soil and cables) through *interface* components, foundations and saddles, which have also an interface/boundary role in the substructure analysis for *layering*.

The substructure analysis is here an effective and simplificative tool for the analysis, because it focuses the attention on the sub-system inserted in a more complex context, reducing the number of degree of freedom and increasing the degree of freedom in the substructures which have a relevant role in the *Meso-Level* response. In this way, for example, the natural modes of the pylon are the first in the substructure model, but they would be very high in the whole bridge modal rank.

The *Performance* targets of the control system – *Efficiency, Robustness, Redundancy* – are outlined, and also the role of Structural Control from the critical erection to the service life, with changes in the structural properties and in the requested performance during the constructive stages.

The multitude of design parameters introduced by multi-device configuration (MTMD) (masses, damping, frequencies, frequency range and criteria of distribution, location of the devices), together with the geometric, structural and loading complexity suggested the adoption of an *Experimental Approach* to explore the response by Finite Element models, and to evaluate the capabilities of the Tuned Mass Dampers in the mitigation of the gust response, according to the fixed tasks.

Seismic analyses in the time domain and in the stationary frequency are collaterally reported in order to verify possible loss of safety introduced by the control systems in respect of the originary uncontrolled configuration.

187

The come out dicotomy between *Safety* and *Robustness* of the control system performance suggest a compromise optimization: a reliability – still experimental (Monte Carlo Simulation)- approach is proposed to identify the optimal solution and to support a technical cost-effective *decision process* on the convenience of the installation.

5.2 Structural Decomposition and Substructuring: the *Meso-level* Pylon-Foundations-Soil System

The size and the complexity of the structure, according to what said in Chapter 2, require the development of more than one structural model, in the different scale of description, starting from the whole bridge, with simple boundaries and global properties of beam, to more refined models representing also soil and foundations.

Global models of the bridge: modes, frequencies involving the pylons and reduction for substructuring
The first dynamic characterization pertains the global properties of the bridge.
For these global (*Macrolevel*) characterizations, frame model have been used, capable of nonlinear geometric effects.

The bridge substructures have been classified as represented in Figure 5.1 and Table 5.I, and modelled through about 1850 beam elements, in 13 different groups, with two different materials (steel) and interconnected in a system of about 1200 nodes with six degrees of freedom. Permanent loads and masses are modelled as distributed along the elements.
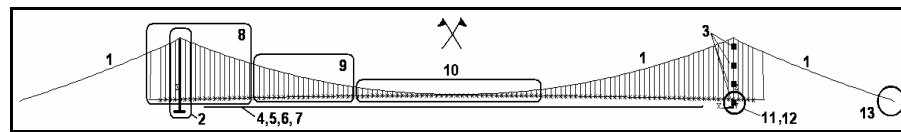
Figure 5.1. Global 3D frame model and element groups (frontal view).
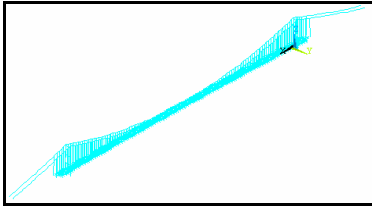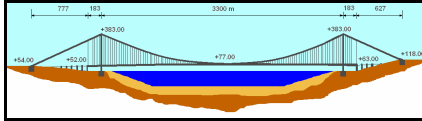
Groups	Substructures	Number of Elements
1	Main Cables	350
2	Pylons Legs	4 x 27
3	Transverses of Pylons (2 x 4)	52
4	Railway Girders	126
5	Roadway Girders	2 x 124
6	Transverses	484
7	Concentrated Masses	232
8	*"Long"* Hangers (Group A)	40
9	*"Medium"* Hangers (Group B)	48
10	*"Short"* Hangers (Group C)	150
11	Control Devices (Longitudinal)	4
12	Control Devices (Transversal)	4
13	Boundary links (Anchorages)	4

Table 5.I. Classification of structural elements for global modeling.

The mechanical global properties and the expected structural damping of the substructures used in the modelling are briefly reported in Table 5.II.

The global models have been used to identify the structural properties of the whole bridge, and to check the modes (and the corresponding frequencies) involving the pylons.
In Figures 5.2 and 5.3 are represented the first 6 modes of the bridge and the histogram of its first 150 modes.

189

Global Model Main Characteristics	Main Features of the Bridge
Number of Nodes: 1190	**Main Cables**: A=2x2x1.01 m^2
Number of Elements: 1850	**Pylon Legs**
Number of Elements types: 13	A=8.4252 m^2 ; Ixx=52.941 m^4 ;
Types of Element: Beam, Contact (devices)	Iyy=131.5288 m^4 Izz=222.3904 m^4
Formulation: High Displacements, Small Strain	**Pylon Transverses:**
	A=1.9792 m^2 ; Ixx=13.9804 m^4 ;
Steel density: 7980 kg/m^3	Iyy=67.2698 m^4 Izz=6.1036 m^4
Young Modulus :	**Railway Girder**:
2.06E11 kg/m^2 (pylons, girders, transverses)	A=0.2996 m^2 ; Ixx=0.6877 m^4 ;
	Iyy=0.2245 m^4 Izz=2.4394 m^4
1.863E11 kg/m^2 (cables, hangers)	Permanent Load: 2700 kg/m
Structural damping: $\xi = 0.5\%$	**Highway Girder**:
	A=0.45 m^2 ; Ixx=1.1642 m^4 ;
	Iyy=0.3589 m^4 Izz=8.0787 m^4
	Permanent Load: 1630 kg/m
	Hangers: Three groups with sections
	A1=0.0327 m^2 ; A2=0.0137 m^2 ;
	A3=0.0117 m^2
	Vertical Forces transmitted by the main cables on the Sicily Pylon under self-weight and Permanent Loads:
	Fz= 0.94963 N = 96802 tons

Table 5.II. Mechanical properties of the bridge substructures.
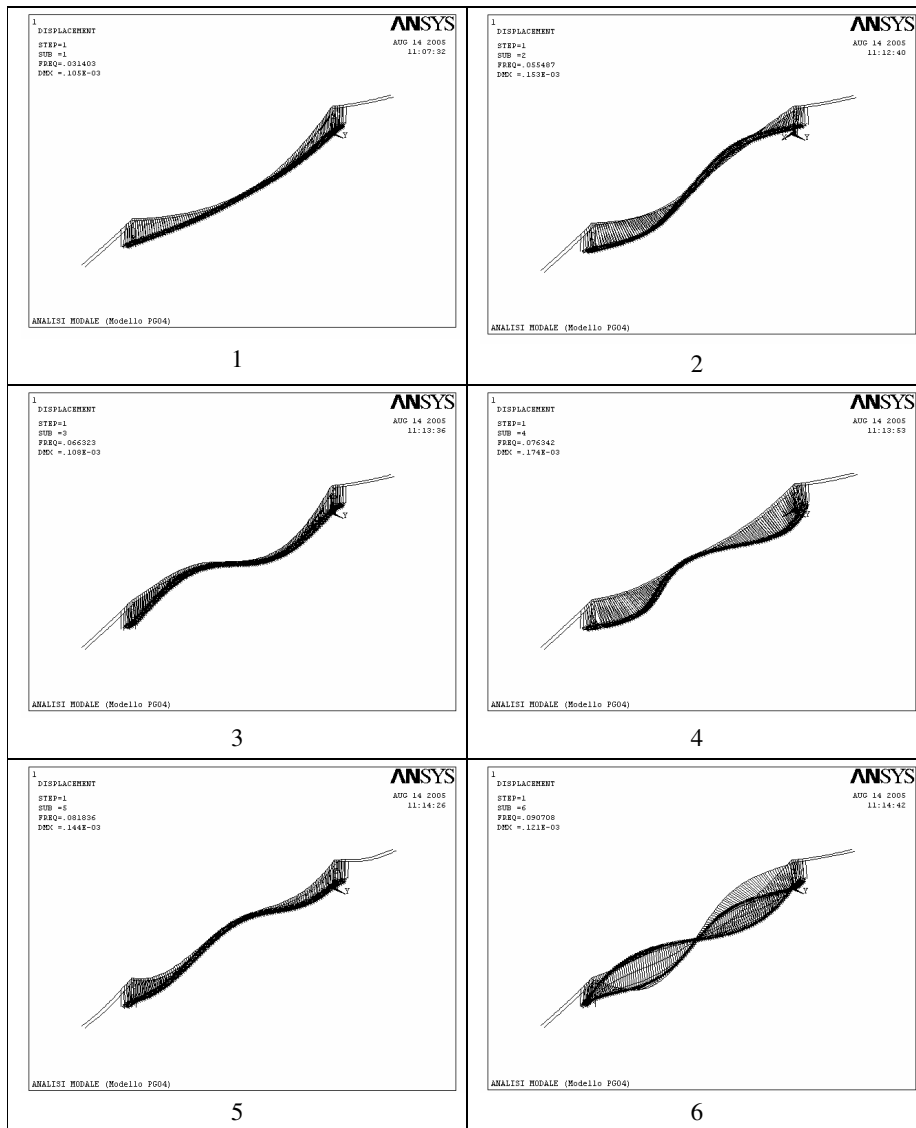
Figure 5.2. Global model of the bridge: Natural modes (Giuliano).
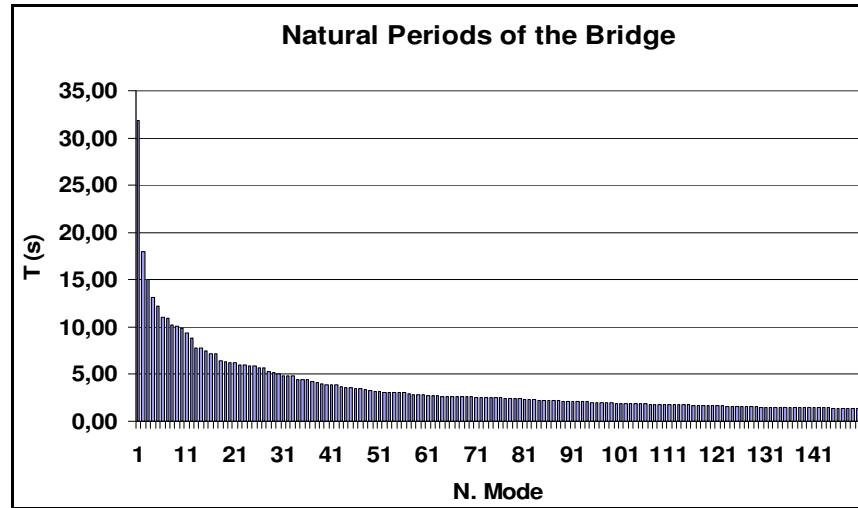
Figure 5.3. Histogram of the first 150 eigen-frequencies of the bridge (Giuliano).

The solution of the eigenvalue problem, solved by the Lanczos algorithm, outlines mode 64 and 90, at frequencies of 0.37 Hz. and 0.47 Hz., respectively, as first exciting the pylon in bending and in torsion (Figure 5.4).

Mode 64: T=2.68 s   Mode 90: T=2.11 s
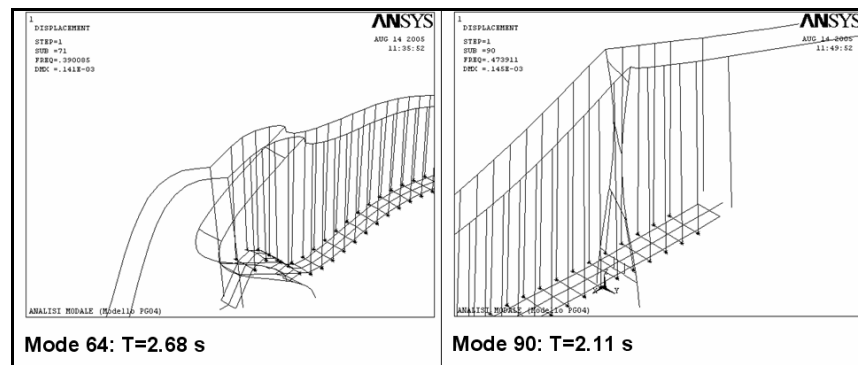
Figure 5.4. First modes (and frequencies) involving the pylon substructure (Casciati & Giuliano, 2006).

The high number of DOF of the global model and the high frequencies of the modes exciting the pylon suggest the adoption of substructuring to focus the pylon response using a reduced number of DOFs and saving time and CPU resources.

The *substructuring* technique has been used to reduce a set of finite elements to only one, represented through a special matrix (superelement).

If $[K]$ is the stiffness matrix, $\{u\}$, $\{F\}$ the displacement and loads vectors of the structural nodes, in the static case the basic equation

$$[K] \cdot \{u\} = \{F\}$$

can be partitioned in accordance to the distinction of master (retained)/slave DOFs:

$$\begin{bmatrix} [K_{mm}] & [K_{ms}] \\ [K_{sm}] & [K_{ss}] \end{bmatrix} \begin{Bmatrix} \{u_m\} \\ \{u_s\} \end{Bmatrix} = \begin{Bmatrix} \{F_m\} \\ \{F_s\} \end{Bmatrix}$$

By substituting the expression of $\{u_s\}$ obtained from the second equation into the first, it is obtained

$$\left([K_{mm}] - [K_{ms}][K_{ss}]^{-1}[K_{sm}]\right) \cdot \{u_m\} = \{F_m\} - [K_{ms}][K_{ss}]^{-1}\{F_s\}$$

that can be synthesised as

$$[\hat{K}] \cdot \{\hat{u}\} = \{\hat{F}\}$$

where

$[\hat{K}] = [K_{mm}] - [K_{ms}][K_{ss}]^{-1}[K_{sm}]$: superelement stiffness matrix;

$\{\hat{F}\} = \{F_m\} - [K_{ms}][K_{ss}]^{-1}\{F_s\}$: superelement force vector;

$\{\hat{u}\} = \{u_m\}$: retained (master) node displacements.

In case of nonlinear analyses it is necessary to update the stiffness matrix at every equilibrium iteration; the updating is not necessary if the substructuring is applied on a linear portion of a more general nonlinear structure, or when a linearized solution of the substructured structure is acceptable.

193

In the dynamic case, the basic solving equation in matrix form

$$[M]\cdot\{\ddot{u}\}+[C]\cdot\{\dot{u}\}+[K]\cdot\{u\}=\{F\}$$

is similarly transformed into

$$[\hat{M}]\cdot\{\ddot{\hat{u}}\}+[\hat{C}]\cdot\{\dot{\hat{u}}\}+[\hat{K}]\cdot\{\hat{u}\}=\{\hat{F}\}$$

where $[\hat{K}]$ and $\{\hat{F}\}$ keep the same previous expression; concerning the mass and damping matrices the partition and condensation are not practicable because of the dependence of the condensed matrices on $\{\dot{u}\},\{\ddot{u}\}$. To overcome this difficulty, Guyan (1965) proposed a simplification for the expression of the mass and damping matrices, giving an approximate solution:

$$[\hat{M}]=[M_{mm}]-[K_{ms}][K_{ss}]^{-1}[M_{sm}]-[M_{ms}][K_{ss}]^{-1}[K_{sm}]+$$
$$+[K_{sm}][K_{ss}]^{-1}[M_{ss}][K_{ss}]^{-1}[K_{sm}]$$

$$[\hat{C}]=[C_{mm}]-[K_{ms}][K_{ss}]^{-1}[C_{sm}]-[C_{ms}][K_{ss}]^{-1}[K_{sm}]+$$
$$+[K_{sm}][K_{ss}]^{-1}[C_{ss}][K_{ss}]^{-1}[K_{sm}]$$

So the stiffness matrix is exact, while the mass and the damping ones are approximate. The accuracy of the solution, consequently, depends strictly on the choice and on the number of master DOFs selected, and so on the dimension of the reduced problem: as it increases, the solution approximates that of the original problem.

The choice of the master DOFs is arbitrary, and different sets can give in the same way acceptable results. The choice, however, must be done in such a way to catch the modes and the frequencies of interest, and so their number must be enough large and their direction such that the directions of the modal vibration are caught. The location must be chosen also considering the place having high masses and relatively low stiffness. This circumstances suggest that master nodes for a suspension bridge are located in the main cables and in the girders.

Other necessary locations are the interface between substructured portion (superelement) and non substructured (nonsuperelement), and the location of any applied force.

For the case-study bridge, the nonsubstructured portion (nonsuperlement) consists of the Pylon legs and transverses: the nodes of the original model are retained, while the other master (retained) DOFs have been located (Figure 5.5):

- in the main cables, with a step of discretization $\Delta x = 90m$, corresponding to three elements in the original model;
- along the railway girder, with a step of discretization $\Delta x = 90m$, corresponding to three elements in the original model;
- in the saddles, which is the interface between pylon and cables.

The nodes are selected in such a way to catch the modes of the bridge, involving the deck and the main cables, while all the available DOFs for each node are considered, according to the type of the incident element (LINK/BEAM).

This choice allows also to consider the dynamic interaction effects between the main cables and the substructure pylon.

The resulting number of nodes of the substructured model is 228 (68 for the pylon+160 for the bridge), while for the original model the number of nodes was 1190.

Concerning the assemblage of the stiffness matrix, the only self weight load configuration is considered, since the longitudinal modelling of the wind impact on the bridge is difficult to implement and there are not data from the wind tunnel tests.

In general, starting from the reduced solution $\{\hat{u}\} = \{u_m\}$, it is possible to expand the results and to get the complete set of the results for the whole structure: as a consequence of the simplifications performed, and the focus on the only substructure *Pylon*, this expansion has not been pursued.
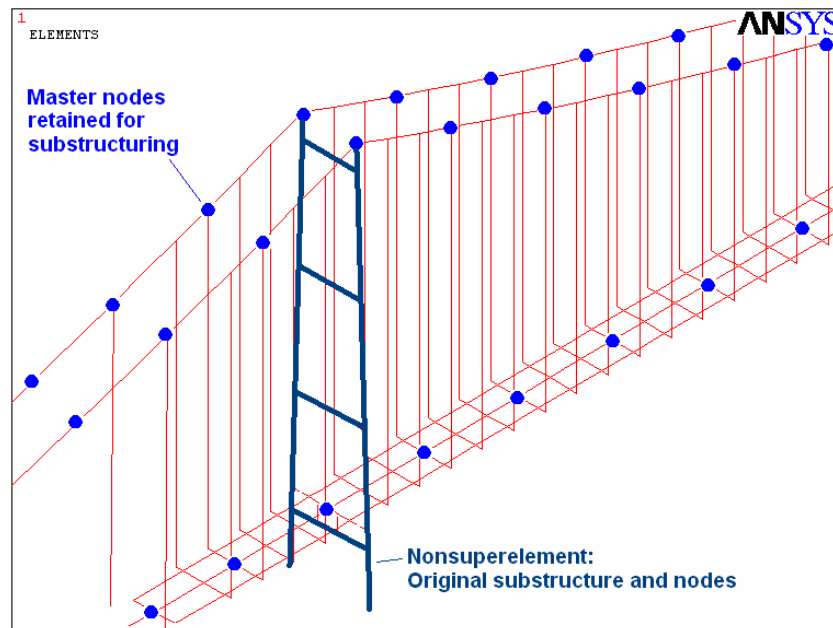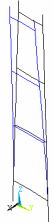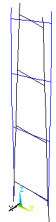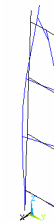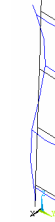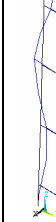
Figure 5.5. Location of master nodes for substructuring and matrix reduction. (Giuliano, 2006).
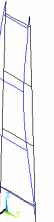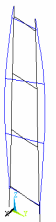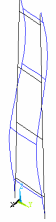
Dynamic properties of the pylon
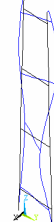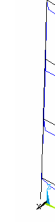
The first dynamic characterization has been done assuming the expected values for the mechanical parameters, in particular for the soil stiffness. The first modes (and the frequencies) of the pylon in the *free-standing* and *in-service* configuration are reported. They are computed through the fixed-base, *substructured* and *pre-stressed* model, in order to reduce the number of degrees of freedom and compute also the further structural modes of the pylon.

The satisfactory agreement of the substructured model frequencies of the pylon with those of the complete global allows the adoption of the substructured model for the investigations on the wind response of the pylon and its mitigation.

196

Free-standing **pylon**: Modes of *substructured* pre-stressed model							
Mode 1 T=10.85	Mode 2 T=4.12 s	Mode 3 T=3.54 s	Mode 4 T=1.66 s	Mode 5 T=1.27 s	Mode 6 T=1.14 s	Mode 7 T=0.60 s	Mode 8 T=0.56 s

Table 5.V. Modes and frequencies of the pylon (substructured model) (Giuliano, 2006).

In-service **pylon**: Modes of *substructured* pre-stressed model							
Mode 1 T=2.74s	Mode 2 T=2.20s	Mode 3 T=1.79 s	Mode 4 T=0.78 s	Mode 5 T=0.73 s	Mode 6 T=0.73 s	Mode 7 T=0.52 s	Mode 8 T=0.38 s

Table 5.VI. Modes and frequencies of the pylon (substructured and pre-stressed model) (Giuliano, 2006).

Numerical models of the pylon: structural configurations, levels of modelling, SSI effects

The numerical modelling of the pylon is conducted from the first stages of the erection to the service life as previously represented.

The numerical modelling of the pylon is conducted in three different levels:

- a single degree of freedom model (SDOF system), representing the first mode of the structure, for which analytical solutions for simple
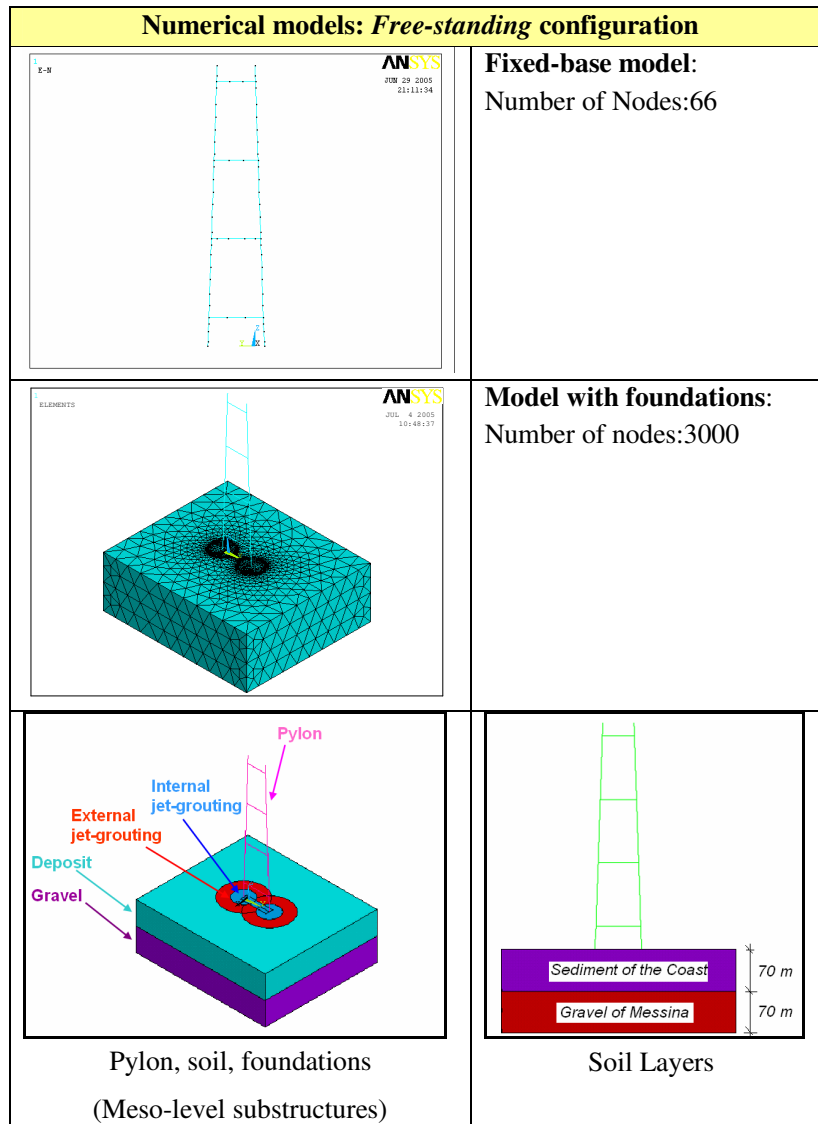
197

excitation are available: these models have been studied for the first dimensioning of the control system after the solution of the eigenvalue problem of the structure;
- a multi-degree of freedom model, in matrix formulation and using the Euler beam formulation. These models have been used for the first evaluation of the structural modes and frequencies of the structure, with simplified boundary conditions: fixed degrees of freedom at the base of the pylon;
- multi-degrees of freedom models, realized by the support of a commercial finite element multi-physics code, *ANSYS*®, at different levels, from the global configuration to *substructured* models, representing in detail geometry and mechanical properties of soil and foundations.

The numerical models have been realized in order to reproduce the structure and its boundaries in different configuration along the constructive process until the service life.

In particular, the modelling assumed (Figures 5.6, 5.7):
- two levels of structural modelling: ***Fixed-base*** models and ***Models with foundations***;
- two structural configurations: the ***Free-standing*** (before the montage of the main cables), and the ***In-service*** configuration, expected when the bridge will be available for the users (in complete or *substructured* formulations, to model the saddle boundaries on the top).

Numerical models: *Free-standing* configuration	
	Fixed-base model: Number of Nodes:66
	Model with foundations: Number of nodes:3000
  Pylon, soil, foundations (Meso-level substructures)	 Soil Layers

Figure 5.6. Numerical models of the pylon: *Free-standing* configuration (Casciati & Giuliano, 2006).

199
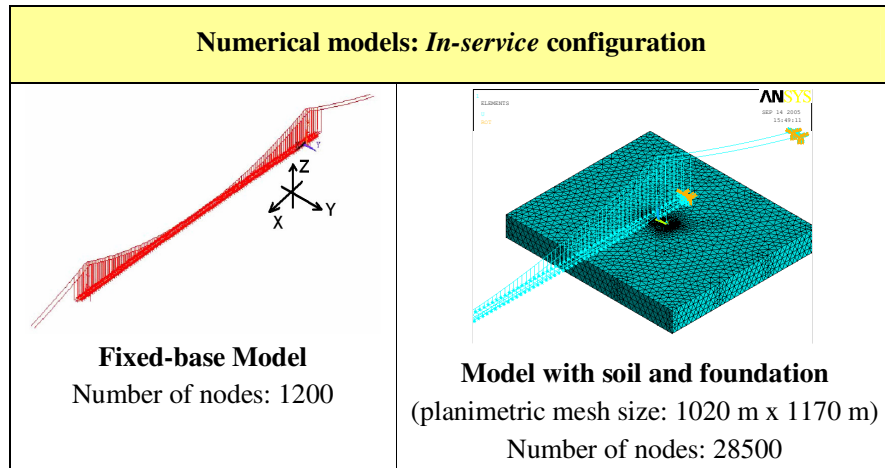
Figure 5.7. Numerical models of the pylon: *In-service* configuration (Giuliano, 2006).

Fixed-base models are frame structures composed by beam elements.

Three different models have been developed: the first, trivial, which has all the displacements and rotations in the base locked. This model can take into account the geometric nonlinearity of the structural behaviour, but the blockage of all the degrees of freedom at the bases of the pylons can be not enough accurate in case compressible soil.

A further updating of the model will be necessary to consider the flexibility of the system structure-foundation in the response, in general frequency dependent, and possible nonlinear effects related to the expected levels of strain in the soil.

Models with foundations are implemented through a direct method from the *Fixed-base* models by substituting the simple boundary conditions with a more realistic representation of the boundaries.

This method allows to simulate, by a finite dimension model, the behaviour of the soil which has indefinite dimension, and to keep into account possible

nonlinear effects, and in a more robust way than any multi-step method (suitable for linear systems coupling kinematical and inertial interaction effects), even if at higher computational costs.

As represented in Appendix B, the soil in the reference site has two layers, one of sediments and one of gravel.

The geometry and the mechanical properties of the foundations and of the soil layers have been modelled on the basis of the drawings of the foundations, using 3D finite elements. In this way one account for the foundation geometry, the actual embedment and the soil mechanical properties as expected after the mechanical treatments.

At first the soil has been modelled using a mesh of tetrahedric/prismatic 3D finite elements (SOLID45 in ANSYS®), with linear elastic and isotropic constitutive law, obtained from the soil characteristics in possession and using empirical relationships of literature. The element is defined by eight nodes having three degrees of freedom at each node: translations in the nodal x, y, and z directions. The element has plasticity, creep, swelling, stress stiffening, large deflection, and large strain capabilities.

The nominal mechanical characteristics of the soils involved, consistent with the strain levels under self weight and permanent load of the bridge, are summarized in Table 5.IV.

Groups	Density γ (kg/m^3)	Modulus of Young E (N/m^2)	Poisson's ratio ν
Internal jet-grouting	2000	1,8e10	0,25
External jet-grouting	2000	1,2e10	0,32
Sediments of the Coast	1800	1,0e8	0,4
Gravel of Messina	2100	2,0e8	0,4

Table 5.IV. Mechanical properties of the model groups.

Concerning the mesh dimension, the volume of the modelled soil has been selected as adequate to describe the morphology and the layers of the site: the extension of the mesh is such to contain the volume of soil significantly affected by the application of the permanent loads of the bridge.

In case of static loading, the modelling of a limited portion of the soil is sufficient, with a fictitious boundary (displacement Dirichlet condition), at an opportune distance from the structure.

In Figure 5.8, 5.9 are represented, in the static field, the vertical and horizontal displacement of the foundation block versus the length of the mesh in the service configuration. The diagrams show that in this case at least a dimension of 800 m is required.
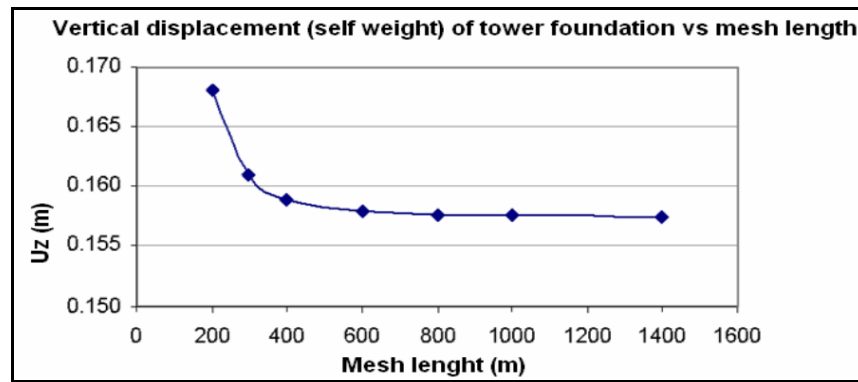
Figure 5.8. Vertical and horizontal displacement vs mesh dimension.
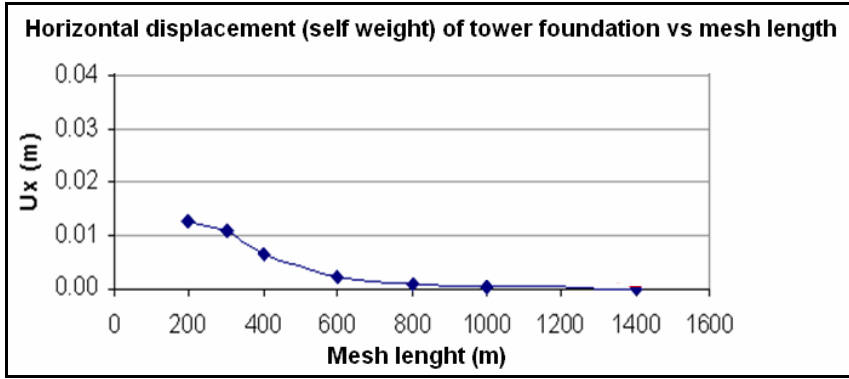
Figure 5.9. Vertical and horizontal displacement vs mesh dimension.

In the case of dynamic loading, a further problem is the reflection of waves by the boundary contour, which does not allow the infinite propagation and return the energy back. The effect of soil damping increase the dissipation, while waves from the structure to the borders are radiated, and the adoption of viscous boundaries is opportune.

Concerning damping, the Rayleigh model is assumed. The global damping is

$$[C] = \sum [\alpha_i [M] + \beta_i [K]]$$

where

α_i, β_i : mass and stiffness damping coefficients;

$[M], [K]$: mass and stiffness matrices of the i-th generic element;

The values of the damping coefficients are selected to assure a damping of 5% as referred for the site soils.

A unit excitation in the point of the foundation is imposed, and the amplitude of the generated displacements is evaluated from the point of application to the borders, in order to evaluate the rate of attenuation in the path.

Analyses have been conducted in order to identify the viscous coefficients necessary to obtain the non reflecting boundaries adsorbing the outgoing waves: the coefficients are selected in such a way that the reflected wave from wind analysis in the time domain has negligible amplitude.

In Figure 5.10 it is possible to observe the ratio between the imposed displacement and that on the border versus the dimension (length) of the mesh. It is possible to observe that if the soil block is of 800 m the residual amplitudes are of about 5%, maximum value admitted by Zheng & Takeda and beyond which the dissipative boundaries are suggested.
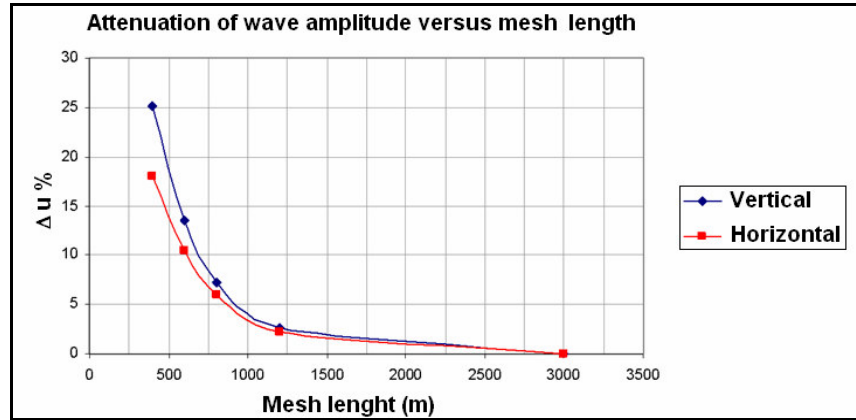
Figure 5.10. Vertical and horizontal displacement vs mesh dimension.

At first also the possible soil sources of nonlinearity have been considered:
-   the material nonlinearities inside the soil – stiffness and damping – depending on the soil strain, while the structure is expected to keep elastic response;
-   the nonlinear nature of the contact between soil and foundations.

In general the soil shear stiffness decrease with shear strain and the hysteresis loop grows wider, resulting in a softer response and a grater damping.
The dynamic soil properties can be expressed in terms of shear modulus ratio G/G_0 and damping ξ curves as function of the shear strain.

Such curves were not available for the reference site: in this study two curves (sand, gravel) from literature have been assumed for sediment deposit and gravel, as representative of such kinds of soils. (Figure 5.11)
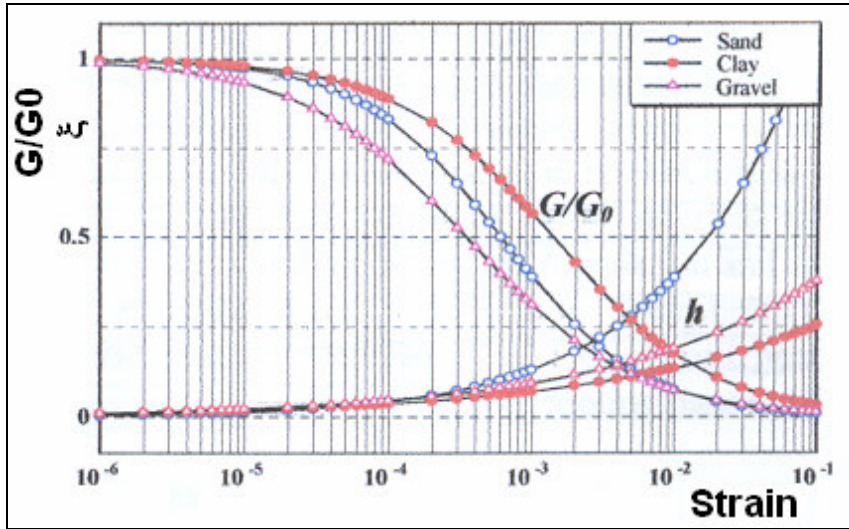
Figure 5.11. Strain-dependent soil material nonlinearity.

Concerning the contact surfaces, the Finite Element modelling has been realized in such a way to catch the opening condition and the frictional sliding which may occur during the time integration, more likely for earthquake analyses.

The opening condition depends on the relative motion between block in contact, with possible detachment; the friction condition depends on the contact force and on the Coulomb friction coefficient between the surfaces in contact.

The contact of two blocks (foundation and soil) gives a nonlinear (unilateral) stiffness in the normal direction and a friction coefficient (assumed $\mu = 0.5$ for the contact foundation-deposit) in the tangential direction.

The contact of surfaces is modelled through the CONTA178 element of Ansys, which represents contact and sliding between two nodes of elements. The element is capable of supporting compression in the contact normal direction and Coulomb friction in the tangential direction, and ensures that adjacent bodies do not overlap and no interaction occurs in case of gap opening.

205

Static analyses (keeping into account the gust dynamic magnification factor) put in evidence that the strain levels induced by permanent loads and wind are small (because of the high dimensions of wells) far from the rupture conditions (about 1/3 of the ultimate stress), all the contacts remain closed for the high weight of the superstructure and linear visco-elastic behaviour can be likely assumed.

These results allow a reduction of soil nonlinear sources in the model, which cannot be accepted for seismic analyses: the soil-foundation system is considered as a visco-elastic mean, and the fixed base models can be updated according to these assumptions.

The models with foundations allow a preliminary evaluation of the effect of soil in the dynamic properties of the system soil-structure, i.e. in terms of the frequencies of the whole system soil-structure.

Updating of the fixed base models

According to the results obtained in the static field through the finite element models with foundations, the contact sliding and the soil nonlinearity for moderate actions in respect of the permanent loads can be assumed as negligible. Consequently the foundation+soil flexibility can be accounted by visco-elastic models, considering lumped damping and stiffness concentrated in the bases of the pylon legs. For these lumped parameters the following expressions from adapted from the Novak's theory of well foundations have been adopted:

Vertical stiffness: $k_{zz} = Gr_0 \left(C_{w1} + \dfrac{G_s}{G} \delta \cdot S_{w1} \right)$

Vertical damping: $c_{zz} = \sqrt{\rho G} r_0^2 \left(C_{w2} + \sqrt{\dfrac{\rho_s}{\rho} \dfrac{G_s}{G}} \delta \cdot S_{w2} \right)$

Horizontal stiffness: $k_{xx} = Gr_0 \left(C_{u1} + \dfrac{G_s}{G} \delta \cdot S_{u1} \right)$ (analogous for y-direction)

Horizontal damping: $c_{xx} = \sqrt{\rho G} r_0^2 \left(C_{u2} + \sqrt{\dfrac{\rho_s}{\rho} \dfrac{G_s}{G}} \delta \cdot S_{u2} \right)$ (analogous for y-direction)

Torsion stiffness: $k_{\zeta\zeta} = G r_0^3 \left(C_{\zeta 1} + \dfrac{G_s}{G} \delta \cdot S_{\zeta 1} \right)$

Torsion damping: $c_{\zeta\zeta} = \sqrt{\rho G} r_0^4 \left(C_{\zeta 2} + \sqrt{\dfrac{\rho_s}{\rho} \dfrac{G_s}{G}} \delta \cdot S_{\zeta 2} \right)$

Rocking x-stiffness (and analogously for y-direction):

$$k_{\psi\psi} - k_{x\psi} =$$

$$= \sqrt{\rho G} r_0^3 \left\{ C_{\psi 1} + \left(\dfrac{h/2}{r_0} \right)^2 C_{u1} + \dfrac{G_s}{G} \delta S_{\psi 1} + \dfrac{G_s}{G} \delta \left(\dfrac{\delta^2}{3} + \dfrac{(h/2)^2}{r_0^2} - \delta \dfrac{h/2}{r_0} \right) S_{u1} \right\} -$$

$$- G r_0 \dfrac{h}{2} C_{u1}$$

Rocking x-damping (and analogously for y-direction):

$$c_{\psi\psi} - c_{x\psi} =$$

$$= \sqrt{\rho G} r_0^4 \left\{ C_{\psi 2} + \left(\dfrac{h/2}{r_0} \right)^2 C_{u2} + \delta \sqrt{\dfrac{\rho_s}{\rho} \dfrac{G_s}{G}} \left[S_{\psi 2} + \left(\dfrac{\delta^2}{3} + \dfrac{(h/2)^2}{r_0^2} - \delta \dfrac{h/2}{r_0} \right) S_{u2} \right] \right\} -$$

$$- \sqrt{\rho G} r_0^2 \dfrac{h}{2} C_{u2}$$

where

ρ: density of the gravel; ρ_s: density of the upper deposit;

G: shear modulus of gravel; G_s: shear modulus of the upper deposit;

r_0: radius of wells; h: height of the wells;

$\delta = \dfrac{h}{r_0}$: relative embedment depth;

207

C_{u1}, S_{u1}, $C_{\zeta 1}$, $S_{\zeta 1}$, $C_{\psi 1}$, $S_{\psi 1}$: stiffness parameters, dependent on the dimensionless frequency a_o (Figure 5.12);

C_{u2}, S_{u2}, $C_{\zeta 2}$, $S_{\zeta 2}$, $C_{\psi 2}$, $S_{\psi 2}$: damping parameters, dependent on the dimensionless frequency a_o (Figure 5.13);

$a_o = r_0 \omega \sqrt{\dfrac{\rho_s}{G_s}}$: dimensionless frequency: it is selected equal to the resonant

frequency ω of the system.
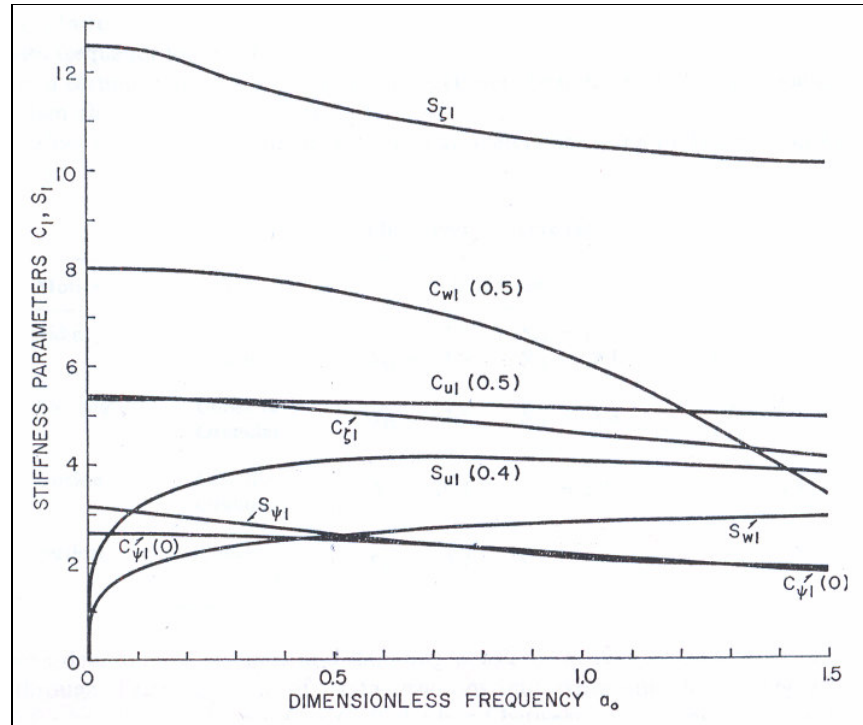
Figure 5.12. Stiffness parameters C_1, S_1 (Novak).

208

Figure 5.13. Damping parameters C_2, S_2 (Novak).

In conclusion, the models with foundations, adopting solid elements, have been used in this study for modal analyses suitable for linear systems, but useful to identify the impact of the soil and its consequences in the performance demand for this specific problem, being more involved than in the case of one-side boundary problems; for the nonli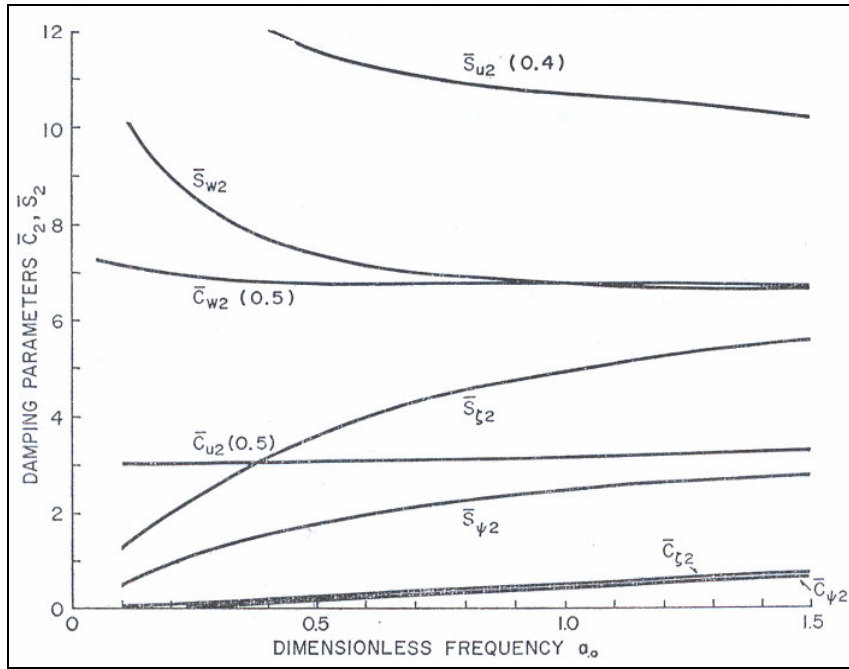near analyses of the wind response in the time domain, which are computationally much more time-consuming for the duration of the signals, the fixed base models with lumped constants have been used to quantify the response and the advantages of the control provisions.

Updating of the dynamic characterization
The undamped modes and the frequencies already computed have been updated using the substructured models, complete of the foundations, and using the expected soil parameters (Table 5.VII).
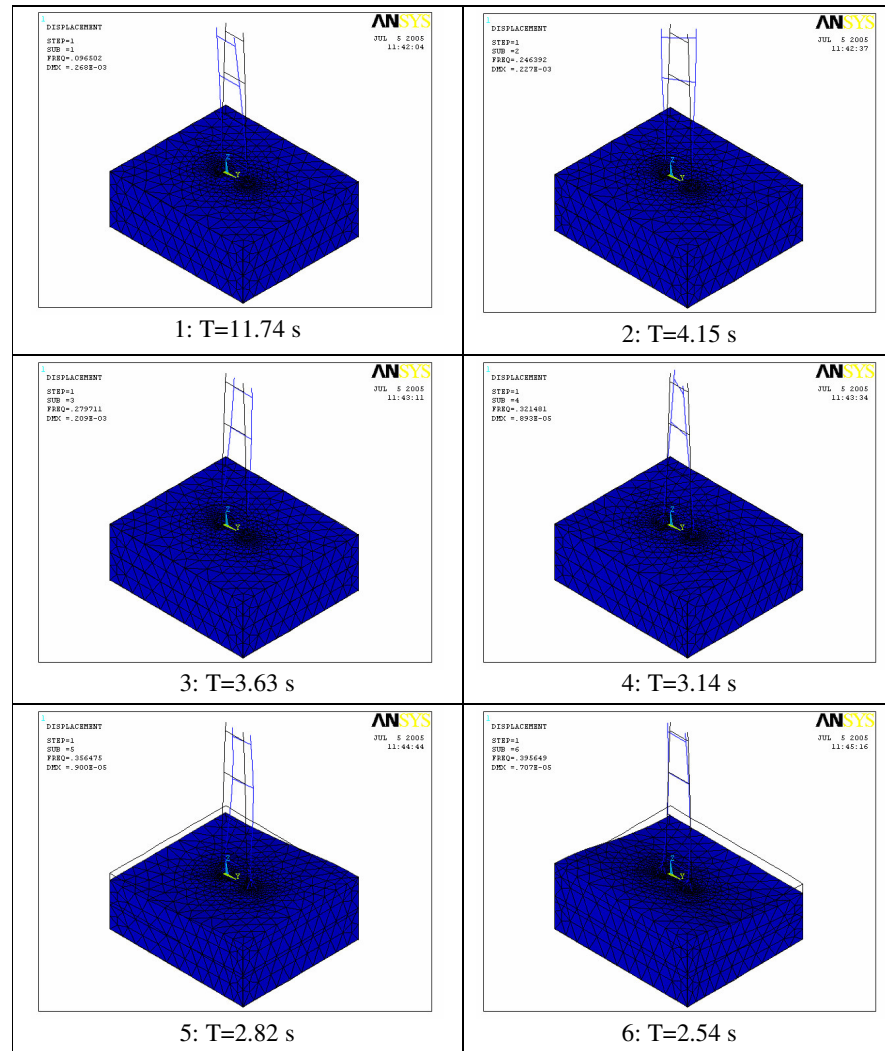
Table 5.VII. *Free-standing* pylon: Modes and frequencies (Giuliano,2006).
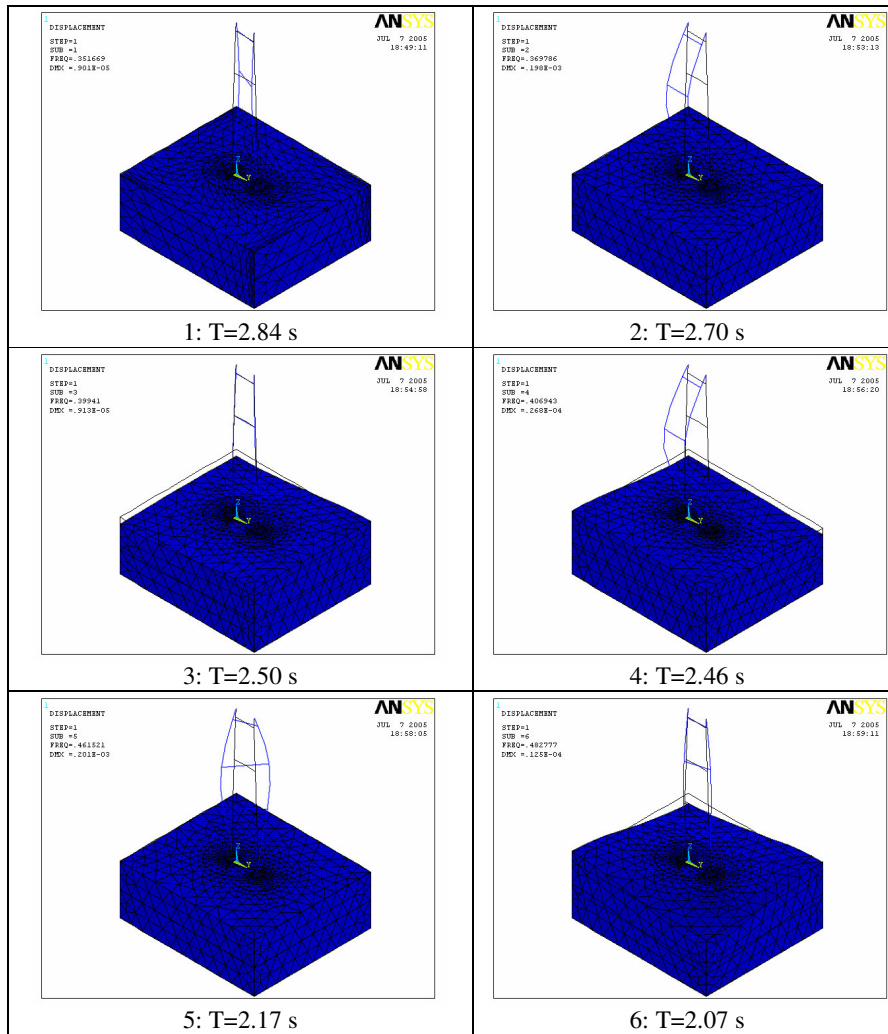
Table 5.VIII. *In-service* pylon: Modes and frequencies (Giuliano, 2006).

If one compares the modes and the frequencies obtained from substructured/full bridge models and from fixed-base and models with soil and foundation, it is possible to assert that (Table 5.IX):

- the foundations and soil have a significant impact in terms of frequency;
- the geotechnical refinement changes the frequency values and the sequence of modes: the geometry of the foundation, in fact, promotes the torsion mode rather than the bending one emphasized by a fixed end model.

The shift of the frequencies is expected because it is related to the soil modelling, while the torsion attitude of the response is related to the geometry of foundation and the soil stiffness.

At this regard a sensitivity analysis of the first frequencies of the pylon in the *free-standing* and in the *service* configuration has been conducted.

The shear wave velocity (V_s) of the surface layer of the soil is assumed as stiffness parameter, since the nature of the surface deposit is softer and more uncertain. It is expressed by:
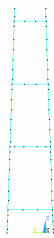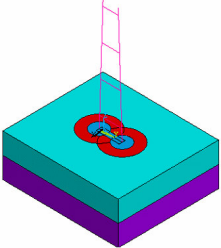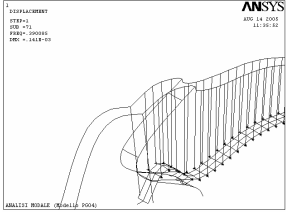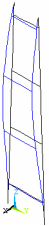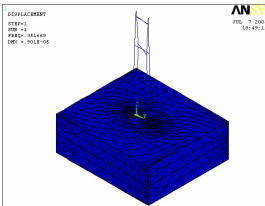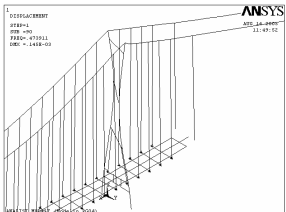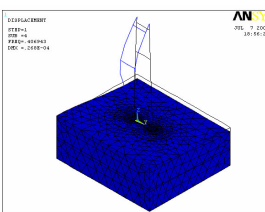
$$V_s = \sqrt{G_s/\rho}$$

where G_s : shear elastic modulus of the surface; ρ : soil density.

The shear wave velocity at the reference site, assumed in the previous results, is $V_s = 140\,m/s$, while the frequency variability was studied in the range from 100 m/s up to the shear wave velocity $V_s = 700\,m/s$ which represent a rock boundary, i.e., a fixed end support for the legs.

In the analyses the jet-grouting properties, the embedded ratio and the dimensions of the foundation are fixed.

FEM global model: (*Macrolevel*)	Fixed-base model (*Mesolevel*)	Model with soil and foundation (*Mesolevel*)
 Mode 64: f=0.37 Hz	 Mode 1: f=0.36 Hz	 Mode 1: f=0.35 Hz
 Mode 90: f=0.47 Hz	 Mode 2: f=0.45 Hz	 Mode 2: f=0.37 Hz

Table 5.IX. Levels of modelling and pylon frequencies (Casciati & Giuliano, 2006).

Figures 5.14 and 5.15 show the natural periods of the *free-standing* and of the *in-service* pylon for different values of the soil stiffness.

213

It is to recognize that the *free-standing* configuration is characterized by the ordinary sequence of modes expected for a cantilever structure, while it is to observe that for soft soils as that expected in the reference site in the service configuration the first mode is torsional instead of flexural as commonly expected. Such circumstance is related to the geometry of the foundation and the soil stiffness, coupled with the inertial properties of the legs and the normal stress applied on them. Soil and foundations have a time-varying effect on the dynamic properties of the structural system during the erection of the structure.
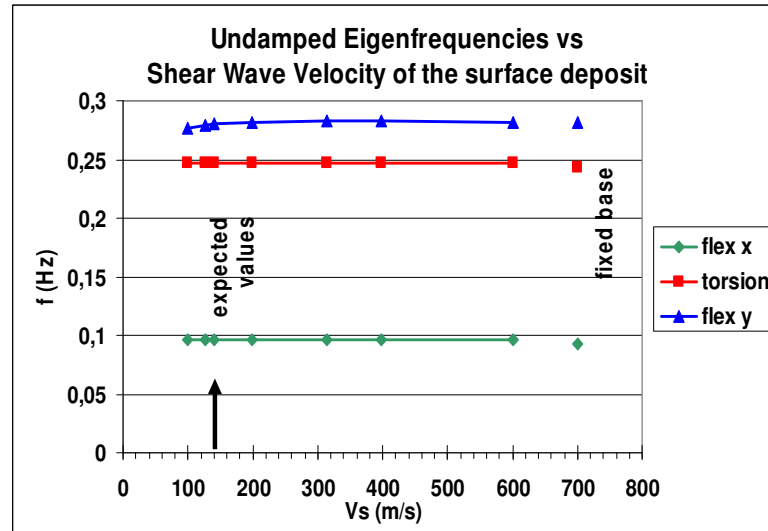
Figure 5.14. *Free-standing* Pylon. Frequencies vs soil shear wave speed Casciati & Giuliano, 2006).

For the *free-standing* configuration the soil stiffness does not affect the dynamic properties of the pylon. They depend mainly on the slenderness and on the mechanical properties of the pylon itself, and any uncertainty depends just on that of materials stiffness, on the geometry and inertial properties of the steel

box section assumed. It makes the designer more confident on the dynamic properties of the system and on its response.

On the contrary for the *in-service* configuration one can observe the high sensitivity of the dynamic properties of the pylon to the soil stiffness. For the expected soil stiffness in the reference site, the natural frequencies and the mode sequence of the pylon are different from those obtained by fixed boundaries (*Fixed base* models), so that an accurate foundation modelling in this configuration is recommended.

The gradient of frequencies makes any control system subjected to significant *mistuning* with high probability of occurrence, decreasing its performance and increasing the demand of robustness.
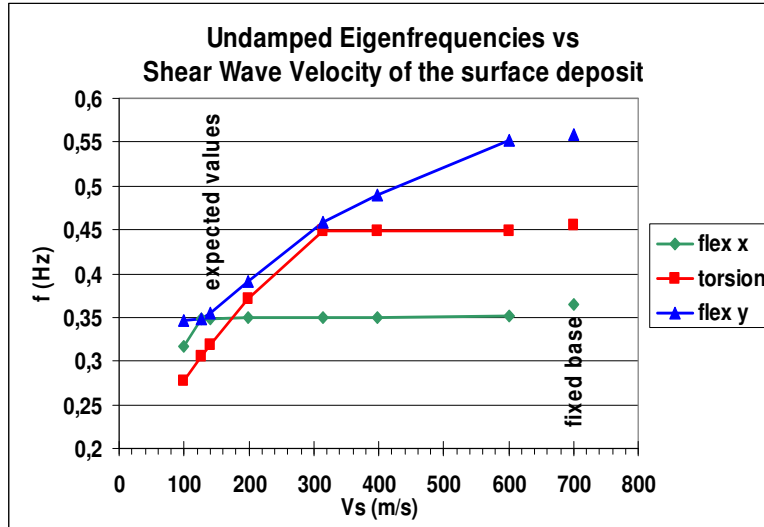
Figure 5.15. *In-service* Pylon. Frequencies vs soil shear wave speed (Casciati & Giuliano, 2006).

In conclusion for the case study the SSI effects and uncertainties on the soil parameters are more relevant and increase the demand of robustness of the

215

control system in the service life. So it is opportune that during the erection, when the soil interaction is weaker, the construction proceeds using active and adaptive control and simultaneously the interaction properties (i.e. *admittance functions*) of the soil are identified and the numerical models updated by data collection campaigns. Any possible fluctuation of the soil properties expected during the service life of the bridge is evaluated in order to limit as much as possible the expected mistuning from the design hypotheses, and reduce the demand of robustness that generally affects the effectiveness capabilities of the control systems.

5.3 Expected Performance and Targets of Design

In the perspective of the Performance Based Design, the design of the substructures of bridges are conducted evaluating the performance levels corresponding to likely *scenarios of contingency* expected in the life of the members, and comparing them with minimum allowed.

During the erection of tall structures, the stresses experienced by the members can be very different from those occurring in the service life, especially for the effects of wind. They can require strengthening or stabilizing provisions such as tendons, temporary equipments and control systems. In these phases the scenarios of contingency can be more hazardous than those of the service-use: *shop* control procedures are generally used to assure that the work is on target and no relevant errors are introduced, and that the geometry of the work and its stressing under normal temperature and permanent loads are in accordance with the *Design Specifications*. The geometric distortions and forced vibrations can induce in the structure secondary bending effects, localized in the substructures, requiring accurate checks during the erection. In fact possible inelastic strains induced can insert dangerous and irreversible damage – often invisible – in the members, reducing their fatigue strength for vibratory motion, or increasing its local buckling attitude.

Also in the service-life the vibratory motion of structures increases stresses, approximating the critical value of local buckling for the stiffened plates, and induces also fatigue effects.

For tall buildings and steel pylons of long span bridges structural control is an effective tool to reduce the response and increase the structural performance, both in the construction stages and in the service life, even if with different philosophies and technologies of intervention.

The evaluation of the satisfaction of the structural targets of the structure along the constructive process can be conducted according to the *Erection Rating Factor (ERF)* procedure (Durkee, Thonaides). This approach is applicable from the first phases of erection to the service life; it lets estimate the adequacy of structure *as designed* or the need of provisions to satisfy the specifications requests. The procedure keeps into account the fact that sometimes the satisfaction of the tolerances on the primary stresses is not sufficient to prevent the damage effects produced by secondary bending, related to joint rigidity and structural deflection.

The evaluation of integrity and reliability of the structure is pursued by comparing the characteristic values of strength and acting forces, related to proper return periods. It can be expressed in general form as follows:

$$S - \Delta S > F + \Delta F \text{ , or } S_k > F_k$$

where

S: nominal strength; ΔS : fractile deviation of the strength; F: nominal or computed force;

ΔF : fractile deviation of the force.

Rearranging the previous equation, a performance parameter *(ERF)* can be identified as

$$ERF \equiv \frac{S}{F} \geq \frac{1 + \dfrac{\Delta F}{F}}{1 - \dfrac{\Delta S}{S}}$$

217

The *ERF* index can be computed with reference to different locations along the members, and also to joints, plates, bolts and welding. The minimum value computed is compared, for each member in each constructive phase, with minimum levels allowed in the design specifications, where tensile/compressive members are distinguished, having different rates $\Delta S/S$ allowed for instability attitude. Simulations of the successive structural configurations of the structure, with geometry, load scenarios, wind action and interaction effects, by mathematical modelling and mechanical tests, in general let evaluate the expected rates $\Delta F/F$. The construction process, and analogously the final design, is conducted at least towards the satisfaction of minimum levels of the *ERF* index. This target can be pursued through different strategies:

- by maximizing the value of S by *strengthening* strategies;
- by minimizing the strength uncertainties ΔS by *quality procedures* of material production, assemblage and *shop control* during the construction;
- by minimizing the value of F by *equipment*, tendon systems, *control strategies*;
- by minimizing the value of ΔF, by numerical and experimental investigations reducing external uncertainties affecting the structural response or the effectiveness of equipment.

The assessment of the numerical values of S, F, ΔS, ΔF, identifying the minimum expected value of the *ERF* index is part of the preliminary investigation on the site of construction and of the design specifications. They contain implicitly the request of efficiency and robustness of the structural system.

The satisfaction of the equation or further increase of the *ERF* index can be obtained also by installing control devices, as already experienced in many structures such as tall buildings and cable-supported bridges.

According to the *Performance-Based Design,* the design of the control system for the mitigation of the response can be conducted through the following steps:

- Modelling and dynamic characterization of structure and loads (*Base of Design and Formulation of the Problem*);
- Statement of the expected performance and requirements (*Specification*): displacements and stresses; for the case study pylon such values are determined according to the allowable stresses against local buckling and fatigue;
- limits, after the characterization of loads by simple models and using an arbitrary criterion of literature; evaluation of the optimal frequency f and damping ξ for the value of μ (*Synthesis*);
- Numerical simulations and verifications (iterative): acceptance or updating and parameter optimization (*Analysis, Evaluation, Riformulation*).

Such steps are conducted with <u>three main Targets</u> (*Performance*) (Casciati & Giuliano, 2006):

  o the **<u>Efficiency</u>**, or adequate reduction of the structural response, in terms of peak and root-mean-square (rms) values;

  o the **<u>Robustness</u>**: the ability to provide a suitable efficiency also in the presence of moderate perturbations (*mistuning*) with respect to the assumed model, as effect of faults, disturbance, errors;

  o the **<u>Redundancy</u>**: the ability to provide a suitable efficiency also in case of out-of-service of one or several devices.

The satisfaction of these targets is done through numerical or experimental analyses, by the evaluation of critical quantities for the structure, such as stresses and strain, or the associated structural displacements.

At first the main structure is idealized as a SDOF system, with frequency equal to the main structural one, coupled to another SDOF system whose properties correspond to the generalized mass, stiffness, damping of the mode to be controlled.

219

The numerical values of the global equivalent device are determined by criteria of literature, hypothesising harmonic excitation at the same structural frequency, to simulate the vortex shedding and *lock-in*, or white noise to simulate gust effects, and neglecting the structural damping for simplicity.

Then the performance of the equivalent system is controlled and refined using the wind spectrum or time-histories, employing the damping for the structure, and re-arranging the optimal values according to the response.

5.4   Interaction Mechanisms: Buffeting Response of the Pylon

Starting from the spectra of the wind speed, two different approaches of description of the gust action have been considered:
- the frequency domain approach (PSD);
- the time domain approach.

It has been considered useful to follow both of the approaches presented, in order to better identify the physical properties of the system and possible control strategies to achieve the control targets, and – finally – to quantify the advantages and the uncertainties of the final proposals.

The frequency domain (PSD) approach

The PSD approach, uses a modal superposition technique to compute the response, in the hypothesis of linear behaviour and stationary processes. It is clear that such hypotheses introduce a relevant degree of error in the quantitative response, but they are useful to emphasises geometric or mechanic effects, relevant for the hypotheses of design – in a small time of elaboration – that are often hidden in a time integration procedure.

The statistics of the motion and of the structural stresses, are computed in the frequency domain in the hypothesis of linear structure, stationary random excitations applied on different structural nodes, and using multiple power spectral densities input (PSD), partially correlated.

The expression of the spectral density of the force applied to the structural nodes is

$$S_{F_D}(\omega) = \rho^2 \overline{U}^2 B^4 c_D^2 \chi(\omega) S_v(\omega)$$

where $\rho = 1.25\, kg/m^3$: air density; $B = 16\,$m : reference length;

$c_D = 1.6$: drag coefficient; $\chi(\omega)$: aerodynamic admittance;

$S_v(\omega)$: Spectral Density of the wind speed;

$\overline{U}$ =mean wind velocity, obtained by the logarithmic profile which increase with the vertical coordinate z:

$$\overline{U}(\underline{z}) = 2.5 u_* \ln(z/z_0) \underline{W}$$

where u_* : tangential velocity; z_0 : characteristic length; $\underline{W}$: velocity direction unit vector.

The response PSDs are computed from the input PSDs through the expressions of transfer functions for single DOF systems $H(\omega)$ by using superposition techniques. For force excitation input, the generic expression of the transfer function of the i-th DOF is

$$H_j(\omega) = \frac{1}{\omega_j^2 - \omega^2 + 2i\xi_j\omega_j\omega}$$

The absolute value of the mean square response of the i-th free-displacement is

$$\sigma_i^2 = \int_0^\infty S_{di}(\omega) d\omega$$

where $S_{di}(\omega) = \sum_{j=1}^n \sum_{k=1}^n \phi_{ij}\phi_{ik} \left(\sum_{l=1}^r \sum_{m=1}^r \gamma_{lj}\gamma_{mk} H_j^*(\omega) H_k(\omega) \cdot \overline{S}_{lm}(\omega) \right)$

n : number of modal shapes considered; ϕ_{ij} : i-th component of the j-th modal shape; r : number of nodal PSD input; γ_{mk} : m-th component of the k-th nodal excitation; $\{\gamma\}_k = \{\phi_k\}^T \cdot \{F\}$; $\{F\}$: load vector.

The time domain approach

The time-domain approach, with a time-integration procedure, takes into account the nonlinear properties of the structure and of the boundaries, if an enough accurate modelling is done.

221

This approach, more time-consuming, require some simplification in the mathematical modelling such as in the geometry, in the boundaries and in the mesh, with possible loss of accuracy when the geometry plays a relevant role. Yet it lets evaluate the structural response of the pylon and give reliable quantification of the performance of the control systems.

Starting from the wind speed spectra, wind-speed time histories have been generated by Monte Carlo procedure, associated to all the return periods of Specifications of the Bridge. For each load different performance are required to the structure.

The time-histories have been generated as random gaussian zero-mean processes, correlated in proportion of the interdistance of the points of observation (Solari-Carassale). The values of the wind speed are obtained by superposition of mean value, from the logarithmic profile and a turbulent Gaussian zero-mean component, obtained by Monte-Carlo simulation from the cross-spectrum of the turbulent components according to the model of Solari Piccardo presented in Chapter 3.

In Figure 5.16 the wind-histories related to periods of return of 2000 years, corresponding to the Ultime Limite State (SLU) are represented, for discrete positions along the pylon height, and in Figure 5.17 the average profile.
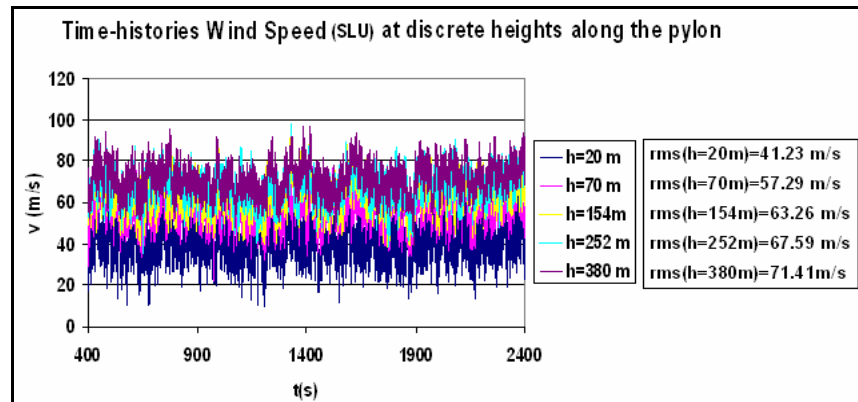
Figure 5.16. Time-histories of wind speed along the pylon height (SLU) and rms values (Solari, 2005).
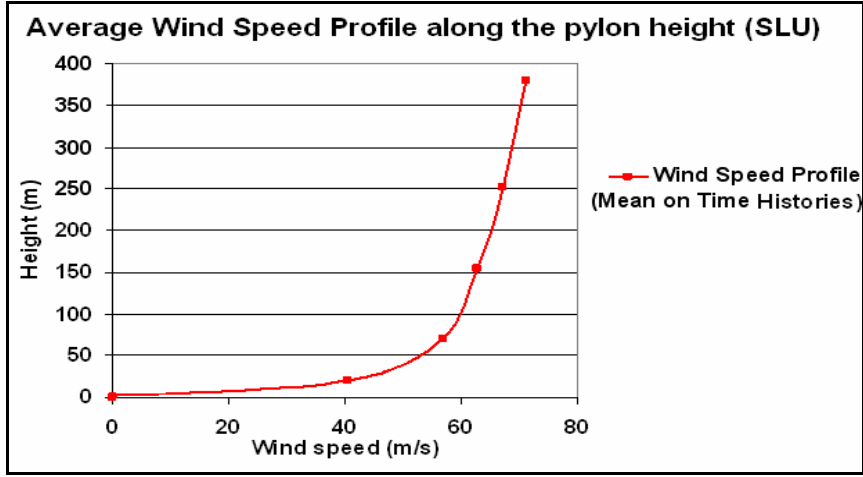
Figure 5.17. Average wind speed profile along the pylon height (SLU).

The force *time-histories*, of duration of one hour, were obtained from field wind velocity *time-histories* based on the stationary theory with aerodynamic coefficient obtained in the wind tunnel and applied to the nodes of the structural finite element model:

$$F_{D,i}(t) = \frac{1}{2} \rho \cdot B \cdot l_i \cdot c_D \cdot v_i(t)^2$$

where l_i = influence length of the *i*-th node; $v_i(t)$ = instantaneous velocity at the *i*-th node.

Numerical analyses have been conducted to evaluate the buffeting response of the structure in the free-standing configuration (expected as the most hazardous) and the service one. The wind is assumed acting in the direction of the tower weak bending plane, longitudinal for the bridge (Figure 5.18).

223
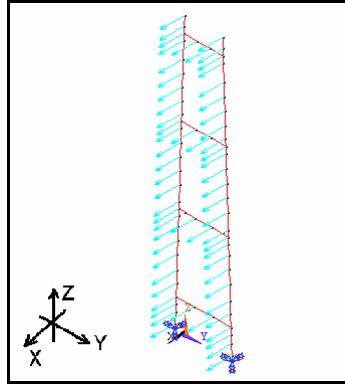
Figure 5.18. Scheme of application of the wind load.

The analyses have been conducted in the frequency and in the time domain (with the respective assumptions), in order to identify the SSI impact and to evaluate the magnitude of the response for design purposes.

The incremental analyses in the time domain are conducted with the Newton Raphson iteration algorithm, with a displacement tolerance on displacements of 0.01.
The Newmark β-algorithm with $\gamma = 0.5; \beta = 0.25$ is used for the time integration: this algorithm is unconditionally stable for linear systems, while a numerical instability can be produced in case of nonlinear systems. To prevent this phenomenon, the time step for the integration has been fixed smaller than 10% of the largest value of frequency in the range of interest. For the case study pylon and the structural configurations investigated, the seventh mode period are:

$$T_7 = 0.60s \ \text{(free-standing configuration)}$$

$$T_7 = 0.52s \ \text{(in-service configuration)}$$

Consequently for all the analyses, a time step of $\Delta t = 0.05s$ has been assumed.

Analyses using smaller values of the time step $\left(\Delta t = 0.025s\right)$ are computationally more time-consuming and the tests did not give sensitive increments on accuracy.

The results of the analyses in the time domain are represented in the Tables 5.X, 5.XI. For both the structural configurations the computed spectra of displacements and accelerations agree with the natural frequencies of the pylon already represented.

The results put in evidence that the structural behaviour and the stresses acting on the structure and its components change in the different constructive stages: in particular the displacements, the stresses and the eccentricity during severe gust load scenarios make the free-standing configuration the most hazardous.

This circumstance suggests the adoption of special provisions such as tendons, active/hybrid strategies, in order to contain the response until the targets established in the *Specifications of Design*.

Concerning the service configuration, the buffeting response is reduced in respect the free-standing also because the increase of the structural frequency shifts the structure towards the lower energy range of the wind power spectrum.

In the Figures 5.19, 5.20 are represented the structural responses of the free-standing and of the in-service pylon, using fixed frame models or models with foundations and soil, and hypothesising different stiffness for the deposit layer.

Figure 5.19 represents the Power Spectral Density of the maximum out-of-plane displacement, occurring at the node167 (the top) for the *free-standing* configuration.

In the *free-standing* configuration the soil stiffness has a smaller effect on the first mode response, but changes the torsion response and shifts the corresponding frequency. For this configuration the fixed base models are adequate only for stiff soils.

Figure 5.20 represents the response in terms of displacements of the node 137, the maximum for the *service* configuration.

Free-Standing Uncontrolled Pylon (Stage 8) – Wind x (SLU)

Time-history x-Displacements of the Top of the free-standing Pylon (Wind x - SLU)

Log-Spectrum of x-Displacements of the Top of the Pylon (Wind x - Mean Speed 21 m/s)

Envelope of Displacements (x) induced by the turbulent wind (x) (SLU) on the free-standing Pylon (T=60 minutes)
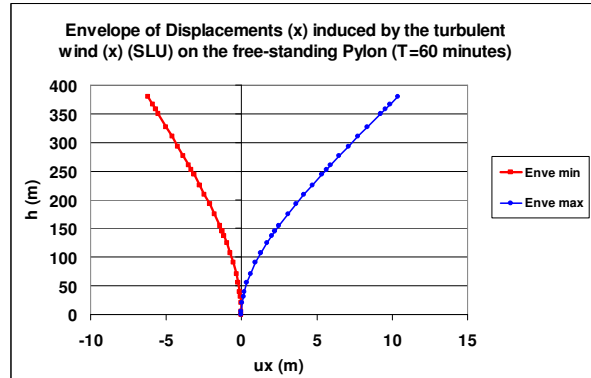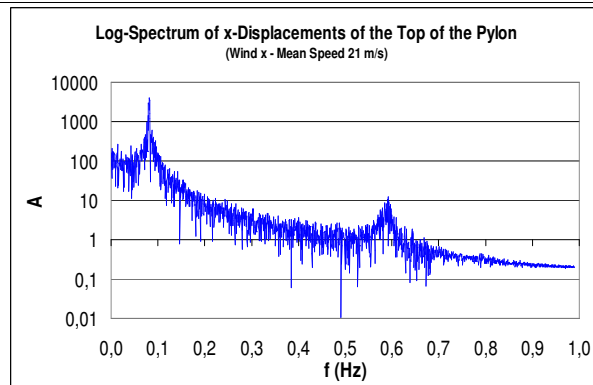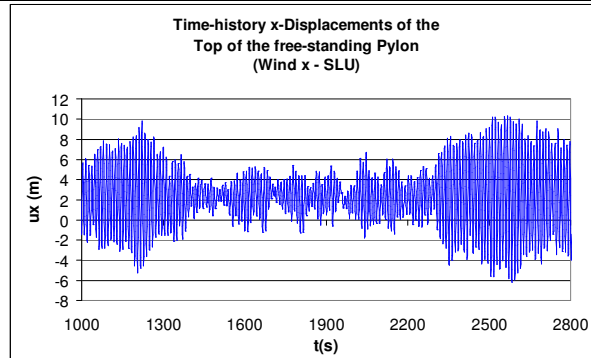
Table 5.X. Buffeting response of the *free-standing* pylon (SLU).

226

In-service Uncontrolled Pylon (Stage 11) - Wind x (SLU)

Time-history x-Displacements of the
Middle of the Pylon (Node137) (Wind x - SLU)

Spectrum of y-Displacements of the Middle of the Pylon
(SLU Wind y)

Envelope of Displacements (x) induced by the turbulent
wind (x) (SLU) on the free-standing Pylon (T=60 minutes)
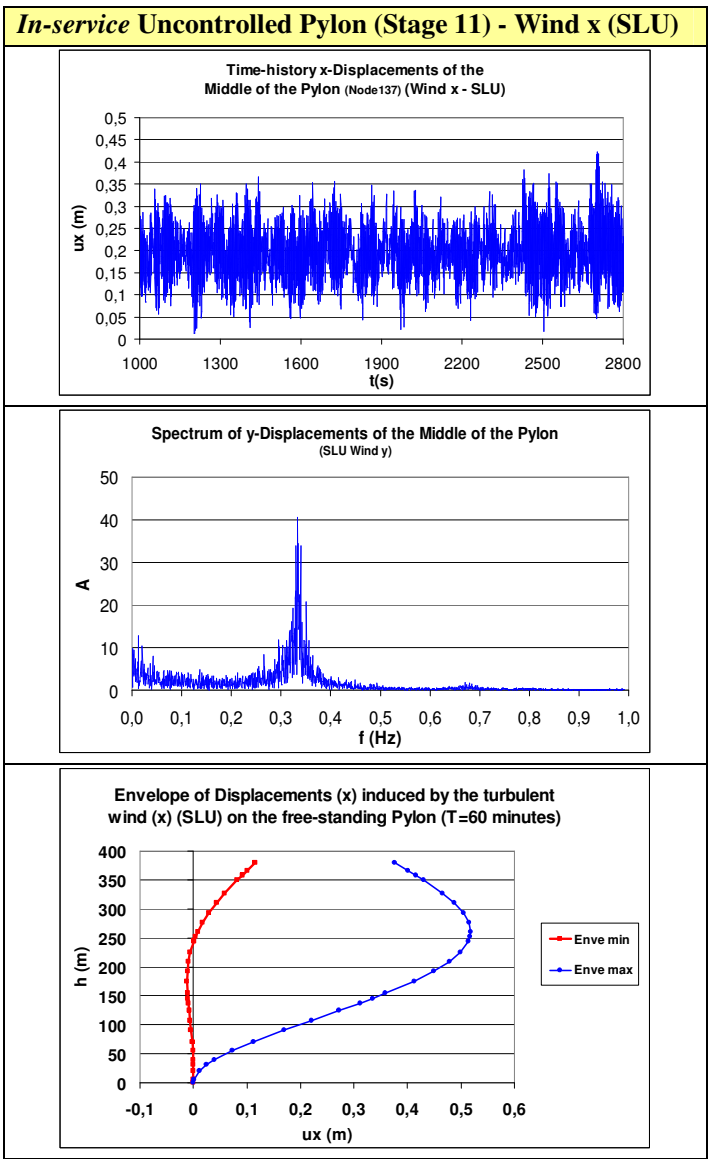
Table 5.XI. Buffeting response of the *in-service* pylon (SLU).
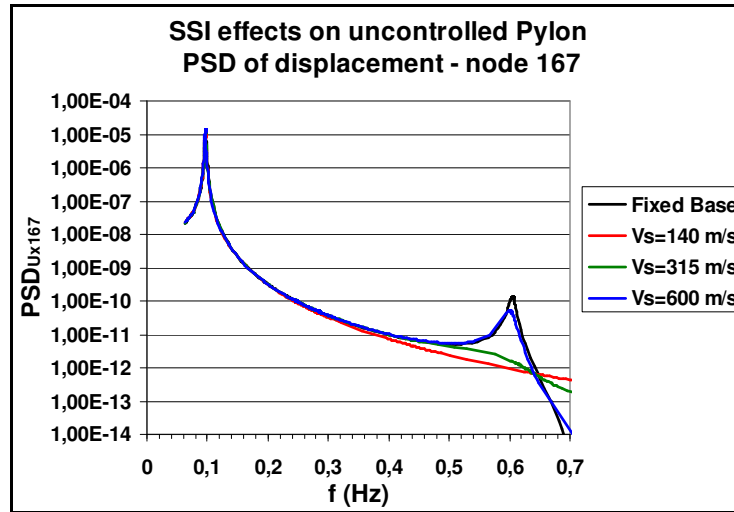
Figure 5.19. *Free-standing* Pylon. Uncontrolled response (Giuliano, 2006).
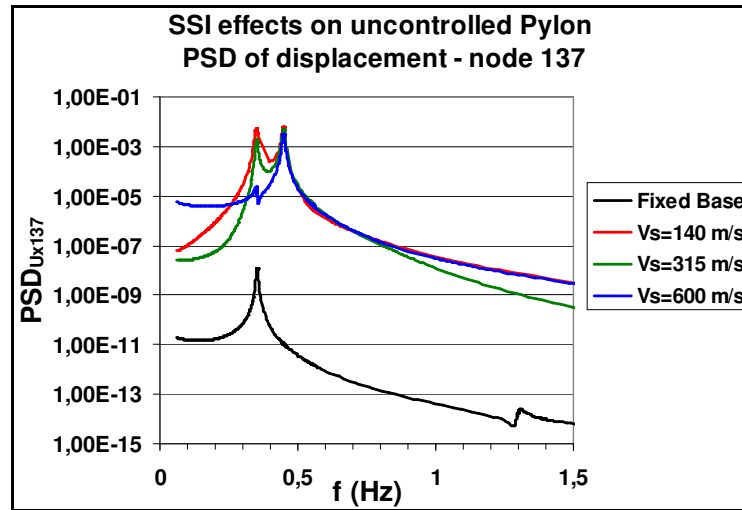
Figure 5.20. *In-service* Pylon. Uncontrolled response in the frequency domain
(Giuliano, 2006).

228

It is possible to observe that:
-   the structural displacement of the fixed model (line black) are underestimated;
-   the introduction of the soil (line red, green, blue), as represented in the previous paragraph, shifts the structural frequencies of the pylon, and gives relevance to the torsional response; this effect is more relevant for soft soils such as that of the site of the Pylon (red line). The diagrams show also that fixed base models, stiffer than those with foundations, are not adequate in representing the dynamic properties and response of the structure in the service configuration, when the main cable impose severe boundary to the legs on the top of the pylon, and the base becomes the flexible side, while the geometry of foundations promotes the torsion response.

5.5   Structural Control from the Erection to the Service Life

The Towers (or pylons) represent a principal component in the structural hierarchy of a suspension bridge. These structures are high and slender, and have low damping, especially for the steel manufacture. These features make them prone to high vibratory motion induced by the wind, both during the constructive stages and in the service life. The erection of the pylons of the bridge is a complex problem for several reasons:
-   the weight of the members to be carried and welded;
-   the high sensitivity to wind-induced vibration;
-   the need of verticality of the members.

Figure 5.21 represents a scheme of the constructive stages of the pylon and the corresponding evolution of its first three natural periods.

The solution of the eigen-value problem of the pylon during its constructive stages, let recognize the evolution of the natural periods of the structure. A maximum value of the natural period is observed when the pylon is completed and *free-standing*.
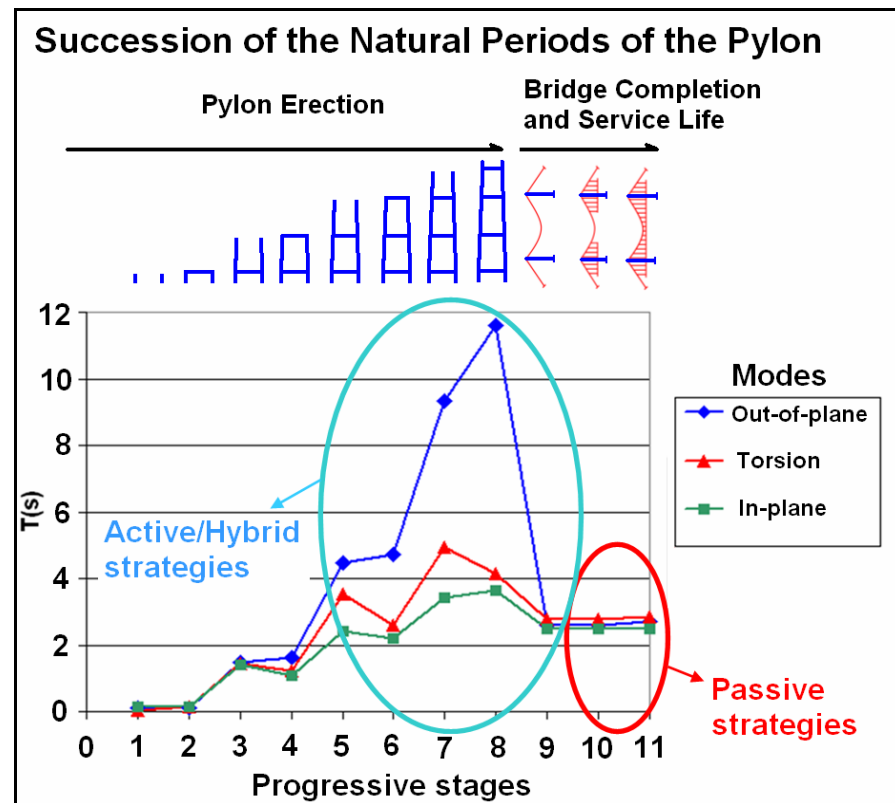
Figure 5.21. Natural Periods along the constructive process of the pylon (Giuliano, 2006).

The succession of the structural configurations during the construction changes the dynamic properties of the pylon for the varying structural slenderness and also the soil flexibility, and similarly changes the effects of interaction with wind. This makes the problem of the reduction of the motion a *time-varying* one, with critical *snap-through* when the main cables are mounted (Phases 8→9).

Wind induces to the Pylon vortex and buffeting vibrations, only partially contrasted by geometric aerodynamic design (*cut-section*).

In the first stages the structure is stiff, and the critical Strouhal wind speed higher, while it decreases and reaches its minimum value in the *free-standing* configuration. The phase 8 is the most critical, because wind static, vortex shedding and gust effects produce maximum displacements and vibrations, and also the most dangerous secondary effects, while the verticality requirement is dominating.

Nevertheless, the wind response must be limited also during the entire lifetime, in order to control the stress levels, the eccentricity, the foundation moments and possible fatigue effects.

The mitigation of these effects by mechanical control devices is allowed in the *Design Specifications* of the case-study bridge.

Moving along the constructive process, the structural problem changes and similarly the targets of structural control. In the first stages the structure is stiff, and the critical Strouhal wind speed higher, while it decreases and reaches its minimum value in the critical *free-standing* configuration, when wind static, vortex shedding and gust effects produce maximum displacements and vibrations, and also the most dangerous secondary effects. The time-variation of the dynamic and aerodynamic properties, and the severity of the wind/seismic problem encouraged successfully the adoption of robust and adaptive *active/hybrid control* for the constructive stages of similar slender pylons, more effective and versatile than passive strategies, even though it required a continuous provision of energy.

In the service time of the bridge the less critical strain and vibratory motion make passive strategies be more attractive because of unnecessary long term energetic support. For pylons of long span bridges TMDs are the most reliable devices for the service life and represent the actual state of art.

The achievement of the objectives of effectiveness, robustness and redundancy is checked by numerical evaluation of some quantities, regarded as critical, as structural displacements or strains.

5.6   Experimental Approach for the Mitigation of the Wind Response

5.6.1 Base of Design: Mitigation of the Vortex-induced Response

As presented in Chapter 4, the Tuned Mass Dampers are effective devices for the reduction of the response of inadequately damped structures. The additional damping provided depends on the tuning ratio f, the mass ratio μ, and the TMD damping ratio ξ_{TMD}. The effectiveness of the TMD system for the structure can be represented also by the effective damping ξ_e of a SDOF system that would have the same response of the structure+TMD. A sensitive increase of the structural damping (Scruton number) can shift the structural response from the *lock-in* region to the forced random vibration.

The idealization of the case-study structure is conducted considering its first mode, and so assuming the corresponding modal mass, stiffness, damping for the evaluation of the mass, frequency and damping ratios.

Since the maximum negative damping ξ_a evaluated in the wind tunnel tests is of about 1.7%, it follows that an effective damping of the system structure+TMD of 2% is evaluated to be effective in suppressing the *lock-in* vibrations:

$$\left(\xi_e\right)_{t\arg et} = \xi_s + \xi_{TMD} = 2\%$$

Since the structural damping is low and affected by some uncertainties, it is conservative and not costly to assume

$$\xi_e \cong \xi_{TMD}$$

A possible optimization criterion is that proposed by Luft (1979), maximizing the effective damping under white noise excitation.

If the mass ratio is given, it provides the tuning ratio $f = f_{opt} = \left(1+1.5\mu\right)^{-\frac{1}{2}}$;

and the TMD damping ratio $\xi_{TMD} = \left(\xi_{TMD}\right)_{opt} = \sqrt{\dfrac{\mu}{4}\left(1-0.75\mu\right)}$.

The effective damping ratio of the system is then

$$\xi_e = (\xi_e)_{opt} = \frac{\xi_{TMD}\mu f}{1 + \left[4\xi_{TMD}^2(1+\mu) - (\mu+2)\right]f^2 + (1+\mu)^2 f^4} =$$

$$= \frac{\mu^{3/2}(1-0.75\mu)^{1/2}(1+1.5\mu)^{-5/2}}{\left(-2.25\mu^4 - 0.75\mu^3 + 7\mu^2 + 16\mu + 8\right)}$$

In Figure 5.22 it is possible to recognize that a minimum mass ratio $\mu_{min} = 0.007$ is adequate to provide an effective damping ratio of 2% for white noise excitation, and even more for harmonic loads.

On the basis of this criterion of design, and assuming the same aerodynamic damping required for the free-standing and in-service configurations, from the statement $\mu_{min} = 0.007$, indicative values of the minimum mass to be provided to the TMD system in the two configurations (*free-standing/in-service*) are computed. The structural configuration of the pylon suggests the provision of symmetrical installations, i.e., each leg mounts a TMD device (or MTMD) identical to another in the other leg.
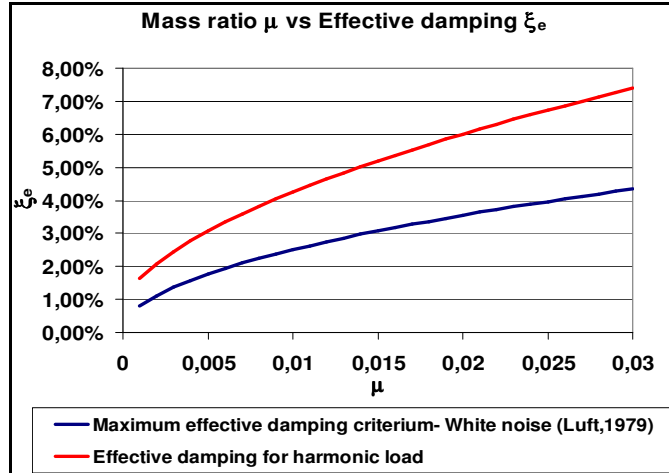
Figure 5.22. Mass ratio vs effective damping for white noise/harmonic excitation.

Free-standing configuration

Fundamental modal mass: $\tilde{m}_1 = \underline{\Phi}_1 [\mathrm{M}] \underline{\Phi}_1^{\mathrm{T}} = 1.3835e + 07 \; kg$

Total mass to be installed to prevent lock-in: $m_{TMD} = \mu * \tilde{m}_1 = 97 \; \mathrm{t}$

In-service configuration

Fundamental modal mass: $\tilde{m}_1 = \underline{\Phi}_1 [\mathrm{M}] \underline{\Phi}_1^{\mathrm{T}} = 2.3984e + 07 \; kg$

Total mass to be installed to prevent lock-in: $m_{TMD} = \mu * \tilde{m}_1 = 167 \; \mathrm{t}$

Once evaluated the minimum amount of mass to be installed to avoid the *lock-in* vibrations, the gust response of the pylon+TMDs is investigated using different control configurations, such as different number of devices, locations, criteria of attribution of the mechanical parameters of the devices. The analyses pursue the optimization of the response, according to the targets of the design already described. After the analyses under the gust wind excitation on the pylon without any device (*uncontrolled* situation), devices of different mechanical properties are added and the response re-evaluated.

5.6.2 Efficiency of TMDs and Optimization of the Buffeting Response

At first the investigations have been conducted using one TMD per leg, with the same mechanical characteristics (*single-TMD* configuration, Figure 5.23).

As outlined in Chapter 4, the effectiveness of the devices increases as the installed mass increases, but the marginal benefit decreases. It is no longer convenient for mass ratios greater than 1-2%, according to the experience collected in similar constructions.

The choice of the masses of the TMDs have been done keeping into account the general benefit of increasing mass as the TMD theory states, but also the possible technical difficulties related to the size and the reliability of too heavy systems.
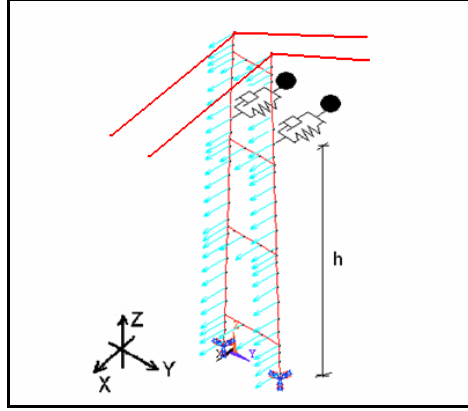
Figure 5.23. Pylon excitation and localization of the TMD devices.

Therefore the gust wind responses are estimated for configurations different each from the other for:

-   the different geometric localization of the devices h/h_{tot} ;

-   the   mass   per   leg,   with $\mu = 0.83\%; 1.25\%; 1.67\%$,
    i.e., $m = 100\,t\,; 150\,t\,; 200\,t\,$;

-   the frequency ratio, f .

The damping ratio first guess is: $\xi_i = \sqrt{\dfrac{3\mu}{8(1+\mu)}}, i = 1,2$

Optimization of the location of the TMDs

The first group of analyses are conducted in order to optimize the location of the TMDs for the control of the out-of-plane response (Mode 1).

For the common building and structures the optimal location of the TMDs corresponds to the maximum of the modal shape to be controlled. Consequently it is worthnoting that for the *free-standing* configuration the optimal location is on the top of the structure.

For the *service* configuration, the first mode is   more influenced by the boundaries of the foundation and the saddle.

The first configuration (*TMD1*) tested to investigate the TMD effectiveness of the TMD against wind action consists of two TMD located in both two legs of the tower at height of 276.5 m, where the previous analyses of the uncontrolled structure showed the maximum dynamic response.

The second configuration (*TMD2*) locates the TMDs on the sections of the maximum displacement of the first modal shape.

In Table 5.XII are reported the two configurations with the properties of TMD inserted in the legs, The out-of-plane responses are compared with those of the uncontrolled pylon in Table 5.XIIIa,b.

Configurations	μ (*mass*)	h/h_{tot} (*h*)
TMD-1	1,67%	0,73 (276 m)
TMD-2	(2x200 tons)	0,59 (226 m)

Table 5.XII. Optimal location: *Single-TMD* control configurations.

The time-histories of x-displacements and accelerations, the envelopes and statistics show that the optimal location for the TMD is better approximated by the first configuration. Furthermore it is possible to note that non optimal location can make ineffective or even depreciatory the installations.

If optimal location is assumed, it is noticeable that the TMD installation mitigates and smoothes the response. It decreases the variance of the controlled quantities when compared with the uncontrolled case.

Any further investigation locates the TMD (or the central TMD) in the optimal location identified.
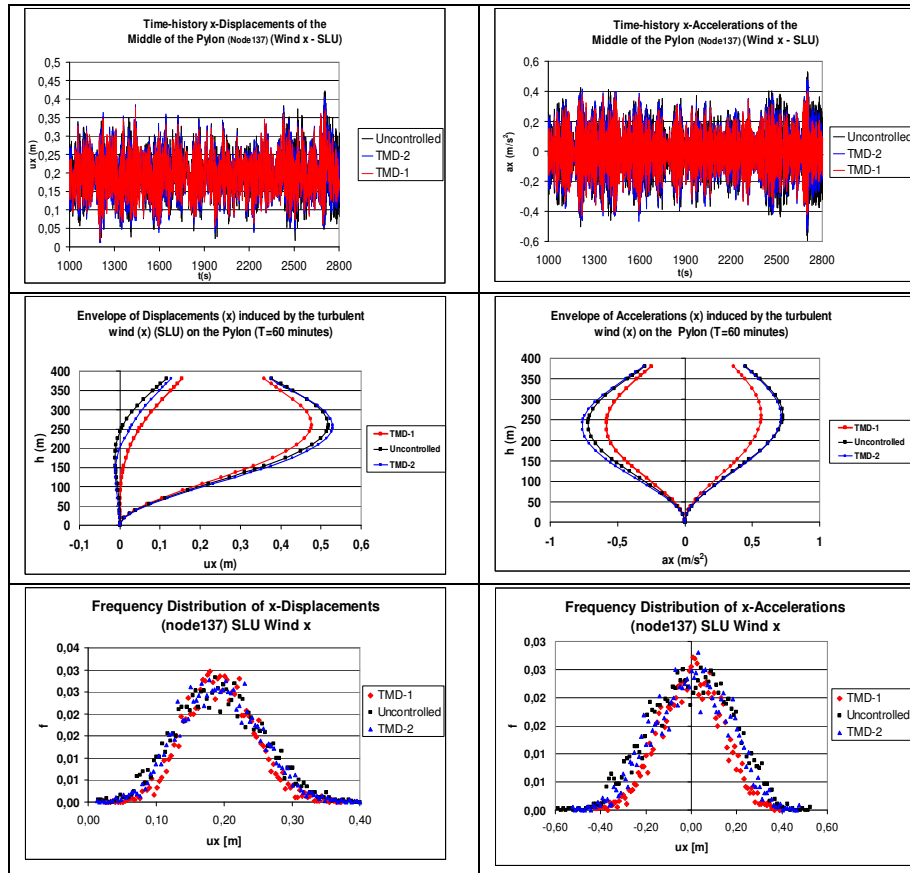
Table 5.XIIIa. Optimal location: comparison of control configurations.

	Mean	Variance	*Max*|•|
Uncontrolled	0,194	0,0038	0,423
With TMD-1	0,194	0,0025	0,378
With TMD-2	0,194	0,0033	0,406

Table 5.XIIIb. Statistics of the x-displacement of the middle section of the in-service pylon.

Effect of the Mass ratio μ

The second group of investigations concerns with the evaluation of the effect of the increase of mass ratio μ on the displacements and acceleration, in terms of envelopes and of statistical quantities.

The investigations are conducted assuming constant values for the other two characteristic parameters of the system structure+ TMD, according to Table 5.XIV.

The frequency ratio assumed has the Warburton value:

$$f_{Warburton} = \frac{1}{1+\mu}\left(1 + \frac{\mu}{2}\right)^{1/2}$$

Configurations (*In-service* pylon)	μ (%) (*mass*)	$f = \omega_a / \Omega$ (k)	h/h_{tot} (h)
TMD-3	0,83 (2x100 tons)	f=f$_{Warburton}$=0,994	
TMD-4	1,25 (2x150 tons)	f=f$_{Warburton}$=0,991	0,73 (276 m)
TMD-5	1,67 (2x200 tons)	f=f$_{Warburton}$=0,988	

Table 5.XIV. Exploration of mass ratio effects: *single-TMD* configurations

The diagram in Figure 5.24 shows, for the configurations of Table 5.XIV, the envelopes of the *out-of-plane* displacements of the pylon, for the wind intensities discussed in the previous section. The diagram shows that the controlled configurations have displacement (and hence stress) peak values lower than the controlled one. In other words the excursions from the static deformed configuration are less significant.

Among others diagrams which could be presented, Figure 5.25 gives evidence of this by a comparison of the 95% fractiles of the bending moment at the base of the pylon leg.

238
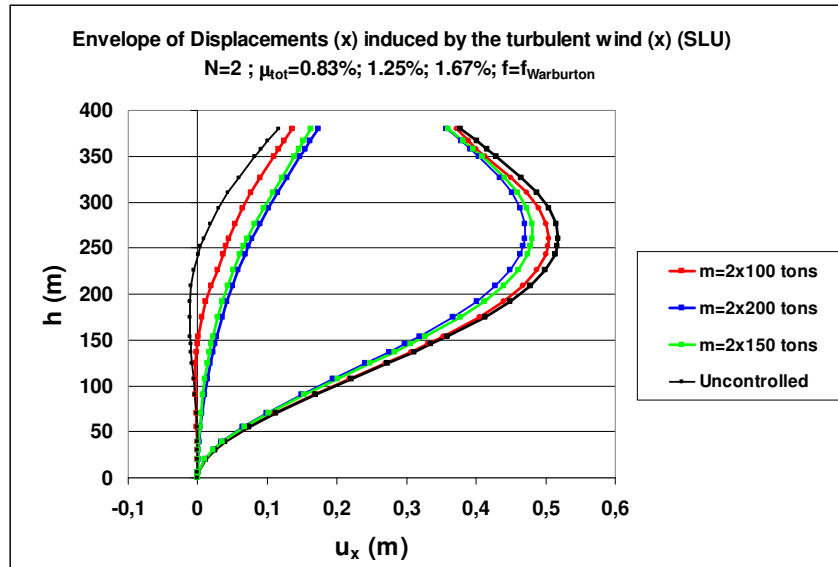
Figure 5.24. Envelope of the out-of-plane displacements for different mass ratios (Casciati & Giuliano, 2006).

It is worth noting that the mitigations effects increases as the mass ratio increases, but the marginal variation decreases: the amount of the mass to be installed arises therefore from a subtle cost-benefit analysis and it would be better to fix its value in the owner's design specifications.

239
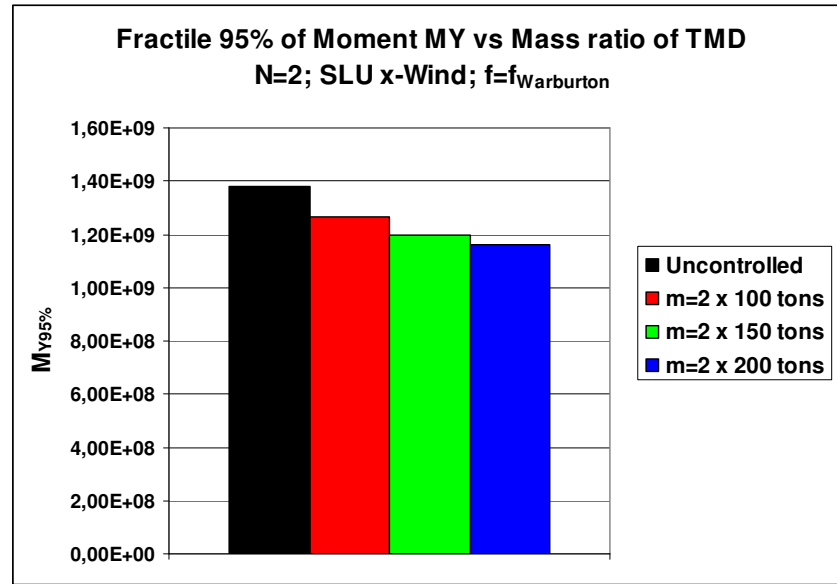
Figure 5.25. Fractile 95% of the bending moment M_Y at the base of one of the tower legs for different values of the mass ratio (Casciati & Giuliano, 2006).

Optimization of the Frequency ratio f

Once established that the mass ratio reduces the response of the pylon, the optimization is conducted by identifying a combination of the parameters μ, f, c/c_c such that the envelope and statistical quantities are minimum, compatibly with technical requirements (i.e. relative displacements, weight of the suspended masses, range of availability of the parameters, costs).

In Table 5.XV are reported the configuration and the properties of TMDs inserted in the legs, with out-of-plane response, used in the parametric analysis for the optimization ($\mu = 0.0125$: suspended masses=150 tons and TMD stiffness variable in order to obtain the frequency ratio expected).

The results of Figure 5.26 confirm the high sensitivity of the efficiency to the tuning ratio f, and so the low robustness of such devices against possible

mistuning, i.e. relevant discrepancy between the control and the structural frequency.

Configurations (*In-service* pylon)	$\mu\ (mass)$	$f = \omega_a / \Omega$	$h / h_{tot}\ (h)$
TMD-4	0.0125 (2x150 tons)	f=f$_{Warburton}$=0,991	0,73 (276 m)
TMD-6		0,704	
TMD-7		1,200	

Table 5.XV. Exploration of frequency ratio effects: *single-TMD* configurations.
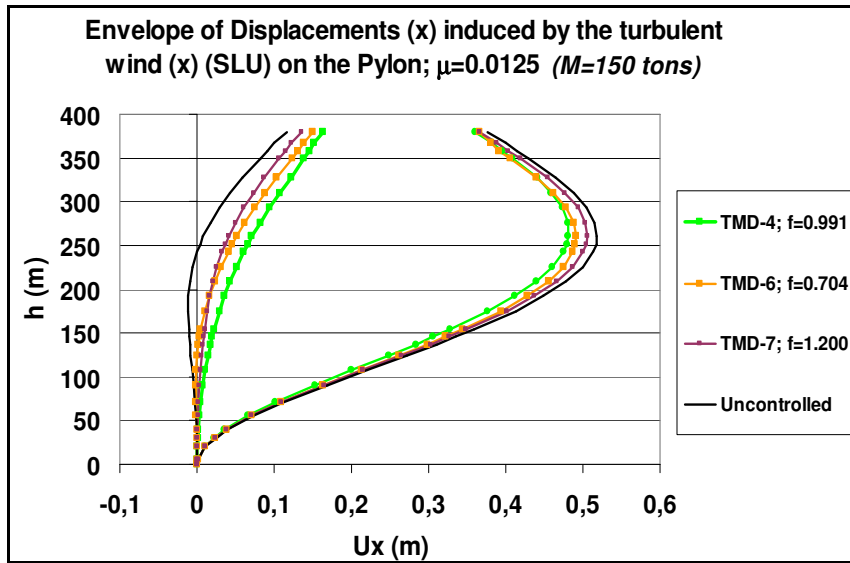
Figure 5.26. Frequency ratio effect: envelopes of out-of-plane response.

The optimal tuning ratio is approximately the same of the white noise defined by Warburton: even if the load spectrum has a non-uniform distribution, the exciting frequency is the resonant one, and the contribution of the other frequency is almost negligible. Assuming a value of the mass ratio $\mu = 0.0125$, corresponding to $M = 150$ tons per leg for the suspended masses, it is possible

241

to get a reduction on the characteristic value of the fractile 95% of the moment M_{yk} of about 9,4%. Furthermore a reduction of 7,7% on the largest horizontal deflection has been obtained, relevant for buckling safety (0,48 m vs 0,52 m).

In Figure 5.27 is represented in the frequency domain the reduction of the response (Power Spectral Density of the out-of-plane maximum displacement), using a mass of 100 tons per leg, and the TMD parameters optimized, using the wind load spectrum defined and the expected soil properties.

It is possible to observe that the couple of TMDs, equivalent to a single TMD, is effective in a small range of frequency, the tuned one, and reduces the response of the mode selected only, while is ineffective for other frequencies, even if they are close like the first two modes of the *in-service* pylon. Such response confirms the small robustness of the TMD, so sensitive to any possible *mistuning*.
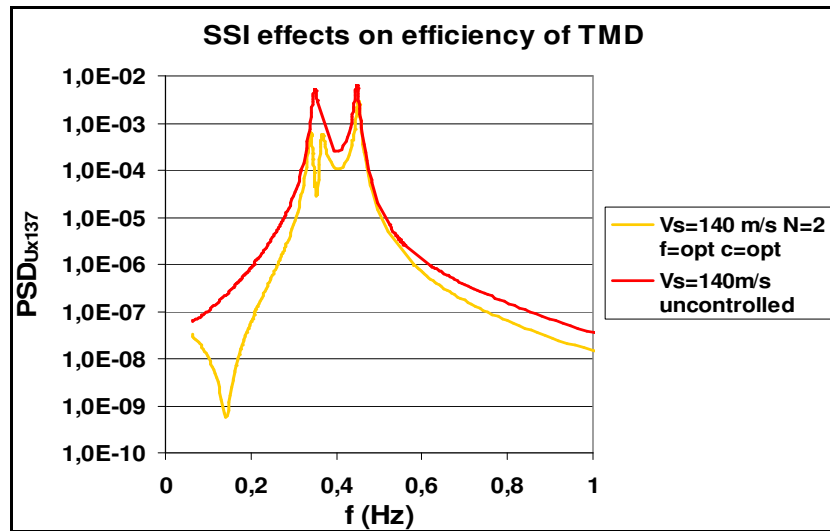
Figure 5.27. Frequency response of uncontrolled and controlled pylon (Giuliano, 2006).

5.6.3 Demand of Robustness of the Soil-Structure-Control System

The result achieved in the previous section, about the ability of a TMD to mitigate the response of a suspended bridge tower, just confirms the data collected during the monitoring of operating bridges. But the design of the device is still open to improvements. In particular one would improve the robustness of the performance, i.e., decrease its sensitivity to perturbations from the adopted optimized design conditions. It is worth mentioning once again, in fact, that TMD devices are very effective in a short frequency range, around the structure fundamental frequency and their performance are quite sensitive to the *mistuning* and, with a lower extent, to the damping property deviations.

Mistuning is mainly due to inaccuracies in:

- the evaluation of the structural frequency of the mode to be controlled;
- the selected material properties of the materials;
- the assumed geometric and inertial properties of the resistant sections;
- the reference boundary conditions.

In addition, unforeseen local behaviours and soil-structure interactions are capable of altering, temporarily but significantly, the structural frequency giving rise to contingency scenarios which could annihilate any benefit from the control device. Robustness is pursued by installing a higher number of devices with suitable mass, frequency and damping values.

The sensitivity of the performance to *soil/device induced mistuning* is here investigated in the frequency domain: the results, due to the linear and stationary process hypotheses are relevant in qualitative sense, while for the numerical quantification it is recommended to refer to the simulations in the time domain and in the nonlinear field.

For the *free-standing* configuration the Performance parameter considered representative of the structural response is the x-displacement (out-of-plane) of

the top (Node167), while for the *in-service* configuration it has been assumed the maximum x-displacement along the legs (occurring at Node137).

Soil stiffness and efficiency of TMDs: soil-induced demand of robustness

In the Paragraph 5.1 the dependence of the structural frequencies on the soil stiffness has been emphasised. Consequently uncertainties and error in the soil parameters, or fluctuations, which have probability of occurrence, can induce mistuning and affect significantly the effectiveness of the TMDs, even if they are optimally designed.

In the diagrams of Figures 5.28, 5.29 is represented the reduction of the response, with reference to different stiffness of the deposit (expressed in terms of soil shear wave speed). *Single-TMD* configurations have been here considered, with mass ratio $\mu = 0.83\%$, corresponding to one mass of 100 tons per leg. Optimal tuning and damping ratios for the devices have been assumed according to Warburton's criterion.

The diagram of Figure 5.28 for the *free-standing* pylon shows a smaller dependence of the effectiveness of TMDs on the soil properties.

For the *in-service* configuration Figure 5.29 shows that the soil stiffness increases the effectiveness in the tuned frequency (the first mode), but gives greater response at low frequencies. Furthermore, the two diagrams show that the TMDs are effective only in a small range of frequency around that of tuning, and are ineffective even in the close frequencies, such as that of the second mode. Such inefficiency, in particular, makes the second mode the most important after the control system installation. The smallness of the effective frequency range reduces the confidence on the *robustness* of such devices against any possible cause of mistuning or disturbance. Such circumstances are almost irrelevant for the *free-standing* pylon, less sensitive to *soil-induced mistuning*, and for which the single TMD solution provides adequate robustness.
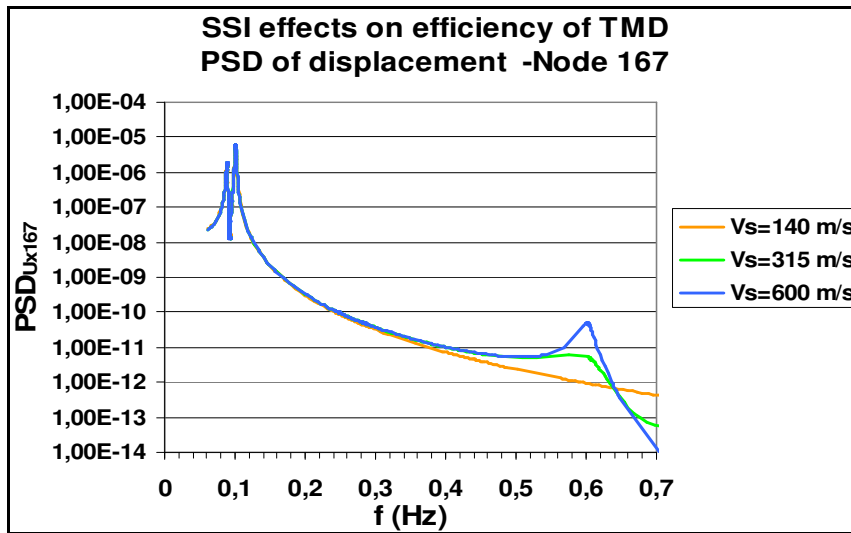
Figure 5.28. *Free-standing* Pylon: Soil stiffness and efficiency of TMD (N=2) (Giuliano, 2006).
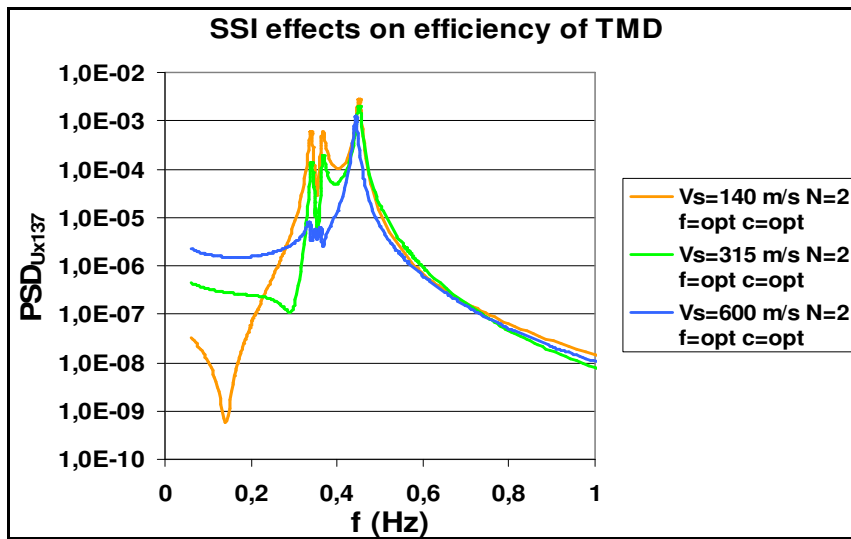
Figure 5.29. *In-service* Pylon: Soil stiffness and efficiency of TMD (N=2) (Giuliano, 2006).

245

Sensitivity to device mistuning: device-induced demand of robustness

Possible *mistuning* of the devices can also affect significantly the effectiveness of the control system, both for the *free-standing*, and for the *in-service* configuration.

The device mistuning can be identified by the device-mistuning parameter:

$$\beta = 1 - \omega_c / \Omega$$

where ω_c = circular frequency of the TMDs; Ω = circular frequency of the controlled mode.

Of course the tests and the quality procedures for the device production reduce the uncertainties on the mechanical properties of the provisions, and so the impact in terms of induced *mistuning*.

Figures 5.30, 5.31 represent the gust response of the pylon with reference to the expected soil stiffness of the site ($V_s = 140 \, m/s$), and using as *mistuning scenarios* $\beta = -0.05$; 0.00 ; $+0.05$.
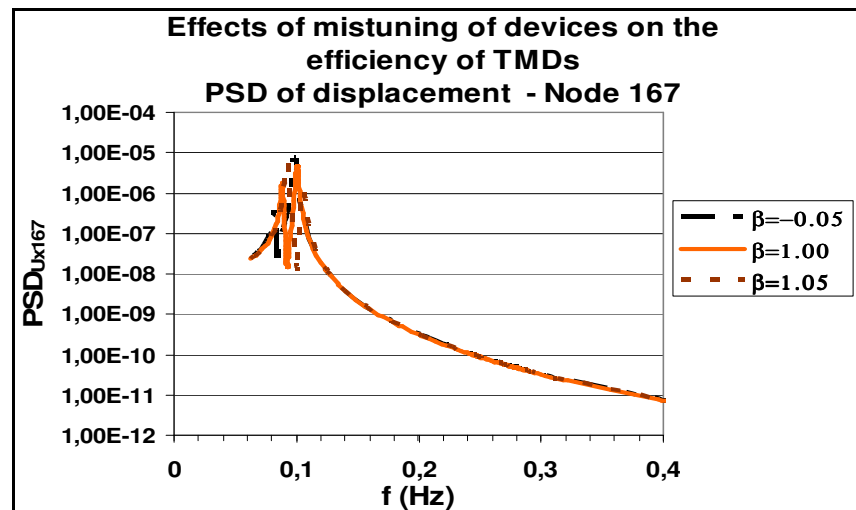
Figure 5.30. *Free-standing* pylon. *Device-induced mistuning* and loss of efficiency.

246
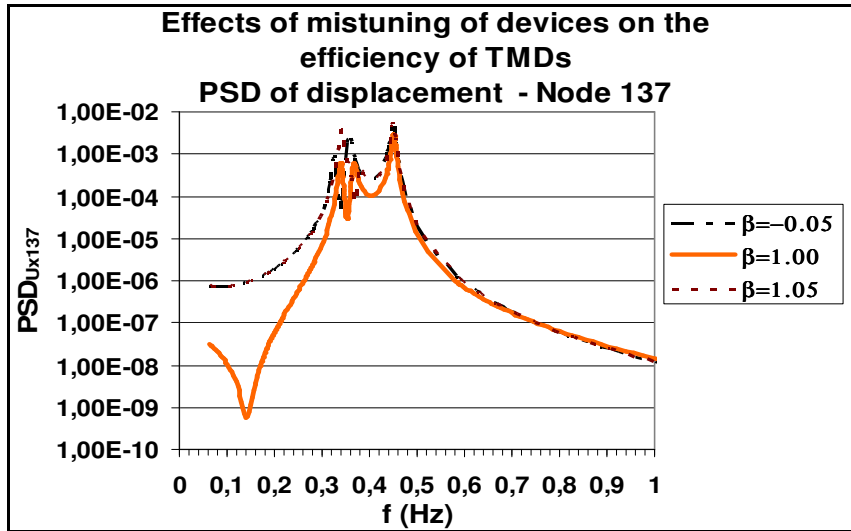
Figure 5.31. *In-service* pylon. *Device-induced mistuning* and loss of efficiency.

The diagrams show that the *free-standing* configuration is less sensitive to *device-mistuning*, and so it keeps its smaller robustness request. In the service configuration the same mistuning affects both the controlled mode response and also the low frequency bandwidth.

5.6.4 Robust Design: MTMD Systems

The previous results show that the *free-standing* is the most severe configuration in the whole life and require maximum effectiveness but lower robustness because the structural properties are very robust and not sensitive to uncertainties and fluctuations. On the contrary the *in-service* one is less hazardous but increases the demand of robustness. In fact the *service* configuration is more sensitive to any cause of *mistuning*, from uncertainties to possible fluctuations on mechanical properties of the structure, of soil, of devices, with different impact.

In the following paragraphs robust configurations are pursued and investigated with reference to the service life of the pylon. At this regard studies of literature

propose the adoption of *multi-TMD* systems to improve the structural response, in terms of *Effectiveness* but principally of *Robustness*.

Effects of multiple design variables in the peak response

The advantages provided by multi-device configurations is represented in terms of Dynamic Amplification Factor D, with reference to the case-study pylon idealized as a SDOF system, studying the effects of the number of devices, their damping, the frequency range covered, on the performance of the control system. In Table 5.XVI are represented the control configurations theoretically investigated by the study of the transfer functions and the resulting dynamic amplification factor as a function of the exciting frequency.

The mass distribution is assumed uniform ($\mu = 0.0083$), and the central frequency of the devices is that of Warburton.

Case	N	$\mu_i \quad i = 1..N$	$\Delta\omega$	ω_{centr}	ξ_i
1	0	-	-		
2	2 (1 per leg)	0.417 %	0		
3	10 (5 per leg)	0.083 %	0.05	2,2858	0,04
4	10 (5 per leg)	0.083 %	0.2		
5	10 (5 per leg)	0.083 %	0.4		

Table 5.XVI. Studied configurations of MTMD systems.

Figure 5.32 represents, for the cases of Table 5.XVI, the response in terms of dynamic amplification for different exciting frequencies. In the absence of devices ($N = 0$) the curve shows its resonant peak. Two equal devices in the two legs ($\Delta\omega = 0$) (equivalent to a *single-TMD* of doubled mass and frequency) produce two peaks. When the number of devices is increased to 10, short ranges of frequencies covered by the devices (f.i., $\Delta\omega = 0.05$) mean the same response of the TMD couple. As $\Delta\omega$ increases, up to an optimal value around 0.02, the response curve shows the expected *flattening* of the curve: it is equivalent to add further damping to the system. After crossing the optimal

threshold, i.e., for $\Delta\omega > \Delta\omega_{opt}$, the response shape go back to the peak feature: indeed some device are no longer effective, since their frequencies are too far from that of the controlled structure.
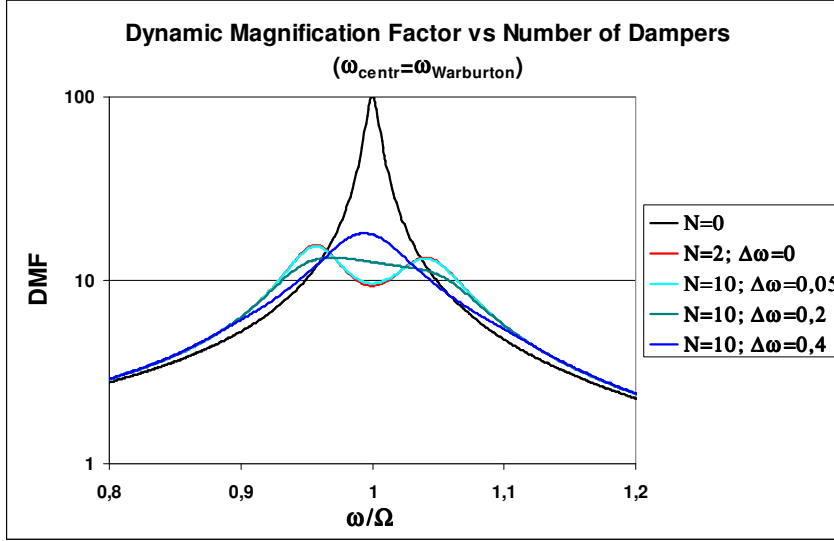
Figure 5.32. Dynamic amplification factor versus the excitation frequency.

Effect of Mass distribution

Figure 5.33 compares, for the same range $\Delta\omega$, the response curves obtained for a uniform distribution of masses and for the non-uniform scheme of the type:

$$\mu_i / \mu_{max} = 0.125 - 0.50 - 1 - 0.50 - 0.125 \quad i = 1...5$$

The latter case produces resonant peaks at the frequencies of the devices of lowest frequency, which result less controllable. Thence, the uniform distribution results the most effective.
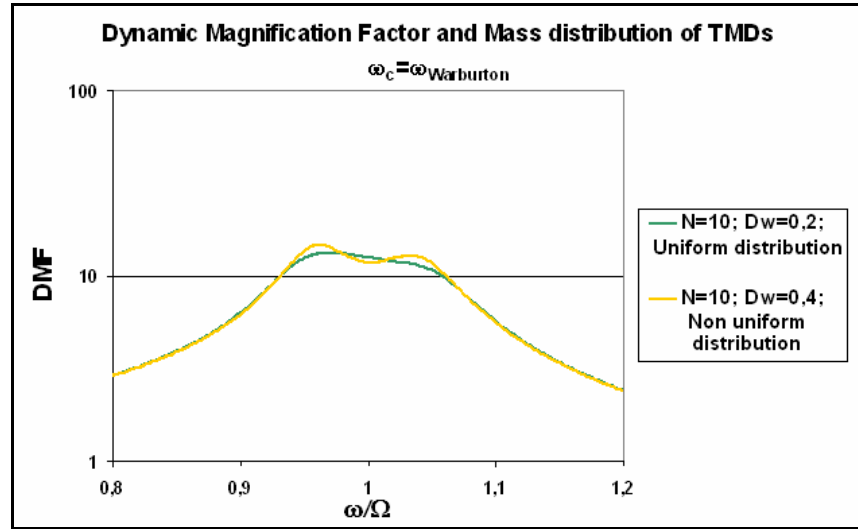
Figure 5.33. Effect of the mass distribution on the structural response.

Effect of damping distribution

In the hypothesis of uniform distribution of damping, together with the expected structural damping, the MTMD response has been investigated with $N = 2x5 = 10$ devices, each with mass $m_1 = 20000\,kg$ (so that $\mu_{tot} = 0.83\%$), central frequency value given by the optimal Warburton value and frequency range of $\Delta\omega = 0.2$. The structural response was investigated for device damping values in the range from 0.0005 to 0.08.

The diagram in Figure 5.34 outlines how too low damping values produce secondary peaks, of number $1 + N/2$, the TMD being symmetrically placed in the two legs. Each couple of TMD devices has its own frequency: too low damping values are not able to mask these peaks and the installation benefit is quite modest.
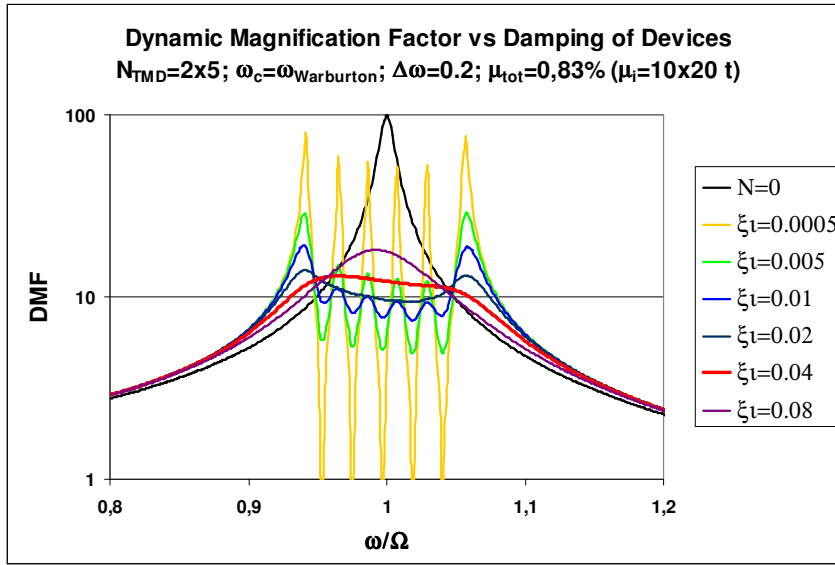
Figure 5.34. Effect of the device damping value on the structural response (Casciati & Giuliano, 2006).

As the damping ratio increases, the structural response becomes regular and the peak response reduces and locates around the main structure frequency.

The diagram also emphasizes the existence of a critical value of the damping ratio, i.e., 0.04: for larger damping values, the structural response increases, since the excessive damping prevents from the desired energy dissipation.

The secondary peaks could be reduced, for the assumed value of $\Delta\omega$, by increasing the number N of devices: in this way the energy content would distribute on a greater number of discrete frequency values. Otherwise, each device must mount a damper providing a sufficient damping.

The estimation of the optimal damping is important in view of producing a reduced and robust response over an extended frequency range. Too low values produces secondary peaks, while too high values produces a resonant peak close to the main structure frequency.

251

It is to note that the optimum damping ratio of the dampers ($(\xi_a)_{opt} \cong 0.04$ if $\mu_{tot} = 0.83\%$) is significantly lower than that of the single TMD (Warburton criterion: $(\xi_a)_{opt} = \sqrt{\dfrac{3\mu}{8(1+\mu)}} = 0.055$).   It confirms that the insertion of TMDs has a global effect of increase of damping.

Combined effect of damping and frequency range
In the same hypotheses of MTMD made of $N = 2x5$ devices, with $\mu_{tot} = 0.83\%$, masses uniformly distributed and central frequency $\omega_c = \omega_{Warburton}$, Figure 5.35 shows the relation between the maximum structural response and the frequency range covered and the damping ratio of the devices. It allows the designer to select the optimal couple $\xi_i - \Delta\omega$ in terms of effectiveness. A neighbourhood of this point will be then explored by numerical simulations in the frequency and time domain.

The diagram of Figure 5.35 is projected on the damping-amplification plane in Figure 5.36. The optimal value $\Delta\omega_{opt}$ of the frequency range is not very sensitive to the value of the device damping ratio. For low values of ξ_i , the optimal value $\Delta\omega_{opt}$ increases, so that the TMD are enlarged around the fundamental frequency and the secondary peaks are reduced. As the damping increases, $\Delta\omega_{opt}$ decreases, and becomes zero for over-damped systems. In this case the MTMD degenerates in a single equivalent TMD and the MTMD benefit is lost.
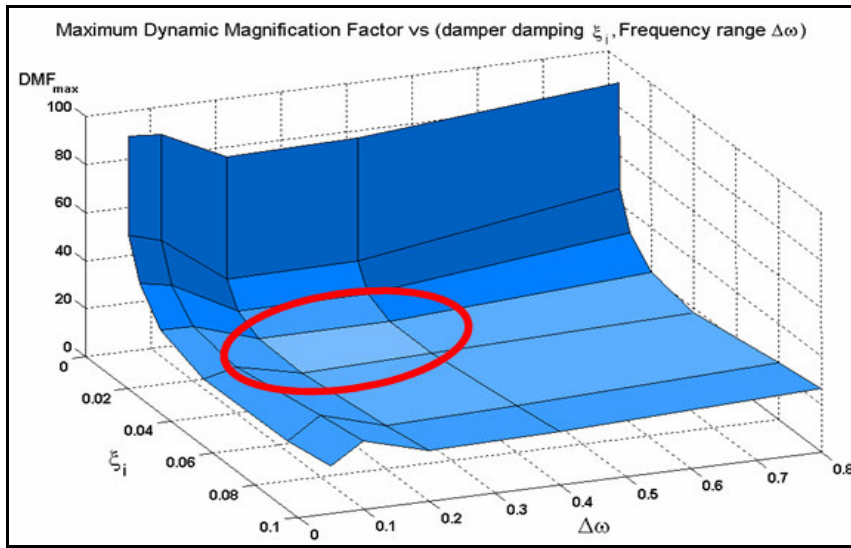
Figure 5.35. Effect of damping ξ_i and frequency range $\Delta\omega$ on the response (Casciati & Giuliano, 2006).
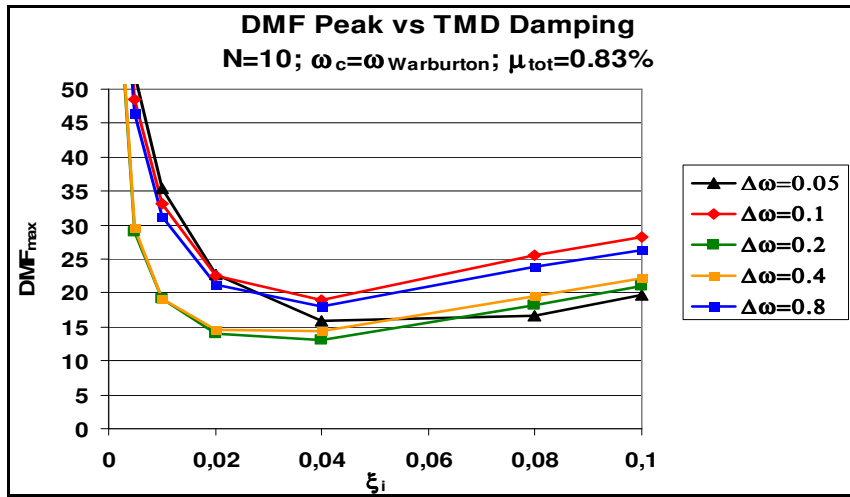
Figure 5.36. Projection of Figure 5.34 on the plane ξ_i-D (Casciati & Giuliano, 2006).

Efficiency, Robustness and Redundancy of multi-device configurations

Most of the discussion developed up to now, is based on a deterministic knowledge of the structural modal parameters and of the (linear) mechanic characteristics of the installed devices. Indeed, both the structural dynamic properties and the design parameters of the TMD devices are affected by uncertainties, which are able to produce *mistuning* and loss of efficiency.

<u>*a. Effectiveness and robustness versus the device damping ratio ξ_i*</u>

If one compares the effectiveness of single-TMD configurations (N=2) and MTMD configurations (N=10) around the Warburton central frequency and with uniform mass distribution (UDM), it is possible to evaluate the effect of the device damping on the robustness of the control performance. This is pursued by studying the response peak as the damping varies. The frequency range is zero for $N = 2$ while it is close to the optimal value for $N = 10$: $\Delta\omega = 0.2$.

Figure 5.37 shows the greater effectiveness of MTMD systems (it could increase for an even higher value of the device number N) even for low values of the damping ratio. Indeed the maximum amplification curve is lower for a wide interval of damping values. Note that the optimal damping value for MTMD systems is lower than that of a single TMD couple. This confirms how the introduction of several devices means a system damping increment. Nevertheless, the selection of the optimal damping cannot forget the secondary peak generated by very low damping values.

Focusing attention on the robustness, the same diagram shows how MTMD systems are less robust than the single TMD (per leg) around the optimal damping, in the sense that the performance decreases more significantly in the former case for variations in the device damping ratio. Actually, for low damping values the MTDM solution shows a greater response gradient, which means a lower robustness level. But for high damping values, the MTDM slope is lower, which means a better robustness.
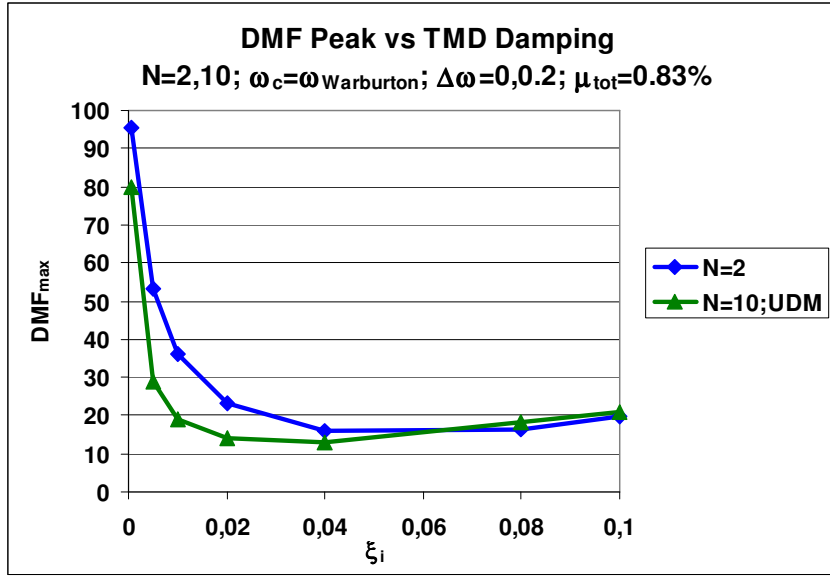
Figure 5.37. Effect of damping and device number on the response (Casciati & Giuliano, 2006).

b. Robustness against mistuning

Any *mistuning* with respect to the main structure frequency decreases the MTDM performance: as the central frequency ω_c varies, several devices behave on frequencies far from the optimal value. Figure 5.38 shows this effect within a likely *mistuning* range for the configurations with $N = 2$ and $N = 10$ with a uniform distribution of mass and damping.

The peak response diagram confirms that an increase of the device number increases the effectiveness (since the peak is reduced at all frequencies) and the robustness (the curve gradient is reduced at all frequencies). It also emphasizes that systems designed with the optimal frequency range, $\Delta\omega_{opt} = 0.2$, i.e. producing maximum response reduction, are less robust in respect of *mistuning*. This inconvenience can be overcome by enlarging the range $\Delta\omega$ of the covered frequencies, so that an higher number of devices work at a frequency close to

the actual main structure frequency. Of course, the price to pay is a lower effectiveness, as outlined by the peak values of the response function around $\omega_c/\Omega = 1$. It follows the need of introducing this aspect in the decision process resulting in the final selection of the design parameters of the control device. The adopted solution will not be the one of maximum effectiveness (minimum peak) achievable in the deterministic case. The final configuration will realize a compromise between effectiveness and robustness, calibrated on the amount of the uncertainty, and on the time variability of the influent factors which should be evaluated in a probabilistic context.
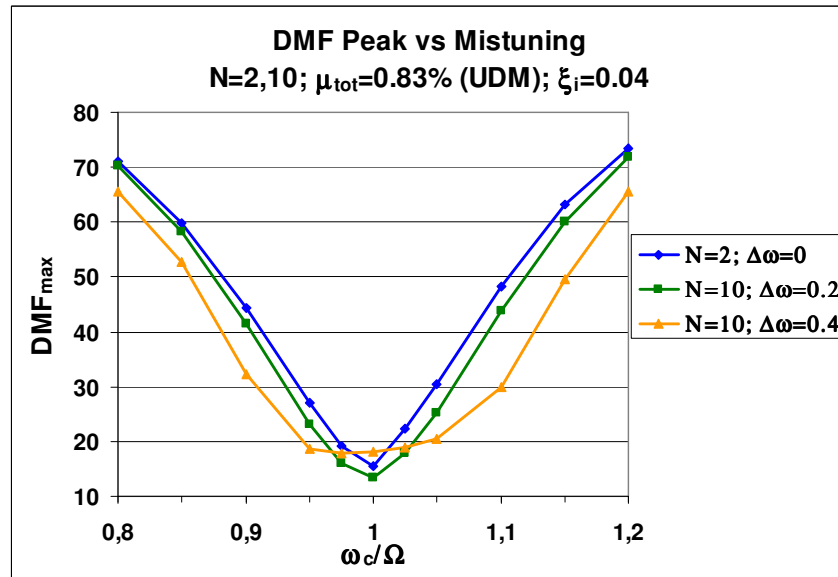
Figure 5.38. Effectiveness reduction due to *mistuning*.(Casciati & Giuliano, 2006).

c. Redundancy of the MTMD system

An evident advantage of MTMD systems relies on the ability to work, even if with reduced performance, when one or more devices undergo maintenance or

out-of-service. The diagram of Figure 5.39 shows for $N = 10$, central frequency and damping optimized, how the effectiveness decreases as the number of working devices decreases: the device of higher effectiveness either in a single leg ($N = 9$) or in both legs ($N = 8$) are removed.
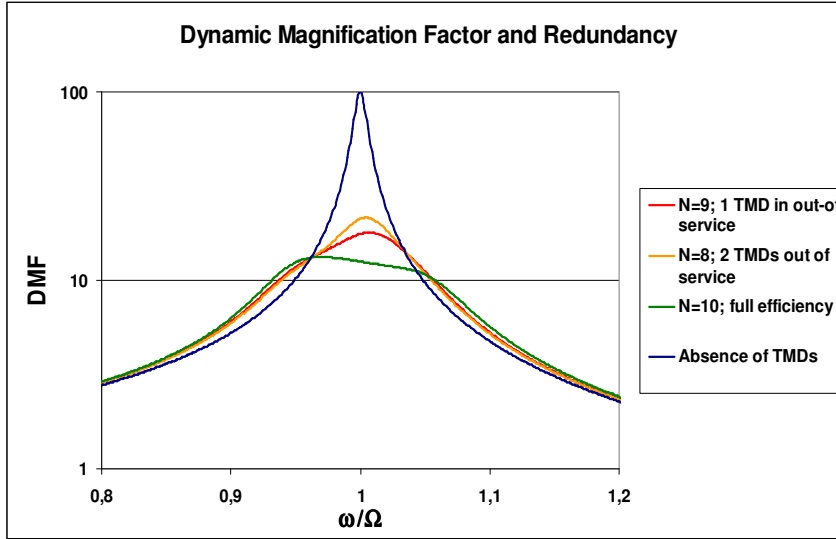
Figure 5.39. Efficiency reduction for partial out-of-service toward MTDM redundancy (Casciati & Giuliano, 2006).

5.6.5   **Performance of MTMD for the Service Life**

The advantages of MTMD systems were emphasized by transfer functions of likely configurations of the tower in its serviceability conditions. They are quantified in this section by numerical simulations.

The analyses are conducted for the installation solutions summarized in Table 5.XVII. The advantage of multi-device configuration is put in evidence in the frequency and time domain, using as soil stiffness parameter that expected for the reference site ($V_s = 140\,m/s$).The main purpose is to quantify effectiveness and robustness and, in case, to update the design on this basis.

Configuration (*In-service* pylon)	Number of devices N	Mass ratio μ_{tot} (Uniform)	Frequency Range $\Delta\omega$	Tuning ω_c/Ω	ξ_i (Uniform)
Uncontrolled	$N = 0$	-	-	-	-
TMD N=2	$N = 2 \times 1$		-		
TMD N=10	$N = 2 \times 5$	0.83%	0.2	$[0.85 - 1.41]$	0.043
			0.4		
			0.65		

Table 5.XVII. Configurations of MTMD systems.

Stationary response: simulations in the frequency domain (PSD approach)

In Figure 5.40 is represented the comparison of the response of the *uncontrolled* pylon, the *single-TMD* (one per leg) solutions, and the *multi-TMD* ones ($N = 2x5$).
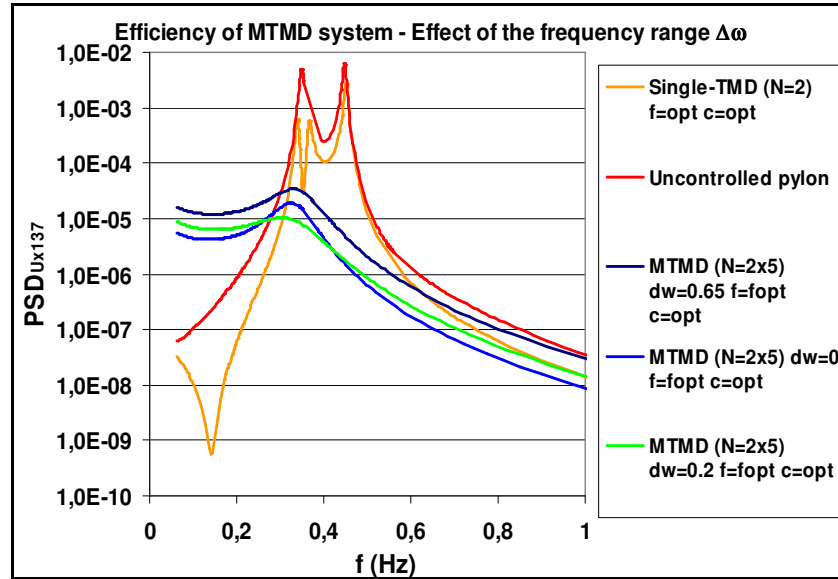
Figure 5.40. *In-service* pylon: Efficiency and robustness of MTMD systems (Giuliano, 2006).

The diagram shows that *multi-TMD* configurations are more efficient than the *single-TMD* per leg, in a larger frequency range, reducing also the second mode response. The increase of the effective bandwidth shows that expected amount of *soil mistuning* would not affect the efficiency of MTMD control systems, providing greater robustness. The advantage of such solution is even further accentuated in respect the *device-induced mistuning*.

Nonstationary response: simulations in the time domain
The advantages of MTMD systems are quantified by numerical simulations in the time domain, were the effects of nonlinearities are included.

The effects of *mistuning* are here represented by exploring the response in a likely range of central *tuning ratios* ω_c/Ω around the optimal value, between 0.85 and 1.41. The other design parameters are kept as represented in the previous Table 5.XVII.

For the different design configurations, the numerical analyses recorded the time histories of displacements, accelerations and load effects at different structure locations. Table 5.XVIII summarizes some statistics of the out-of-plane bending moment M_Y at the bottom of one of the two legs. The results confirm that, for given values of installed mass and central frequency, the solution with $N=10$ devices, of uniformly distributed frequency, is more effective than the solution with $N=2$ devices. The results confirm also that the effectiveness of MTDM systems decreases as the frequency range $\Delta\omega$ exceeds an optimal threshold. On the other side, for a given $\Delta\omega$, it is possible to evaluate an optimal tuning ratio $f=\omega_c/\Omega$. If the ratio $f=\omega_c/\Omega$ is far from the optimal value, then the response peak can become even more severe than those recorded in the *uncontrolled* structure.

The robustness features of MTMD configurations against any cause of *mistuning* is represented with reference to the 95% fractile of the bending

259

moment M_Y at the bottom of the leg. Figure 5.41 provides the fractile values as a function of the frequency range $\Delta\omega$ and of the tuning ratio $f = \omega_c/\Omega$.

Configuration	Freq. range $\Delta\omega$	Central tuning ω_c/Ω	Response: Bottom moment M_y (Nm) (per leg)		
			Maximum	Mean	Standard deviation
Uncontrolled	-	-	2.176E+09	7.738E+08	3.683E+08
TMD N=2 (1 TMD per leg)	0.0	0.85	2.163E+09	7.737E+08	3.497E+08
		0.94	2.107E+09	7.737E+08	3.310E+08
		1.03	1.922E+09	7.737E+08	3.001E+08
		1.27	2.199E+09	7.738E+08	3.580E+08
		1.41	2.211E+09	7.738E+08	3.634E+08
TMD N=10 (5 TMD per leg)	0.2	0.85	2.156E+09	7.737E+08	3.460E+08
		0.94	2.077E+09	7.737E+08	3.242E+08
		1.03	1.896E+09	7.737E+08	2.957E+08
		1.27	2.181E+09	7.738E+08	3.516E+08
		1.41	2.204E+09	7.738E+08	3.587E+08
	0.4	0.85	2.150E+09	7.737E+08	3.436E+08
		0.94	2.050E+09	7.737E+08	3.196E+08
		1.03	1.926E+09	7.737E+08	2.994E+08
		1.27	2.177E+09	7.738E+08	3.502E+08
		1.41	2.202E+09	7.738E+08	3.582E+08
	0.65	0.85	2.120E+09	7.737E+08	3.363E+08
		0.94	2.012E+09	7.737E+08	3.146E+08
		1.03	1.961E+09	7.738E+08	3.068E+08
		1.27	2.163E+09	7.738E+08	3.466E+08
		1.41	2.198E+09	7.738E+08	3.568E+08

Table 5.XVIII. Configurations of MTMD systems and bottom-leg bending moment M_Y.
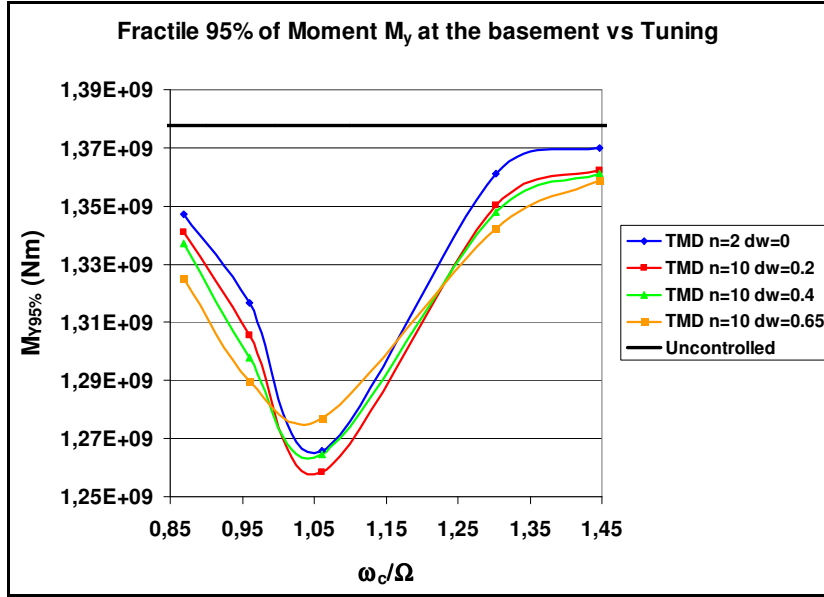
Figure 5.41. Fractile 95% of the moment M_Y at the leg bottom for different values of f and $\Delta\omega$ (Casciati & Giuliano, 2006).

The following remarks are expressed with numerical quantification:

- the system effectiveness generally increases with the device number;
- the optimal value of $\Delta\omega$ increases with the tuning ratio $f = \omega_c/\Omega$ since it makes some devices closer to the optimal frequency which reduces the response;
- solutions with high $\Delta\omega$ decrease the effectiveness but increase the robustness.

The selection of the design parameters, as $\Delta\omega$ and device damping ratios and frequencies, should pursue the maximum effectiveness in the expected *contingency scenarios*.

261

If one selects as effectiveness parameter the 95% fractile of the bending moment at the bottom of the tower referred to its uncontrolled value ($\Delta M_{Y95\%}$), the robustness of the solution can be studied by the decrease of effectiveness due to the defined mistuning index β.

The diagrams in Figures 5.42 and 5.43 show that in the expected range of structural frequencies, control systems of the MTMD type are more robust and effective and that it is possible to stabilize the performance by increase the frequency range $\Delta \omega$.
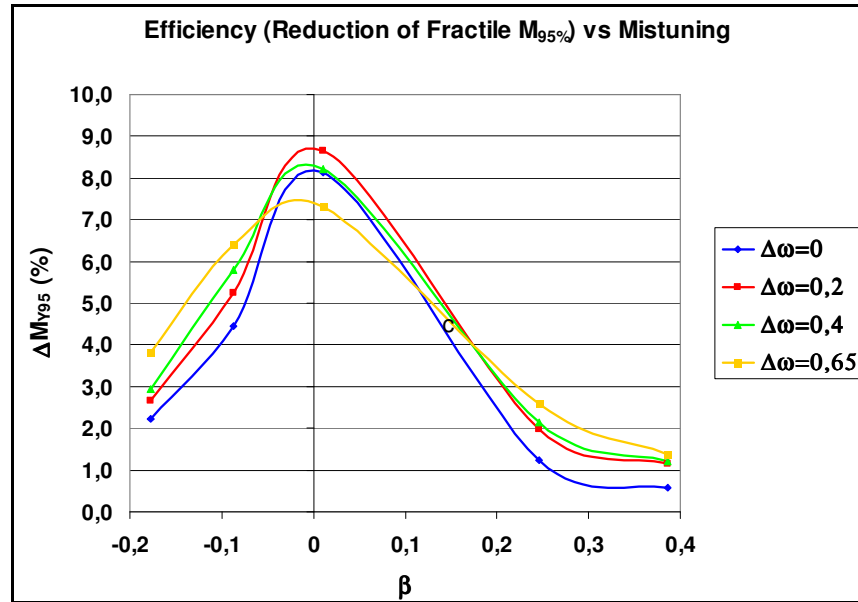
Figure 5.42. Effectiveness reduction and robustness due to *mistuning* (Casciati & Giuliano, 2006).
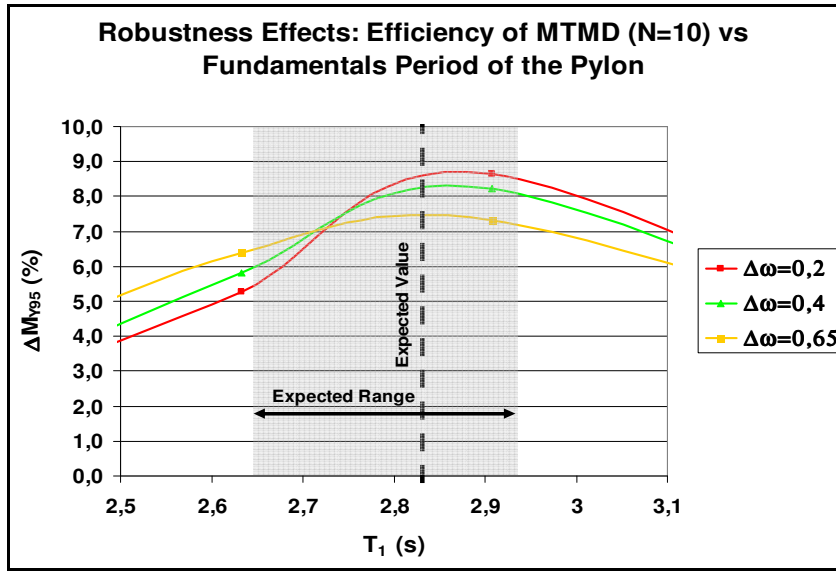
Figure 5.43. Effectiveness and robustness of the performance in the natural frequency range (Casciati & Giuliano, 2006).

Using a total amount of 100 ton per leg, reductions of 7% in the moment fractile are in this way achieved, against the original 9%. Of course, by reducing the uncertainties, one reduce the robustness demand and this turns into a better performance effectiveness. Coming back to Figure 5.28, the tower is located in a region of the curve $\Omega - V_s$ showing a significant slope. Therefore, the approximation in establishing the soil mechanical properties leads one to increase the robustness demand and hence to overestimate the frequency range $\Delta\omega$. The performance optimization, therefore, is better pursued by a campaign of data acquisition to be mainly planned during the construction stage, to also incorporate the consequent soil properties alteration.

Redundancy properties
The effectiveness of control systems with a higher number of devices comes together with a higher redundancy level. This is quantified in the histograms of

Figure 5.44, always in terms of 95% fractiles of the bending moment at the bottom of the tower. The failure of the device of central frequency (the more effective) is assumed. Frequency ratio and frequency range $\Delta \omega$ are fixed at the optimal values and configurations with $N = 2\,;6\,;10$ are studied.

When moving to the extreme conditions, the action of the TMD could result critical. A possible solution in this case would be to put the TMD out-of-service as soon as some sensors detect values beyond a pre-selected threshold. This aspect could be the matter of investigation.
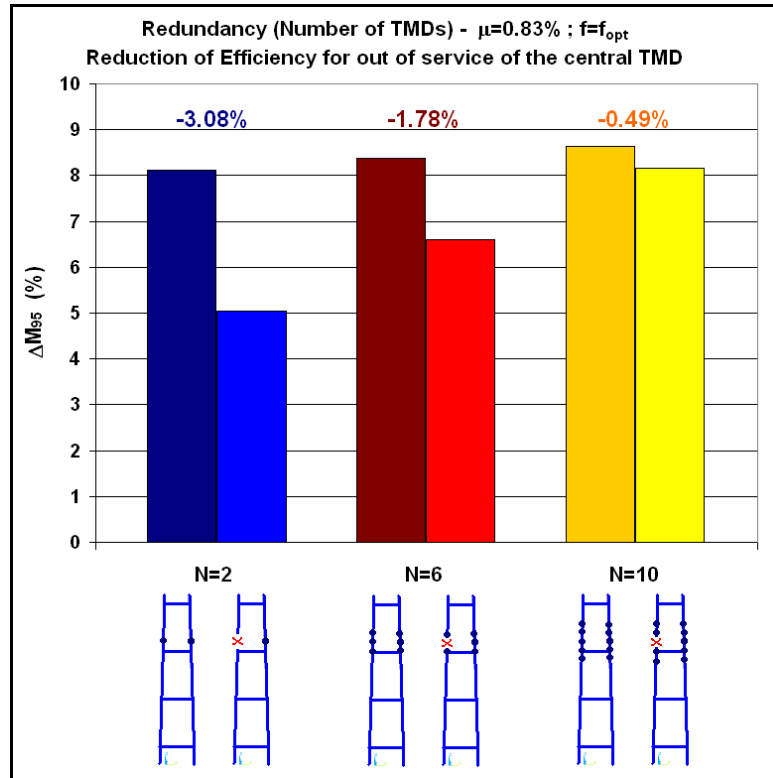
Figure 5.44. Redundancy: Effectiveness reduction for out-of-service of one device (Casciati & Giuliano, 2006).

5.7   Performance of TMDs under Seismic Loadings

If the efficiency of Tuned Mass Dampers in reducing the wind induced response is well recognized, the efficiency against the seismic actions is less pronounced. In general under earthquake-type excitations, the effective forces acting on the system structure+TMD are proportional to the masses. The performance of TMD can be improved by increasing the mass ratio μ. Yet the increase on the force acting on the secondary mass m due to the increase of μ reduces the TMD efficiency, since the inertia force acting on m is in phase with that acting on the main mass M. Also the optimum frequency f_{opt} and damping ratio $(\xi_a)_{opt}$ are shifted to new values in respect of those minimizing the wind response.

Furthermore, the passive nature of TMD requires the motion of the primary structure. If the loading has a strong impulsive content, and the maximum response occurs early in the record, the TMD can have no enough time to produce significant effect.

Furthermore the high frequency content of the seismic excitation is high, involving the higher modes of the structure. Tuned Mass Dampers are generally tuned for the first modes, and the mistuning with the higher mode can produce a slight increase of the response.

The efficiency of MTMD in suppressing the seismic response is emphasised by analyses in the time and frequency domain.

The monitored quantities are the nodal maximum x-displacements of the leg (node137) and the moment M_Y at the bottom of the pylon (node 99), in terms of time-histories, peaks, ratios in respect of the uncontrolled response.

Frequency domain analyses
Seismic analyses have been conducted also in the frequency domain, in order to identify the sensitivity of the response to the frequency content of the excitation, in the hypothesis of stationary random process.

The earthquake is modelled as a white-noise process, filtered by the Kanai-Tajimi filter.

The PSD function of the base-acceleration is

$$S_{\ddot{x}_g}(\omega) = S_0 \frac{1 + 4\xi_g^2 (\omega/\omega_g)^2}{\left[1 - (\omega/\omega_g)^2\right]^2 + 4\xi_g^2 (\omega/\omega_g)^2}$$

where S_0: intensity of the input white-noise; ξ_g: damping ratio of the ground filter; ω_g: predominant ground frequency.

The power spectrum of the white noise is related to the maximum peak of the ground acceleration by the following expression (Buchholdt, 1997)

$$S_0 = \frac{0.141 \xi_g \ddot{x}_{g0}^2}{\omega_g \sqrt{1 + 4\xi_g^2}}$$

Concerning the peak ground acceleration it has been assumed $\ddot{x}_{g0} = 5.7 \, m/s^2$, according to the *Design Specifications* of the case-study bridge.,

Frequency content of excitation and efficiency of TMDs

At first the evaluation of the efficiency of TMDs has been investigated assuming two kinds of soil (and consequent excitation content). For soft soils it has been assumed $\xi_g = 0.3$, $\omega_g = 3.14 \, rad/s$ ($f = 0.5 Hz$), while for firm soils it has been assumed $\xi_g = 0.6$, $\omega_g = 15.71 \, rad/s$ ($f = 2.5 Hz$) (Figure 5.45).

For soft soils the exciting frequencies are closer to the structural one and a greater response is expected.

In Figure 5.46, 5.47 the spectra of the out-of-plane displacements of node137 are represented, for soft and stiff soil, in the uncontrolled and MTMD configurations, with $\Delta\omega = 0$, 0.2, 0.4 and central tuning ratio $f_c = 0.94$.
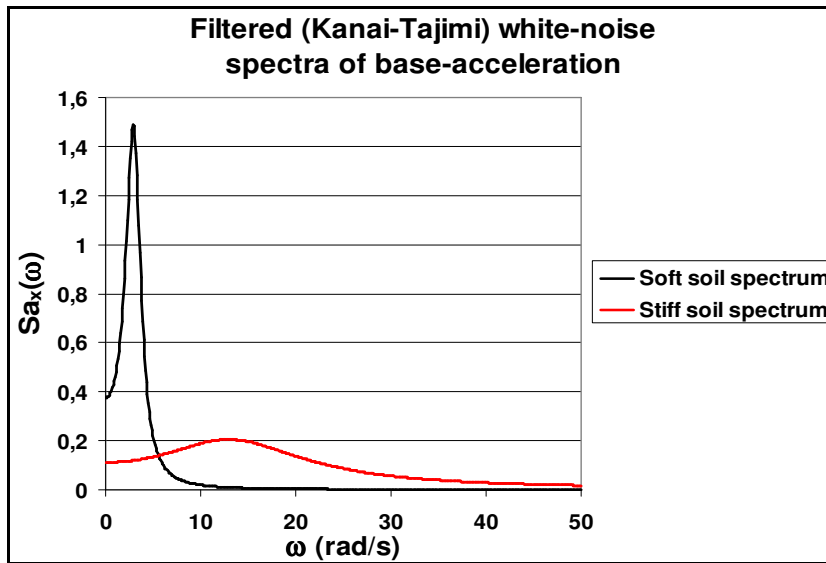
Figure 5.45. Spectrum of filtered stationary white-noise base acceleration.
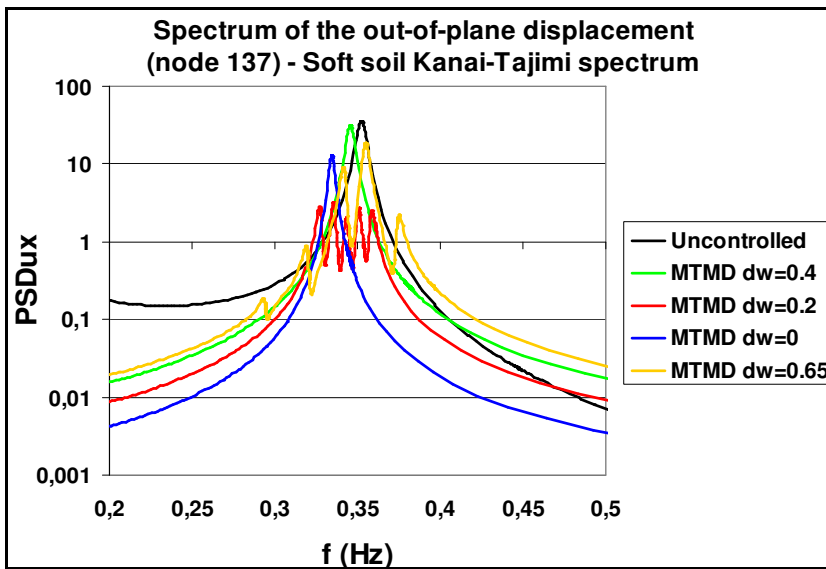
Figure 5.46. PSD response of displacement (soft soil spectrum).

267
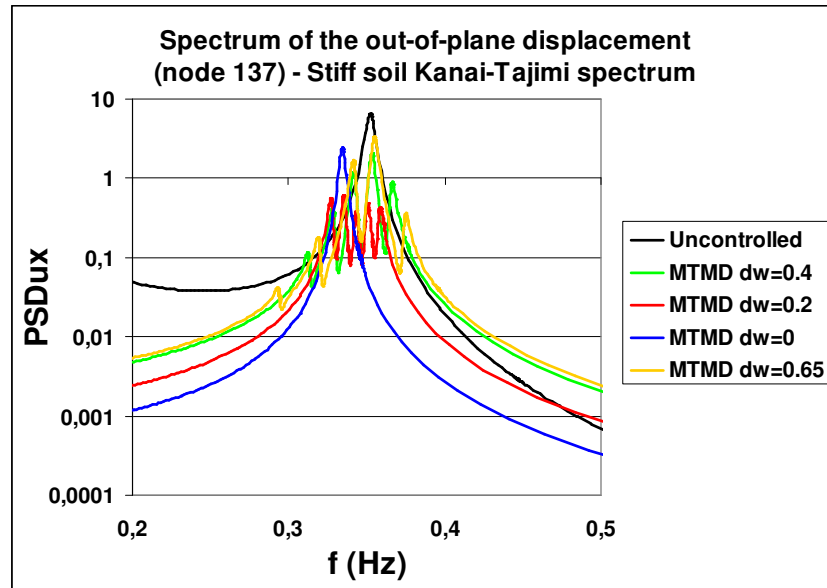
Figure 5.47. PSD response of displacement (stiff soil spectrum).

It is possible to observe that :

- in case of soft soil the response is higher because the exciting frequency is closer to the natural frequency of the structure $\Omega = 2.21\,rad/s$;

- the optimal value of the frequency range is smaller than the optimum identified for the buffeting loading; too high frequency range produce almost ineffectiveness of the control devices;

- for the stiff soil spectrum the efficiency of system with higher frequency range increases, because of the frequency content of the excitation involving also the mistuned devices.

If changes in the dominant ground acceleration ω_g are produced, in such a way that the ratio $\omega_g/\Omega = 0.25,\ 0.50,\ 0.75,\ 1.00,\ 1.50,\ 2.50,\ 4.00$, and the

268

damping ratio of the ground filter $\xi_g = 0.6$, the influence of the frequency content of the excitation can be investigated.

In Figure 5.48 are represented the input spectra of the acceleration used.
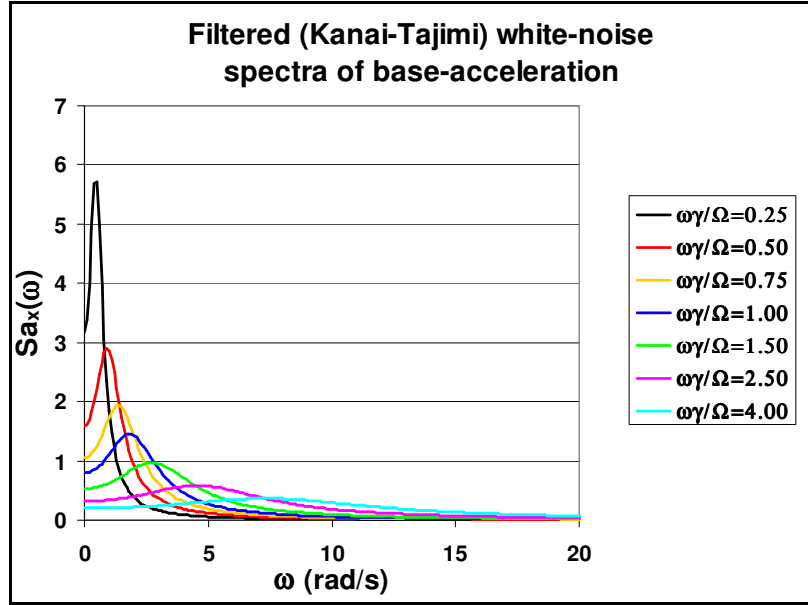
Figure 5.48. Spectra of filtered white-noise.

Figure 5.49 reports the diagram of the ratio of the standard deviations of the out-of-plane displacements in respect of the uncontrolled values. The controlled configuration (MTMD) have $n = 10$, $\Delta\omega = 0.2$, $\xi_{ai} = 0.04$, $f_c = 0.94$.

It is possible to observe that the frequency content of the excitation changes the efficiency of the devices. The efficiency (ratio $\sigma_{ux}/\sigma_{ux,0}$) is lower at the low frequencies of excitation, and remains constant for ratios $\omega_g/\Omega > 1$.
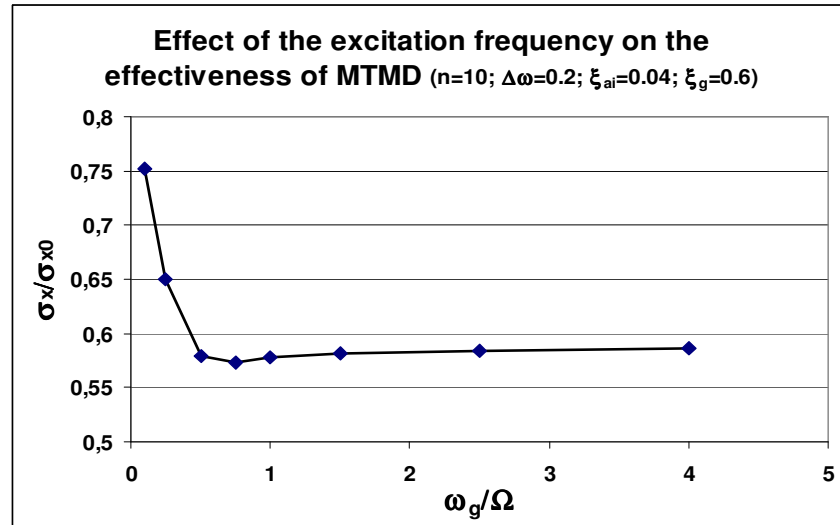
Figure 5.49. Effect of the excitation frequency on the efficiency of MTMD.

Time-domain analyses

The analyses in the time-domain use a seismic signal (E1/1992) generated *ad hoc* for the reference site of the bridge and for analyses at the Ultimate Limit State. The choice of the record has been conducted in order to excite the first natural frequencies of the pylon, and the analyses are focused on the efficiency of the Tuned Mass Dampers or to check possible loss of safety. In any case, further investigations are recommended for the case-study.

The size of the bridge impose that asynchronous signals were used for the analyses, with different excitations for the pylon legs and the anchorages of the two sides.

The input signals are converted in terms of displacement time-histories for the boundary nodes, generated from time-history of ground acceleration applying a bandpass Butterworth filter correction of the fourth order with frequency $f_1 = 0.1 Hz$, $f_2 = 25 Hz$.

270

The bandpass filtering is employed to remove unwanted frequency components from the given signal: it allows signals within a given frequency range (f_1 to f_2) bandwidth to pass through. This target is pursue using the Butterworth classical infinite-impulse-response (IIR) filter type. Digital IIR filters Butterworth can achieve a given set of filtering characteristics (e.g. smoothness, roll-off steepness, etc.) with a much lower filter order than a corresponding FIR filter, thus minimizing computing requirements.

The Butterworth filter features a maximally flat response in the passband (i.e. practically no deviation from unity), albeit at the cost of a smaller roll-off steepness (in comparison to a Chebyshev filter of the same order), that can be overcome by the use of a higher order filter. The adequate value of the order must be determined through a user-driven sensitive study.

In Appendix C are represented the three-component acceleration, velocity, displacement time-histories of the seismic record used, in the original and corrected form, and the corresponding spectra of the acceleration.

In Table 5.XIX the MTMD control configurations analyzed are reported.

In Table 5.XX the MTMD maximum (peak) M_Y moment are reported with reference to the control configurations of Table 5.XIX, with their percent reduction in respect of the values of the uncontrolled configurations.

Configuration	Number of devices N	Mass ratio μ_{tot} (Uniform)	Frequency Range $\Delta\omega$	Central tuning ω_c / Ω	ξ_i (Uniform)
Uncontrolled	$N = 0$	-	-	-	-
TMD N=10	$N = 2 \times 5$	0.83%	0.20	$[0.85 - 1.41]$	0.043
			0.40		
			0.65		

Table 5.XIX. Configurations of the MTMD control systems.

271

Configuration	Frequency Range $\Delta\omega$	Tuning ω_c/Ω	Response: My (kNm) (per leg)	
			Maximum	Reduction
Uncontrolled	-	-	6710370	-
MTMD N=10 (5 TMD per leg)	0.2	0.85	6703390	-0,104%
		0.94	6645880	-0,961%
		1.03	6639220	-1,060%
		1.27	6498800	-3,153%
		1.41	6511970	-2,957%
		1.60	6575580	-2,009%
	0.4	0.85	6685010	-0,378%
		0.94	6645960	-0,960%
		1.03	6635310	-1,119%
		1.27	6504630	-3,066%
		1.41	6511650	-2,961%
	0.65	0.85	6705550	-0,072%
		0.94	6669290	-0,612%
		1.03	6651670	-0,875%
		1.27	6525460	-2,756%
		1.41	6514280	-2,922%
		1.60	6564020	-2,181%

Table 5.XX. MTMD control configurations and maximum (peak) moments at the bottom of the leg of the pylon.

Figure 5.50 shows the reduction of the peak moment at the leg basement of the pylon vs tuning ratio and frequency range. The diagram shows that the efficiency of the TMD installed is lower than for buffeting loading; furthermore the optimal tuning ratio is higher and the optimal frequency range lower. The increase of the optimal tuning ratio is related to the fact that the higher modes are involved by the frequency content of the excitation: higher tuning ratios get some devices resonant with the consequent motion. For too high or too low tuning ratios (and high mistuning) the optimal frequency range increases, in order to get more resonant devices at the dominant frequencies.

It is possible to assert that the TMDs installed to contrast the buffeting effects are likely inefficient for seismic excitations.
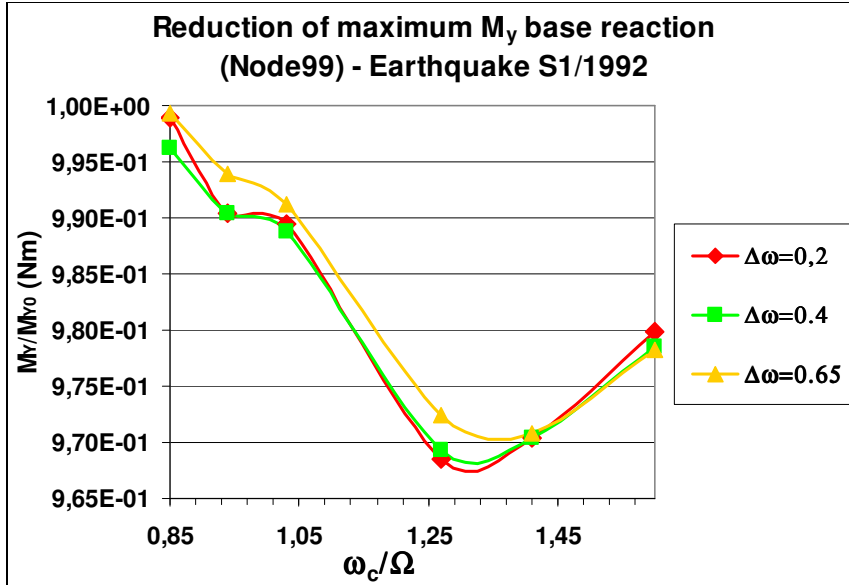
Figure 5.50. Reduction of the maximum (peak) base moment in respect of the uncontrolled configuration vs tuning ratio and frequency range.

In Figure 5.51, 5.52, 5.53 are represented the time-histories of the of the out-of-plane x-displacement (at node 137, the maximum) of the uncontrolled pylon and of a controlled configuration with central tuning ratio $f_c = \omega_c/\Omega = 1.27$ and frequency range $\Delta\omega = 0.4$.

The diagrams show that the TMDs take some seconds to move in anti-resonance with the structure, say at the end of the forced regime for this record: consequently they are effective in reducing the free vibrations, increasing the rate of decay of the amplitudes; yet they are not effective in the first peaks reduction and so for any high impulsive loading.

273
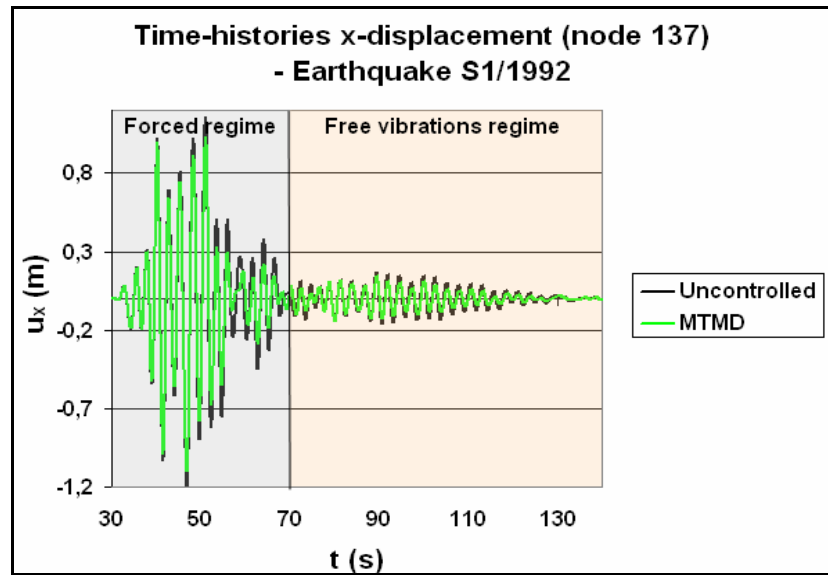
Figure 5.51. Time-history of out-of-plane x-displacements (node 137).
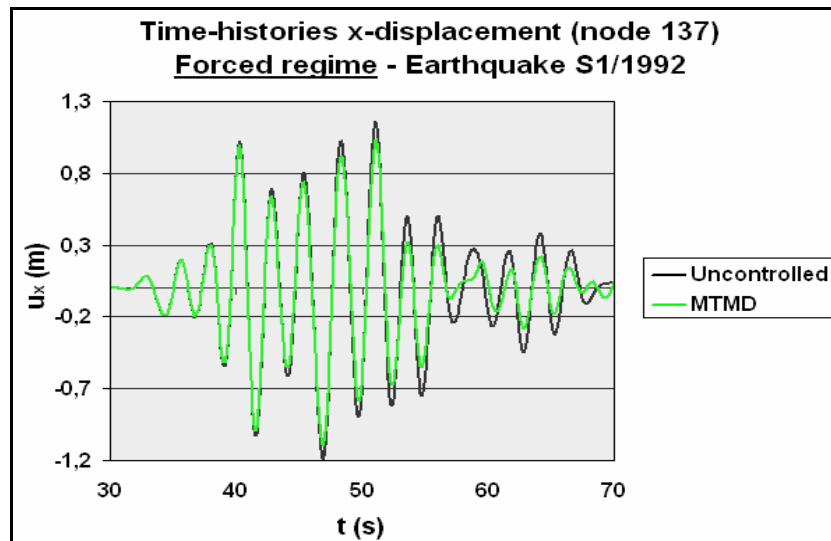
Figure 5.52. Time-history of x-displ. (node137) (Forced regime).
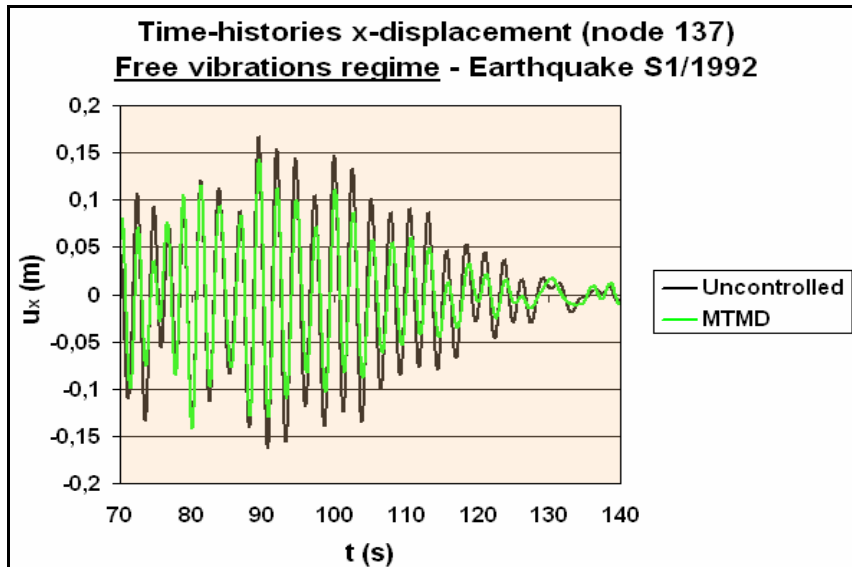
Figure 5.53. Time-history of x-displ. (node 137) (Free vibrations).

5.8 Remarks and Proposal of a Reliability-based

Optimization for a Decision Process

For a given structure such as the pylon of a suspension bridge, whose modal properties are known, and for which the number of devices and the mass amount to be installed is established according to the targets of design:

1. Passive Control Strategies like TMDs are efficient in the reduction of the gust response;
2. The modelling of the geometry and mechanics of foundation is necessary for the design of the TMD system, especially for soft soils.
3. Uncertainties and fluctuations on the soil properties can affect the efficiency of the TMDs.
4. MTMD systems can overcome the intrinsic small robustness of single TMDs, cover more than one frequency and increase the efficiency.

275

5. There is an optimal MTMD system that optimize the response in terms of efficiency (reduction of the response), if deterministic properties of the soil-structure-environment system is assumed: optimal distributions of device damping and frequencies can be determined;

6. MTMD systems can be more efficient than *single-TMD* configurations (N=2) if maximum efficiency is pursued;

7. MTMD can be more robust in respect of the *single-TMD* configurations in respect of *mistuning* scenarios. The robustness can be larger if the range of the covered frequencies is larger than that of maximum efficiency $\Delta\omega > \Delta\omega_{opt}$. The range $\Delta\omega$ has a primary role in the design of the MTMD control system, because of its ability of improving/degrading the efficiency and robustness capabilities.

8. Maximum efficiency does not correspond to maximum robustness of the design. An optimal compromise between Efficiency and Robustness must be pursued.

9. Strategies of data collection and model updating during the construction can reduce the uncertainty amount, limit the demand of robustness to fluctuation effects and pursue greater efficiency.

10. Tuned Mass dampers have smaller effectiveness in reducing the seismic response. In particular it is possible to assert that the TMDs installed to contrast the buffeting effects are likely inefficient for seismic excitations. The efficiency concerns the rate of decrease of the free vibrations, while the reduction of the peak response is almost negligible. The optimal design parameters are shifted in respect those of buffeting loadings. The high frequency content of the excitation promote the mistuned higher responses, with possible negative effects of the dampers, and generally with higher structural response. For the seismic efficiency active/hybrid devices seems to be more attractive.

In the previous paragraphs it has been demonstrated that the control system can mitigate the response of the case-study pylon. The state of art of the design of the case-study bridge certifies that the box sections (whose area and inertia have

been assumed in the previous computations) already satisfy the safety and serviceability requirements of the Design Specifications. These properties are assumed as *locked-data*, because the provision of the control system is intended for the improvement of the response but not to be decisive for the satisfaction of the minimum expected performance.

It is worthnoting that if all the design variables were free, greater margins of cost reduction could be theoretically available, but it would give a strategic relevance to the control system, whose reliability is often its major weakness. In this sense the limitation of the role of the structural control must be intended as a redundant robustness resource, but it reduces heavily the margins of convenience of the installation.

Furthermore uncertainties on the mechanical properties of the structure, soil or devices can reduce the performance of the control system and consequently degrade the structural response, and that the most efficient control system is not the most robust. Since the demand of robustness is related to the uncertainties of the relevant factors, it is natural to consider the probabilistic approach as an attractive tool to measure the performance and to identify optimal design solutions: the reliability methods allow a contextual maximization of efficiency and robustness.

Reliability analyses, whose definitions and methods are outlined in Appendix E, are used to evaluate the probability of survival (or the satisfaction of a performance criterion) of a component (element reliability, i.e. a substructure) or of the whole system (system reliability, i.e. the whole bridge).

A reliability analysis includes the uncertainties in the evaluation of the performance, and requires that the uncertainties are described as random variables. They are generally modelled in terms of the mean (central tendency), the variance (dispersion about the mean), the probability density and distribution functions. These data could be transformed in randomly generated samples (i.e. through the Monte Carlo Simulation), input for deterministic analyses. It realizes the fourth step of the *Experimental Approach* as outlined in Chapter 1.

Design variables $\underline{x}$

The control problem assumes the mechanical properties of the pylon as locked data, subjected only to the uncertainties, while the MTMD control parameters are assumed as design variables $\underline{x}$. The values of the sectional properties of the legs and transverses are assumed as locked data because they satisfy the Design Specifications which state that for service-state scenarios (SLE) the response of the members is in the elastic field, while for ultimate-state scenarios (SLU) the stresses are lower than the rupture values, with proper safety coefficients.

A more general approach could consider the sectional properties as a free design variable, in order to conduct the optimization in terms of minimization of the cost function; this procedure is not allowed by the Design Specifications because the provisions of control devices is conceived only in terms of improvement of the structural behaviour (i.e. increase of fatigue life) without being decisive for the satisfaction of the safety requirements.

In conclusions, the design variables considered are (Table 5.XXI):

- x_1: number of devices n: since it is a discrete number, it can be assumed constant and repeat the reliability optimization using different values of n; it is a deterministic variable;

- x_2: devices mass m_i (uniform distribution assumed) (deterministic);

- x_3: devices damping c_i (uniform) (random variable);

- $x_4,...x_{3+n}$: device frequencies (uniform distribution of frequency is hypothesised: the central frequency and the frequency range are consequent).

Because of the uncertain characteristics of the design variables, also their statistic distribution and the standard deviations can be considered.

The mean values of the design parameters are the target (design point) of the reliability-based optimization analysis, while the standard deviations of the design parameters σ_m, σ_c, σ_ω depend on the quality control procedures of the industrial production and must be specified in the contractual documents with the furnisher industry.

278

Design variables $\underline{x}$ of the MTMD system			Distribution type	Standard deviation
x_1	Number of devices	n	Deterministic and discrete: 0-2-4-6-8-10	-
x_2	Nominal devices mass ratio	μ_i	Normal	σ_m
x_3	Nominal devices damping ratio	ξ_i	Normal	σ_c
$x_4,...x_{3+n}$	Nominal devices frequency ratio	f_i	Normal	σ_ω

Table 5.XXI. Presumed statistics (scheme) of the design variables for the case-study pylon.

The reliability-based optimization consists of the identification of the design point $\underline{x}^*$, or the combination of the parameters that satisfies the constraint equations, minimizes the cost function and guarantees the target reliability index β_0 (corresponding to a target probability of failure $p_{f,0}$).

Since the number of devices is a discrete variable, the procedure of optimization must be conducted for different values, from $n = 0$ (uncontrolled pylon) to $n = n_{max} = 10$, comparing the costs for the same reliability indices.

Random variables $\underline{v}$

The random variable $\underline{v}$ that can be considered are (Table 5.XXII):

- the shear wave speed of soil V_s (eventually time-dependent);
- the sectional properties A, I of the legs and of the transverses;
- the characteristic yield stress of steel f_{yk} and elastic modulus E;
- the wind/seismic loading characteristics.

A first approximation could also consider the sectional properties of legs and transverses and the mechanical properties of the steel as deterministic data.

Random Variables $\underline{v}$			Substr.res	Distribution Type	Mean Value	St. Dev.
v_1	Elastic modulus (N/m^2)	E	Leg, Transverses	Normal	2.06e11	σ_E
v_2	Yield stress (N/mm^2)	f_{yk}	Leg, Transverses	Normal	510	$\sigma_{f_{yk}}$
v_3	Rupture stress (N/mm^2)	f_{yu}	Leg, Transverses	Normal	355	$\sigma_{f_{yu}}$
v_4	Cross sectional Area (m^2)	A_1	Leg	Lognormal	8.425	σ_{A_1}
v_5		A_2	Transverses	Lognormal	1.979	σ_{A_2}
v_6	Sect. moments of inertia (m^4)	I_{1x}	Leg	Lognormal	131.529	$\sigma_{I_{1x}}$
v_7		I_{1y}	Leg	Lognormal	222.390	$\sigma_{I_{1y}}$
v_8		I_{2x}	Transverses	Lognormal	6.104	$\sigma_{I_{2x}}$
v_9		I_{2y}	Transverses	Lognormal	67.2670	$\sigma_{I_{2y}}$
v_{10}	Structural damping (to be identified during erection)	ξ	Leg, Transverses	Normal	0.05	σ_ξ
v_{11}	Shear wave speed (m/s) (to be identified during erection)	$V_s(t)$	Soil	Normal	140	σ_{V_s}
v_{12}	Turbulent wind: return coeff. – SLE	α_r	-	Normal	1.07	$\sigma_{\alpha_r,SLE}$
v_{13}	Turbulent wind: return coeff. - SLU)	α_r	-	Normal	1.20	$\sigma_{\alpha_r,SLU}$

Table 5.XXII. Presumed statistics (scheme) of the random variables for the case-study pylon.

Constraint functions

The constraint functions are such that the physical properties of material are not violated. In the reliability problem, the constraint equation are expressed in the form

$$f^{j} \leq 0 \quad j \in J$$

For the control system of the pylon, the constraint function can be written as

$f^{1} = -x_{2}$: devices mass; $f^{2} = -x_{3}$: devices damping;

$f^{3} = -x_{4}; \ldots ; f^{2+n} = -x_{3+n}$: devices frequency.

The last constraint function prevents the lock-in vibrations, assuring a minimum damping amount greater than 1.7%:

$$f^{3+n} = 0.017 - \xi_{e,TOT} = 0.017 - \sum_{i=1}^{x_{1}} \left[\frac{\mu_{i}}{2} \sqrt{1 + \left(\frac{2\xi}{\mu_{i}} + \frac{1}{2\xi_{i}} \right)^{2}} \right] \geq 0.017 - \sum_{i=1}^{x_{1}} \left[\frac{x_{2}}{2} \sqrt{1 + \left(\frac{1}{2x_{3}} \right)^{2}} \right]$$

Limit-state functions

The limit-state functions have implicit form and take into account the stochastic nature of the variables and action:

1. Members stresses at service-state (SLE):

    $g_{1}^{p}{}'(\underline{x}, \underline{v}) = \dfrac{f_{yk}}{\gamma_{s}} - \sigma_{eq,SLE}(\underline{x}, \underline{v})$: the response of the members must be in the elastic field;

2. Members stresses at ultimate-state

    (SLU): $g_{2}^{p}{}'(\underline{x}, \underline{v}) = \dfrac{f_{uk}}{\gamma_{s}} - \sigma_{eq,SLU}(\underline{x}, \underline{v})$: the stress of the members must be lower than the rupture value.

Provided that the first two limit-state are already satisfied by the intrinsic sectional properties assumed for the pylon, without the control devices, the control system must provide an improvement of the structural performance in the service (SLE) and in the ultimate states (SLU). Since it has to be satisfied the equation $\beta\left(\underline{x}^{*}\right)_{controlled} > \beta_{uncontrolled}$, the previous limit-state functions, if control system is considered, become

281

$$g_1^p(\underline{x}, \underline{v}) = \frac{f_{yk}}{\gamma_s} - \varepsilon^1 - \sigma_{eq,SLE}(\underline{x}, \underline{v})$$

$$g_2^p(\underline{x}, \underline{v}) = \frac{f_{uk}}{\gamma_s} - \varepsilon^2 - \sigma_{eq,SLU}(\underline{x}, \underline{v})$$

where σ : equivalent stress (rms value in case of stochastic excitation);

$\varepsilon^1, \varepsilon^2$ are arbitrary quantities greater than zero.

The last statements imply that

$$\bigcup_{k=1}^{2}\left[g_k^p(\underline{x}, \underline{v}) \le 0\right] \subset \bigcup_{k=1}^{2}\left[g_k^{p\,\prime}(\underline{x}, \underline{v}) \le 0\right]$$
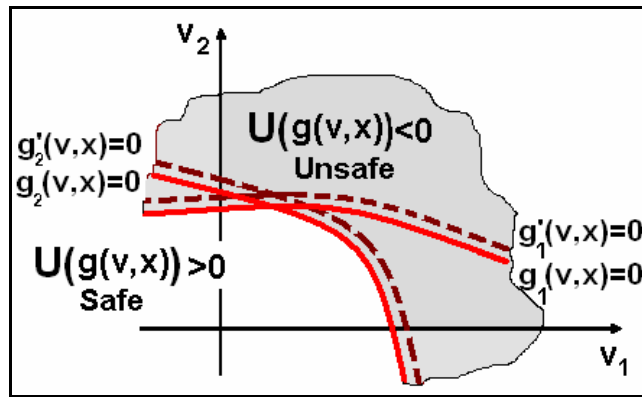
Figure 5.54. Allowed impact of the control system and Limit State functions.

3. Maximum out-of-plane displacement (secondary bending effects):

$$g_3^p(\underline{x}, \underline{v}) = \sigma_{ox_{max}} - \sigma_{x_{max}}(\underline{x}, \underline{v})$$

where σ : rms of maximum out-of-plane displacement;

4. Relative displacements of devices:

$$g_i^p(\underline{x}, \underline{v}) = \sigma_{oY,i} - \sigma_{Y,i}(\underline{x}, \underline{v}), \qquad i = 4, ..., (n+3)$$

where σ : rms of relative device displacement;

282

5. Fatigue effects: number of cycles guaranteed and corresponding stress levels allowed (from the SN curves) :

$$g_1^p\left(\underline{x},\underline{v}\right)=\sigma_{0,SN}-\sigma_{eq,fatigue}\left(\underline{x},\underline{v}\right)$$

The resultant failure domain is still identified as

$$\Omega(\underline{x},\underline{v})=\left\{\bigcup_k\left[g_k^p\left(\underline{x},\underline{v}\right)\le 0\right]\right\}.$$

Design and optimization

The construction of the implicit limit-state is difficult for the complexity of the problem: nonlinearities, multiplicity of design and random variables, loading, structural features. The construction of the approximate expressions of the function is possible through the Monte Carlo Simulation method (MCS) presented in Appendix E.

This method in general allows an *experimental* identification of the design point (the most probable failure point) and of the reliability index.

It is possible to use it also as an optimization tool, to identify in the space of the design variables, including the control system parameters, the configuration which minimizes the failure probability (or non satisfaction of minimum performance levels or violation of at least one of the Limit State functions introduced).

The maximum levels of reliability that can be obtained must be compared with those of the uncontrolled configuration; if the control system provides an improvement of the structural behaviour in a *cost-effective* way, the installation of the control system will be provided.

In conclusion, the MCS reliability-based design and optimization could be a useful mean:

a. to determine the <u>optimal design point</u> $\underline{x}^*$, that just minimizes the failure probability;

b. to   allow   a   <u>decision   making</u>:   assumed   that $\beta\left(\underline{x}^*\right)_{controlled}>\beta_{uncontrolled}$ (the   installation   of   the   control   system

provides an increase of the reliability index), the installation of the control system is convenient if it allows a reduction of the costs:

$$f^0\left(\underline{x}^*\right)_{controlled} < f^0_{uncontrolled}$$

where the cost function f^0 assumes different forms in case of uncontrolled/controlled configuration:

$$f^0_{uncontrolled} = f_{construction} + f_{failure} \cdot p_f + f_{maintenance-pylon}$$

$$f^0\left(\underline{x}\right)_{controlled} = f_{construction} + f_{control}\left(\underline{x}\right) + f_{failure} \cdot p_f\left(\underline{x}\right) + f_{maintenanceTMD}\left(\underline{x}\right) +$$

$$+ f_{maintenance-pylon}\left(\underline{x}\right) + f_{failure,TMD} \cdot p_{f,TMD}$$

In the hypotheses done and with the consideration about the cost and reliability requirements to be satisfied to <u>produce a decision</u> of installing a control system, and using the notation introduced in Appendix E, the reliability-based optimization problem can be formalized as

$$P : \min\left\{ f^0(\underline{x}) \begin{vmatrix} \text{if } f^0\left(\underline{x}^*\right)_{controlled} < f^0_{uncontrolled} : \\ \beta_0 \leq \beta_{uncontrolled} < \beta(\underline{x})_{controlled} ; \quad f^j(\underline{x}) \leq 0, \quad j \in J \\ \text{if } f^0\left(\underline{x}^*\right)_{controlled} \geq f^0_{uncontrolled} : \text{Decision making : No control} \end{vmatrix} \right\}$$

where

β : reliability index (β_0 : minimum allowed value); f^j : constraint functions.

The Monte Carlo Simulation allows also sensitivity analyses for the evaluation of the Importance Factors in the response: as previously demonstrated, it is expected that the soil mechanical properties have the higher weight.

The statistical methods can provide also a measure of the necessary confidence on the mechanical parameters (and so the refinement of data from investigations and monitoring) to obtain certain targets of the reliability index. This information enter in the cost function in the construction term $f_{control}$, and so have a certain impact in the decision process.

In any case it is to remember again that a refinement of the knowledge of the input data from monitoring shift the to optimal design, increase the efficiency, robustness, reliability of the final product.

CONCLUSIONS

Vibratory motion of slender and low-damped structures such as steel pylon of long span bridges increase stresses, induce localized irreversible damage, affect fatigue strength and safety performance from the erection to the service life.

Passive and active control strategies have been employed in several tall and slender structures and showed effectiveness in the reduction of the response. Actually Tuned Mass Dampers are the most adopted devices for the motion control of structures.

Yet these devices are not robust, being their effectiveness sensitive to many mistuning causes, such as the mechanical properties of foundations and soil. Furthermore the macroscopic soil properties such as its stiffness can introduce deep change in the structural properties, with shift of frequencies and insertion of spurious modes, with different consequences along the constructive process.

Such effects are not valuable by fixed base models, and are also soil-stiffness dependent.

Finite Element analyses in the domain of frequency, even if stationary of the wind process and linearity of structural response is at first assumed, can

285

emphasize such effects of structure-soil-TMD interaction, and be useful in the preliminary design of the control system, when the identification of the dynamics of soils interested by the intervention is not complete yet.

Particular attention must be paid in the modelling of the soil-structure-TMD system: the geometry of the contact structure-soil, the structural configuration, the soil properties and uncertainty, the finite element meshing, the PSD functions of the loads, the uncertainty on the device constants, and so the global request of effectiveness, robustness, redundancy of the control system.

The degree of sensitivity of the performance to time-fluctuations of the boundary conditions or soil uncertainties, the request of robustness, the decrease of effectiveness to be paid, and eventually effective and robust solutions for the expected scenarios of contingency can be identified.

The numerical investigations on the case study show that the in-service configuration is less flexible but affected by a larger amount of uncertainties, related to the SSI effects, and make convenient the adoption of multi-TMD control systems, intrinsically more robust. If time-fluctuations of the boundary conditions or the soil uncertainties are relevant, the demand of robustness can be high and its satisfaction is paid by a decrease of effectiveness of the control system. In this sense the final choice will realize an optimal compromise between effectiveness and robustness, whose demand should be limited as much as possible in order to pursue maximum reduction of the structural response. Such task must be pursued through data collection during the constructive stages: the non adaptivity of the passive strategies require that the final design of the control system, i.e. the definitive choice of the design parameters, is completed only at the end of the constructive stages.

Appendix A

Substructure Analysis by the Displacement Method

For large and complex structures, with a high number of elements or of scale of description, the number of d.o.f. necessary to describe the response and the structural performance can exceed the capacity of computer programs: a possible way to solve this difficulty is the *structural partitioning* and the analysis of *substructures*.

This approach is effective when a local performance depending on *Macro-level* response must be evaluated.

The structure is divided into a certain number of substructures, separated each other by arbitrary boundaries.

If we know the stiffness properties of the substructures, it is possible to treat them as complex elements, and to apply the usual displacement (force) method.

After finding the displacements (forces) on the substructure boundaries, each substructure can be analyzed, also with a better scale of description, under known systems of displacements (forces).

Let's consider a structure, with a known stiffness matrix $[K]$, subjected to an external load vector $\underline{P}$: the set of equilibrium equations, stated that any free-body motion are suppressed and $[K]$ is non singular, are

$$[K]\underline{U} = \underline{P},$$

where $\underline{U}$ is the vector of the nodal displacements.

The substructure analysis divides the structures into a set ob substructures, introducing interior boundaries; the column matrix of boundary displacements common to more than one substructure is denoted by $\underline{U}_b$, while the matrix of interior displacements of a substructure is denoted by $\underline{U}_i$.

Using this partitioning, and denoting with $\underline{P}_b$ and $\underline{P}_i$ the corresponding external forces, the equilibrium equations can be written

$$\begin{bmatrix} [K_{bb}] & [K_{bi}] \\ [K_{ib}] & [K_{ii}] \end{bmatrix} \begin{bmatrix} \underline{U}_b \\ \underline{U}_i \end{bmatrix} = \begin{bmatrix} \underline{P}_b \\ \underline{P}_i \end{bmatrix}$$

The total displacements of the structure can be seen also as the superposition of two matrices

$$\underline{U} = \underline{U}^{(\alpha)} + \underline{U}^{(\beta)},$$

where $\underline{U}^{(\alpha)}$: vector of displacements due to $\underline{P}_i$ but fixing the boundaries so that $\underline{U}_b = \underline{0}$;

$U^{(\beta)}$: vector of corrections to the vector $U^{(\alpha)}$ to get the boundary displacements $\underline{U}_b$ for $\underline{P}_i = \underline{0}$.

Consequently the vector of displacements may be expressed as follows:

$$\underline{U} = \begin{bmatrix} \underline{U}_b \\ \underline{U}_i \end{bmatrix} = \begin{bmatrix} \underline{U}_b^{(\alpha)} \\ \underline{U}_i^{(\alpha)} \end{bmatrix}_{\substack{boundaries \\ fixed}} + \begin{bmatrix} \underline{U}_b^{(\beta)} \\ \underline{U}_i^{(\beta)} \end{bmatrix}$$

where, by definition, $\underline{U}_b^{(\alpha)} = \underline{0}$.

Similarly, corresponding to $\underline{U}^{(\beta)}$ and $\underline{U}^{(\alpha)}$, the external forces can be separated into

$$\underline{P} = \underline{P}^{(\alpha)} + \underline{P}^{(\beta)}, \text{ or } \underline{P} = \begin{bmatrix} \underline{P}_b^{(\alpha)} \\ \underline{P}_i^{(\alpha)} \end{bmatrix} + \begin{bmatrix} \underline{P}_b^{(\beta)} \\ \underline{P}_i^{(\beta)} \end{bmatrix}$$

where, by definition, $\underline{P}_i^{(\alpha)} = \underline{P}_i$ and $\underline{P}_i^{(\beta)} = \underline{0}$.

In the displacement method each substructure is at first analyzed separately, assuming that the adjacent substructures are completely fixed; these boundaries are then relaxed simultaneously, and the actual boundary displacements are determined from the equations of equilibrium of forces at the boundary joints, involving a very smaller number of unknowns on respect with the complete structure without partitioning.

a. Let's consider a substructure: if its boundaries are fixed, $\underline{U}_b = \underline{0}$, from the equilibrium equations, $\underline{U}_i^{(\alpha)} = [K_{ii}]^{-1} \underline{P}_i$

and $\underline{P}_b^{(\alpha)} = [K_{bi}]\underline{U}_i^{(\alpha)} = [K_{bi}][K_{ii}]^{-1} \underline{P}_i = \underline{R}_b$: this term represents the boundary reactions necessary to keep $\underline{U}_b = \underline{0}$ while the interior forces $\underline{P}_i$ are applied.

Since the boundary displacements are set equal to zero, the substructures are isolated from each other, and the application of an interior force causes displacement in only one substructure: the interior displacements $\underline{U}_i^{(\alpha)}$ with boundaries fixed can be calculated for each substructure separately by

$$\underline{U}_i^{(\alpha)} = [K_{ii}]^{-1} \underline{P}_i$$

b. When the substructure boundaries are relaxed, the boundary displacements $\underline{U}^{(\beta)}$ can be computed also through the equilibrium equations:

$$\underline{U}_i^{(\beta)} = -[K_{ii}]^{-1}[K_{ib}]\underline{U}_b^{(\beta)}$$
$$\underline{U}_b^{(\beta)} = [K_b]^{-1} \underline{P}_b^{(\beta)}$$

where $[K_b] = [K_{bb}] - [K_{bi}][K_{ii}]^{-1}[K_{ib}]$: boundary stiffness matrix (of smaller order than $[K]$); $\underline{P}_b^{(\beta)} = \underline{P}_b - \underline{P}_b^{(\alpha)} = \underline{P}_b - \underline{R}_b = \underline{S}_b$.

The substructure analysis is composed by three main steps.

1. <u>The substructure displacements and forces with boundary fixed</u>

The stiffness of the generic substructure, considered as a free body, can be partitioned as follows:

$$[K]^{(r)} = \begin{bmatrix} [K_{bb}]^{(r)} & [K_{bi}]^{(r)} \\ [K_{ib}]^{(r)} & [K_{ii}]^{(r)} \end{bmatrix}$$

where b and i refer to boundary and interior displacements, and $[K_{bi}]^{(r)} = [K_{ib}]^{(r)}$.

The displacements of the substructure can be related to the external forces by the equation

$$[K]^{(r)}\underline{U}^{(r)} = \underline{P}^{(r)}, \text{ or } \begin{bmatrix} [K_{bb}]^{(r)} & [K_{bi}]^{(r)} \\ [K_{ib}]^{(r)} & [K_{ii}]^{(r)} \end{bmatrix}\begin{bmatrix} \underline{U}_b^{(r)} \\ \underline{U}_i^{(r)} \end{bmatrix} = \begin{bmatrix} \underline{P}_b^{(r)} \\ \underline{P}_i^{(r)} \end{bmatrix}$$

If we fix the substructure boundaries (Figure A.1) and it is sufficient to avoid any rigid motion of the substructure, the interior displacement of the substructure and the boundary reaction due to $\underline{P}_i^{(r)}$ when $\underline{U}_b^{(r)} = \underline{0}$ can be determined by

$$\left[\underline{U}_i^{(r)}\right]_{\substack{boundary \\ fixed}} = \left[K_{ii}^{(r)}\right]^{-1}\underline{P}_i^{(r)}$$

and

$$\underline{R}_b^{(r)} = \left[K_{bi}^{(r)}\right]\left[K_{ii}^{(r)}\right]^{-1}\underline{P}_i^{(r)}$$

where the matrix inversion of $\left[K_{ii}^{(r)}\right]$ can be inverted because fixing of boundaries avoids any rigid motion.

290
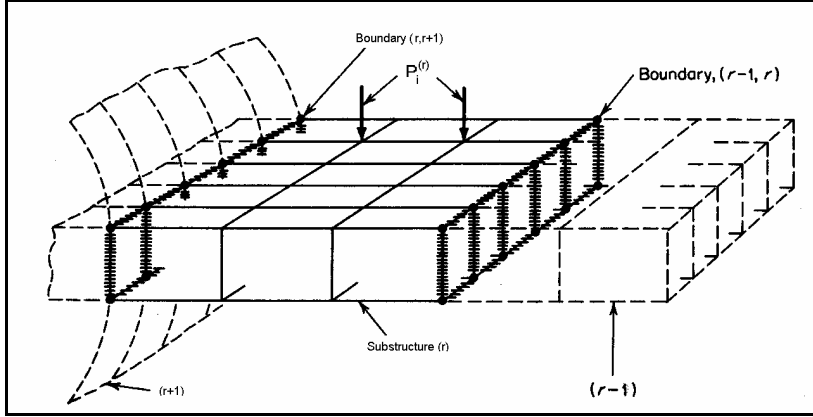
Figure A.1. Example of substructure and fixed boundaries (Przemieniecki).

The stiffness of the substructure associated to $\underline{U}_b^{(r)}$ is given by

$$\left[K_b^{(r)}\right] = \left[K_{bb}^{(r)}\right] - \left[K_{bi}^{(r)}\right]\left[K_{ii}^{(r)}\right]^{-1}\left[K_{ib}^{(r)}\right]$$

This matrix is used in the assemblage of the boundary stiffness $\left[K_b\right]$ of the complete structure.

2. The substructure relaxation: general solution for boundary displacements

Once determined the substructure stiffness $\left[K_b^{(r)}\right]$ and the reactions $\underline{R}_b^{(r)}$ due to specific interior loading, all the boundaries are simultaneously relaxed: the boundary reactions and the external forces applied on the boundaries are not in balance, so that the boundary relaxation induces displacements of boundaries such that the equilibrium at each joint of the boundary is satisfied.

It is possible to calculate the boundary displacement considering the structure as the assemblage of all the substructures, subjected to external loading

$$\underline{S}_b = -\sum_r \underline{R}_b^{(r)} + \underline{P}_b$$

where $\underline{P}_b$ is the loading matrix for external forces applied on the boundaries.

291

In Figure A.2 there is a typical joint on the common boundary between two substructures.
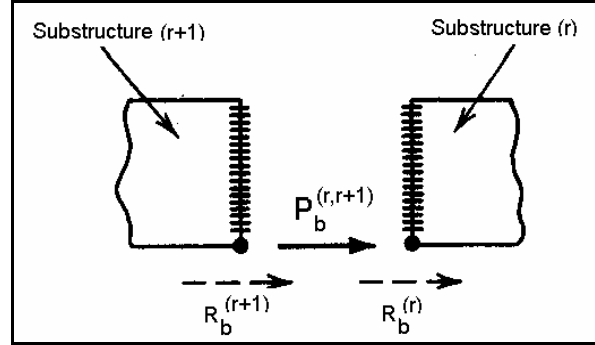
Figure A.2. Joint loads before boundary relaxation.

The equations of equilibrium in terms of boundary displacements for the complete structure are $[K_b]\underline{U}_b = \underline{S}_b$.

where $[K_b]$ is obtained by putting the submatrices $\left[K_b^{(r)}\right]$ in their correct position in the boundary stiffness matrix for the complete structure, and summing the overlapping terms.

By restraining an adequate number of d.o.f. all the rigid motions are suppressed and the matrix $[K_b]$ is nonsingular and the displacements $\underline{U}_b$ can be determined by

$$\underline{U}_b = [K_b]^{-1}\underline{S}_b$$

The relative positions of the submatrices $\left[K_b^{(r)}\right]$ into the matrix $[K_b]$ depend on the progressive numeration of the boundaries; the coupling matrices between two substructures will be nonzero if they have common boundaries, while the unconnected substructures will have coupling matrices equal to zero. It is advantageous to number the substructures in way that the component of $[K_b]$ will fill a band around the principal diagonal, to reduce the computing time.

A possible substructure arrangement is that shown in the Figure A.3: the arrangement leads to a quintuple band matrix for $[K_b]$.

$$[K_b] = \begin{bmatrix} [1,1] & [1,2] & [0] & [0] & [0] & [0] \\ [2,1] & [2,2] & [2,3] & [2,4] & [0] & [0] \\ [0] & [3,2] & [3,3] & [3,4] & [0] & [0] \\ [0] & [4,2] & [4,3] & [4,4] & [4,5] & [4,6] \\ [0] & [0] & [0] & [5,4] & [5,5] & [5,6] \\ [0] & [0] & [0] & [6,4] & [6,5] & [6,6] \end{bmatrix}$$

where the row and column numbers denote the substructure boundary numbers.
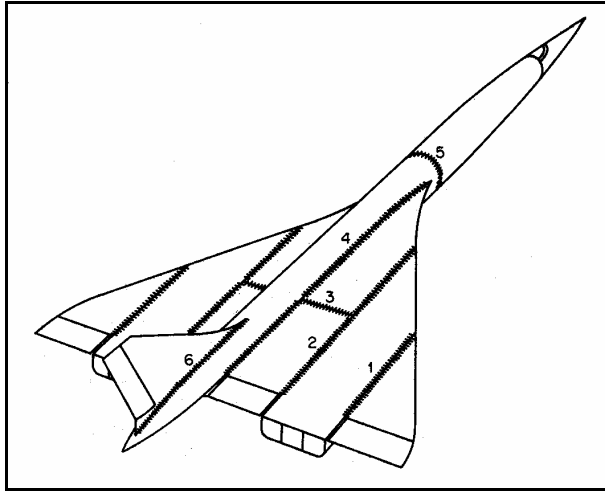
Figure A.3. Example of substructural arrangement (Przemieniecki).

3. <u>The substructure displacements and forces: boundaries relaxed</u>

Once determined the boundary displacements on each substructure $\underline{U}_b^{(1)}, \underline{U}_b^{(2)}, \underline{U}_b^{(3)}...$, it is possible to analyze the substuctures separately under the external loading $\underline{P}_i^{(r)}$ together with known boundary displacements $\underline{U}_b^{(r)}$.

293

From $\begin{bmatrix} [K_{bb}]^{(r)} & [K_{bi}]^{(r)} \\ [K_{ib}]^{(r)} & [K_{ii}]^{(r)} \end{bmatrix} \begin{bmatrix} \underline{U}_b^{(r)} \\ \underline{U}_i^{(r)} \end{bmatrix} = \begin{bmatrix} \underline{P}_b^{(r)} \\ \underline{P}_i^{(r)} \end{bmatrix}$ it follows that the interior

displacements $\underline{U}_i^{(r)}$ of the substructure due to the force $\underline{P}_i^{(r)}$ and boundary

displacements $\underline{U}_b^{(r)}$ are given by

$$\underline{U}_i^{(r)} = \left[K_{ii}^{(r)} \right]^{-1} \underline{P}_i^{(r)} - \left[K_{ii}^{(r)} \right]^{-1} \left[K_{ib}^{(r)} \right] \underline{U}_b^{(r)}$$

Consequently

$$\begin{bmatrix} \underline{U}_b^{(r)} \\ \underline{U}_i^{(r)} \end{bmatrix}_{\substack{biundary \\ relaxed}} = \begin{bmatrix} \underline{0} \\ \underline{U}_i^{(r)} \end{bmatrix}_{\substack{boundary \\ fixed}} + \begin{bmatrix} [I] \\ -\left[K_{ii}^{(r)} \right]^{-1} \left[K_{ib}^{(r)} \right] \end{bmatrix} \underline{U}_b^{(r)}$$

or $\qquad \left[\underline{U}^{(r)} \right]_{\substack{boundary \\ relaxed}} = \left[\underline{U}^{(r)} \right]_{\substack{boundary \\ fixed}} + \begin{bmatrix} \text{displacements due to} \\ \text{boundary relaxation} \end{bmatrix}$

Figure A.4 represents the framework of the substructure analysis by the displacements method: the procedure of assemblage of the individual substructures to form the boundary stiffness, the boundary force matrices for the complete structure, the calculation of the substructure boundary displacements used to determine displacements and forces in each substructure independently.
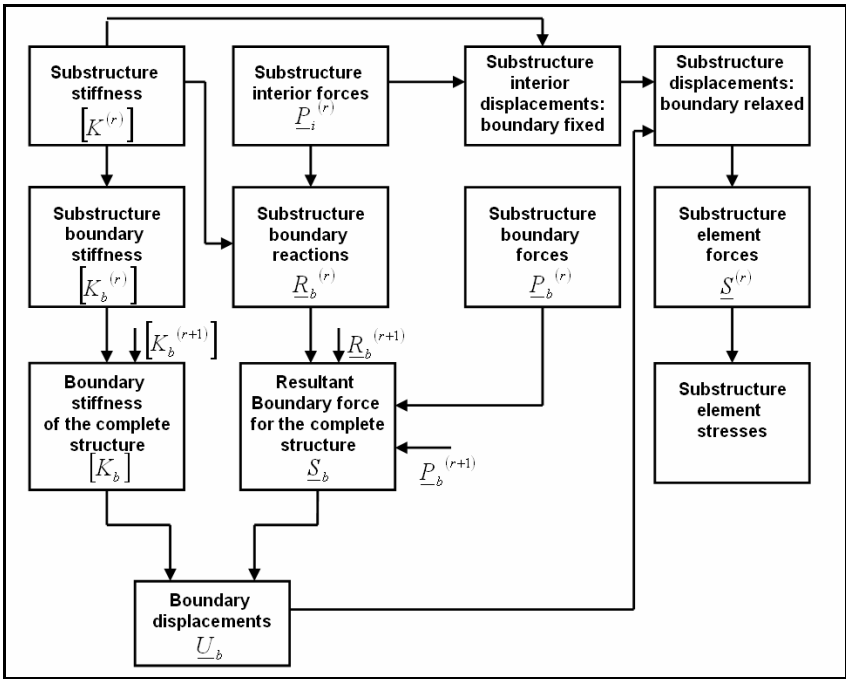
Figure A.4. Substructure analyses by the displacement method.

Appendix B

B.1 General Description of the Case-Study Structure

The link between Sicily and Calabria (Figure B.1), in the Southern Italy, is one of the most innovative challenge of Civil Engineering in Italy.

The structural solution studied to realize it consists in a cable suspension bridge and two pylons located one in Sicily and one in Calabria.

The Messina Strait Bridge, as described in the web site at www.strettodimessina.it, has a main span of *3300m*, while the total length of the deck, *60m* wide, is *3666m*, including the side spans. The global geometry established for the work is reported in Figure B.2.

This bridge has been assumed as case-study structure for the investigations of the present work.

The two pylons are *383m* high and the deck, in the middle section of the bridge, is enough high to provide vertical clearance for the navigation channel – over a length of *600m*. The bridge suspension system relies on two pairs of steel cables with a total length, between the anchor blocks, of about *5300m*, sustaining the deck by a system of hangers, of different sections, with constant step of *30m*.

The deck is composed by three box sections, the external ones for roadways and the central for railways. The roadway deck has three lanes for each carriageway, each *3.75m* wide; the railway box has two tracks (Figure B.3).
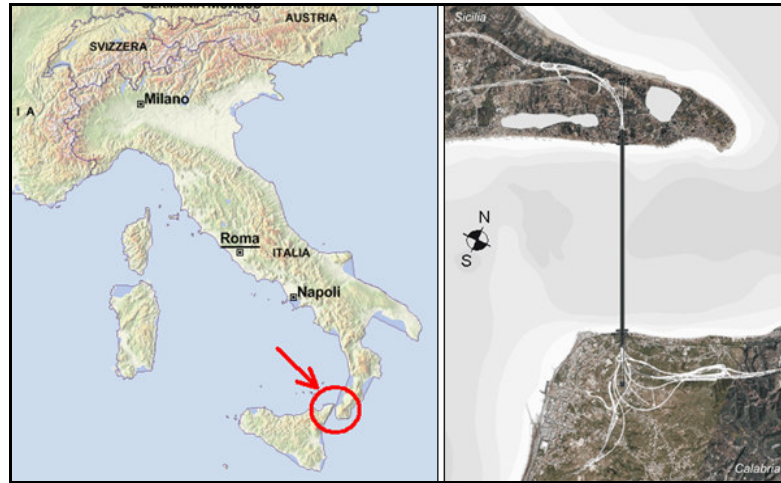
Figure B.1. Geographic location of the Messina Strait Bridge.
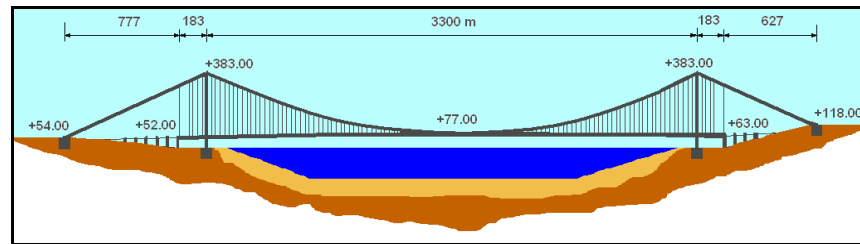
Figure B.2. Global geometry of the Messina Strait Bridge.
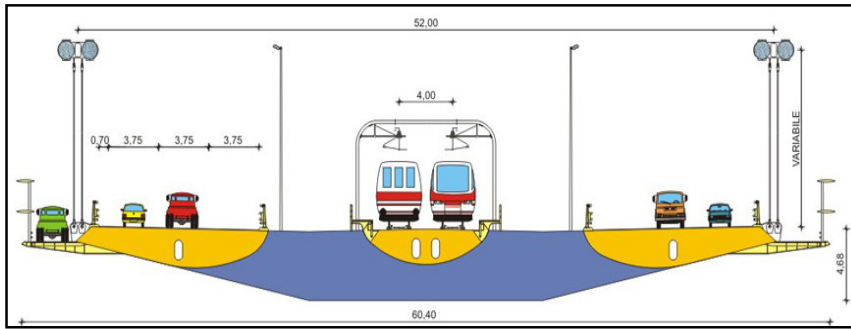
Figure B.3. **Composition of the deck of the Messina Strait Bridge.**

B.2 The Design Environment

The design environment of the pylon consists of the complex of boundaries or actions stressing the structure, with also possible interaction effects changing its response.

It is expressed by the wind actions, the geomechanical properties of the surrounding soil and their consequences on the structural dynamics, the seismic environment, the traffic actions on the bridge. In this section the geologic and the characterization of the wind actions are summarized.

B.2.1 Geology

In Figure B.4 the geologic formations of the reference site are reported: concerning the Sicilian side, the soil on which the pylons will be built consists of olocenic sediment of the coast (about 65 m deep), on a base of pleistocenic gravel (Gravel of Messina, about 200 m deep).

Geognostic investigations have been done: the profile of the N_{SPT} test and the granulometry for the Sicilian side used for modelling are briefly reported (Figure B.5).

These available data have been the basis of the assumptions on the soil properties for the analyses. No data are available on the nonlinear properties of the soil nor on the frequency dependance of the geomechanical parameters.

299
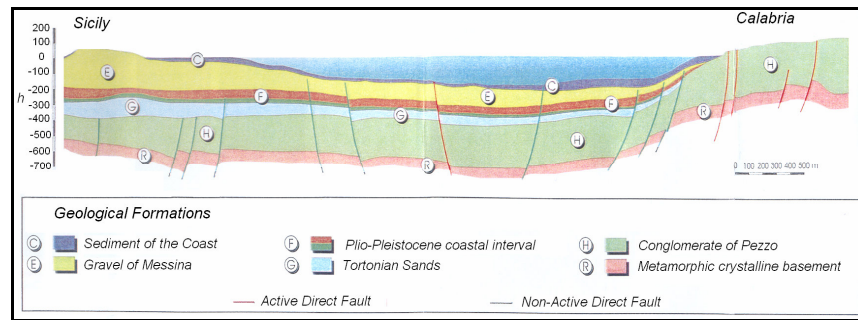
Figure B.4. Geological section of the Strait of Messina.
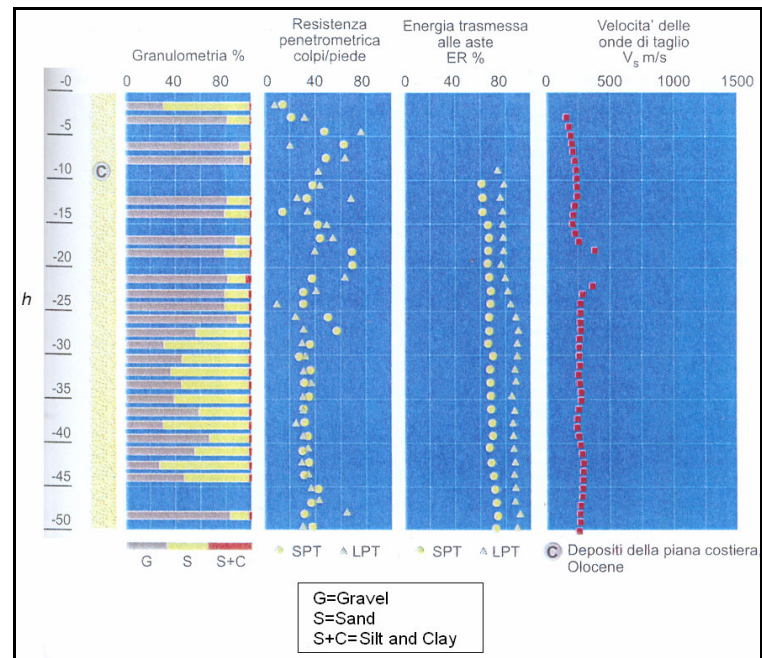
Figure B.5. N$_{SPT}$ test and composition of the superficial formations.

B.2.2 Wind loads

The wind actions, the most significant for slender structures as long suspension bridges and towers, are here modelled in terms of wind speed spectra acting along the exposed surfaces, or in terms of time-histories of wind speed field. The wind speeds (or the PSD functions) are then transformed in corresponding forces (or their PSD functions) on the structure, by applying the aerodynamic coefficients obtained in the wind tunnel tests, and, where significant, adopting aeroelastic formulations of the forcing system, keeping into account possible *self-excited* resonant phenomena.

Wind speed spectra

The description of wind loads acting on the pylon comes from field observations and statistical treatment in the reference site.

The results of the observations consists of power density spectra (PSD) of the wind speed, at different nodes of the finite element structural model of the structure.

The wind speed auto-spectrum of the turbulence components is that of Solari-Piccardo:

$$S_{v_j v_j}\left(\underline{x};n\right) = \sigma_{v_j}^2\left(\underline{x}\right)\lambda_j \frac{L_{v_j}\left(\underline{x}\right)}{\left\|U\left(\underline{x}\right)\right\|}\left(1+1.5\lambda_j n \frac{L_{v_j}\left(\underline{x}\right)}{\left\|U\left(\underline{x}\right)\right\|}\right)^{-\frac{5}{3}} \qquad j=1,2,3$$

where $\lambda_1 = 6.868$, $\lambda_1 = 9.434$, $\lambda_1 = 6.103$;

L_{v_j} : integral scale of the gust component $v_j\left(\underline{x},t\right)$;

$$L_j = 300\beta_j\left(\frac{z}{200}\right)^{0.67+0.05\ln z_0}; \ \beta_1 = 1.00, \ \beta_2 = 0.25, \ \beta_1 = 0.10;$$

$$\sigma_{v_j}^2 = \left[6-1.1\arctan\left(\ln z_0 +1.75\right)\right]u_*^2\alpha_j; \ \alpha_1 = 1.00, \ \alpha_2 = 0.75, \ \alpha_3 = 0.25.$$

The generic cross-spectrum terms are obtained by

$$S_{v_i v_j}\left(\underline{x};\underline{x}';\omega\right) = \sqrt{S_{v_i v_i}\left(\underline{x};\omega\right)S_{v_j v_j}\left(\underline{x}';\omega\right)} \cdot Coh_{v_i v_j}\left(\underline{x};\underline{x}';\omega\right) \qquad i,j=1,2,3$$

where the two-point coherence of the turbulence component decrease with separation distance and frequency according to the following equation:

301

$$Coh_{v_i^{(h)}v_j^{(k)}}(\omega) = \exp\left[-\frac{\dfrac{\omega}{2\pi}\left\|\left(C_j^{(h)}+C_j^{(k)}\right)\left(\underline{x}^{(h)}-\underline{x}^{(k)}\right)\right\|}{\left\|U^{(h)}\right\|+\left\|U^{(k)}\right\|}\right]; \quad j=1,2,3; \ k=1,2...n$$

where

$$C_j^{(k)} = \sum_{s=1}^{3} C_{js}\,\underline{f}_s^{(k)} \otimes \underline{f}_s^{(k)} \quad j=1,2,3; \ k=1,2...n \ ; \ [C] = \begin{bmatrix} 3.0 & 3.0 & 0.5 \\ 10.0 & 6.5 & 6.5 \\ 10.0 & 6.5 & 3.0 \end{bmatrix};$$

$$\underline{f}_1^{(k)} = \frac{\underline{U}^{(k)} - U_3^{(k)}\underline{e}_3}{\sqrt{\left\|\underline{U}^{(k)}\right\|^2 - U_3^{(k)2}}}, \ \underline{f}_2^{(k)} = \underline{e}_3 \times \underline{f}_1^{(k)}, \ \underline{f}_1^{(k)} = \underline{e}_3;$$

$\underline{U}^{(k)}$: mean wind speed in the *k*-th point.

B.3   The Pylons of the Bridge and the Foundations

The main characteristics of the pylon of the case-study bridge and its dynamic properties are summarized, with regard to the Sicilian side as regards the soil and foundation modelling.

The pylons consist of a frame structure in the transversal plan of the bridge. Each pylon, 380m high, has two legs and four transverses. The legs have an inclination so that the distance between the legs varies from 52 m on the top to 78 m on the base. On the top of the pylons there are the saddles that bear the main cables of the bridge.

During the service life each leg, connected to the main suspension system, is subjected to a normal stress of 0.95E+06 kN.

The geometry of the legs, transverses, saddles are represented in Figures B.6, B.7, B.8, B.9. (from www.strettodimessina.it)

The Preliminary Design of the bridge contains a proposal for the Foundations, on the basis of the geognostic investigations done (Figure B.10).

The foundations consist of a rigid block on a shaft, with two jet-grouting groups: the first with higher density of the concrete, composed by two cylinder under the legs of the pylon, and the second, external, with lower density and mechanical properties; the groups are separated by diaphragms. The depth of the foundation is of 50 m.

The foundation is sustained by the deepest layer of the sediment, since the gravel formation is at lower depth; the base rock is at a depth of about 600 m.
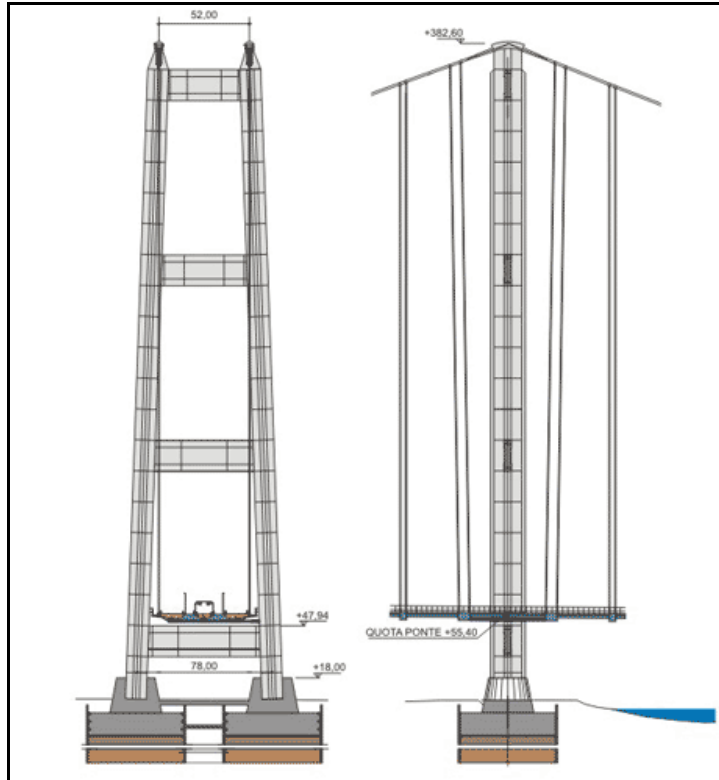
Figure B.6. Frontal views of the Pylon.
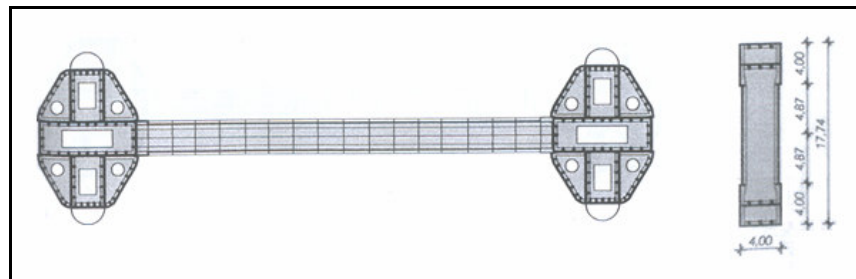
Figure B.7. Pylon and transverse sections.
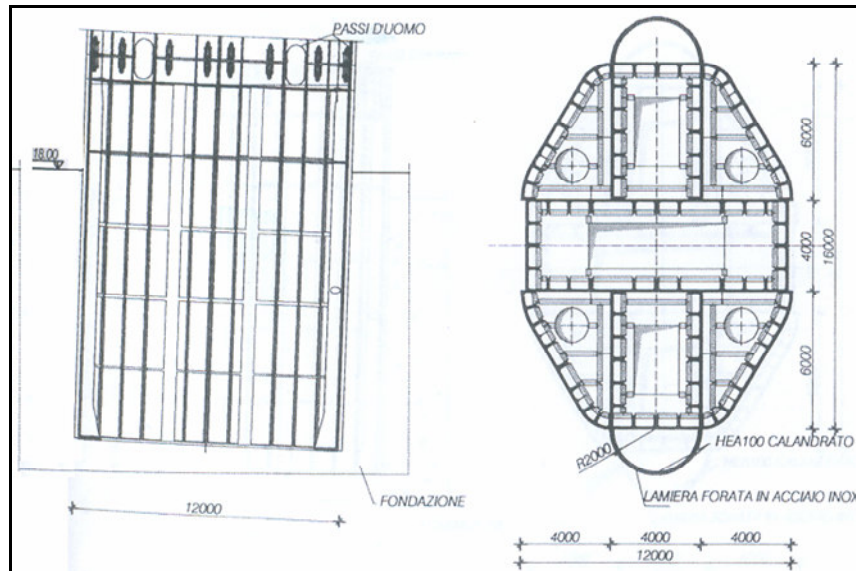
Figure B.8. Section of foundation and first foundation block.
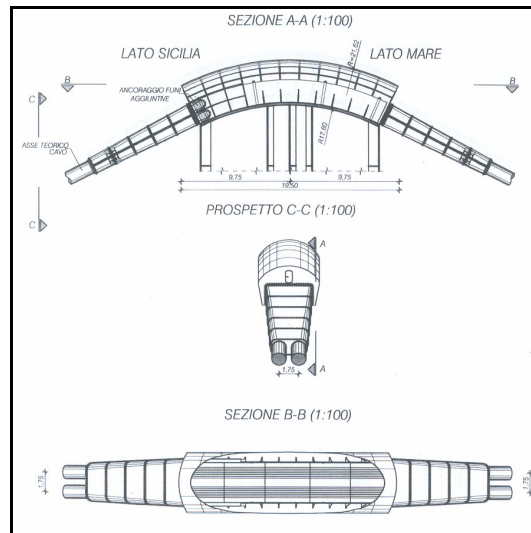
Figure B.9. Saddle of the Pylon.
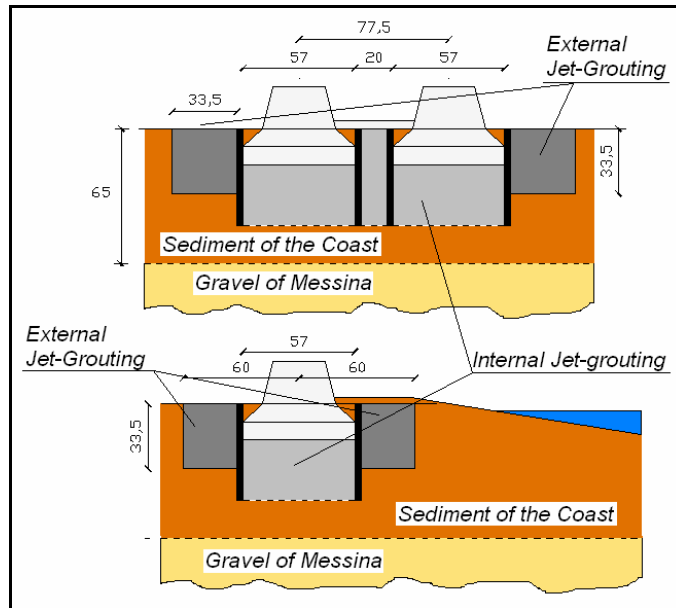
Figure B.10. Geometry of the foundation of the pylon (Sicilian side).

B.4   Aerodynamic and Aeroelastic Properties of the Pylon

In the past years several wind tunnel test have been conducted by the Polytechnic of Milan and the Danish Maritime Institute in order to evaluate the aerodynamic and aeroelastic properties of the case-study bridge and of its sub-structures, with different configurations and at different Reynolds numbers. Most of the results are available in the scientific literature already published.

Tests have been done with sectional and full models of the bridge, with laminar and turbulent flows.

The main purposes of the tests involving the pylon substructure were:

- the evaluation of the static aerodynamic coefficients of the section for different angles of attack (static polar diagrams) and the derivative diagrams;
- the accelerations induced by vortex-shedding excitation;
- the evaluation of the buffeting response to turbulent wind.

The similitude between the real structure and the models is resumed by the Reynolds number (*Re*), the Strouhal number (*St*) and the Scruton number (*Sc*), while the effect of Froude (*Fr*) number has been neglected.

Correct Scruton number was obtained through a calibration of mass and damping of the model, Strouhal number by a well-defined reproduction of geometry and details, but Reynolds number was not reproduced because of the size effects. The test were conducted using $Re \square 10^4$-10^5, while the Reynolds numbers that the pylon will experience are of the order of $Re \square 10^8$, that is a value in the ipercritic zone of the diagram C_L-Re for cylinders: the experiments overestimate the lift forces and also the vortex oscillations induced, since the turbulence of the flow reduce their amplitude.

The tests conducted on sectional models mounted on springs, to get a two degree-of-freedom motion, reproduced the across-wind and torsion response.

Other tests were conducted on 3D-models, to reproduce the behaviour of the pylons for conditions closer to those of the full-scale structure, with 3D effects of the flow around the top and between the legs, with sensors to record the

306

structural response. The model was built in such a way to reproduce the first modes of the pylon at proper frequencies.

Similar tests have been conducted simulating the service configuration, when the top of the pylon is restrained.

Aerodynamic coefficients

The tunnel tests conducted on sectional models led to the identification of the aerodynamic coefficients of the sections assumed. They are represented in the diagrams of Figure B.11 together with their derivatives with angle of wind incidence. Concerning the aerodynamic properties of the section of the pylon, the drag component along wind was considered, using the aerodynamic coefficients reported in Table B.I.
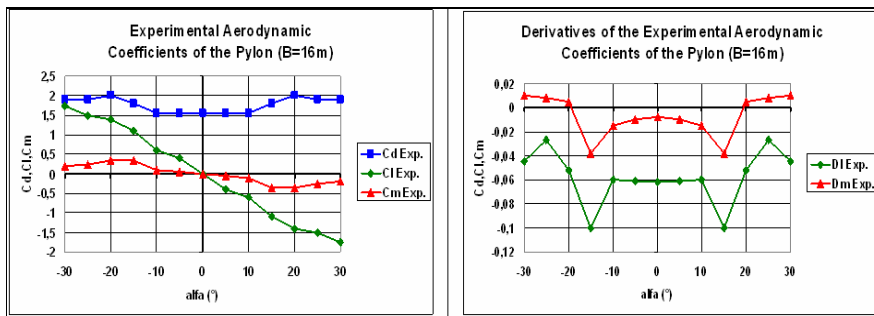
Figure B.11. Experimental aerodynamic coefficients and derivatives of the pylon section.

Pylon	c_D	B
Wind x (out-of-plane)	1.00	12.00
Wind y (in-plane)	1.40 (leeward leg) 0.60 (windward leg)	16.00
Transverse		
Wind x	1.00	16.90

Table B.I. Experimental aerodynamic coefficients of legs and transverses.

307

Response to laminar and turbulent wind and Vortex shedding excitation

The wind tunnel tests showed that concerning wind actions, vortex-shedding governs the response, at least at low wind speeds and especially in the *free-standing* configuration.

For the particular geometry of the pylon of a suspension bridge, the results of the Vickery's model can be not adequately reliable, especially for the strong interaction and disturb in the flow from the downwind leg to the second: the vortex shedding from the first leg gives harmonic load to the second leg, and the wind speed on the surface of the second leg is also reduced.

The prediction of the response to vortex shedding should be determined by semi-empirical MDOF models keeping into account the geometry of the problem, the harmonic forces induced in the second leg by the vortex-shedding from the first, the reduction of the wake on the second, the motion dependent forces induced.

For wind acting in the longitudinal direction of the bridge no interaction between the legs occurs. In any case the most reliable data for design are those from the experimental tests in the wind tunnel.
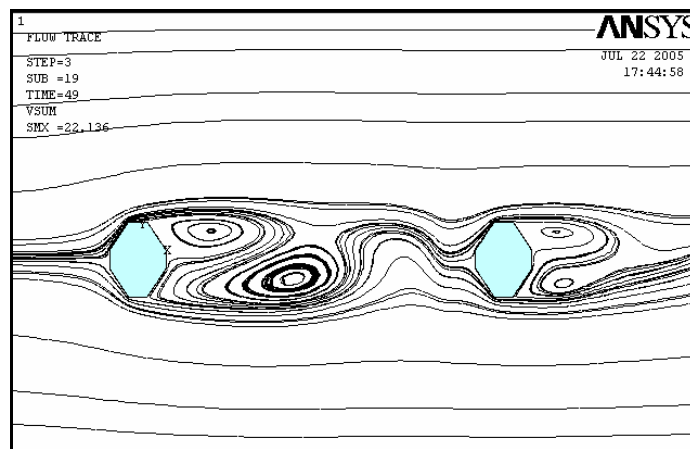
Figure B.12. Vortex shedding and interaction between the legs of the pylon: disturbed flow (Giuliano).

308

The vortex-induced vibrations are governed mainly by the Strouhal number, depending on the shape and related to the frequency of the fluctuations of the forces at different wind speeds, and by the Scruton number depending on the structural damping and affecting the adsorption of energy by the structure and consequently the maximum amplitudes of the oscillations.

The wind tunnel tests demonstrated that the aerodynamic behaviour of the pylon is dominated by vortex induced oscillations, observed for angle of wind incidence from 0° to 20° in smooth and turbulent flow. The tests gave also the values of Strouhal number, calculated by the maximum of the PSD of the lift force, between 0.1 and 0.15 for flexible models, and 0.17 for fix models, for which the forces measured depend only on the vortex shedding and not on the flow-structure synchronous motion.

If one assumes the pylon as a cylinder, since the minimum natural frequency calculated for the free standing pylons is of 0.1 Hz, it can be asserted that the *lock-in* affects the structure in the across-wind direction for a wind speed of about 13 m/s at the top, quite usual for the reference site, while for higher speeds the response decreases, out of the *lock-in* range.

In the service configuration, the Pylon, with greater stiffness and main frequency of 0.3 Hz, has the first *lock-in* at wind speed of about 40 m/s.

Furthermore, the light weight, the low structural damping and the high slenderness make the construction phase more critical: the most hazardous configuration is the *free-standing* one, with wind normal to the bridge axis, and critical velocity of about 10 m/s.

The geometry of the Pylon makes it more similar to a system of cylinders in tandem rather than only one: the consequence is that the structure has two Strouhal numbers, and two peaks in the diagram response vs wind speed, corresponding the first to the shedding from the first leg and the second to that from the second, excited by the disturbed wake of the first leg, and so at higher levels of wind speed. (at this regard, see also the reduction of drag coefficients between the legs).

Different wind speed generate vortex induced vibrations and *lock-in* for different angles of attack.

Through the record of time-histories of the vortex induced vibrations, the tests evaluated also the amount of energy adsorbed by the pylon at *lock-in*, when the structure starting from a small vibratory state grows in its movement until a certain limit proper of the phenomenon. The record of this transitory stage (*build-up*) let evaluate the amount of energy introduced in terms of the negative non-dimensional damping ratio *h*, or of the Scruton number: the greater is the amount of energy adsorbed, the greater are the induced vibrations.

The tunnel tests let also evaluate the necessary damping of the system to suppress the vortex shedding excitation (1st mode): the value estimated is at least of 1.7% on respect the critical for the weak axis response: so if the structural damping of the pylon is more than 2% no *lock-in* vortex-shedding oscillations are expected. This value of damping is assumed in the next sections as target of the design process against vortex induced vibrations.

By growing the wind speed from zero, two range of wind speed with negative damping h have been checked: in these ranges energy is adsorbed by the system and the oscillations increase their amplitude. At the first range of speeds, between 10 m/s and 20 m/s, h is negative, with a minimum of -1.7%, giving energy to the first flexural mode; the torsion mode is excited in a range of wind speed between 50 m/s and 70 m/s (Figure B.13).
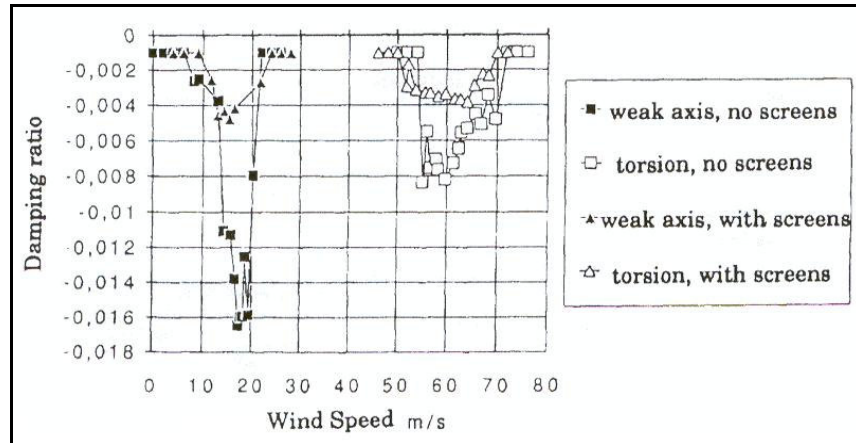
Figure B.13. Energy introduction (negative damping ratio) vs wind speed.

In Table B.II are summarized some results of the aeroelastic tests, used for the design of the control system for the mitigation of the wind response.

Strouhal numbers	Excitation for the shedding from the first leg	0.14
	Excitation for the shedding from the second leg	0.08
Aerodynamic maximum negative damping ratio = -1.7%		
Free-standing configuration		
Structural eigenfrequencies		
1st flexural	0.09 Hz	
Torsional	0.24 Hz	
Critical wind speeds		
Shedding from the first leg (1st mode excited)	10 m/s	
Shedding from the second leg (1st mode excited)	18 m/s	
Torsional excitation	50-70 m/s	
Service configuration		
Structural eigenfrequencies		
1st flexural	0.39	
Torsional	0.47	
Critical wind speeds		
Shedding from the first leg (1st mode excited)	45 m/s	
Shedding from the second leg (1st mode excited)	78 m/s	

Table B.II. Experimental results of wind tunnel tests.

Appendix C

Seismic Records for the Reference Site of the Bridge

Side S (Pylon and Anchorages)

313
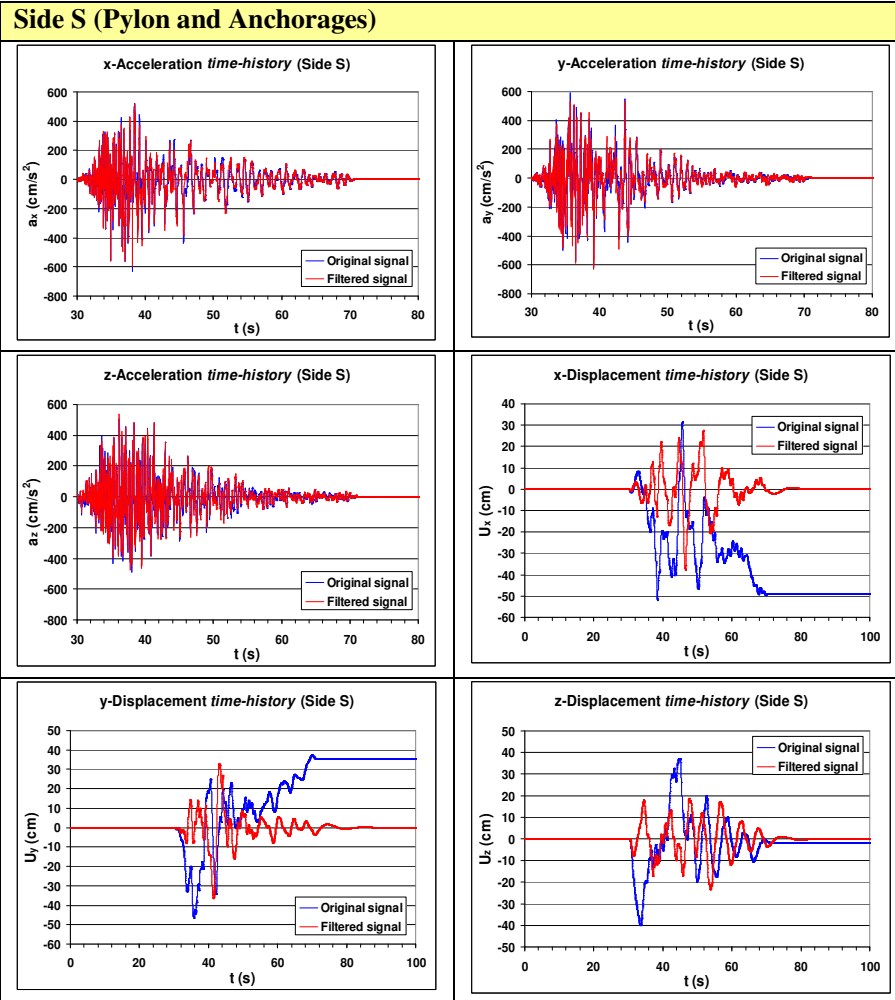
Table B.I. Seismic record – side S.
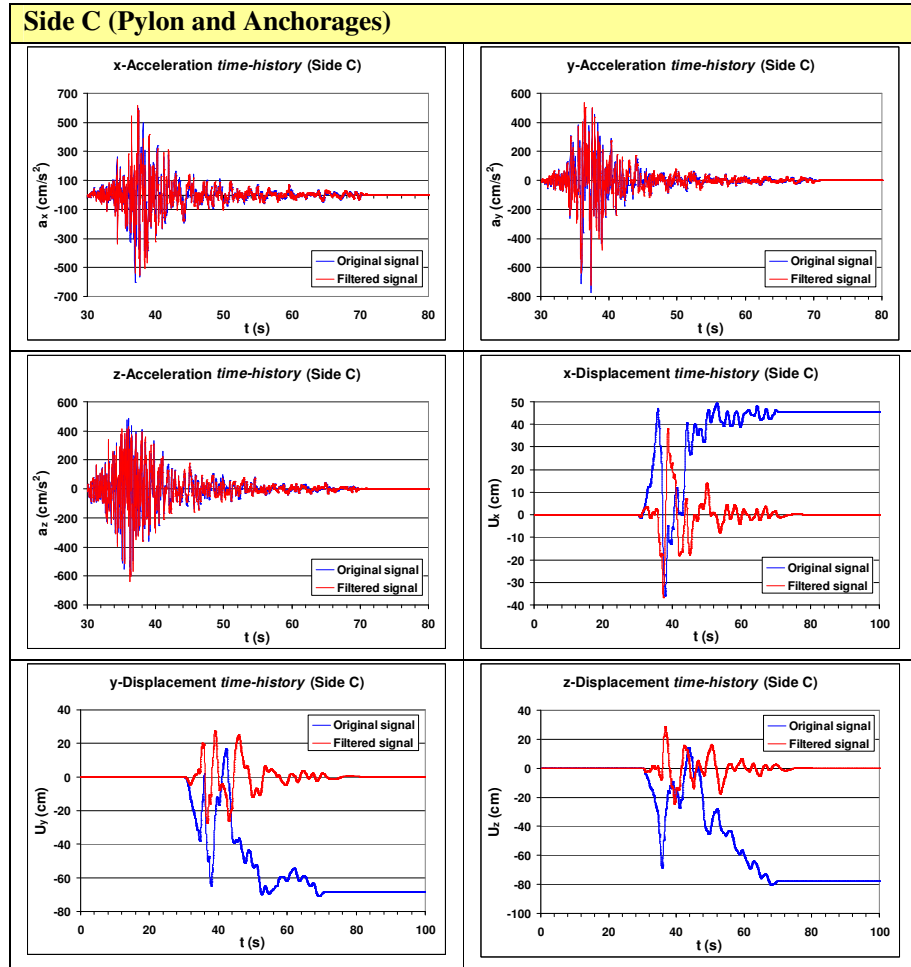
Table B.II. Seismic record – side C.
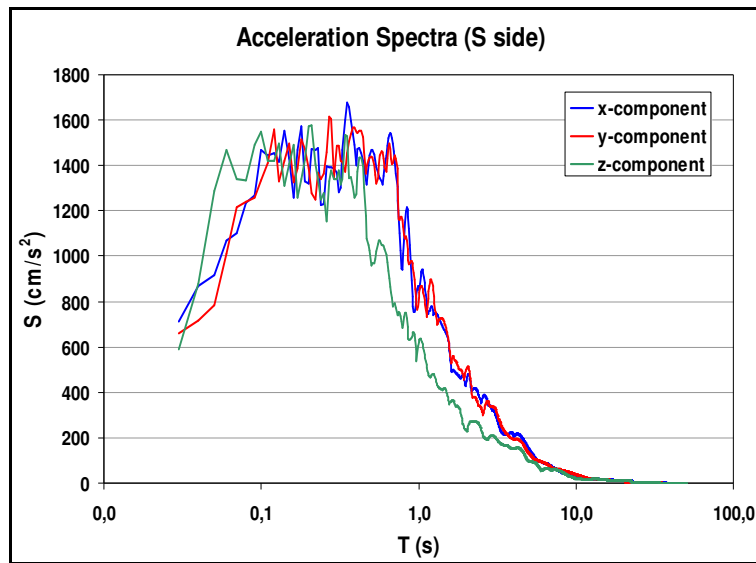
Figure. B.1. Spectra of x/y/z-acceleration of the record – side S.
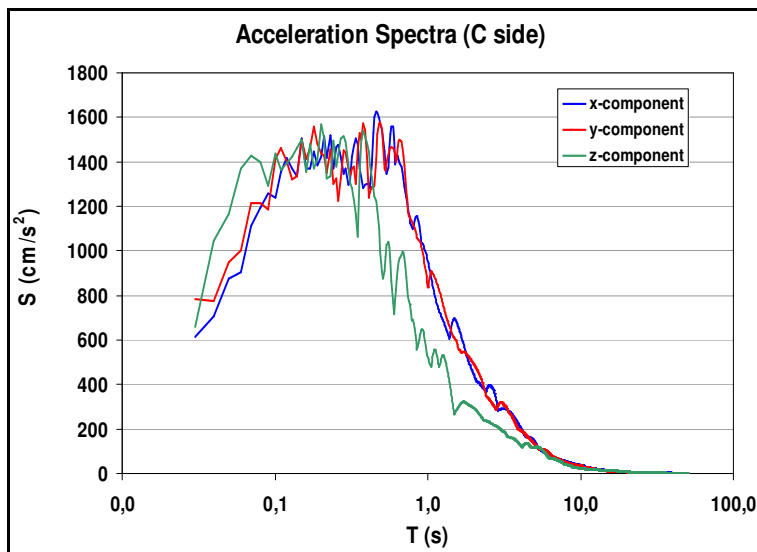
Figure. B.2. Spectra of x/y/z-acceleration of the record – side C.

315

Appendix D

D.1 Structural Response under Random Excitation

The purpose of Random Dynamics is to determine the random characteristics of the response of mechanical systems, if the characteristics of the random excitation process are known.

The response of a SDOF system subjected to a random excitation is a random process which have statistical properties such as moments, cumulants, probability density function, etc. The evaluation of these parameters can be conducted both in the domain of time and frequency, like in the deterministic field.

The Gaussian processes have a prominent role in Random Dynamics because they are characterized by simple mathematical relations:

- the probability density function depends only on the first and second order moments;
- the marginal and conditioned densities are also gaussian;
- the linear combination of gaussian processes is gaussian, so that if a the excitation is gaussian and the system (i.e. SDOF) is linear, the response is also a gaussian process.

Consequently the definition of the probability densities of the excitation and of the response requires only the evaluation of the multiple-time average or the correlations until the second order.

Such computational advantages are also supported by the Central Limit Theorem, that states that the distribution of experimental data can be well represented by the gaussian distribution.

So in what follows the fundamentals for the evaluation of the mean, of the covariance, of the correlation functions and of the moments, that characterize the gaussian probability function of a SDOF will be exposed.

Stationary Random Response of SDOF Systems

Let's hypothesise a stationary gaussian excitation for a SDOF System: as already defined, such a process $X(t)$ in the domain of time has a mean value μ_X independent on time, and an autocorrelation function $R_{XX}(\tau)$ that depends only on the interval τ between the times in which the process is studied:

$$E[X(t)] = \mu_X(t) = \mu_X$$
$$R_{XX}(\tau) = R_X(\tau) = E[X(t)X(t+\tau)] - \mu_X^2$$

Furthermore the autocorrelation function of a stationary random process is continuous, symmetric on respect of $\tau = 0$, where its value is equal to the variance σ_X^2 of $X(t)$:

$$E[X(t)X(t+\tau)] = E[X(t+\tau)X(t)] \Rightarrow R_{XX}(\tau) = R_{XX}(-\tau)$$
$$R_{XX}(0) = E[X^2(t)] - \mu_X^2 = \sigma_X^2$$

The mean and the variance do not depend on time.

In Random Dynamics the random response of a SDOF system is a bi-variate process identified by the displacement and velocity random processes.

The velocity random process $\dot{X}(t)$, derivate from the displacement process $X(t)$, in the stationary case has zero mean: $\mu_{\dot{X}} = 0$.

Furthermore the following relations are valid for the evaluation of the direct and cross correlation functions for the components of the bi-variate process $[X(t)\dot{X}(t)]$:

$$\frac{d}{d\tau}R_{XX}(\tau) = R_{X\dot{X}}(\tau) = -R_{\dot{X}X}(\tau)$$

$$\frac{d^2}{d\tau^2}R_{XX}(\tau) = R_{X\ddot{X}}(\tau) = -R_{\dot{X}\dot{X}}(\tau)$$

For stationary gaussian random processes, the spectral density power function (PSD) has in the domain of frequency an analogous role of that of autocorrelation function in the domain of time: in the domain of time the mean and the autocorrelation function characterized completely the process; in the domain of frequency the process is characterized by its mean and the PSD function, defined as the Fourier Transform of the autocorrelation function:

$$S_{XX}(\omega) = S_X(\omega) = \frac{1}{2\pi}\int_{-\infty}^{+\infty} R_{XX}(\tau)e^{-i\omega\tau}d\tau \quad (1^{st} \text{ Relation of Wiener-Khinchine)}$$

where $S_{XX}(\omega)$ is a real positive function, also symmetric on respect of $\omega = 0$.

The inverse Transform $R_{XX}(\tau) = \int_{-\infty}^{+\infty} S_{XX}(\omega)e^{i\omega\tau}d\omega$ (2nd Relation of Wiener-Khinchine)

leads to state that the variance is the area under the PSD function:

$$\sigma_X^2 = R_{XX}(0) = \int_{-\infty}^{+\infty} S_{XX}(\omega)d\omega.$$

The previous relations are useful to compute the cross-PSD $S_{X\dot{X}}(\omega)$ between $X(t)$ and $\dot{X}(t)$, and the PSD $S_{\dot{X}\dot{X}}(\omega)$ of the derived random process $\dot{X}(t)$:

$$\frac{d}{d\tau}R_{XX}(\tau) = R_{X\dot{X}}(\tau) = i\int_{-\infty}^{+\infty}\omega S_{XX}(\omega)e^{i\omega\tau}d\omega$$

$$\frac{d^2}{d\tau^2}R_{XX}(\tau) = -R_{\dot{X}\dot{X}}(\tau) = -\int_{-\infty}^{+\infty}\omega^2 S_{XX}(\omega)e^{i\omega\tau}d\omega$$

Using the relations of Wiener-Khinchine we obtain

$$S_{X\dot{X}}(\omega) = i\omega S_{XX}(\omega)$$

$$S_{\dot{X}\dot{X}}(\omega) = \omega^2 S_{XX}(\omega)$$

Since the time derivatives of the mean value μ_X are zero, we can write

$$R_{X\dot{X}}(0) = \sigma_{X\dot{X}} = E\left[X(t)\dot{X}(t)\right] = \int_{-\infty}^{+\infty}i\omega S_{XX}(\omega)d\omega = 0$$

because $S_{XX}(\omega)$ is symmetric on respect of $\omega = 0$, and the processes $X(t)$ and $\dot{X}(t)$ have correlation coefficient equal to zero; furthermore

$R_{\dot{X}\dot{X}}(0) = \sigma_{\dot{X}\dot{X}} = \sigma_{\dot{X}}^2 = E\left[\dot{X}^2(t)\right] = \int_{-\infty}^{+\infty}\omega^2 S_{XX}(\omega)d\omega$ is a positive quantity.

Other significant quantities in Random Dynamics are the spectral moments $\lambda_{i,X}$ by which it is possible to evaluate the probability distribution of the maximum of the response (peak):

$$\lambda_{i,X} = \int_{0}^{+\infty}\omega^i G_{XX}(\omega)d\omega \quad i = 0,1,...$$

where $G_{XX}(\omega)$ is the unilateral spectral power density:

$$G_{XX}(\omega) = \begin{cases} 2S_{XX}(\omega) & 0 \le \omega \le +\infty \\ 0 & \omega < 0 \end{cases}$$

Besides the following relations are valid between the first spectral moments and the statistic moments of the bi-variate process $\left[X(t)\dot{X}(t)\right]$:

$$\lambda_{0,X} = \int_{0}^{+\infty} G_{XX}(\omega)d\omega = \int_{-\infty}^{+\infty} S_{XX}(\omega)d\omega = \sigma_X^2 = E\left[X^2(t)\right] - \mu_X^2$$

$$\lambda_{1,X} = \int_{0}^{+\infty} \omega G_{XX}(\omega)d\omega \neq \int_{-\infty}^{+\infty} \omega S_{XX}(\omega)d\omega = 0$$

$$\lambda_{2,X} = \int_{0}^{+\infty} \omega^2 G_{XX}(\omega)d\omega = \int_{-\infty}^{+\infty} \omega^2 S_{XX}(\omega)d\omega = \sigma_{\dot{X}}^2 = E\left[\dot{X}^2(t)\right]$$

The first spectral moment $\lambda_{0,X}$ is the variance of the random process $X(t)$, while the third $\lambda_{2,X}$ is that of $\dot{X}(t)$; the second moment $\lambda_{1,X}$ is not coincident with the covariance between $X(t)$ and $\dot{X}(t)$ which is zero.

Concerning the physical dimensions of the quantities introduced, the correlation functions $R_{XX}(\tau)$, $R_{X\dot{X}}(\tau)$, $R_{\dot{X}\dot{X}}(\tau)$ have respectively the dimension of $X^2(t)$, $X(t)\dot{X}(t)$ and $\dot{X}^2(t)$; those of the PSD functions $S_{XX}(\omega)$, $S_{X\dot{X}}(\omega)$, $S_{\dot{X}\dot{X}}(\omega)$ are those of $t * X^2(t), t * X^2(t)$ and $t * X^2(t)$.

Random Response in the domain of time

For the properties previously described for the gaussian processes, it possible to state that the derivate and the integral of a gaussian random process are gaussian: in fact the derivate can be considered as the limit of the incremental ratio and so as a linear combination of gaussian processes, while the integral, from Riemann definition, can also be seen as a linear combination of gaussian variables and so it is gaussian.

So also the joint probabilities between the variable, its derivative and its integral are gaussian.

The solution of the differential equation of the motion of a SDOF system is the sum of the integral of Duhamel and a function that depends on the initial conditions; consequently it is not an integral in the sense of Riemann and the response process in general is not gaussian; yet if the excitation and the initial conditions are gaussian (jointly or independent on excitation), the random

response is gaussian too. In particular, if the initial conditions are deterministic, they can be considered gaussian with variance equal to zero.

So the random response of a SDOF system subjected to gaussian excitation is usually a gaussian process, and its complete characterization in the domain of time requires only the mean value and the autocorrelation function.

The random response $U(t)$ of a SDOF system with mass M and viscous damping and deterministic initial conditions and random excitation $F(t)$ is governed by the following second order differential equation:

$$M\ddot{U}(t) + 2\zeta_0\omega_0\dot{U}(t) + \omega_0^2 U(t) = F(t) , \quad P\left[\left(U(t_0) = u_0\right) \cap \left(\dot{U}(t_0) = \dot{u}_0\right)\right] = 1$$

where ζ_0, ω_0: damping ratio and the natural circular frequency of the system.

Let the random excitation $F(t)$ be stationary and gaussian, and the generic trial $F^{(k)}(t)$ defined in $(-\infty, +\infty)$: the random response is stationary for $t \geq 0$, if the initial condition are imposed at the time $t_o \to -\infty$. The convolution integral of Duhamel, keeping into account that the initial condition are imposed for $t_o \to -\infty$, can be written for the generic trial $U^{(k)}(t)$ in the following form:

$$U^{(k)}(t) = \frac{1}{M} \int_{-\infty}^{t} h(t-\tau)F^{(k)}(\tau)d\tau \quad t > 0$$

where $h(t)$ is deterministic: $h(t) = \frac{1}{\overline{\omega}_0}\sin\left(\overline{\omega}_0 t\right)\exp\left(-\zeta_0\omega_0 t\right)$;

$\overline{\omega}_0 = \omega_0\sqrt{1-\zeta_0^2}$: reduced circular frequency.

After imposing $\rho = t - \tau$ and changing variables in the integral, we get

$$U^{(k)}(t) = \frac{1}{M} \int_{0}^{+\infty} h(\rho)F^{(k)}(t-\rho)d\rho \quad t > 0$$

The previous expression lets evaluate the deterministic response of the SDOF system assumed subjected to a generic trial of the stationary random excitation.

322

The mean value of the response random process $U(t)$ can be evaluated by the application of the stochastic mean operator to the members of the previous expression and commutation property between stochastic mean and integral:

$$E[U(t)] = E\left[\frac{1}{M}\int_0^{+\infty}h(\rho)F(t-\rho)d\rho\right] = \frac{1}{M}\int_0^{+\infty}h(\rho)E[F(t-\rho)]d\rho \quad t > 0$$

Since the excitation is stationary, $\mu_F(t) = E[F(t)] = const \quad \forall t$, we get a mean value for the response:

$$\mu_U = E[U(t)] = \frac{1}{M}\mu_F\int_0^{+\infty}h(\rho)d\rho = \frac{\mu_F}{M\omega_0^2}$$

The autocorrelation function of the response process $U(t)$ can be determined by the relation already written for the generic $X(t)$ stationary gaussian process:

$$R_{UU}(\tau) = E[U(t)U(t+\tau)] - \mu_U^2$$

From this relation it can be demonstrated that the autocorrelation function can be computed by solving the following double integral:

$$R_{UU}(\tau) = \frac{1}{M^2}\int_0^{+\infty}\int_0^{+\infty}yh(\rho_1)h(\rho_2)R_{FF}(\tau-\rho_2+\rho_1)d\rho_1 d\rho_2 \quad \tau \geq 0$$

The variance of the response process can be computed imposing $\tau = 0$:

$$\sigma_U^2 = R_{UU}(0) = \frac{1}{M^2}\int_0^{+\infty}\int_0^{+\infty}h(\rho_1)h(\rho_2)R_{FF}(-\rho_2+\rho_1)d\rho_1 d\rho_2 \quad \tau \geq 0$$

By successive derivations from the autocorrelation function of the random process it is possible to determine the cross correlation functions between the random displacement and velocity processes and the autocorrelation of the velocity process; these quantities can be used to evaluate the covariance between the response processes displacement-velocity and the variance of the velocity response process.

Once evaluated all these quantities, and keeping into account that the mean value of the velocity response is zero, it is possible to characterize completely in the domain of time the bi-variate gaussian random process $\underline{Y}(t) = [U(t) \ \dot{U}(t)]^T$

Random Response in the domain of frequency

In the domain of frequency the bi-variate stationary gaussian process $\underline{Y}(t) = [U(t) \ \dot{U}(t)]^T$ is completely characterized if we know the mean values μ_U, $\mu_{\dot{U}}$ and the PSD functions $S_{UU}(\omega)$, $S_{U\dot{U}}(\omega)$, $S_{\dot{U}\dot{U}}(\omega)$.

The mean values are the same previously computed:

$$\mu_U = \frac{\mu_F}{M\omega_0^2}, \mu_{\dot{U}} = 0$$

The spectral density power of the displacement random process $U(t)$ can be written by the already written expression

$$R_{UU}(\tau) = \frac{1}{M^2} \int_0^{+\infty}\int_0^{+\infty} y h(\rho_1)h(\rho_2)R_{FF}(\tau - \rho_2 + \rho_1)d\rho_1 d\rho_2 \quad \tau \ge 0$$

and using the Wiener-Khinchine relation:

$$R_{UU}(\tau) = \int_{-\infty}^{+\infty} |H(\omega)|^2 S_{FF}(\omega)e^{i\omega\tau}d\omega = \int_{-\infty}^{+\infty} S_{UU}(\omega)e^{i\omega\tau}d\omega.$$

The variance of the displacement response can be obtained imposing $\tau = 0$:

$$\sigma_U^2 = \int_{-\infty}^{+\infty} |H(\omega)|^2 S_{FF}(\omega)d\omega = \int_{-\infty}^{+\infty} S_{UU}(\omega)d\omega$$

The expression $S_{UU}(\omega) = |H(\omega)|^2 \dfrac{S_{FF}(\omega)}{M^2}$ represents the power spectrum of the displacement response process, while the expression $|H(\omega)|^2$ represents the Energy Transfer Function:

$$|H(\omega)|^2 = \frac{1}{\left(\omega_0^2 - \omega^2\right)^2 + 4\zeta_0^2\omega_0^2\omega^2}$$

So for random stationary processes the PSD of the response process is the product of the PSD of the excitation and the Energy Transfer Function, that are scalar quantities; such operation is easier than that for the autocorrelation function that require the solution of the double integral.

Like for the deterministic excitation, also for the random excitation the nSDOF system filters the energy content of the input and exalts the output at its natural frequency: also if the excitation have different content of power at different frequencies (narrow band/large band/ white noise, etc.) (different PSD of the excitation), the response have the same frequency contents, evident from the Energy Transfer Function and the PSD of the response.

The cross spectral power density displacement-velocity $S_{U\dot{U}}(\omega)$ and the spectral power density of velocity $S_{\dot{U}\dot{U}}(\omega)$ of the bi-variate response process are

$$S_{U\dot{U}}(\omega) = i\omega |H(\omega)|^2 S_{FF}(\omega)$$

$$S_{\dot{U}\dot{U}}(\omega) = \omega^2 |H(\omega)|^2 S_{FF}(\omega)$$

and the covariances can be determined by integrating on the whole domain of PSD:

$$\sigma_{U\dot{U}} = \int_{-\infty}^{+\infty} i\omega |H(\omega)|^2 S_{FF}(\omega) d\omega = 0$$

$$\sigma_{\dot{U}}^2 = \int_{-\infty}^{+\infty} \omega^2 |H(\omega)|^2 S_{FF}(\omega) d\omega$$

The first spectral moments can be computed after having introduced the unilateral spectral power density $G_{UU}(\omega)$:

$$\lambda_{0,U} = \int_0^{+\infty} G_{UU}(\omega) d\omega = \int_0^{+\infty} |H(\omega)|^2 G_{FF}(\omega) d\omega = \sigma_U^2$$

$$\lambda_{1,U} = \int_0^{+\infty} \omega G_{UU}(\omega) d\omega = \int_0^{+\infty} \omega |H(\omega)|^2 G_{FF}(\omega) d\omega \neq \sigma_{U\dot{U}} = 0$$

325

$$\lambda_{2,U} = \int_0^{+\infty} \omega^2 G_{UU}(\omega)d\omega = \int_0^{+\infty} \omega^2 |H(\omega)|^2 G_{FF}(\omega)d\omega = \sigma_{\dot{U}}^2$$

White Noise Random Excitation

Let the excitation $F(t)$ be a white noise process $W(t)$ with mean zero and spectral power density $S_{FF}(\omega) = S_W$ constant in the domain $(-\infty, +\infty)$ of ω.

The autocorrelation function is $R_{FF}(\tau) = 2\pi S_W \delta(\tau)$.

The autocorrelation function of the response random process can be demonstrated that is

$$R_{UU}(\tau) = \sigma_U^2 \left[\cos(\overline{\omega}_0 |\tau|) + \frac{\zeta_0}{\sqrt{1-\zeta_0^2}} \sin(\overline{\omega}_0 |\tau|) \right] \exp(-\omega_0 \zeta_0 |\tau|)$$

where σ_U^2 : variance of the displacement random process $U(t)$:

$$\sigma_U^2 = \frac{\pi S_W}{ck} = \frac{\pi S_W}{M^2 2\zeta_0 \omega_0^3}$$

The autocorrelation function of the velocity response process $\dot{U}(t)$ can be evaluated by deriving the expression of $R_{UU}(\tau)$:

$$R_{\dot{U}\dot{U}}(\tau) = -\frac{d^2 R_{UU}(\tau)}{d\tau^2} = \sigma_{\dot{U}}^2 \left[\cos(\overline{\omega}_0 |\tau|) + \frac{\zeta_0}{\sqrt{1-\zeta_0^2}} \sin(\overline{\omega}_0 |\tau|) \right] \exp(-\omega_0 \zeta_0 |\tau|)$$

where the variance of the process $\dot{U}(t)$ is

$$\sigma_{\dot{U}}^2 = \frac{\pi S_W}{cm} = \frac{\pi S_W}{M^2 2\zeta_0 \omega_0}$$

The spectral power density of the displacement response random process of a SDOF subjected to white noise excitation can be evaluated:

$$S_{UU}(\omega) = |H(\omega)|^2 \frac{S_{FF}(\omega)}{M^2} = |H(\omega)|^2 \frac{S_W}{M^2}$$

Introducing the unilateral spectral power density of the white noise excitation

$$G_W = \begin{cases} 2S_W & \omega \geq 0 \\ 0 & \omega < 0 \end{cases}$$

it is possible to evaluate the first three moments of the response:

$$\lambda_{0,U} = G_W \int_0^{+\infty} |H(\omega)|^2 \, d\omega = \sigma_U^2 = \frac{\pi G_W}{2ck} = \frac{\pi G_W}{4\zeta_0 \omega_0^3 M^2}$$

$$\lambda_{1,U} = G_W \int_0^{+\infty} \omega |H(\omega)|^2 \, d\omega = \frac{G_W}{4\zeta_0 \omega_0 \overline{\omega}_0 M^2} \left[\pi - 2\arctan\left(\frac{\zeta_0}{\sqrt{1-\zeta_0^2}} \right) \right]$$

$$\lambda_{2,U} = G_W \int_0^{+\infty} \omega^2 |H(\omega)|^2 \, d\omega = \sigma_{\dot{U}}^2 = \frac{\pi G_W}{2Mc} = \frac{\pi G_W}{4\zeta_0 \omega_0 M^2}$$

The white noise excitation is very important in the Stochastic Dynamics: several natural phenomena like wind and earthquake actions can be modelled as filtered white processes, that are random processes solution of systems of linear differential equations, where the known terms are white noise processes.

The random process solution of the differential equation is said filtered because the uniform power density of the white process is filtered by the energy transfer function of the filter, to get a random process which has power spectrum meaningful of that of experimental derivation. Furthermore the modelling of the excitation as a filtered white noise signal is actually the best way to characterize the stationary and non-stationary random response of nonlinear structures and of structures subjected to non-gaussian processes.

In the following figure the autocorrelation functions and the spectral density power of the response are represented, in terms of displacements and velocity, for a SDOF system subjected to white noise: the system amplifies the power content of the excitation corresponding to its natural frequency.

Extension to MDOF Systems

The characterization of the random response of MDOF systems consists of the determination of all the statistical significant quantities.

The analyses of the response are more complicate than the deterministic ones; at first a proper distinction is necessary concerning the nature of the random excitation, that in general can be multi-variate and mono-correlated (like the earthquake) or multi-correlated (like the wind action).

Multivariate Gaussian Excitation: Equation of the Motion

The equations of the motion of a MDOF structure subjected to multivariate excitation and deterministic initial condition are

$$[M]\underline{\ddot{U}}(t) + [C]\underline{\dot{U}}(t) + [K]\underline{U}(t) = \underline{F}(t) , \quad P\left[\left(\underline{U}(t_0) = \underline{u}_0\right) \cap \left(\underline{\dot{U}}(t_0) = \underline{\dot{u}}_0\right)\right] = 1$$

where $\underline{U}(t)$ is the n-dimension vector of displacements and represents a multi-variate process according to the random nature of the excitation; $\underline{u}_0$ and $\underline{\dot{u}}_0$ are the vectors of the deterministic initial conditions; $[M], [C], [K]$ are the usual mass, damping and stiffness matrixes, the formers symmetric and definite positive, the latter symmetric and semi definite (definite) positive.

The modal approach requires the usual coordinate transformation as

$$\underline{U}(t) = [\Phi]\underline{Q}(t) = \sum_{j=i}^{m} Q_j(t)\underline{\phi}_j$$

where $[\Phi]$ is the matrix of the modes.

The equations of the motion become

$$\underline{\ddot{Q}}(t) + [\Xi]\underline{\dot{Q}}(t) + [\Omega^2]\underline{Q}(t) = [\Phi]^T \underline{F}(t) ,$$
$$P\left[\left(\underline{q}(t_0) = [\Phi]^T[M]\underline{u}_0\right) \cap \left(\underline{\dot{q}}(t_0) = [\Phi]^T[M]\underline{\dot{u}}_0\right)\right] = 1$$

where $[\Omega^2]$ is the spectral matrix, $[\Xi]$ is the modal damping matrix and $Q(t)$ is the vector of the response in modal coordinates.

The following relations are valid:

$$[K]^{-1}[M][\Phi] = [\Phi][\Omega^{-2}]; \ [\Phi]^T[M][\Phi] = [I_m]$$

$$\left[\Omega^{-2}\right] = \begin{bmatrix} \dfrac{1}{\omega_1^2} & 0 & ... & ... & 0 \\ 0 & \dfrac{1}{\omega_2^2} & 0 & ... & ... \\ ... & 0 & ... & 0 & ... \\ ... & ... & 0 & \dfrac{1}{\omega_{m-1}^2} & 0 \\ 0 & ... & ... & 0 & \dfrac{1}{\omega_m^2} \end{bmatrix}$$

where $\left[\Omega^{-2}\right]=$ (above) : inverse of the spectral matrix

and $\left[I_m\right]$ is the unity matrix of order m.

For classically damped structures $\left[\Xi\right]$ is diagonal:

$$\left[\Xi\right] = \begin{bmatrix} 2\zeta_1\omega_1 & 0 & ... & ... & 0 \\ 0 & 2\zeta_2\omega_2 & 0 & ... & ... \\ ... & 0 & ... & 0 & ... \\ ... & ... & 0 & 2\zeta_{m-1}\omega_{m-1} & 0 \\ 0 & ... & ... & 0 & 2\zeta_m\omega_m \end{bmatrix}$$

where ζ_j : damping ratio corresponding to the j$^{\text{th}}$ mode.

The equations of the motion are uncoupled:

$$\ddot{Q}_j(t) + 2\zeta_j\omega_j\dot{Q}_j(t) + \omega_j^2 Q_j(t) = \underline{\phi}_j^{\;T} \underline{F}(t) \;,$$
$$P\left[\left(Q_j(t_0) = q_{0,j}\right) \cap \left(\dot{Q}_j(t_0) = \dot{q}_{0,j}\right)\right] = 1$$

where $q_{0,j}$, $\dot{q}_{0,j}$: initial conditions for the generic oscillator.

If the multi-variate excitation is monocorrelate then it is possible to assume $\underline{F}(t) = F(t)\underline{\tau}$, where $F(t)$ is a random process and $\underline{\tau}$ is the *influence vector*, which represents the influence of the excitation on the different degree of freedom.

In this hypothesis the equations of the motion become

$$\underline{\ddot{Q}}(t) + \left[\Xi\right]\underline{\dot{Q}}(t) + \left[\Omega^2\right]\underline{Q}(t) = \underline{s}F(t)$$

where $\underline{s} = [\Phi]^T \underline{\tau}$

or $\ddot{Q}_j(t) + 2\zeta_j \omega_j \dot{Q}_j(t) + \omega_j^2 Q_j(t) = s_j F(t), \quad \left(s_j = \underline{\phi}_j^T \underline{\tau}\right)$ for   classically

damped structures.

If we assume initial conditions equal to zero, as happens for earthquake, and a generic trial $\underline{F}^{(k)}(t)$ of the multivariate excitation, the solution of the equations governing the motion have the following integral form:

$$[Q]^{(k)}(t) = \int_0^t [h(t-\tau)][\Phi]^T \underline{F}^{(k)}(\tau) d\tau = \int_0^{+\infty} [h(t-\tau)] U(t-\tau)[\Phi]^T \underline{F}^{(k)}(\tau) d\tau$$

or $Q_j^{(k)}(t) = \int_0^t h_j(t-\tau) \underline{\phi}_j^T \underline{F}^{(k)}(\tau) d\tau = \int_0^{+\infty} h_j(t-\tau) U(t-\tau) \underline{\phi}_j^T \underline{F}^{(k)}(\tau) d\tau,$

where $[h(t)U(t)]$: response matrix to the unity impulse for MDOF systems; for classically damped structures it is a diagonal matrix which has in the j-th element the response function of the corresponding degree of freedom subjected to the impulse.

If we characterize the response in terms of modal coordinates, we have to introduce the response vector in the form:

$$[Z(t)] = \begin{bmatrix} \underline{Q}^T(t) \\ \underline{\dot{Q}}^T(t) \end{bmatrix}$$

The equations of the motion can be written

$$[\dot{Z}(t)] = [D_M][Z(t)] + [V_M]\underline{F}(t) \quad P[[Z(0)] = [z_0]] = 1$$

where $[D_M] = \begin{bmatrix} [0] & [I_m] \\ -[\Omega^2] & -[\Xi] \end{bmatrix}, \ [V_M] = \begin{bmatrix} [0] \\ [\Phi]^T \end{bmatrix}.$

For classically damped structures the equation of the motion of the jth oscillator are

$$\underline{\dot{Z}}(t) = [D_j]\underline{Z}(t) + \underline{V}_j \underline{F}(t)$$

where $\underline{Z}_j = \begin{bmatrix} Q_j(t) \\ \dot{Q}_j(t) \end{bmatrix}$, $[D_j] = \begin{bmatrix} 0 & 1 \\ -\omega_j^2 & -2\zeta_j\omega_j \end{bmatrix}$, $\underline{V}_j = \begin{bmatrix} 0 \\ \underline{\phi}_j^T \end{bmatrix}$.

Using the modal coordinates the solution of the motion in the integral form is

$$[Z]^{(k)}(t) = \int_0^t \underline{h}_M(t-\tau)\underline{F}^{(k)}(\tau)d\tau = \int_0^t [\Theta_M(t-\tau)][V_M]\underline{F}^{(k)}(\tau)d\tau$$

or $\underline{Z}_j^{(k)}(t) = \int_0^t \underline{h}_j(t-\tau)\underline{F}^{(k)}(\tau)d\tau = \int_0^t [\Theta_j(t-\tau)]\underline{V}_j\underline{F}^{(k)}(\tau)d\tau$

where $[\Theta_M(t)]$, $[\Theta_j(t)]$: transition matrixes;

$$\underline{h}_M(t) = [\Theta_M(t)][V_M] = \begin{bmatrix} h(t)[\Phi]^T \\ \dot{h}(t)[\Phi]^T \end{bmatrix}, \quad \underline{h}_j(t) = [\Theta_j(t)]\underline{V}_j = \begin{bmatrix} h_j(t)\underline{\phi}_j^T \\ \dot{h}_j(t)\underline{\phi}_j^T \end{bmatrix}.$$

In the domain of frequency the solution of the motion with zero initial condition has the form

$$[Q]^{(k)}(\omega) = [H_M(\omega)][\Phi]^T \underline{F}^{(k)}(\omega)$$

where $\underline{F}^{(k)}(\omega)$, $[Q]^{(k)}(\omega)$: Fourier transforms of the excitation trial $\underline{F}^{(k)}(t)$ and of the modal response $[Q]^{(k)}(t)$.

$[H_M(\omega)]$ is a matrix defined in the modal space and that transforms the excitation quantities in those of the response:

$$[H_M(\omega)] = \int_{-\infty}^{+\infty} h_M(\tau)U(\tau)e^{-i\omega\tau}d\tau = [\Omega^2 - \omega^2 I_m + i\omega\Xi]^{-1}$$

For classically damped structures such matrix is diagonal, so that it is possible to evaluate the response of the jth in the domain of frequency:

$$Q_j^{(k)}(\omega) = H_{M,j}(\omega)\underline{\phi}_j^T \underline{F}^{(k)}(\omega)$$

where $H_{M,j}(\omega)$: j[th] element of $[H_M(\omega)]$; it represents the transfer function of the jth oscillator:

$$H_j(\omega) = H_{M,j}(\omega) = \frac{1}{\omega_j^2 - \omega^2 + 2i\omega_j\zeta_j\omega}$$

331

Characterization of the random response

If the excitation $\underline{F}(t)$ is a gaussian non-stationary multivariate process (monocorrelate or multicorrelate), and the initial conditions of the motion are deterministic, the response is a gaussian multivariate process, characterized by the mean values $\underline{\mu}_U(t)$, $\underline{\mu}_{\dot{U}}(t)$ and the matrixes of correlation $[R_{UU}(t_1,t_2)]$, $[R_{U\dot{U}}(t_1,t_2)]$, $[R_{\dot{U}\dot{U}}(t_1,t_2)]$.

If the excitation is gaussian, the response is gaussian and the mean values do not depend on time, $\underline{\mu}_U(t)=\underline{\mu}_U$, $\underline{\mu}_{\dot{U}}(t)=\underline{\mu}_{\dot{U}}$, while the correlation matrixes depend only on the parameter τ, $[R_{UU}(t_1,t_2)]=[R_{UU}(\tau)]$, $[R_{U\dot{U}}(t_1,t_2)]=[R_{U\dot{U}}(\tau)]$, $[R_{\dot{U}\dot{U}}(t_1,t_2)]=[R_{\dot{U}\dot{U}}(\tau)]$. In the domain of frequency the characterization has the PSD matrixes that depend on the circular frequency $S_{UU}(\omega)$, $S_{U\dot{U}}(\omega)$, $S_{\dot{U}\dot{U}}(\omega)$.

The statistical quantities in the nodal coordinates can be expressed in the modal coordinates; the following general relation can be demonstrated:

$\underline{\mu}_U(t)=[\Phi]\underline{\mu}_Q(t)$ (with no time dependence for stationary excitation);

$[R_{UU}(t_1,t_2)]=[\Phi][R_{QQ}(t_1,t_2)][\Phi]^T$ ($[R_{UU}(\tau)]=[\Phi][R_{QQ}(\tau)][\Phi]^T$ for stationary excitation);

and the covariance matrix

$[C_{UU}(t)]=[R_{UU}(t,t)]=[\Phi][C_{QQ}(t)][\Phi]^T$ (with no time dependence for stationary excitation).

The PSD matrix in the nodal and modal spaces are related by

$$[S_{UU}(\omega)]=[\Phi][S_{QQ}(\omega)][\Phi]^T$$

Multivariate mono-correlated stationary processes: response in the domain of frequency of classically damped structures

The multivariate mono-correlated excitation is typical of seismic analysis.

The analyses in the domain of frequency are easier than in the domain of time, since it requires the computation of simple integral instead of double convolution integrals.

For classically damped structures it is possible to compute the first m modes of the structure: the statistical quantities until the second order of the modal response can be determined by combining those of the m single oscillators of unity mass (*modal oscillators*).

After computing the quantities in the modal space

$$\mu_{Q_j} = \frac{1}{\omega_j^2} s_j \mu_F$$

$$R_{Q_j Q_k}(\tau) = s_j s_k \int_0^{+\infty} \int_0^{+\infty} h_j(\rho_1) h_k(\rho_2) R_{FF}(\tau - \rho_2 + \rho_1) d\rho_1 d\rho_2$$

$$S_{Q_j Q_k}(\omega) = s_j s_k H_j^*(\omega) H_k(\omega) S_{FF}(\omega)$$

where * represents the complex conjugate. The last equation states that the cross power spectral density between $Q_j(t)$ and $Q_k(t)$ is a complex quantity equal to the product of the PSD of the excitation and of the transfer function of two oscillators.

By derivation by τ we get the cross correlation functions of the derived processes:

$$\frac{d}{d\tau} R_{Q_j Q_K}(\tau) = R_{Q_j \dot{Q}_K}(\tau) = -R_{\dot{Q}_j Q_K}(\tau); \quad \frac{d^2}{d\tau^2} R_{Q_j Q_K}(\tau) = -R_{\dot{Q}_j \dot{Q}_K}(\tau)$$

The spectral power density of derived processes can be computed as

$$S_{Q_j \dot{Q}_k}(\omega) = i\omega S_{Q_j Q_k}(\omega), \ S_{\dot{Q}_j Q_k}(\omega) = -i\omega S_{Q_j Q_k}(\omega), \ S_{\dot{Q}_j \dot{Q}_k}(\omega) = \omega^2 S_{Q_j Q_k}(\omega)$$

Introducing the unilateral power spectrum of the excitation

$$G_{FF}(\omega) = \begin{cases} 0 & \omega < 0 \\ 2S_{FF}(\omega) & \omega \geq 0 \end{cases}$$

it is possible to determine the spectral moments in the modal space:

$$\lambda_{0,Q_j Q_k} = s_i s_j \lambda_{0,jk}, \ \lambda_{1,Q_j Q_k} = s_i s_j \lambda_{1,jk}, \ \lambda_{2,Q_j Q_k} = s_i s_j \lambda_{2,jk},$$

333

where $\lambda_{i,jk} = \lambda^{*}_{i,kj} = \int\limits_{0}^{+\infty} \omega^{i} H^{*}_{j}(\omega) G_{FF}(\omega) d\omega$.

The direct spectral moments are real quantities, while the cross modal spectral moments are complex and related to the covariances:

$$\mathrm{Re}\{\lambda_{0,Q_{j}Q_{k}}\} = \sigma_{Q_{j}Q_{k}}$$
$$\mathrm{Im}\{\lambda_{1,Q_{j}Q_{k}}\} = \sigma_{\dot{Q}_{j}Q_{k}}$$
$$\mathrm{Im}\{\lambda_{1,Q_{j}Q_{k}}\} = -\sigma_{Q_{j}\dot{Q}_{k}}$$
$$\mathrm{Re}\{\lambda_{2,Q_{j}Q_{k}}\} = \sigma_{\dot{Q}_{j}\dot{Q}_{k}}$$

Multivariate multi-correlated stationary processes: response in the domain of frequency of classically damped structures

For classically damped structures subjected to multivariate and multi-correlated gaussian excitation, it can be shown that statistical quantities assume the following values:

$$\mu_{Q_{j}} = \frac{1}{\omega_{j}^{2}} \underline{\phi}^{T}_{j} \underline{\mu}_{F}$$

$$R_{Q_{j}Q_{k}}(\tau) = \underline{\phi}^{T}_{j} \int\limits_{0}^{+\infty} \int\limits_{0}^{+\infty} h_{j}(\rho_{1}) h_{k}(\rho_{2}) [R_{FF}(\tau - \rho_{2} + \rho_{1})] d\rho_{1} d\rho_{2} \underline{\phi}_{k}$$

$$S_{Q_{j}Q_{k}}(\omega) = \underline{\phi}^{T}_{j} H^{*}_{j}(\omega) S_{FF}(\omega) H_{k}(\omega) \underline{\phi}_{k}$$

where $[R_{FF}(\tau)]$ is the matrix of correlation and $[S_{FF}(\omega)]$ is the matrix of spectral power density (PSD) of the multivariate process $\underline{F}(t)$ and $\underline{\mu}_{F}$ is the vector of mean values.

If we introduce the unilateral PSD matrix $[G_{FF}(\omega)] = \begin{cases} [0] & \omega < 0 \\ 2[S_{FF}(\omega)] & \omega \geq 0 \end{cases}$

it is possible to determine the rth spectral moment

$$\lambda_{r,Q_{j}Q_{k}} = \underline{\phi}^{T}_{j} \int\limits_{0}^{+\infty} \omega^{r} H^{*}_{j}(\omega) H_{k}(\omega) G_{pq}(\omega) d\omega \underline{\phi}_{k}.$$

Appendix E

Reliability Analysis: Definitions and Basic Methods

E.1   Definitions

Design variables and random variables
In a design problem a first classification distinguishes the design parameters $\underline{x}$ that must be chosen in order to satisfy specific targets (performance or probability of failure), in presence of uncertainties that are represented by random variables $\underline{v}$.

The first step consists of the identification of the probability density functions of the relevant random parameters and the functional relationship among them.
In general also the design parameters have random nature and could be consequently treated.

Limit-state functions
The failure surface (limit-state performance function) can be defined as
$$g(\underline{x},\underline{v}) = 0$$
It represents the boundary between the safe and the unsafe (satisfied/unsatisfied performance) region in the design parameter space (Figure E.1).

In the case of system-reliability or multi-performance required, more than one limit-state is defined and the unsafe region is configured as (Figure E.2):

$$\Omega(\underline{x}, \underline{v}) = \left\{ \bigcup_{i=1}^{N} g_i [\underline{x}, \underline{v}] \leq 0 \right\}$$
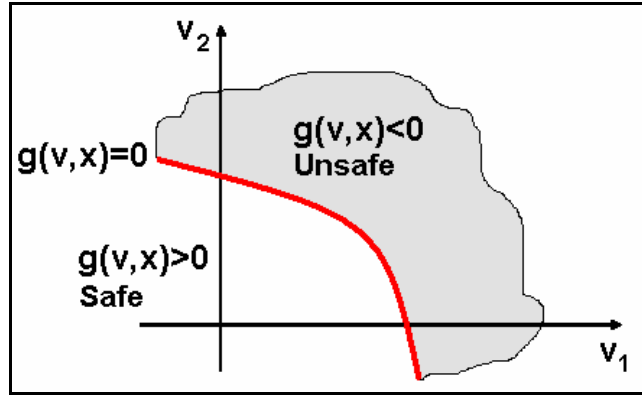
Figure E.1. Limit-state function for two random variables (Der Kiureghian).
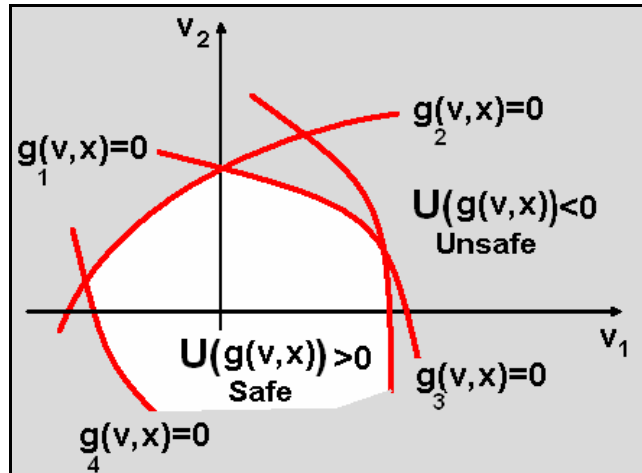
Figure E.2. Multiple limit-state function for two random variables (Der Kiureghian).

The limit-state function can be expressed in explicit or implicit form; its complexity suggests the reliability method to be chosen.

Failure probability and reliability index

The reliability analysis pursues the computation of the failure probability p_f which is the probability that one or more response limit-states $g_i(\underline{x}, \underline{v}) = 0$ are violated in an established time t_f (reasonable larger than the disturbance time):

$$p_f = \max_{0 \leq t \leq t_f} P\left\{ \bigcup_{i=1}^{N} g_i[\underline{x}, \underline{v}; t] \leq 0 \right\}$$

In the hypothesis of stationary response the previous expression becomes

$$p_f = \max_{0 \leq t \leq t_f} P\left\{ \bigcup_{i=1}^{N} g_i[\underline{x}, \underline{v}] \leq 0 \right\}$$

If the equation is expressed in terms of probability density functions one obtains

$$p_f = \int_{\Omega(\underline{x}, \underline{v})} f(\underline{x}, \underline{v}) d\underline{v}$$

where f is the joint probability density function of the random variables. The integral is performed in the region where $g_i(\underline{x}, \underline{v}) \leq 0$, $i = 1..N$

$$\Omega(\underline{x}, \underline{v}) = \left\{ \bigcup_{i=1}^{N} g_i[\underline{x}, \underline{v}] \leq 0 \right\}$$

If the random variables are statistically independent, the joint density function can be replaced by the product of the individual density function.

The solution of this integral is the classic reliability problem; it identifies the failure probability and the design point, defined as the most probable combination of random variables corresponding to failure occurrence.

In addition to the classic reliability analysis, a reliability-based optimal control design consists of the identification of a combination of the design parameters

$\underline{x}^*$ (*optimal design point*) that minimizes the costs, given the structural constraints, or maximizes the reliability index given the allowed costs. In the former case:

$$P : \min\left\{ f^0(\underline{x}) \middle| p_f(\underline{x}) \le p_{f_0}; \quad f^j(\underline{x}) \le 0, \ j \in J \right\}$$

where $f^0(\underline{x})$: cost function; $f^j(\underline{x})$, $j \in J$: constraint function;

p_{f_0} : target failure probability; $p_f(\underline{x})$: actual failure probability.

E.2   Reliability methods

In general the joint probability density function of random variables is impossible to obtain or the computation of the integral can be very complicated. several techniques exist to perform structural reliability analyses or optimization: they can be divided into three main categories:

- FORM and SORM (First/Second-order Reliability Method);
- RSM (Response Surface Method);
- MCS (Monte Carlo Simulation).

FORM and SORM
FORM and SORM are the earliest and most widely used methods: they estimate the probability of failure using first/second-order approximations of the limit-state function at the design point. They require the evaluation of the derivatives of the response functions or limit state functions with respect to the random variables. When the limit-state function are explicit, the calculation of the derivatives is easy; for complicate structures the limit-state functions are generally implicit and the derivatives are not available. In these case the FORM/SORM methods need to be associated to probabilistic finite element analyses to compute the gradients of the response.

FORM can be used when $g(\underline{x}, \underline{v})$ is a linear function of uncorrelated normal variables or when $g(\underline{x}, \underline{v})$ is approximated by a linear (first-order) approximation, tangent in the design point; SORM is used for nonlinear limit-

state functions with correlated non-normal variables by a second-order approximation.

FORM and SORM are a second-moment method, because it uses the information on first and second moments of the random variables. Means and covariances appear in the Taylor series approximations of the limit-state function:

$$g(\underline{x},\underline{v}) \equiv g(\underline{X}) = g(\overline{X}) + \sum_{i=1}^{n} \frac{\partial g}{\partial X_i} (X_i - \overline{X}_i) +$$

$$+ \frac{1}{2} \sum_{i=1}^{n} \sum_{j=1}^{n} \frac{\partial^2 g}{\partial X_i \partial X_j} (X_i - \overline{X}_i)(X_j - \overline{X}_j) + \dots$$

where

$\overline{X}_i$: mean value of X_i; $g(\overline{X}) = g(\overline{X}_1, \overline{X}_2, \dots, \overline{X}_u)$: mean value of $g(\underline{x},\underline{v})$;

$\sigma^2 \cong \sum_{i=1}^{n} \sum_{j=1}^{n} \frac{\partial^2 g}{\partial X_i \partial X_j} COV(X_i, X_j)$: approximated variance of $g(\underline{x},\underline{v})$.

For variables statistically independent the variance is

$$\sigma^2 = \sum_{i=1}^{n} \left(\frac{\partial g}{\partial X_i} \right)^2 VAR(X_i)$$

If we introduce the reduced standard variables (Hasofer-Lind Method)

$$X_i^{'} = \frac{X_i - \overline{X}_i}{\sigma_i} \quad i = 1,2\dots n$$

which have zero mean and unit standard deviation, the limit-state equation $g(\underline{x},\underline{v}) \equiv g(\underline{X}) = 0$ in the reduced limit-state becomes $g(\underline{X}') = 0$.

The standard normal space has the advantage of rotational symmetry, exponential decaying density in radial and tangential directions.

If all the random variables X_i are statistically independent normal variables and $g(\underline{x},\underline{v})$ is a linear combination of the X_i (or if the random variables X_i

339

are statistically independent lognormal variables and $g(\underline{x}, \underline{v})$ is a multiplicative function of the X_i), then $g(\underline{x}, \underline{v})$ (or $\ln g(\underline{x}, \underline{v})$) is normal and the failure probability can be expressed as

$$p_f = \Phi(-\beta)$$

where Φ is the cumulative distribution function for a standard normal variable; β: reliability index

The reliability of a structure is then commonly expressed by

$$\beta = \Phi^{-1}\left[1 - p_f(\underline{x}, \underline{v})\right]$$

The index β can be represented by the minimum distance between the origin of the axes in the reduced coordinate system and the limit-state (failure) surface (Figure E.3):

$$\beta = \sqrt{\left(\underline{X}^{'*}\right)^T \left(\underline{X}^{'*}\right)}$$

where $\underline{X}^{'*}$: most probable failure point in the reduced space.
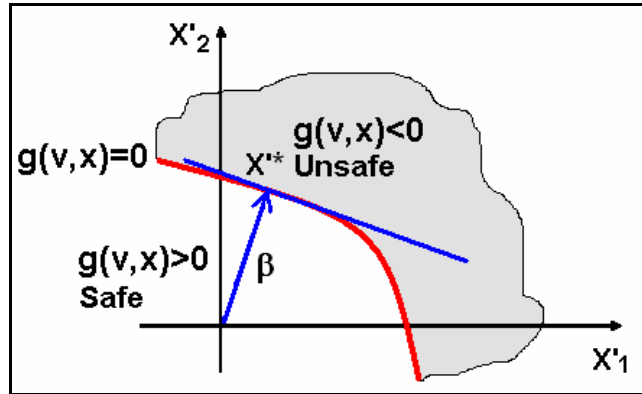
Figure E.3. Meaning of the Reliability Index β.

For nonlinear limit-state the identification of the most probable failure point $\underline{X}^{'*}$ is an optimization problem:

$$\min\left\{\beta = \sqrt{\left(\underline{X}^{'*}\right)^{T}\left(\underline{X}^{'*}\right)}\right\}/\ g\left(\underline{X}^{'*}\right) = 0$$

It can be solved by the Lagrange multipliers method (Shinozuka, 1983):

$$\beta = -\frac{\sum\limits_{i=1}^{n} X_{i}^{'*}\left(\dfrac{\partial g}{\partial X_{i}^{'}}\right)^{*}}{\sqrt{\sum\limits_{i=1}^{n}\left(\dfrac{\partial g}{\partial X_{i}^{'}}\right)^{2*}}}$$

The most probable failure point is then identified by

$$X_{i}^{'*} = \alpha_{i}^{*}\cdot\beta \quad i = 1,2...n$$

where $\alpha_{i}^{*} = -\dfrac{\left(\dfrac{\partial g}{\partial X_{i}^{'}}\right)^{*}}{\sqrt{\sum\limits_{i=1}^{n}\left(\dfrac{\partial g}{\partial X_{i}^{'}}\right)^{2*}}}$ (dir. cosines).

In the space of the original variables the most probable failure point is

$$X_{i}^{*} = \mu_{X_{i}} - \alpha_{i}^{*}\sigma_{X_{i}}\beta$$

The computation of β, $\underline{X}^{'*}$ requires the approximation of $g\left(\underline{X}\right)$ and can be conducted through the iterative algorithm developed by Rackwitz. The algorithm makes a linear approximation of $g\left(\underline{X}\right)$ in the successive failure points instead of the mean and so takes into account also the statistics of the random variables (i.e. the variances), until convergence. The algorithm works as follows:

1. Assumption of the initial failure point $X_{i}^{'*}$, $i = 1,2...n$,

   $$X_{i}^{*} = \frac{X_{i}^{*} - \overline{X}_{i}}{\sigma_{i}}\ ;$$

341

2. Approximation of $g(\underline{X}')$ and computation of $\left(\dfrac{\partial g}{\partial X_i'}\right)^*$ in $\underline{X}'^*$ and

computation of $\alpha_i^* = -\dfrac{\left(\dfrac{\partial g}{\partial X_i'}\right)^*}{\sqrt{\displaystyle\sum_{i=1}^{n}\left(\dfrac{\partial g}{\partial X_i'}\right)^{2*}}}$;

3. Computation of $\beta = -\dfrac{\displaystyle\sum_{i=1}^{n} X_i'^*\left(\dfrac{\partial g}{\partial X_i'}\right)^*}{\sqrt{\displaystyle\sum_{i=1}^{n}\left(\dfrac{\partial g}{\partial X_i'}\right)^{2*}}}$;

4. Computation of the new failure point $\underline{X}'^*$: $X_i^* = \mu_{X_i} - \alpha_i^* \sigma_{X_i} \beta$;

5. Repeat from point 2 to 4 until convergence is obtained.

Response Surface Method (RSM)

The performance limit-state is usually very complicated or implicit; furthermore also the structural response must be computed through deterministic finite element analyses.

RSM allows the reliability analysis using a polynomial approximation of $g(\bullet)$ obtained through a series of simulations chosen in the neighbourhood of the most probable failure point. Regression analyses are used to obtain explicit expression of the limit-state function. Finally the FORM/SORM methods already outlined are used to complete the reliability analysis.

Monte Carlo simulation method (MCS)

MCS is another method used when the limit-state function is implicit: it uses randomly generated samples of the input variables for each deterministic

analysis; the frequency of the failure occurrence approximate the probability of failure if the number of simulations is enough large.

The Monte Carlo Simulation Reliability Method is composed by the following steps:

1. Definition of the system: assumption of the random variables, their statistical moments and distribution types;
2. Generation of the input variables (*trials*): the number of trials is the same of the simulation that will be performed. More simulation increase the accuracy of the results and the computational costs.
3. Construction of the mechanical model: finite element models allow deterministic analyses for complex structure; additional variables can account the modelling uncertainties (coefficient of variation);
4. Evaluation of the model: trials of the output are obtained; their number is the same of the input trials generated and of the simulation performed;
5. Statistical analysis of the response: mean, variance, distribution types of the physical quantities monitored (and of the performance) are evaluated. In particular the frequency of violation of one or more limit-state function is monitored. For high number of simulation, it approximates the failure probability:

$$p_f = \lim_{N_{tot} \to \infty} \frac{N_f}{N_{tot}} = \lim_{N_{tot} \to \infty} \overline{p}_f$$

where N_{tot}: total number of simulations; N_f: number of simulations for which at least one limit-state is violated $N_f / \exists g_i(\underline{x},\underline{v}) \le 0, \quad i = 1,...N$.

The accuracy of the method can be evaluated in terms of variance or coefficient of variation of the failure probability computed:

$$VAR(\overline{p}_f) = \frac{(1 - \overline{p}_f)\overline{p}_f}{N} ; \quad COV(\overline{p}_f) = \frac{\sqrt{\dfrac{(1 - \overline{p}_f)\overline{p}_f}{N}}}{\overline{p}_f}$$

343

For coefficient of variation enough small a sufficient (arbitrary) accuracy is obtained.

Because of the high computational costs, alternative techniques have been introduced: the RSM-based Monte Carlo Importance Sampling (RMS-MCIS) use RSM to approximate the limit-state function and applies the Monte Carlo Importance Sampling to evaluate the structural reliability. The Importance Sampling Method performs numerical simulations in the neighbourhood of the presumed design point (sampling point) instead of using trials from the actual distributions. The expression of the failure probability assumes the following form:

$$p_f = \lim_{N_{tot} \to \infty} \frac{N_f}{N_{tot}} = \lim_{N_{tot} \to \infty} I_f \frac{f(\underline{x}, \underline{v})}{h(\underline{x}, \underline{v})}$$

where

I_f : failure indicator function: it is 0 in case of failure, 1 vice-versa;

$f(\underline{x}, \underline{v})$: joint density function of the random variables evaluated at every input generation;

$h(\underline{x}, \underline{v})$: importance function (sampling density function) evaluated at every input generation.

The efficiency of the method depends highly on the choice of the form of $h(\underline{x}, \underline{v})$.

BIBLIOGRAPHY

Abdel - Ghaffar A. M., e Rood J. D. (1982). "Simplified earthquake analysis of suspension bridge towers", *Journal of the Engineering Mechanics Division, ASCE*, 108, 291 - 308 .

Abe M., Fujino Y. (1994). "Dynamic Characterization of Multiple Tuned Mass Dampers and Some Design Formulas", *Earthquake Engineering and Structural Dynamics*, 23, 813-835.

American Institute of Steel Construction (AISC).(1986). *Manual of steel construction: Load and Resistance Factor Design*. Chicago: American Institute of Steel Construction.

Ang, G.K.I., Wyatt, D.P. (1998). "The role of performance specifications in the design agenda", *Proceedings of the Design Agenda Conference*, Brighton, UK, September 1– 18.

ANSYS Reference Guide: www.ansys.com, ANSYS Inc.

Astashev, V. K.; Babitsky, V. I.; Kolovsky, M. Z. (2000). *Dynamics and Control of Machines*, Ed. Springer.

Augusti G., Baratta A., Casciati F. (1984). *Probabilistic Methods in Structural Engineering*, London, Chapman & Hall.

Avizienis, A., Laprie, J.C. & Randell, B.(2004). "Dependability and its threats- A taxonomy". *IFIP Congress Topical Sessions*.

Avrenli K.A., Gencturk B., Keten S., Lus H. (2004). "Structural Control – A brief review", *Civil news 3*, 6.

Ayyub B.M., Haldar A. (1984). "Practical structural reliability techniques", *J. of Structural Engineering, American Society of Civil Engineers*, 110 (8), 1707-1724.

Ayyub B.M., McCuen R. (1995). "Simulation-based reliability methods", *Probabilistic Structural Mechanics Handbook*, Ed. By C.R.

Bathe KJ. (1996). *Finite Element Procedures*. NJ: Prentice Hall.

Belloli M., Diana G., Resta F., Rocchi D., Zasso A. (2003). "Wind effects on suspension bridges: the case of the Messina strait bridge", *5th International Symposium on Cable Dynamics*, 15-18 September, Santa Margherita Ligure, pp. 469-484.

Betti R., Abdel – Ghaffar A. M., Niazy A. S. (1993). "Kinematic soil - structure interaction for long - span cable - supported bridges", *Earthquake Engineering and Structural Dynamics*, 22, 415-430.

Biondini F., Frangopol D.M., Malerba P.G. (2006). "Time-variant structural performance of the Certosa cable-stayed bridge". *Journal of the International Association for Bridge and Structural Engineering (IABSE),* 16 (3), pp. 235-244.

Blanchard, B.S. (1997). *System Engineering Management*. New York: Wiley-Interscience.

Bontempi F, Catallo L, Sgambi L. (2004). "Performance-based design and analysis of the Messina Strait Bridge". *Proceedings of ASRANET 2004*, Barcelona.

Bontempi, F. Giuliano F. (2005). "Multilevel Approaches to the Analysis and Synthesis of the Serviceability Performance of a Long Span Suspension Bridge", Proceeding of the Tenth International Conference CC-2005, August 31st , September 2nd, Rome.

Bontempi F, Gkoumas K, Arangio S. (2005). "System Engineering Framework for the knowledge based analysis of complex structural system", *Proceedings of ICOSSAR'05*, Rome.

Bontempi F., Malerba P. G. (1996). "Il controllo della formulazione tangente per la soluzione di problemi strutturali non lineari", *Studi e Ricerche*, 17, Politecnico di Milano.

Bryson A.E. Ho Y.C. Jr. (1975). *Applied optimal control*, Washington: Hemisphere Publishing Corporation.

Bucher C.G.(1988)."Adaptive sampling – an iterative fast Monte Carlo procedure", *Structural Safety*, 5, 119-126.

Buchholdt H.(1997). *Structural dynamics for engineering*, London: Thomas Teldfort.

Cakmark A.S. (1987). "Soil-structure interaction", *Developments in Geotechnical Engineering*, 43, Ed. Elsevier.

Cakmark A.S., Herrera I. (1989). *Structural Dynamics and soil structure interaction*, Computational Mechanics Publications.

Calzona R.(2005). "Epistemological Aspects of Safety concerning the challenge of Future Construction: the Messina Strait Bridge", *Proceeding of the 10th*

International Conference on Civil, Structural and Environmental Engineering Computing, CC2005, Rome.

Caputo V. (1991). "Equivalent elastic analysis of piled foundation", *Proceeding X European conference of soil mechanic engineering*, Florence.

Caputo V. (1995). *Interazione fondazione terreno modelli matematici e metodi numerici*; Ed. Hevelius.

Casciati F., De Stefano A., Matta S. (2003). "Simulating a Conical Tuned Liquid Damper", *Simulation Modelling Practice and Theory*, 11, 353-370.

Casciati F., Faravelli L., F. Casciati, L. Faravelli, M. Battaini. (2001). "Ultimate vs. serviceability limit state in designig bridge energy dissipation devices", *Earthquake Engineering Frontiers in the New Millennium*, B.F. Spencer Jr, Y.X. Hu, 293-297.

Casciati F. and Faravelli L.(1991). *Fragility Analysis of Complex Structural Systems*, Taunton, UK, Research Studies Press.

Casciati F., Magonette G., Marazzi F. (2006). *Semiactive Devices and Applications in Vibration Mitigation*, Chichester, UK: John Wiley & Sons.

Casciati F., Giuliano F. (2006). "Tuned Mass Dampers in the Towers of Long Span Suspension Bridges", *Proceeding of the 5th International Conference on Engineering Computational Technology*, Las Palmas, Spain, 11-15 September.

Casciati S., Borja R. I. (2004). "Dynamic FE analysis of South Memnon Colossus including 3D soil-foundation-structure interaction", *Computers & Structures*, 82, 1719-1736.

Casciati S., Osman A. (2005). "Damage assessment and retrofit study for the Luxor Memnon Colossi ", *Journal of Structural Control and Health Monitoring*, 12 (2), 139-156.

Catallo L, Biondini F, Bontempi F, Frangopol DM. (2004). "Robust reliability-based design optimization of Suspension Bridges", *Proceedings of the 7th International Conference on Probabilistic Safety Assessment and Management, PSAM 7–ESREL04*, Berlin.

Cigada A., Diana G., Zappa E. (2003). "Messina Bridge Complex Aerodynamic Admittance Function Measurement", *Proceeding of International Conference on Wind Engineering (ICWE 2003)*, Lubbock, TX, USA, 2-5 June, pp. 123-130.

Clough R.W., Penzien J. (1993). *Dynamics of structures*, Singapore: Mc-Graw Hill Int. Ed.

Como M., Grimaldi A., Lembo M. (1987). "On the statical behaviour of cable-stayed /suspension bridges", *Proceeding of the Int. Conf. on cable-stayed bridges*, Bangkok.

Connor J.J. (2003). Introduction to structural Motion Control, MIT-Prentice Hall, NJ.

Connor J.J. (2003). Structural Motion Control, NJ: Prentice Hall.

Del Grosso A., Inaudi D., Pardi L. (2002). "Overview of European Activities in the Health Monitoring of Bridges", *Proceeding IABMAS'02 Bridge Maintenance, Safety and Management* (J.R. Casas, D.M. Frangopol, A.S.Nowak Eds.), CIMNE, Barcelona.

Den Hartog J.P. (1956). *Mechanical Vibrations*, New York: McGraw-Hill 4th Ed.

Der Kiureghian A., Lin H.Z., Hwang S.J. (1987). "Second-order reliability approximations", *J. Eng. Mech. ASCE*, 113 (8), 1208-1225.

Diana G., Bocciolone M., Manenti A., Zasso A. (1994). "Passive control system for reducing hangers wind induced vibrations design criteria and application to Messina Straits Bridge", *IABSE/FIP Int. Conference*, Deauville (France).

Diana G., Resta F., Rocchi D., Zasso A. (2003). "Effects of the yaw angle on the flutter derivatives and vortex shedding of the Messina multi-box girder deck section", *Proceeding of International Conference on Wind Engineering (ICWE 2003)*, Lubbock, TX, USA, 2-5 June, pp. 139-146.

Di Paola M. "Digital simulation of wind field velocity", *J. Wind Engineering Industrial Aerodynamics*, vol. 74-76, 91-109.

Ditlevsen, O., H. O. Madsen (1996). *Structural Reliability Methods*. Chichester, West Sussex, England: John Wiley and Sons Ltd.

Durkee, J.L., Thonaides S.S. "Erection Strength Adequacy of Long Truss Cantilevers", *J. Struct. Div., ASCE*.

Falcon K.C., Stone B.J., Simcock W.D, Andrew C. (1967). "Optimization of Vibration Absorbers: a Graphical Method for Use on Idealized Systems with Restricted Damping". *Journal of Mech. Engineering Science*, no. 9, 374-381.

Fellows R, Liu A. (1997). *Research Methods for Construction*, Blackwell Science.

Foliente, G.C. (2000). "Developments in performance-based building codes and standards", *Forest Products Journal*, 50 7/8: 12-21.

Frangopol D., Imai K. (2000). "Geometrically nonlinear finite element reliability analysis of structural systems II: applications", *Comput. Struct.*, 77, 693-709.

Fujino Y., Sun L., Pacheco B.M., Chaiseri P.(1992). "Tuned Liquid Damper (TLD) for Suppressing Horizontal Motion of Structures", *Journal of Engineering Mechanics ASCE*, 118 (10), 2017-2030.

Fujino Y., Abe M.(1993). "Design Formulas for Tuned Mass Dampers Based on Perturbation Technique", *Earthquake Engineering and Structural Dynamics*, 22, 833-854.

Fujino, Y.(2002). "Vibration, control and monitoring of long-span bridges – recent research, developments and practice in Japan", *Journal of Constructional Steel Research,* 58, 71-97.

Gawronski W.K. (2004). *Advanced Structural Dynamics and Active Control of Structure*, Ed. Springer.

Gimsing NJ. (1983) *Cable Supported Bridges, concept and design.* New York: J. Wiley & Sons.

Giuliano F. (2005). "Sensitivity Analysis of Devices and Motion Control Design for Cable-Suspension Bridges", Proceedings of ICOSSAR'05, Rome.

Giuliano F. (2006). "Reliability of Soil-Structure-TMD Response to buffeting Loads by Spectrum Analyses", *Proceeding of the 4th World Conference on Structural Control and Monitoring*, San Diego (U.S.A.), July 11-13.

Giuliano F, Gkoumas K, Petrini F. (2005). "Load scenarios and serviceability tests for the Messina Strait Bridge by time-history simulations". Third MIT Conference. Boston.

Guyan, R. J. (1965). "Reduction of Stiffness and Mass Matrices", *AIAA Journal*, Vol. 3, No. 2.

Harbitz A. (1983). "Efficient and accurate probability of failure calculation by FORM-SORM and updating by importance sampling", *Proceeding of the 5th International Conference on Applications of Statistics and Probability Theory in Civil Engineering*, A.Augusti, A. Borri, G. Vannucchi Ed., 825-836.

Haldar A., Mahadevan S. (1995). "First-order and second-order reliability methods", *Probabilistic Structural Mechanics Handbook*, Ed. By C.R. Sundararajan, New York: Chapman & Hall.

Hasegawa K., Kelly J.M. (1992). *Application of a mass damping system to bridge structures*, Report no. UCB/EERC-92/12, Earthquake Engineering Center, University of California at Berkeley.

Hata K., Masaaki T. (1998). "Vibration control of the main towers of the Akashi Kaikyo bridge", *Proceeding of the IABSE Conference Symposium,* Kobe, Japan.

Housner G.W. et al. (1997). "Structural Control: Past, Present, and Future", *ASCE Journal of Engineering Mechanics*.

IAI. (1997). *IFC end user guide.* Washington DC: Industry Foundation Classes - Release 1.5, International Alliance for interoperability.

349

Igusa T., Xu K. (1994): "Vibration control using multiple tuned mass dampers", *Journal of sound and vibration*, 175, 491-503.

Imai K, Frangopol D.M.(2002). "System reliability of suspension bridges", *Structural Safety*, 24.

Ioi T., Ikeda K. (1978). "On the Dynamic Vibration Damped Absorber of the Vibration System", *Bulletin of Japanese Society of Mechanical Engineering*, vol. 21 no. 151, 64-71.

Irvine H.M. (1975). *Cable structures*. MIT Press.

Jacquot R.G: and Hoppe D.L. (1973). "Optimal Random Vibration Absorbers", *Journal Engineering Mechanics ASCE*, 99, 612-616.

Jangid R.S.(1995). "Dynamic characteristics of structures with multiple tuned mass dampers", *Structural Engineering and Mechanics*, 3, 497-509.

Jiyu A.(2003). *Design of Experiments*, Oxford: Butterworth Heinemann.

Kanya A.M., Veneziano D.(1981). "Seismic effectiveness of tuned mass dampers", *J. Struct Div. ASCE*; 107, 1465-1484.

Kareem A., Kline S. (1995). "Performance of multiple tuned mass dampers under random loading", *Journal of Structural Engineering (ASCE)*, 121, 348-361.

Koshimura K., Tatsumi M., Hata, K. (1994), " Vibration Control of the Main Towers of the Akashi Kaikyo Bridge". *Proceedings of the First World Conference on Structural Control (1WCSC)*, Los Angeles, California, USA.

Kramer S.L. (1996). *Geotechnical earthquake engineering*, Ed. Prentice-Hall.

Larose G.L., M. Falco, Cigada A. (1995). "Aeroelastic response of the towers for the proposed bridge over Stretto di Messina", *Journal of Wind Engineering and Industrial Aerodynamics* 57; 363-373.

Lazzari M., Saetta A., Vitaliani R.V. (2001). "Non-linear dynamic analysis of cable-suspended structures subjected to wind actions", *Computer & Structures*, 79, 953-969.

Li C.(2002). "Optimum multiple tuned mass dampers for structures under the ground acceleration based on DDMF and ADMF", *Earthquake Engineering and Structural Dynamics*, 31, 897-919.

Li C., Liu Y.(2003). "Optimum multiple tuned mass dampers for structures under the ground acceleration based on the uniform distribution of system parameters", *Earthquake Engineering and Structural Dynamics*, 32, 671-690.

Lin Y.K. (1967). *Probabilistic theory of structural dynamics,* Malabar, Florida: McGraw-Hill, Inc.

Luft R.W. (1979): "Optimal Tuned Mass Dampers for Building", *J. Struct. Div., ASCE*, 105 (12), 2766-2772.

Madsen H.O., Krenk S., Lind N.C.(1986). *Methods of Structural Safety*, Englewood Cliffs, NJ: Prentice Hall Inc.

Malerba P.G., *Appunti dal Corso di Tecnica delle Costruzioni*.

Melchers, R. E. (1999). *Structural Reliability Analysis and Prediction* (2nd ed.). Chichester, West Sussex, England: John Wiley and Sons Ltd.

Mestat P., Prat M. (1999) *Ouvrage en interaction* (in French) Hermes Science.

Moore P.J. (1985). *Analysis and design of foundations for vibration*, Ed. Balkema.

Muscolino G. (2002). *Dinamica delle Strutture* (in Italian), McGraw Hill.

National Aeronautics and Space Administration (NASA) (1995). *Systems Engineering Handbook*, available on line at:
http://ldcm.gsfc.nasa.gov/library/Systems_Engineering_Handbook.pdf

Nishimura I., Sakamoto M, Yamada T., Koshika N., Kobori T.(1994). "Acceleration Feedback Method Applied to Active-Passive Composite Tuned Mass Damper", *Journal of Structural Control*, 1, 103-116.

Norme Tecniche per le Costruzioni – Testo Unitario, 23/09/2005 (in Italian).

Novak M. (1974). "Effect of soil on structural response to wind and earthquake", *Earthquake Eng. And Struct. Dynamics,* 3, 79-96.

Novak M., El Hifnawy L.(1988). "Structural response to wind with soil-structure interaction", *J. Wind Eng. Ind. Aerodyn*. 28, 329-338.

O'Connor C. (1971). *Design of bridge superstructures*, New York: John Wiley.

Ostenfeld K.H., Larsen A. (1992). "Bridge Engineering and Aerodynamics", *Proceeding of the 1st Int. Symp. on aerdynamics of large bridges*, Copenhagen, Balkema Publishers.

Papadimitriou C., Katafygiotiss L.S., Au S.K.(1997). "Effects of Structural Uncertainties on TMD Design: a Reliability-based Approach", *Journal of Structural Control*, 4, 65-88.

Park J., Reed D.(2001). "Analysis of uniformly and linearly distributed mass dampers under harmonic and earthquake excitation", *Engineering Structures*, 23, 802-814.

PeBBu Final Report EUR 21990 ISBN 90-6363-051-4. (2005) "Performance based building: conceptual framework"

Petrini F., Giuliano F., Bontempi F. (2006) "Comparison of time domain techniques for the evaluation of the response and the stability in long span suspension bridges", *Computers & Structures*, accepted paper.

Podolny W., Scalzi .J.B. (1976). *Construction and design of cable-stayed bridges*, New York: John Wiley.

Preumont A. (2002). *Vibration Control of Active Structures*, Ed. Springer.

Przemieniecki J.S. (1985). *Theory of Matrix Structural Analysis*, New York, Dover Publication.

Rackwitz R. (2000). "Optimization – the basis of code-making and reliability verification", *Structural Safety*, 22, 27-60.

Rackwitz R. (2001). "Reliability analysis – A review and some perspectives", *Structural Safety*, 23, 365-395.

Rega G:, Troger H. (2005). "Dimension Reduction of Dynamical Systems: Methods, Models, Applications", *Nonlinear Dynamics*, 41, 1-3; 1 - 15.

Rosenblatt, M. (1952). "Remarks on a multivariate transformation", *The Annals of Mathematical Statistics*, 23, 470–472.

Scanlan R. (1992). "Wind dynamics of long-span bridges", *Proceeding of the 1st Int. Symp. on aerdynamics of large bridges*, Copenhagen, Balkema Publishers.

Schmitendorf W.E.(2000). "Designing tuned mass dampers via static output feedback: a numerical approach", *Earthquake Engineering and Structural Dynamics*, 29, 127-137.

Schodek, D.L. (1998). *Structures*, Third Edition, Ohio: Prentice Hall-Columbus.

Schueller G.I., Bucher C.G., Bourgund U., Ouypornprasert W. (1989). "An efficient computational scheme to calculate structural failure probabilities", Probabilistic Eng. Mechanics, 4 (1), 10-18.

Shinozuka M. (1983). "Basic analysis of structural safety", *ASCE Journal of Struct. Eng.*, 109(3), 721-740.

Silvestri M, Bontempi F. (2003). "Strategy and formulation levels of the structural performance analysis of advanced systems", *Proceedings of the Second International Conference on Structural and Construction Engineering, ISEC03*, Rome.

Simiu E., Scanlan R.H. (1996). *Wind effects on structures*. New York: 3rd Ed., John Wiley & Sons.

Simon H.A. (1998). *The Sciences of the Artificial. Cambridge*, The MIT Press.

Singh M.P., Maldonado G.O.(1991). "An Improved Response Spectrum Method for Calculating Seismic Design Response – Part I: Classically Damped Structures", *Earthquake Engineering and Structural Dynamics*, 20, 621-635.

Singh M.P. and Suarez L.E. (1998). "Nonstructural Components and Civil Infrastructure Systems", in Casciati et al. (eds.), Civil Infrastructure Systems: Intelligent Renewal, World Scientific, Singapore.

Skelton R.E. (2002). "Structural System: a marriage of structural engineering and system science", *Journal of Structural Control*, Vol. 9, pp. 113-133.

Skogestad S., Postlethwaite I. (2005). *Multivariable feedback control*, Chichester, England: John Wiley & Sons Ltd.

Sladek J.R., Klingner R.E. (1983). "Effect of Tuned Mass Dampers on Seismic Response", *J. Struct. Eng., ASCE*, 109 (8), 2004-2009.

Smith I.(2001). "Increasing Knowledge of Structural Performance", *Structural Engineering International*, 12 (3), 191-195.

Solari G. (1985). "Mathematical model to predict 3-D wind loading on buildings", *J. of Eng. Mechanics ASCE*, 111, 2, 254-276.

Solari G., Carassale L.(2005). "Monte Carlo simulation of wind velocity fields on complex structures", *Proceedings of ICOSSAR2005*, Rome

Solari G., Piccardo G. "Probabilistic 3-D turbulence modelling for gust buffeting of structures", *Probabilistic Engineering Mechanics*, vol.17,327-335.

Solnes J. (1997). *Stochastic processes and random vibration,* Chichester, England: John Wiley & Sons Ltd.

Soong T.T., Dargush G.F. (1997). *Passive Energy Dissipation Systems in Structural Engineering*, Chichester, England: John Wiley & Sons.

Soong T.T. (1990). *Active structural control: theory and practice*, New York: John Wiley & Sons.

Spencer B.F.Jr., Sain M.K., Won C.H., Kaspari D.C., Sain P.M. (1994). "Reliability-based measures of structural control robustness", *Structural Safety*, 15, 111-129.

Spencer B.F., Soong T.T. (1999). "New Applications and Development of Active, Semi-Active and Hybrid Control Techniques for Seismic and Non-Seismic Vibration in the USA", *Intl. Post-SMiRT Conference*, Korea.

Steinman D.B. (1922). *A practical treatise on suspension bridges*, New York: John Wiley & Sons, Inc.

Stewart J. P., Seed R. B., Fenves G. L.: "Empirical evaluation of inertial soil - structure interaction effects",http://peer.berkeley.edu/publications/PEER-199807/intro.pdf.

Stretto di Messina S.p.A., Preliminary Project, 1992, available at http://www.strettodimessina.it .

Szigeti F., Davis G. (2005). *Performance Based Building: Conceptual Framework*. EUR21990 ISBN90-6363-051-4 Final Report, http://www.pebbu.nl.

Tanaka H., Mak C.Y. (1983) "Effect of TMD on Wind Induced Response of Tall Buildings", *Journal of Wind Engineering and Industrial Aerodynamics*, 11, 357-368.

Tewari A. (2002). *Modern Control Design*, Chichester, England: John Wiley & Sons Ltd.

Thoft-Christensen, P., Baker M.J. (1982). *Structural Reliability Theory and its Applications*. Berlin:Springer-Verlag.

Thompson A.G. (1981). "Optimum Tuning and Damping of a Dynamic Vibration Absorber Applied to a Force Excited and Damped Primary System", *Journal of Sound and Vibration*, 77, 403-415.

Thomson W.T. (1972).*Theory of vibrations with applications,* Cheltenham, UK: Prentice Hall.

Troitsky M.S. (1977). *Cable-stayed bridges. Theory and design*. Corsby Lockwood Staples.

Tvedt L. (1990). "Distribution of quadratic forms in normal space – application to structural reliability", J. of the Engineering Mechanics Division, American Society of Civil Engineers, 116 (6), 1183-1197.

Vickery B.J. (1990). "Progress and problems in the prediction of the response of prototype structures to vortex-induced oscillation", *J. Wind Eng. Ind. Aerodyn*, 33, 181-196.

Vickery B.J., Basu R.I. (1983). "Across-wind vibrations of structures of circular cross-section - Part 1", *J. Wind Eng. Ind. Aerodyn*, 12, 2, 49-73.

Warburton G.B., Ayorinde E.O. (1980): "Optimal Absorber Parameters for Simple Systems", *Engineering and Structural Dynamics*, 8, 197-217.

Warburton G.B.(1982). "Optimal Absorber Parameters for Various Combinations of Response and Excitation Parameters", *Earthquake Engineering and Structural Dynamics*, 10, 381-401.

Wirsching P.H., Paez T.L., Ortiz K. (1995). *Random vibrations,* New York: John Wiley & sons, Inc.

Wirsching P.H., Campbell G.W. (1974). "Minimal Structural Response under Random Excitation Using the Vibration Absorber", *Earthquake Eng. Struct. Dyn*., 2, 303-312.

Wolf J.P. (1988). *Soil-structure interaction in time domain*, Ed. Prentice-Hall.

Wolf J. P. (1994). *Foundation vibration analysis using simple physical model*, Ed. Prentice-Hall.

Xu Y.L., Kwok K.C.S. (1992). "Wind Induced Response of Soil-Structure-Damper system", *Proceedings 8th Int. Conf. Wind Eng.*, Ed. A.G. Davenport et al., London, Ontario, Canada, 2057-2068.

Xu Y.L., Kwok K.C.S., Samali B. (1992). "Control of wind-induced tall building vibration by tuned mass dampers", *Journal of Wind Engineering and Industrial Aerodynamics*, 40, 1-32.

Xu K., Igusa T. (1992). "Dynamic Characteristics of Multiple Substructures with Closely Spaced Frequencies", *Earthquake Engineering and Structural Dynamics*, 21, 1059-1070.

Yamagata M., Yasuda M., Nitta A. e Yamamoto S. (1996). "Effects on the Akashi Kaikyo Bridge", *Special Issue of Soils and Foundations*, 179 - 187.

Yamaguchi H., Harnpornchai N. (1993). "Fundamental characteristics of multiple tuned mass dampers for suppressing harmonically forced oscillations", *Earthquake Engineering and Structural Dynamics*, 22, 51-62.

Zhao Y.G., Ono T. (1999). "A general procedure for first/second-order reliability method (FORM/SORM), *Structural Safety*, 21, 95-112.

Zuo D. "Numerical modeling of dynamic soil – structure interaction during earthquakes",
http://www.ce.jhu.edu/dzuo/earthquake/Earthquake_rtp02.PDF.